

## INFORMATION TO USERS

This manuscript has been reproduced from the microfilm master. UMI films the text directly from the original or copy submitted. Thus, some thesis and dissertation copies are in typewriter face, while others may be from any type of computer printer.

**The quality of this reproduction is dependent upon the quality of the copy submitted.** Broken or indistinct print, colored or poor quality illustrations and photographs, print bleedthrough, substandard margins, and improper alignment can adversely affect reproduction.

In the unlikely event that the author did not send UMI a complete manuscript and there are missing pages, these will be noted. Also, if unauthorized copyright material had to be removed, a note will indicate the deletion.

Oversize materials (e.g., maps, drawings, charts) are reproduced by sectioning the original, beginning at the upper left-hand corner and continuing from left to right in equal sections with small overlaps.

Photographs included in the original manuscript have been reproduced xerographically in this copy. Higher quality 6" x 9" black and white photographic prints are available for any photographs or illustrations appearing in this copy for an additional charge. Contact UMI directly to order.

ProQuest Information and Learning  
300 North Zeeb Road, Ann Arbor, MI 48106-1346 USA  
800-521-0600

UMI<sup>®</sup>



**University of Alberta**

**Behaviour of Sleeper-supported Line Pipe**

by

**Jeffrey David DiBattista**



A thesis submitted to the Faculty of Graduate Studies and Research in partial fulfillment  
of the requirements for the degree of Doctor of Philosophy

in

Structural Engineering

Department of Civil and Environmental Engineering

Edmonton, Alberta

Spring 2000



National Library  
of Canada

Acquisitions and  
Bibliographic Services

395 Wellington Street  
Ottawa ON K1A 0N4  
Canada

Bibliothèque nationale  
du Canada

Acquisitions et  
services bibliographiques

395, rue Wellington  
Ottawa ON K1A 0N4  
Canada

*Your file Votre référence*

*Our file Notre référence*

The author has granted a non-exclusive licence allowing the National Library of Canada to reproduce, loan, distribute or sell copies of this thesis in microform, paper or electronic formats.

The author retains ownership of the copyright in this thesis. Neither the thesis nor substantial extracts from it may be printed or otherwise reproduced without the author's permission.

L'auteur a accordé une licence non exclusive permettant à la Bibliothèque nationale du Canada de reproduire, prêter, distribuer ou vendre des copies de cette thèse sous la forme de microfiche/film, de reproduction sur papier ou sur format électronique.

L'auteur conserve la propriété du droit d'auteur qui protège cette thèse. Ni la thèse ni des extraits substantiels de celle-ci ne doivent être imprimés ou autrement reproduits sans son autorisation.

0-612-59950-7

**Canada**

**University of Alberta**

**Library Release Form**

**Name of Author:** Jeffrey David DiBattista

**Title of Thesis:** Behaviour of Sleeper-supported Line Pipe

**Degree:** Doctor of Philosophy

**Year This Degree Granted:** 2000

Permission is hereby granted to the University of Alberta Library to reproduce single copies of this thesis and to lend or sell such copies for private, scholarly, or scientific research purposes only.

The author reserves all other publication and other rights in association with the copyright in the thesis, and except as hereinbefore provided, neither the thesis nor any substantial portion thereof may be printed or otherwise reproduced in any material form whatever without the author's prior written permission.



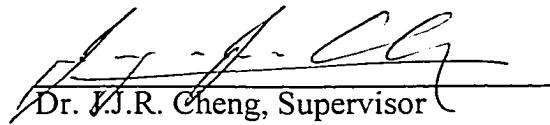
11824-8 Avenue  
Edmonton, AB  
CANADA  
T6J 6Z9

*April 7, 2000*

**University of Alberta**

**Faculty of Graduate Studies and Research**

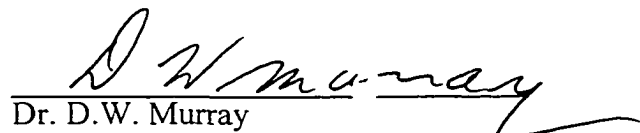
The undersigned certify that they have read, and recommend to the Faculty of Graduate Studies and Research for acceptance, a thesis entitled Behaviour of Sleeper-supported Line Pipe submitted by Jeffrey David DiBattista in partial fulfillment of the requirements for the degree of Doctor of Philosophy in Structural Engineering.

  
Dr. J.J.R. Cheng, Supervisor

  
Dr. R.W. Brachman

  
Dr. G.Y. Grondin

  
Dr. A.W. Lipsett

  
Dr. D.W. Murray

  
Dr. J.M. Roesset

*April 4, 2000*

*to my family*

## ABSTRACT

Buried high-pressure large-diameter pipes for hydrocarbon products are sometimes supported by flat concrete footings known as ‘sleepers.’ Current design methods for sleeper-supported pipes are not rational and are believed to be excessively conservative. An improved understanding of sleeper-supported piping behaviour is required to provide more economical designs while still maintaining appropriate margins of safety.

Full-size line pipes were examined to determine their behaviour when subjected to bearing forces induced at the sleeper supports. Of particular concern were the distortion of the cross-section and the identification of potential buckling or wrinkling problems. The goal was to develop a new design approach that is consistent with the limit states design philosophy.

Results from full-scale laboratory tests show that sleeper-supported pipes behave in a stable and ductile manner, but cross-sectional distortion is considerable and is likely to be the governing limit state. Finite element models of the specimens, which incorporate non-linear material properties and account for large strains and deformations, were developed. The numerical results compare favourably with the test data in terms of both strength and deformation criteria.

Modifying the modelling procedures allowed simulation of idealized *in situ* conditions. This idealized model was used to examine how the relationship between soil pressure and out-of-roundness is affected by pipe size, wall thickness, steel grade, and also by sleeper size and spacing. Non-linear regression analysis of this data led to the

development of simplified empirical equations that accurately predict the behaviour of idealized *in situ* sleeper-supported piping.

Based on the available literature and on the results from this study, reasonable limits on pipeline distortion are 8.5% out-of-roundness at zero internal pressure and 5% out-of-roundness at operating pressure. However, there is a need for the pipeline industry to clarify the specific design requirements for their lines in order to identify more objective limits on cross-sectional distortion. A new method for the design of sleeper-supported pipes is proposed using such limits in conjunction with the regression equations developed in this work. The equations will relieve the designer of the need to perform detailed finite element analyses for routine design scenarios and provide solutions that are more rational than those that were available previously.

## ACKNOWLEDGEMENTS

This study was conducted with the financial assistance of the Natural Sciences and Engineering Research Council of Canada (NSERC) and NOVA Gas Transmission Ltd. (a subsidiary of TransCanada PipeLines Limited). The author also acknowledges support, in the form of scholarships, provided by the Killam Trusts, NSERC, the Steel Structures Education Foundation, NOVA, Petro-Canada, Gulf Canada Resources, the University of Alberta, and the Offshore Mechanics and Arctic Engineering Society.

At the University of Alberta, students Andrew Boucher, Chris Jordan, and Kelty McColl were invaluable assistants in the preparation of the full-scale tests. As usual, the wizardry of Mr. Richard Helfrich, technician at the I.F. Morrison Structural Lab, made the testing program run smoothly. Thanks are also extended to Dr. Gilbert Grondin who provided comments on all aspects of the work that were invariably insightful and practical. Dr. Alaa Elwi also provided useful suggestions for the finite element procedures. Throughout the work, my office colleagues, in particular Christophe Deniaud, Alfred Dorey, and Marc Kuzik, provided valuable technical advice and consultation. Dr. Roger Cheng acted as the supervisor of the project, and Dr. David Murray's contribution was of particular importance during the early stages of the project.

The comments of Dr. K.L. Mehra and Dr. N.G. Prasad of the Department of Mathematical Sciences were helpful in the development of experimental design and regression work presented in Chapter 6. The opinions of Dr. David DiBattista from the Department of Psychology at Brock University helped me to gain a new perspective on the statistical work, and have made it more intelligible to non-engineers.

In industry, Dr. Joe Zhou of NOVA Gas Transmission Ltd. first identified the limitations of the existing design technique for sleeper-supported piping. He brought the problem to the attention of researchers at the U of A, obtained funding from NOVA to support the research, and played a key role in the conceptual development of the project. Dr. Laurie Collins and Mr. Brian Nelson of IPSCO Saskatchewan Incorporated made their Research and Development facility in Regina available for the hydraulic ring expansion tests. Their assistance is acknowledged with thanks.

Finally, I wish to extend special gratitude to my wife, Traci, who has provided patient support throughout.

## TABLE OF CONTENTS

<b>1</b>	<b>INTRODUCTION AND LITERATURE REVIEW.....</b>	<b>1</b>
1.1	THE SLEEPER-SUPPORT CONCEPT.....	1
1.1.1	Statement of the Problem.....	2
1.1.2	Scope and Objectives.....	2
1.2	LITERATURE REVIEW.....	4
1.2.1	Design Philosophies.....	4
1.2.1.1	<i>Working Stress Design</i> .....	5
1.2.1.2	<i>Limit States Design</i> .....	6
1.2.2	Current Design Method for Sleeper-supported Piping.....	9
1.2.3	Limit States for Sleeper-supported Piping.....	12
1.2.4	Cross-sectional Distortion of Thin-walled Pipes.....	14
1.2.4.1	<i>Quantitative Measures of Distortion</i> .....	15
1.2.4.2	<i>Existing Cross-sectional Distortion Design Criteria</i> .....	16
1.2.4.2.1	Limits on Ovalization.....	17
1.2.4.2.2	Limits on Ovality.....	18
1.2.4.2.3	Limits on Out-of-Roundness.....	18
<b>2</b>	<b>EXPERIMENTAL PROGRAM.....</b>	<b>22</b>
2.1	FULL-SCALE LABORATORY TESTS.....	22
2.1.1	Selection of Parameters.....	22
2.1.2	Description of Specimens.....	23
2.1.3	Test Set-up and Procedure.....	24
2.1.4	Instrumentation and Monitoring.....	26
2.1.4.1	<i>Initial Measurements</i> .....	26
2.1.4.2	<i>Strain Gauges</i> .....	27
2.1.4.3	<i>Internal Pressure</i> .....	28
2.1.4.4	<i>Displacement Measurements</i> .....	28
2.1.4.5	<i>Cross-sectional Distortion</i> .....	28
2.2	ANCILLARY TESTS.....	29
2.2.1	Material Properties of Pipeline Steels.....	29
2.2.2	Tension Coupon Tests.....	30
2.2.3	Hydraulic Ring Expansion Tests.....	31

<b>3</b>	<b>FINITE ELEMENT ANALYSIS OF TEST SPECIMENS .....</b>	<b>40</b>
3.1	GOALS OF FINITE ELEMENT STUDY .....	40
3.2	DESCRIPTION OF MODELS .....	41
3.2.1	Finite Element Formulation .....	41
3.2.2	Elements.....	42
3.2.3	Boundary Conditions .....	44
3.2.4	Contact Formulation .....	45
3.2.5	Material Model.....	46
3.2.6	Initial Geometry and Residual Stresses .....	48
3.2.7	Mesh Selection and Refinement .....	49
<b>4</b>	<b>DISCUSSION OF EXPERIMENTAL AND NUMERICAL RESULTS.....</b>	<b>56</b>
4.1	RESULTS: FULL-SCALE LABORATORY TESTS.....	56
4.1.1	Qualitative Observations.....	56
4.1.2	Quantitative Observations.....	57
4.1.2.1	<i>Consideration of Random Errors</i> .....	57
4.1.2.2	<i>Load versus Sleeper Displacement</i> .....	59
4.1.2.3	<i>Out-of-Roundness versus Sleeper Displacement</i> .....	61
4.2	RESULTS: ANCILLARY MATERIAL TESTS.....	62
4.2.1	Tension Coupon Test Results .....	62
4.2.2	Hydraulic Ring Expansion Tests .....	64
4.3	RESULTS OF MODELLING AND COMPARISON WITH LABORATORY TESTS.....	66
4.3.1	Qualitative Observations.....	66
4.3.2	Quantitative Observations.....	67
<b>5</b>	<b>FINITE ELEMENT MODELLING OF <i>IN SITU</i> CONDITIONS.....</b>	<b>87</b>
5.1	IDEALIZATION OF <i>IN SITU</i> SLEEPER-SUPPORTED PIPING .....	87
5.1.1	Soil Loads on Pipelines.....	88
5.1.2	Selection of a Soil Model.....	89
5.1.3	Empirical and Semi-empirical Estimation of Soil Pressures .....	90
5.1.3.1	<i>Vertical Downward Soil Pressure</i> .....	90
5.1.3.2	<i>Vertical Upward and Lateral Soil Pressures</i> .....	92
5.1.4	Equilibrium of the Idealized System.....	93
5.1.5	Critical Examination of the Idealization .....	94

5.2	FINITE ELEMENT MODELLING OF IDEALIZED SLEEPER-SUPPORTED PIPING .....	96
5.2.1	Kinematic Boundary Conditions.....	96
5.2.2	Loads.....	96
5.2.3	Selection of a Solution Technique .....	98
5.2.4	Material Representation, Residual Stresses, and Initial Geometry.....	100
5.3	SELECTION OF REPRESENTATIVE MODEL PARAMETERS .....	100
5.3.1	Simplification of the Parametric Study—Dimensional Analysis .....	101
5.3.2	Application of Dimensional Analysis to Sleeper-supported Pipe Problem	102
5.3.3	Representative Ranges of the $\pi$ -Parameters .....	104
5.4	PERFORMANCE ASSESSMENT OF THE <i>IN SITU</i> MODEL .....	106
5.4.1	Suitability of Non-dimensional Parameters.....	106
5.4.2	Examination of the Deformed Shape.....	108
5.4.3	Influence of the Second-order Soil Loads .....	109
5.4.4	Numerical Stability of the Model .....	109
<b>6</b>	<b>DEVELOPMENT OF SIMPLIFIED DESIGN EQUATIONS.....</b>	<b>121</b>
6.1	RESPONSE SURFACE METHODOLOGY .....	121
6.1.1	Mathematical Description of a Response Surface .....	122
6.1.2	Design of Experiments: An Overview.....	125
6.2	APPLICATION OF RESPONSE SURFACE METHODOLOGY TO THE SLEEPER-SUPPORTED PIPE PROBLEM: SCREENING STUDY.....	127
6.2.1	Combinations of $\pi$ -Parameters for the Screening Study.....	128
6.2.2	Results and Discussion of Screening Study.....	129
6.2.3	Establishing Consistency in the Data Set for Use in Regression Analyses	131
	6.2.3.1 <i>Special Consideration of Factor <math>w/\sigma_y</math> (<math>\pi_6</math>)</i> .....	131
	6.2.3.2 <i>Ensuring Uniformity of the Output Data</i> .....	132
6.3	EXPERIMENTAL DESIGN AND THE DEVELOPMENT OF PREDICTION EQUATIONS.....	133
6.3.1	Parametric Study of $p/p_y=0.5$ .....	133
	6.3.1.1 <i>Experimental Design, <math>p/p_y=0.5</math></i> .....	133
	6.3.1.2 <i>Results of Parametric Study and Prediction Equation Development, <math>p/p_y=0.5</math></i> .....	134
6.3.2	Parametric Study of $p/p_y=0.8$ .....	138
	6.3.2.1 <i>Screening Study and Experimental Design, <math>p/p_y=0.8</math></i> .....	138

6.3.2.2 <i>Results of Parametric Study and Prediction Equation Development, p/p<sub>y</sub>=0.8</i> .....	139
6.3.3 Parametric Study of p/p <sub>y</sub> =0 .....	140
6.3.3.1 <i>Screening Study and Experimental Design, p/p<sub>y</sub>=0</i> .....	140
6.4 DISCUSSION OF REGRESSION TECHNIQUES .....	143
<b>7 ASSESSMENT OF PREDICTION EQUATIONS AND THEIR APPLICATION TO DESIGN .....</b>	<b>170</b>
7.1 PREDICTION OF BEHAVIOUR OBSERVED IN FULL-SCALE LABORATORY TESTS .....	170
7.2 USE OF EQUATIONS AND APPLICATION OF LIMIT STATES DESIGN .....	174
7.3 COMPARISON OF PREDICTION EQUATIONS WITH EXISTING DESIGN EQUATION .....	177
<b>8 SUMMARY, CONCLUSIONS, AND RECOMMENDATIONS .....</b>	<b>189</b>
8.1 SUMMARY .....	189
8.2 CONCLUSIONS .....	190
8.3 RECOMMENDATIONS .....	193
<b>REFERENCES .....</b>	<b>195</b>
<b>APPENDIX A—PROPAGATION OF RANDOM EXPERIMENTAL ERRORS ..</b>	<b>199</b>
<b>APPENDIX B—RESULTS OF ANCILLARY TESTS .....</b>	<b>202</b>
<b>APPENDIX C—FINITE ELEMENT ANALYSIS RESULTS FOR PARAMETRIC STUDY OF p/p<sub>y</sub>=0 .....</b>	<b>210</b>

## LIST OF TABLES

Table 2.1	Nominal specimen parameters .....	33
Table 5.1	Parameters for investigation of potential scale effects .....	111
Table 5.2	Parameters for investigation of potential scale effects if E is considered to be a constant.....	111
Table 6.1	Set of variables for screening study of all parameters .....	147
Table B.1	Measured specimen parameters .....	203

## LIST OF FIGURES

Figure 1.1	Typical sleeper-supported pipe installation .....	20
Figure 1.2	Sleeper-supported pipe geometry.....	21
Figure 1.3	Typical distorted cross-sectional shapes .....	21
Figure 2.1	Typical fabrication of spiral weld pipe .....	34
Figure 2.2	Typical fabrication of pipe by the U and O method .....	34
Figure 2.3	Schematic of test set-up .....	35
Figure 2.4	Typical test set-up .....	35
Figure 2.5	Typical strain gauge layout (762 mm specimen).....	36
Figure 2.6	Typical strain gauge layout (406 mm specimen).....	37
Figure 2.7	Ring specimen mounted in testing machine .....	38
Figure 2.8	Rubber gasket installed .....	38
Figure 2.9	Cable transducer mounted for strain measurement.....	39
Figure 2.10	Lid bolted into position and guards installed.....	39
Figure 3.1	Overall finite element mesh.....	52
Figure 3.2	Kinematic boundary conditions .....	52
Figure 3.3	Refined Mesh layout .....	53
Figure 3.4	Coarse Mesh layout.....	53
Figure 3.5	Optimal Mesh layout.....	54
Figure 3.6	Correlation of strength behaviour .....	54
Figure 3.7	Correlation of distortional behaviour.....	55
Figure 4.1	Typical deformation of sleeper-to-pipe contact region, unpressurized specimen .....	69
Figure 4.2	Typical deformation of pressurized pipe showing bulge at edge of sleeper .....	70
Figure 4.3	Load vs. sleeper displacement, Specimen S1 .....	71
Figure 4.4	Load vs. sleeper displacement, Specimen S2 .....	71
Figure 4.5	Load vs. sleeper displacement, Specimen S3 .....	72
Figure 4.6	Load vs. sleeper displacement, Specimen S4 .....	72
Figure 4.7	Load vs. sleeper displacement, Specimen S5 .....	73
Figure 4.8	Load vs. sleeper displacement, Specimen S6 .....	73
Figure 4.9	Load vs. sleeper displacement, Specimen S7 .....	74
Figure 4.10	Load vs. sleeper displacement, Specimen S8 .....	74

Figure 4.11	Load vs. sleeper displacement, Specimen S9 .....	75
Figure 4.12	Load vs. sleeper displacement, Specimen S10 .....	75
Figure 4.13	Load vs. sleeper displacement, Specimen S11 .....	76
Figure 4.14	Idealized load vs. sleeper displacement relationship, unpressurized specimens.....	76
Figure 4.15	Decreased stiffness evident as the pipe wall reverses in curvature along the centreline of contact, Specimen S5 .....	77
Figure 4.16	Mid-span out-of-roundness vs. sleeper displacement, Specimen S1 .....	78
Figure 4.17	Mid-span out-of-roundness vs. sleeper displacement, Specimen S2 .....	78
Figure 4.18	Mid-span out-of-roundness vs. sleeper displacement, Specimen S3 .....	79
Figure 4.19	Mid-span out-of-roundness vs. sleeper displacement, Specimen S4 .....	79
Figure 4.20	Mid-span out-of-roundness vs. sleeper displacement, Specimen S5 .....	80
Figure 4.21	Mid-span out-of-roundness vs. sleeper displacement, Specimen S6 .....	80
Figure 4.22	Mid-span out-of-roundness vs. sleeper displacement, Specimen S7 .....	81
Figure 4.23	Mid-span out-of-roundness vs. sleeper displacement, Specimen S8 .....	81
Figure 4.24	Mid-span out-of-roundness vs. sleeper displacement, Specimen S9 .....	82
Figure 4.25	Mid-span out-of-roundness vs. sleeper displacement, Specimen S10 .....	82
Figure 4.26	Mid-span out-of-roundness vs. sleeper displacement, Specimen S11 .....	83
Figure 4.27	Typical progression of deformation, unpressurized specimen (S1).....	84
Figure 4.28	Typical progression of deformation, pressurized specimen (S3).....	85
Figure 4.29	Deformed configuration from finite element model, Specimen S1 (unpressurized).....	86
Figure 4.30	Deformed configuration from finite element model, Specimen S3 (pressurized).....	86
Figure 5.1	Idealization of <i>in situ</i> sleeper-supported piping.....	112
Figure 5.2	Finite element mesh for <i>in situ</i> model.....	113
Figure 5.3	Kinematic boundary conditions for <i>in situ</i> model.....	113
Figure 5.4	Uniform soil pressure distributed as work-equivalent nodal forces .....	114
Figure 5.5	Second-order loads resulting from distortion .....	114
Figure 5.6	Second-order effect for an individual element.....	115
Figure 5.7	Standard Newton solution approach .....	116
Figure 5.8	Sleeper spacing for typical parameters based upon design equation by Kormann and Zhou (1995).....	117

Figure 5.9	Effect of varying model scale while maintaining $\pi$ -parameters as constants.....	118
Figure 5.10	Effect of varying model scale while maintaining $E=207\,000$ MPa .....	118
Figure 5.11	Progression of deformation, 80-0.5-1.0-7-2.33 .....	119
Figure 5.12	Influence of second-order soil loads .....	120
Figure 6.1	Flow chart of the development of knowledge used as part of response surface methodology proposed by Khuri and Cornell (1996) .....	148
Figure 6.2	Effect of variation of $D/t$ ( $\pi_1$ ).....	149
Figure 6.3	Effect of variation of $p/p_y$ ( $\pi_2$ ) .....	149
Figure 6.4	Effect of variation of $2b/D$ ( $\pi_3$ ).....	150
Figure 6.5	Effect of variation of $L/D$ ( $\pi_4$ ) .....	150
Figure 6.6	Effect of variation of $\epsilon_y$ ( $\pi_5$ ).....	151
Figure 6.7	Variation of response with soil load .....	151
Figure 6.8	$w/\sigma_y$ redefined as the response variable, $\sigma$ as a factor .....	152
Figure 6.9	Data redefined at 2.5% increments of $\sigma$ to provide uniformity in the data set .....	152
Figure 6.10	Overall layout of parametric finite element analysis study.....	153
Figure 6.11	Results from finite element analyses for parametric study at $p/p_y=0.5$ ...	154
Figure 6.12	Comparison of predicted response by equation [6-11] with finite element data for $p/p_y=0.5$ .....	155
Figure 6.13	Predicted response by equation [6-11] versus finite element response for $p/p_y=0.5$ .....	156
Figure 6.14	Comparison of predicted response by equation [6-13] with finite element data for $p/p_y=0.5$ .....	157
Figure 6.15	Predicted response by equation [6-13] versus finite element response for $p/p_y=0.5$ .....	158
Figure 6.16	Effect of variation of $D/t$ ( $\pi_1$ ) when $p/p_y=0.8$ .....	159
Figure 6.17	Effect of variation of $2b/D$ ( $\pi_3$ ) when $p/p_y=0.8$ .....	159
Figure 6.18	Effect of variation of $L/D$ ( $\pi_4$ ) when $p/p_y=0.8$ .....	160
Figure 6.19	Effect of variation of $\epsilon_y$ ( $\pi_5$ ) when $p/p_y=0.8$ .....	160
Figure 6.20	Variation of response with soil load when $p/p_y=0.8$ .....	161
Figure 6.21	Results from finite element analysis for parametric study at $p/p_y=0.8$ ....	162
Figure 6.22	Comparison of predicted response by equation [6-14] with finite element data for $p/p_y=0.8$ .....	163

Figure 6.23	Predicted response by equation [6-14] versus finite element response for $p/p_y=0.8$ .....	164
Figure 6.24	Effect of variation of $D/t$ ( $\pi_1$ ) when $p/p_y=0$ .....	165
Figure 6.25	Effect of variation of $2b/D$ ( $\pi_3$ ) when $p/p_y=0$ .....	165
Figure 6.26	Effect of variation of $L/D$ ( $\pi_4$ ) when $p/p_y=0$ .....	166
Figure 6.27	Effect of variation of $\varepsilon_y$ ( $\pi_5$ ) when $p/p_y=0$ .....	166
Figure 6.28	Variation of response with soil load when $p/p_y=0$ .....	167
Figure 6.29	Predicted response by equation [6-16] versus finite element response for $p/p_y=0$ .....	167
Figure 6.30	Residual errors versus cumulative probability for $p/p_y=0, 0.5,$ and $0.8$ ...	168
Figure 6.31	Residual errors versus predicted response for $p/p_y=0, 0.5,$ and $0.8$ .....	169
Figure 7.1	Free-body, shear force, and bending moment diagrams of laboratory tests and the <i>in situ</i> idealization .....	182
Figure 7.2	Comparison of laboratory test, finite element solution, and regression prediction equation for Specimen S1 .....	183
Figure 7.3	Comparison of laboratory test, finite element solution, and regression prediction equation for Specimen S2 .....	183
Figure 7.4	Comparison of laboratory test, finite element solution, and regression prediction equation for Specimen S3 .....	184
Figure 7.5	Comparison of laboratory test, finite element solution, and regression prediction equation for Specimen S4 .....	184
Figure 7.6	Comparison of laboratory test, finite element solution, and regression prediction equation for Specimen S5 .....	185
Figure 7.7	Comparison of laboratory test, finite element solution, and regression prediction equation for Specimen S6 .....	185
Figure 7.8	Comparison of laboratory test, finite element solution, and regression prediction equation for Specimen S7 .....	186
Figure 7.9	Comparison of laboratory test, finite element solution, and regression prediction equation for Specimen S8 .....	186
Figure 7.10	Comparison of laboratory test, finite element solution, and regression prediction equation for Specimen S9 .....	187
Figure 7.11	Comparison of laboratory test, finite element solution, and regression prediction equation for Specimen S10 .....	187
Figure 7.12	Comparison of laboratory test, finite element solution, and regression prediction equation for Specimen S11 .....	188
Figure B.1	Ancillary test results, Specimen S1 .....	204
Figure B.2	Ancillary test results, Specimen S2 .....	204

Figure B.3	Ancillary test results, Specimen S3 .....	205
Figure B.4	Ancillary test results, Specimen S4 .....	205
Figure B.5	Ancillary test results, Specimen S5 .....	206
Figure B.6	Ancillary test results, Specimen S6 .....	206
Figure B.7	Ancillary test results, Specimen S7 .....	207
Figure B.8	Ancillary test results, Specimen S8 .....	207
Figure B.9	Ancillary test results, Specimen S9 .....	208
Figure B.10	Ancillary test results, Specimen S10 .....	208
Figure B.11	Ancillary test results, Specimen S11 .....	209
Figure C.1	Results from finite element analysis for parametric study of $p/p_y=0$ when $D/t=40$ .....	211
Figure C.2	Results from finite element analysis for parametric study of $p/p_y=0$ when $D/t=60$ .....	211
Figure C.3	Results from finite element analysis for parametric study of $p/p_y=0$ when $D/t=80$ .....	212
Figure C.4	Results from finite element analysis for parametric study of $p/p_y=0$ when $D/t=100$ .....	212
Figure C.5	Results from finite element analysis for parametric study of $p/p_y=0$ when $D/t=120$ .....	213

## LIST OF SYMBOLS

### *Latin Symbols*

A	accidental load effects
A	axial force on idealized pipe segment
$A_p$	projected area of element on a horizontal plane
b	one-half length of sleeper in longitudinal direction of pipe
$b_0, b_1, b_2 \dots$	coefficients of the predicted response function
B	$\left[12(1 - \nu^2)\right]^{\frac{1}{8}} = 1.348$ for steel
$c_o$	critical distance for activation of viscous contact forces
D	outside diameter of pipe; nominal outside diameter of pipe
$D_{\max}$	maximum diameter of deformed pipe
$D_{\min}$	minimum diameter of deformed pipe
e	experimental error
E	environmental load effects; modulus of elasticity
F	pipeline design factor
G	permanent gravity load effects
H	depth of cover
J	pipeline design joint factor
$k$	number of experimental factors
$\ell$	span length of pipe between reactions in experimental tests
L	sleeper support spacing; length dimension; pipeline design location factor
M	mass dimension
M	bending moment acting on idealized pipe segment
n	number of observed values of the response variable
$n$	number of variables included in a dimensional matrix
$o$	out-of-roundness
$p$	number of regression coefficients in a complete polynomial
p	actual level of pipeline internal pressure
$p_y$	pressure at which $\sigma_h$ equals $\sigma_y$
P	total force on sleeper-to-pipe contact area; pipeline design pressure

$P_i$	cumulative probability
$q$	distributed load transferred between sleeper and pipe
$Q$	operational load effects
$r$	pipe outside radius
$r_i$	residual error $i$
$r$	rank of the dimensional matrix
$R$	nominal resistance (load limit, strain limit, deflection limit, etc.)
$R^2$	coefficient of multiple determination
$S$	specified minimum yield strength (SMYS)
$t$	pipe wall thickness
$t$	finite element incrementation time
$T$	time dimension; pipeline design temperature derating factor
$u_1, u_2, u_3$	global displacement co-ordinates
$w$	uniform downward soil pressure
$X_1, X_2, \dots, X_k$	experimental factors
$Y_i$	$i$ th observed value of the response
$\hat{Y}$	predicted value of the response
$\hat{Y}_i$	$i$ th predicted value of the response
$\bar{Y}$	mean observed value of the response

*Greek Symbols*

$\alpha$	soil bedding constant
$\alpha_G$	gravity load factor
$\alpha_Q, \alpha_E, \alpha_A$	live load factors
$\beta_0, \beta_1, \beta_2 \dots$	coefficients of the true response function
$\gamma$	importance (class) factor
$\gamma_{fill}$	backfill weight density
$\gamma_{steel}$	steel weight density
$\Delta A_p$	change in projected area of element on a horizontal plane
$\Delta \theta^{crit}$	critical ovalization deformation limit
$\Delta \theta$	ovalization deformation

$\varepsilon_\ell$	engineering strain in longitudinal direction of pipe
$\varepsilon_{\text{nom}}$	nominal strain (engineering strain)
$\varepsilon_{\text{in}}^{\text{pl}}$	plastic component of the logarithmic strain
$\varepsilon_y$	strain at which yielding begins
$\eta$	true value of the response
$\mu$	coefficient of viscous damping
$\mu_0$	maximum value of damping coefficient
$\mu\varepsilon$	microstrain ( $1 \mu\varepsilon = 1 \times 10^{-6}$ )
$\nu$	Poisson's ratio
$\pi$	3.14159...
$\pi_1$	$D/t$
$\pi_2$	$p/p_y$
$\pi_3$	$2b/D$
$\pi_4$	$L/D$
$\pi_5$	$\varepsilon_y$
$\pi_6$	$w/\sigma_y$
$\pi_7$	$o$
$\sigma_2$	circumferential membrane stress
$\sigma'_2$	circumferential bending stress on outside of pipe
$\sigma_h$	engineering stress in hoop direction of pipe
$\sigma_\ell$	engineering stress in longitudinal direction of pipe
$\sigma_{\text{nom}}$	engineering stress (force per initial unit area)
$\sigma_{\text{true}}$	true stress (force per actual unit area)
$\sigma_y$	static yield strength
$\phi$	resistance (performance) factor
$\phi_1, \phi_2, \phi_3$	nodal rotations
$\phi$	true response function
$\psi$	load combination factor $\leq 1.0$

# **1 INTRODUCTION AND LITERATURE REVIEW**

The petroleum products industry in North America and internationally has begun to rely more heavily on pipelines for the efficient and safe transportation of petroleum, natural gas, and other liquid and gaseous hydrocarbon products. In Canada, more than 540 000 km of pipelines are in service, of which over 100 000 km are large-diameter long-distance transmission lines (Petroleum Communication Foundation, 1995). Increased reliance on pipelines is governed chiefly by economics—it is the cheapest way to get the product to the market—and improvements in technology continue to make pipelines even more efficient. With the increased capital expenditure on new lines and maintenance of existing lines, the economies that may be realized by using optimal design methods have become more important. At the same time, this increased use of pipelines has also brought issues of safety to the forefront, since pipelines are often built near populated or environmentally sensitive areas. The need for economy and safety continually presents new challenges to the industry, especially as resources are exploited in areas that have severe environments, such as in the Arctic. All of these factors combine to make the pursuit of rational design procedures and improved understanding of pipeline behaviour of ever-increasing importance.

In the design or evaluation of a pipeline the engineer must account for all potentially harmful forces—corrosion, thermal variation, settlement, gravity loads, vibration, earthquakes, and others—to ensure that it is likely to perform in a satisfactory manner. Because of the diverse range of conditions that must be considered, pipeline behaviour is an ongoing area of research in many fields. In this report, the focus is specifically on the interaction between line pipe and concrete ‘sleeper’ supports. Sleepers are used most often in the yards of compressor stations for natural gas pipelines, but are also used on mainline piping where heavy valves or tee connections must be supported.

## **1.1 THE SLEEPER-SUPPORT CONCEPT**

All pipelines require compressor stations at intervals along their lengths for pumping and routing of the contents. Most of the complex network of piping in a compressor station yard is buried in order to keep the surface free from encumbrances.

These buried pipes must withstand forces that arise from surface loads or differential soil settlements. Traditional methods of protecting the pipe necessitate extensive preparation of bedding materials in the trench, resulting in costly installations. Flat reinforced concrete footings, known as ‘sleepers,’ are sometimes used in the pipeline industry to support buried pipes directly so as to ensure satisfactory performance while realizing cost savings. The sleepers also serve to aid in the accurate alignment of piping during installation and to reduce the influence that inclement weather might have on the construction process by elevating the pipe above the bottom of the trench (Kormann and Zhou, 1995). A typical sleeper-supported pipe installation under construction is shown in Figure 1.1. To the author’s knowledge, NOVA Gas Transmission Ltd. (a subsidiary of TransCanada PipeLines Limited) is the only major pipeline operator that regularly uses sleepers for the support of buried pipes. Other pipeline operators may choose to implement the use of sleepers as more information on their design becomes available.

### **1.1.1 Statement of the Problem**

The contact condition between the sleeper and the pipe can impose high levels of stress in the pipe wall and can potentially cause significant deformation of the cross-section. Although these local effects are of concern to the designer, there is currently no rational method by which to approach this problem. Present methods for design are based upon elastic solutions for a load distributed along the initial line of contact between the sleeper and the undeformed pipe, which is an unrealistic over-simplification of the behaviour. The available design equation used by industry, which is based on this model, has proved to be safe and adequate, but it is believed to result in supports that are too closely spaced (Kormann and Zhou, 1995). This leads to unnecessary installation costs. An additional limitation of the current design method is that it uses stress as the only design criterion; no consideration is given to the deformation of the cross-section, which may place additional constraints on the support spacing.

### **1.1.2 Scope and Objectives**

In order to investigate the interaction between sleeper supports and line pipe, a series of 11 full-size line pipe specimens were tested at the University of Alberta. The

tests were designed in such a way as to simulate field installations of sleeper-supported piping as closely as practicable. The parameters that are of primary interest in the tests are the pipe diameter and wall thickness, the internal pressure, and the size of the sleeper support. Of course, items such as the spacing between the supports and soil-pipeline interaction are also issues for consideration in the design process, but it is necessary to understand first the local behaviour between the pipe and a single support. Consequently, the initial stages of this research aim to investigate the interaction between a pipe and a single sleeper in terms of both strength and local deformation criteria.

The experimental work is complemented by a series of finite element analyses that provide a numerical simulation of the behaviour of the laboratory specimens. The geometry and boundary conditions of the finite element models match those present in the laboratory tests, and each pipe specimen is modelled using 4-node doubly curved shell elements. Large deformations and non-linear material behaviour are accounted for in the analyses. The goal of the numerical study is to develop a general modelling technique that can be used with confidence to model other configurations and sizes of sleeper-supported line pipe.

Upon the development of a reliable numerical modelling procedure for the laboratory specimens, the boundary and loading conditions are modified to reflect idealized *in situ* conditions. This *in situ* finite element model is then used in a parametric study to establish a base of information on the influences of pipe diameter, wall thickness, yield strength and yield strain. Sleeper dimensions and level of internal pressure are also considered in the parametric study. This finite element work should preclude the need to perform additional costly full-scale laboratory or *in situ* tests. The database of information is then used in the development of simplified empirical design equations for sleeper-supported pipes, relieving the designer of the need to perform detailed finite element analyses for routine design scenarios.

In summary, the primary objectives of this study are to:

1. review design philosophies in the context of the sleeper-supported pipe problem;
2. identify and describe the limitations of existing design techniques;
3. characterize limits on the acceptable performance of sleeper-supported pipelines;

4. determine the behavioural characteristics of sleeper-supported line pipe based on laboratory tests;
5. develop a set of finite element modelling techniques that accurately predicts the load-carrying capacity and deformational behaviour of the laboratory specimens;
6. propose a idealization that approximates the conditions of *in situ* sleeper-supported pipes;
7. construct a finite element model of the idealization using the techniques developed in step No. 5;
8. perform a parametric study using the finite element model of *in situ* conditions to examine the influences of the variables that control sleeper-supported pipeline behaviour;
9. develop simplified empirical equations to predict the behaviour of sleeper-supported pipes by making use of the results from the parametric study;
10. propose limits of acceptable performance to be used in conjunction with the empirical equations so as to form a new design approach for sleeper-supported line pipes.

The author believes that this work will help lead to a new generation of sleeper-supported piping systems that are more economical yet still maintain appropriate margins of safety.

## **1.2 LITERATURE REVIEW**

This section contains information on design philosophies, current design techniques, and previous studies related to the sleeper support problem. Relevant portions of standards that govern the design of high-pressure pipelines are also discussed.

### **1.2.1 Design Philosophies**

In the design of civil engineering structures, two basic philosophies exist: *working stress design (WSD)* and *limit states design (LSD)*. Until recently, almost all design standards incorporated working stress design principles. Limit states design methods, which are developed upon a statistical and rational basis, began to be introduced during the 1970's (see, for example, Kennedy, 1974). The first North American design code to implement these new procedures was the Canadian structural steel design code, CSA

S16.1-1974 *Steel Structures for Buildings—Limit States Design* (Canadian Standards Association, 1974).

#### **1.2.1.1 Working Stress Design**

Working stress design usually applies a *factor of safety* on the yield strength or ultimate strength of a material in order to control undesirable behaviour. Most current pipeline design codes make use of the working stress design method, as is done in the governing Canadian design standard CSA Z662-96 *Oil and Gas Pipeline Systems* (Canadian Standards Association, 1996). The application of this method is simple and convenient, but upon closer investigation severe limitations are apparent, as described below.

It is obvious that the level of safety inherent in any design must be a function of the statistical variability of both the applied loads *and* the strength and stiffness of the structural members. In this context, the level of safety must be construed as the probability of failure of the structure during a specified period of time. Since it is impossible to design a structure so as to guarantee that failure is prevented, the probability of failure must be set at an acceptably small level. Despite this reality, the WSD philosophy takes no specific account of the effect of the loading and resistance probability distributions on the level of safety. Instead, a ‘global’ factor of safety is most often used for the entire structure with no regard to the underlying variability associated with each component. As a consequence, the probability of failure achieved in the design is not well controlled and the structure may not provide a suitable level of economy.

Other limitations of WSD are apparent. For example, there is usually no consideration given to the behaviour of individual components (e.g., whether the failure mode will be ductile or brittle), or to the behaviour of the system (e.g., whether failure of one component causes total collapse, contained collapse, or local failure only). Because WSD does not necessarily involve the explicit identification of failure conditions, the level of safety achieved in a design will vary depending upon the failure mode. Consequently, the designer is left ignorant of the approximate probability of failure of the structure.

As in any design situation, the criteria used to ensure adequate strength, which are usually based on stresses, must be supplemented by criteria to limit deformations if those deformations might interfere with the serviceability of the structure. However, this is not always done in WSD, primarily because there is not necessarily explicit identification of the failure mode.

### ***1.2.1.2 Limit States Design***

The approach taken in limit states design (also known as ‘load and resistance factor design’ in the United States) is fundamentally different from that of working stress design. The first stage of this design process involves the identification of all of the ‘limit states’ at which the structure no longer fulfils its intended function. Once identified, the objective in the design process is to control the probability of failure associated with each limit state to an acceptably small level. The current Canadian structural steel design code CAN/CSA-S16.1-94, entitled *Limit States Design of Steel Structures*, includes the following definition (Canadian Standards Association, 1994):

Limit States—those conditions of a structure in which the structure ceases to fulfil the function for which it was designed. Those states concerning safety are called the ultimate limit states and include exceeding of load-carrying capacity, overturning, sliding, fracture, and fatigue. Those states that restrict the intended use and occupancy of the structure are called serviceability limit states and include deflection, vibration, and permanent deformation.

Of course, this definition is tailored to the use of steel in buildings and other structures, but a parallel definition may be made for any type of material used in any type of structure, be it concrete in a bridge, wood in a house, or steel in a pipeline.

Adoption of limit states design methods is beginning in the pipeline industry. Internationally, for example, the well-established standard *Rules for Submarine Pipeline Systems* (Det Norske Veritas, 1996) has been converted from WSD to LSD principles to obtain a more adaptable design approach and more consistent level of safety (Collberg and Mørk, 1999). In Canada, newly introduced to the 1996 edition of CSA Z662 *Oil and Gas Pipeline Systems* is Appendix C, “Limit States Design,” which is a non-mandatory

part of the Standard. (Because the CSA Z662 Limit States Design standard would govern the design of pipelines in Canada, only its requirements are described in detail herein. The approach taken in international LSD standards for pipelines is similar to that of the Canadian standard.) In the context of pipelines, ultimate limit states are defined in Appendix C of CSA Z662 as “those concerning burst or collapse” of the pipeline and consist of rupture, yielding caused by primary loads, buckling resulting in collapse or rupture, and fatigue. Serviceability limit states are defined as “those that restrict normal operations or affect durability.” These limit states include yielding caused by secondary loads and buckling not resulting in collapse. Examples of serviceability limit states include displacements or deformations that adversely affect the operation of the pipeline; local damage such as local yielding, stable wrinkle growth, dents, corrosion, or non-through-thickness cracking that adversely affects the use or durability of the pipeline; and motion, including vibration, that adversely affects the operation or durability of the pipeline.

It is important to appreciate the difference between primary and secondary loads. Primary loads are defined as those that are independent of deformations and induce internal forces that are necessary to satisfy the laws of static equilibrium. In this case, yielding of the material does not diminish the level of internal forces. Examples include internal pressure, self-weight, buoyancy, weight of soil overburden, and the like. Secondary loads are those that are induced by structural deformations or the restraint of deformations. Because boundary conditions for this case are kinematic, yielding of the material diminishes any internal forces that arise. This is usually the case, for example, for those loads in a pipe that arise from lateral ground movements. Consequently, secondary loads do not have to be taken into account where they do not affect the capacity of the member to resist primary loads.

Once the limit states are identified for a particular problem, the engineer is to consider each one in the design process and ensure that a sufficiently low probability of failure is maintained. This is done by taking into consideration the statistical variation of both the loads and the properties of the structure as related to each potential failure mode such that the following relation is satisfied:

$$\text{factored resistance} \geq \text{effect of factored loads.} \quad [1-1]$$

Mathematically, this can be represented as follows (Zimmerman et al., 1992):

$$\phi R \geq \gamma[\alpha_G G + \psi(\alpha_Q Q + \alpha_E E + \alpha_A A)] \quad [1-2]$$

where,

$\phi$	=	resistance factor [or performance factor]
R	=	[nominal] resistance (load limit, strain limit, deflection limit, etc.)
$\gamma$	=	importance [class] factor
$\alpha_G$	=	gravity load factor
$\alpha_Q, \alpha_E, \alpha_A$	=	live load factors
$\psi$	=	load combination factor $\leq 1.0$
G	=	permanent gravity load effects
Q	=	operational load effects
E	=	environmental load effects
A	=	accidental load effects.

In general, the nominal loads are multiplied by load factors that are greater than unity. This is done in order to account for the fact that the actual load might be greater than the nominal value. Similarly, the nominal resistance is multiplied by a performance factor less than unity, thereby accounting for the possibility that the actual strength of the component might be less than the nominal value. In order to maintain a reasonably consistent and acceptable level of safety, these factors must be calibrated for each specific load and resistance case. Usually, the target level of safety is similar to that inherent in other applicable WSD standards, but optimization of the calibration is also performed. (Obtaining load and resistance factors that give a reasonably uniform and appropriate probability of failure are ongoing areas of study. For example, see Price and Anderson, 1991.) The load combination factor is intended to reduce the effect of the live loads somewhat to account for the relatively low probability that live loads from different sources might reach their peak values concurrently. This load combination factor is not yet included in Appendix C of CSA Z662; omitting this factor tends towards a safer but less economical design. The importance factor (called the class factor in Z662-96),  $\gamma$ , is intended to take into account the consequences of failure. For example, failure resulting in leakage of a 'sour' gas pipeline (i.e., one that carries toxic hydrogen sulphide gas) is more hazardous to the public and the environment than leakage of a non-sour line.

Consequently, the importance factor is greater for the former case. Further calibration of this part of the CSA Z662-96 standard is ongoing (Canadian Standards Association, 1996).

Although the limit states design appendix is not a mandatory part of CSA Z662 at this time, it is the opinion of the author that it represents a significant step towards the development of a rational design methodology that will serve to provide an appropriate level of safety and serviceability. The recent Workshop on Pipeline Safety Needs sponsored by the American Society of Civil Engineers has also emphasized the benefits of implementing the limit states design concept into the pipeline design field (Sterling, 1996).

In summary, the limit states design concept is more rational and can provide a more uniform level of safety than working stress design. Because it is apparent that limit states design offers significant advancements in the design of pipelines and other structures, it is within this scope that the investigation into the behaviour of sleeper-supported pipe is being considered.

### 1.2.2 Current Design Method for Sleeper-supported Piping

The current design method used for gas pipelines supported by concrete sleepers is based upon experience and the working stress design concept. The existing design equation has the following form (Zhou and Kormann, 1995):

$$L = 20000 D \frac{S}{H} \left( \frac{D}{t} \right)^{-1.75} \quad [1-3]$$

where,

L	=	sleeper spacing in mm
D	=	outside pipe diameter in mm
H	=	depth of cover in mm
t	=	pipe wall thickness in mm
S	=	specified minimum yield strength (SMYS) in MPa.

Kormann and Zhou (1995) developed this equation based upon an elastic solution for a cylindrical shell (the pipe) subjected to a line load over a very short length (the sleeper) in the longitudinal direction. The underlying assumptions are that the pipe is

pressurized to give a hoop stress of 50% of the SMYS in the pipe wall, the sleeper has a length equal to 1.5 times the outside diameter of the pipe, and the backfill has a density of 15 kN/m<sup>3</sup>. The self-weight of the pipe is considered in the gravity force calculation, but the weight of the contents is neglected. Furthermore, it is assumed that the sleepers carry all of the gravity forces acting on the pipe and that no load is carried by the soil in direct contact with the underside of the pipe.

The stresses under examination are the membrane and bending components of stress in the hoop direction at the centreline of contact between the sleeper and the pipe. It is noteworthy that the derivation performed by Kormann and Zhou (1995) is based upon stress equations given by Roark and Young (1975). In the most recent edition of this text (Young, 1989), one of these stress equations has been corrected. A new derivation of the design equation proposed by Kormann and Zhou (1995) follows, using the same underlying assumptions but the updated stress equation.

From Young (1989):

$$\begin{aligned}\sigma_2 &= -0.13B Pr^{\frac{3}{4}} b^{-\frac{3}{2}} t^{-\frac{5}{4}} \\ \sigma'_2 &= -1.56B^{-1} Pr^{\frac{1}{4}} b^{-\frac{1}{2}} t^{-\frac{7}{4}}\end{aligned}\tag{1-4}$$

where,

- $\sigma_2$  = circumferential membrane stress
- $\sigma'_2$  = circumferential bending stress on outside of pipe
- $r$  = pipe outside radius
- $t$  = pipe wall thickness
- $P$  = force on contact area
- $2b$  = loaded length (along longitudinal axis of pipe)
- $B$  =  $\left[12(1 - \nu^2)\right]^{\frac{1}{8}} = 1.348$  for steel
- $\nu$  = Poisson's ratio = 0.3 for steel.

Using the weight of backfill and steel acting on the tributary length for one sleeper:

$$\begin{aligned}P &= \gamma_{\text{fill}} DLH + \gamma_{\text{steel}} \pi DtL \\ &= 15DLH \times 10^{-6} + 242DtL \times 10^{-6} \\ &\approx 15DL(H + 16t) \times 10^{-6}\end{aligned}\tag{1-5}$$

where,

- $P$  = force on contact area in N

H	=	depth of cover in mm
D	=	pipe outside diameter in mm
L	=	sleeper spacing (o/c) in mm
$\gamma_{fill}$	=	15 kN/m <sup>3</sup>
$\gamma_{steel}$	=	77 kN/m <sup>3</sup> .

Combining [1-4] with [1-5] gives:

$$\begin{aligned}\sigma_2 &= -2.41 \times 10^{-6} L(H + 16t)D^{\frac{1}{4}}t^{\frac{-5}{4}} \\ \sigma'_2 &= -16.85 \times 10^{-6} L(H + 16t)D^{\frac{3}{4}}t^{\frac{-7}{4}}\end{aligned}\quad [1-6]$$

It is assumed next that the internal pressure contributes a hoop stress equal to 50% of the SMYS (based on the maximum allowable stress in the pipe wall using a location factor of 0.625 for compressor stations and a design factor of 0.8 for steel pipe as given in CSA Z662-96). Therefore, the maximum total tensile stress on the inside surface of the pipe wall is given by:

$$\begin{aligned}\sigma_{circ} &= 0.5S + \sigma_2 - \sigma'_2 \\ \sigma_{circ} &= 0.5S + 16.85 \times 10^{-6} L(H + 16t)D^{\frac{3}{4}}t^{\frac{-7}{4}} (1 - 0.143t^{\frac{1}{2}}D^{\frac{-1}{2}}) \\ \text{and, after neglecting small terms} \\ \sigma_{circ} &\approx 0.5S + 16.85 \times 10^{-6} LHD^{\frac{3}{4}}t^{\frac{-7}{4}}\end{aligned}\quad [1-7]$$

For the case of combined membrane and bending stress, the ASME Boiler and Pressure Vessel Code, Section VIII, Division 2 (1992), limits the allowable stress to 1.5 times the general membrane stress, which in this case is 0.5S. Therefore:

$$\sigma_{allow} = 1.5 \times 0.5 \times S = 0.75 \times S \quad [1-8]$$

Setting  $\sigma_{circ} = \sigma_{allow}$  and solving for L gives:

$$L = 14840 D \frac{S}{H} \left( \frac{D}{t} \right)^{-1.75} \quad [1-9]$$

Comparing [1-9] to the current design equation [1-3], it is apparent that the corrected version is about 35% more conservative than the current equation.

Although the current design method given by equation [1-3] has provided safe and adequate designs in recent years, it is regarded as being unsatisfactory for several reasons (Zhou and Kormann, 1995). First, the hoop stress caused by internal pressure and the

circumferential bending stress caused by local effects from sleeper–pipe interaction are assumed to be directly additive because elastic design methods are used. Local stresses will, in reality, be limited by the yield strength of the material. Second, the potentially beneficial effects of internal pressure on the circumferential bending stresses caused by local effects are neglected. Third, the contact condition of the sleeper–pipe interaction is assumed to be a uniform line load for the current design equation, whereas it is known that for the true interaction the contact condition changes as displacements increase. Fourth, Zhou and Kormann (1995) argue, based upon engineering judgement, that the existing design equation requires the spacing between sleepers to be too short. Finally, the current equation is based on working stress design; limit states design principles applied to this problem would probably result in more rational solutions.

In effect, the intent of the current design method is to prevent local yielding in the pipe wall, even though a confined amount of yielding will likely have no effect on the ability of the pipe to perform its function. In addition, the current design equation does not take into account the length of the sleeper as measured in the longitudinal direction of the pipe; it is assumed that the length of the sleeper is  $1.5D$  (length  $2b$  in Figure 1.2). For a particular design scenario the sleeper length will not necessarily have this length, since space limitations in the compressor station yard may be severe. Consequently, the designer may desire to use sleepers shorter than  $1.5D$ . However, minimum limits on the physical size of the sleeper must be maintained in order to ensure an adequate soil bearing area unless other means of support, such as piles, are used.

Clearly, the prospect of achieving a more rational and efficient design method is economically desirable and should be possible if these limitations can be removed. Ideally, a new design method will be founded on the basis of limit states design. Given that the current design equation [1-3] appears to be excessively conservative, the modified design equation [1-9] based upon the revised stress equations [1-4] is also not satisfactory because it is even more conservative.

### **1.2.3 Limit States for Sleeper-supported Piping**

It is clear that the current design method for sleeper supported piping, given in equation [1-3], is based on the working stress design approach, that is, an attempt is made

merely to limit the stresses in the pipe wall to levels below the yield strength of the material. Consideration is not given to the consequences, if any, that may result if the stresses in the wall reach the yield value. In order to approach this design problem, one must pose the question: If the yield stress is reached as a result of sleeper-to-pipe contact forces, will any of the limit states be attained? It is not difficult to imagine that the pipe could be allowed to deform plastically to some degree without causing the pipeline to reach those limit states set out in Section 1.2.1.2.

One of the goals of the research reported herein is necessarily the identification of the limiting states that govern the behaviour of sleeper-supported piping. Only after these states are defined can a rational means be developed by which these systems can be designed. For sleeper-supported piping, ultimate limit states include the collapse of the cross-section of the pipe resulting from external soil pressure or local buckling collapse initiated by bending of the pipe at the edge of the sleeper. The serviceability limit state is likely to be governed by the magnitude of the cross-sectional distortion, which may influence a number of aspects of its functionality. For example, distortion of the cross-section may influence flow through the pipe, or excessive strains may result in debonding of coatings and produce susceptibility to corrosion. Another critical serviceability limit state is controlled by the ability of a pipeline to allow the passage of so-called *pigging devices*, which are described below.

Several studies indicate that pigging operations are essential in order to ensure satisfactory performance and long-term life of a pipeline (see, for example, Brooks and Smith, 1995; Tiratsoo, 1987). Pigging devices serve to provide pipeline operators with a means to inspect or repair the inside of lines while they are in service. Various types of 'pigs' are available and their primary functions are to act as an interface to separate different fluids; inspect and monitor the location and growth of cracks or corrosion; remove debris or make repairs; or survey the location and depth of the line. Consequently, the success of pigging operations must be considered as a limit state in the design process in terms of a limit on cross-sectional distortion. If a pig becomes stuck in a line it can cause a major and costly disruption of service. At worst, the line may have to be cut open to retrieve the device. However, with the wide variety of functions that different types of

pigs provide, it is difficult to determine specifically the amount of deformation of the pipe cross-section that can be allowed. Consequently, the work reported herein is not immediately useful unless the industry is able to define the level of deformation at which the performance of the pipeline is not satisfactory. It is, therefore, a critical assumption of the author that the pipeline industry will evaluate the performance requirements of their lines in such a way as to be compatible with the limit states design philosophy, that is, to identify quantitatively those conditions in which the structure ceases to fulfil the function for which it was designed.

#### **1.2.4 Cross-sectional Distortion of Thin-walled Pipes**

Distortion of the cross-section of a thin-walled pipe can arise from a variety of sources and can influence both ultimate limit states and serviceability limit states. Generally, cross-sectional flattening will arise in a pipe when it is loaded in bending about an axis normal to its length. As the pipe curves about this axis, the longitudinal compression on the inner side of the pipe and the longitudinal tension on the outer side of the pipe both have a component directed towards the centre of the cross-section. These forces tend to flatten the section. This behaviour, known as Karman's effect, was first investigated by Brazier (1927). Flattening can lead to premature sectional collapse, because the flattening tends to decrease the moment of inertia of the overall cross-section as moment increases. When excessive moment is applied to a pipe segment, localized buckling may result. These buckles tend to form in either a 'diamond' mode (inward buckle) or a 'bulging' mode (outward buckle). A thorough description of buckling instability can be found in the work of Yoosef-Ghodsii et al. (1994).

Transverse loads can also cause cross-sectional distortion. This occurs, for example, when different soil forces act in the vertical and horizontal directions on the circumference of a buried pipe. Concentrated loads, such as loads induced by pipe supports, also cause distortion of the cross-section. Combinations of all of these loading situations are also possible, as is the case for sleeper-supported piping.

### 1.2.4.1 Quantitative Measures of Distortion

In the consideration of the strength of the pipe, it is reasonably easy from test results to determine the amount of load at which ultimate limit states, such as collapse, buckling, or rupture, are attained. However, for limit states related to cross-sectional distortion it is necessary to examine the criterion that is to be used to describe pipe behaviour. Although there does not appear to be consensus within the pipeline industry regarding definitions for measures of cross-sectional distortion, three measures are commonly used: *ovalization*, *ovality*, and *out-of-roundness*.

Ovalization deformation is defined by the following relation (see, for example, Canadian Standards Association, 1996; Row et al., 1987):

$$\Delta_{\theta} = \frac{2(D_{\max} - D_{\min})}{D_{\max} + D_{\min}} \quad [1-10]$$

where,

$$\begin{aligned} \Delta_{\theta} &= \text{ovalization deformation} \\ D_{\max} &= \text{maximum diameter of deformed pipe} \\ D_{\min} &= \text{minimum diameter of deformed pipe.} \end{aligned}$$

Ovality is given as (see, for example, Price and Barnette, 1987):

$$\text{ovality} = \frac{D - D_{\min}}{D} \quad [1-11]$$

where,

$$D = \text{nominal outside diameter.}$$

Finally, out-of-roundness is defined by the following relation (see, for example, Det Norske Veritas, 1996; Troitsky, 1982):

$$o = \frac{D_{\max} - D_{\min}}{D} \quad [1-12]$$

where,

$$o = \text{out-of-roundness.}$$

Although these definitions are representative of standard practice, one should not consider them to be authoritative—no industry-wide convention on the precise meaning of each term exists. For example, in the Det Norske Veritas (1996) rules, both ovalization

and out-of-roundness are defined by the expression given in equation [1-12]. Consequently, when interpreting information in the literature related to cross-sectional distortion, particular care must be taken to ensure that the underlying definitions are understood properly. For all work reported herein, the definitions set out in equations [1-10] through [1-12] are used.

Because the minimum diameter is the only variable included in the calculation of ovality, this measure is often used a descriptor of local distortion caused by dents or in the assessment of potential flattening and buckling in the presence of longitudinal compressive bending stresses. Ovalization and out-of-roundness calculations incorporate both the minimum and maximum diameters, so these measures tend to be more useful general descriptors of overall distortion. In practice, the values of ovalization and out-of-roundness for a particular pipe are often quite similar. If the distorted shape is approximately elliptical, the magnitude of the increase in diameter is nearly equal to the magnitude of the decrease in diameter, and the resultant of [1-10] will be similar to the resultant of [1-12]. The choice of whether to use ovalization or out-of-roundness as the measure of distortion appears to rely only on personal preference.

Figure 1.3 shows typical shapes and dimensions of cross-sectional distortion that may result from transverse loads that act on a cross-section or from local buckling in the compression region of a pipe loaded in flexure.

#### ***1.2.4.2 Existing Cross-sectional Distortion Design Criteria***

Currently, it appears that there is no single preferred measure of cross-sectional distortion in use in the pipeline industry, nor is there any convention on what limits should be placed on distortion. Dinovitzer and Smith (1998) provide a review of existing American, Australian, British, Canadian, German, and Norwegian standards. This review is particularly useful because many of the international standards are not well appreciated in North America. On the subject of cross-sectional distortion, Dinovitzer and Smith show that most standards specify that the maximum allowable level of distortion for pipes is at the discretion of the designer. In particular, the designer must satisfy a general requirement that distortion should not adversely affect serviceability of the line nor promote structural failure. This approach is reasonable, but the need to satisfy these

requirements should be obvious to the experienced designer. Consequently, these standards can not be considered as particularly helpful. Furthermore, no guidance is given to the designer on how the amount of distortion is to be calculated. (The British standard does give equations for the calculation of distortion, but only for distortion induced by cold-bending.) Based on the information provided by Dinovitzer and Smith, two standards in particular are worthy of further investigation: the Australian and the Norwegian. Specific design requirements and recommendations from these standards, the Canadian standard, and other applicable literature are described below.

#### *1.2.4.2.1 Limits on Ovalization*

In CSA Z662-96 Appendix C—Limit States Design, cross-sectional distortion resulting from bending is considered in terms of limits on ovalization for both ultimate and serviceability criteria. The Standard states:

In order to prevent sectional collapse, the critical ovalization deformation limit of the pipe wall,  $\Delta_{\theta}^{\text{crit}}$ , shall be determined by valid analysis methods, or physical tests, or both, taking into account internal and external pressure, initial imperfections, residual stresses and the shape of the material stress-strain curve. In the absence of more detailed information, this limit shall be taken as  $\Delta_{\theta}^{\text{crit}} = 0.03$ .

This requirement is probably based upon recommendations given by Row et al. (1987).

To consider the serviceability limit state in Appendix C of Z662-96, the following note is added:

Where it can be shown that premature sectional collapse will not occur as a result of excessive deformation, the critical ovalization deformation,  $\Delta_{\theta}^{\text{crit}}$ , may be increased to such a value that unhindered passage of internal inspection devices is still ensured. In the absence of more detailed information, this limit shall be taken as  $\Delta_{\theta}^{\text{crit}} = 0.06$ .

In other words, CSA Z662-96 implements a limit on ovalization of 6% to allow pigging operations to take place unhindered.

#### 1.2.4.2.2 *Limits on Ovality*

Ovality is a measure of denting or flattening of the pipe, and it is typically used as a limit on the deformation that may be caused by large local forces such as pipe supports. According to the Australian design standard, *Pipelines—Gas and Liquid Petroleum* (Standards Australia, 1997), ovality is to be limited to 5% unless approved otherwise (presumably by the engineer-in-charge). This requirement is intended primarily to reduce the likelihood that distortion will interfere with the passage of pigging devices. An associated general statement is made that the pipe should be checked to ensure that buckling or denting as a result of transverse loads is avoided, particularly when the level of internal pressure in the pipe is low.

In the main body of the CSA Z662-96 design standard (i.e., not the Limit States Design appendix), no specific requirements are set out for limits on cross-sectional distortion. Instead, it is stated only that pipes are to be inspected for defects, including such items as flattening or ovality. However, there is a requirement regarding the maximum allowable size of plain dents in Clause 6.3.3.2 of the Standard. (A plain dent is one that does not have significant stress-raising characteristics or affect wall thickness adversely.) This clause limits the depth of dents to 6% of the nominal pipe outside diameter by means of a calculation that is identical to that given for ovality in equation [1-11]. Furthermore, recommendations are made to consider limiting dent size to 2% and to assess the influences of dents on the passage of pigging devices. The former recommendation is quite conservative as compared to the requirements given in the Australian standard.

#### 1.2.4.2.3 *Limits on Out-of-Roundness*

Price and Anderson (1991) report different out-of-roundness limits for various conditions. For acceptance of the pipe at installation, a maximum out-of-roundness of 2.5% is recommended. For operations at zero pressure, the limiting value of out-of-roundness is 15.0%, while at full pressure 6.0% is considered to be a maximum. For the last case, the lower value of allowable out-of-roundness accounts for the significant stiffening effect caused by the internal pressure. These values are to be used in the context of limit states design, with a ‘partial safety factor’ (i.e., performance factor) of

1.0 for installation acceptance, 0.75 for operations at zero pressure, and 1.0 at full pressure. However, no specific justification is given in the paper for the choice of these limits or performance factors—they are probably based only on engineering judgement and experience.

The Det Norske Veritas (1996) rules have been adopted as part of the Norwegian pipeline design standard (NORSOK, 1997). In these rules, total out-of-roundness (also called ovalisation therein) as result of both fabrication and operational loads is not to exceed 3%. This requirement may be relaxed if the moment capacity is correspondingly reduced; operational requirements, such as pigging, are not hindered; and cyclic stresses induced by ovalization are considered. The limitation of out-of-roundness to 3% would appear, at first glance, to be extremely conservative as compared to the requirements described by Price and Anderson (1991). However, the Det Norske Veritas rules govern submarine pipelines rather than buried or elevated lines. Submarine pipelines will likely carry significant external hydrostatic pressure—if internal pressure is lost, excessive out-of-roundness may lead to rapid and progressive collapse of the line. On this basis, the Det Norske Veritas rules are reasonable, but can not be viewed as useful guidance for the design of buried pipelines.

As an example of industrial practice, it is known that NOVA Gas Transmission Ltd. currently uses 5% as a maximum allowable out-of-roundness at full operating pressure to minimize difficulties associated with pigging operations. This value is considered to be a conservative estimate of the limiting distortion that can be accommodated by pigging devices. With the ever-improving technology of pigging devices, it may be possible to increase limiting values of out-of-roundness in years to come.



**Figure 1.1** Typical sleeper-supported pipe installation

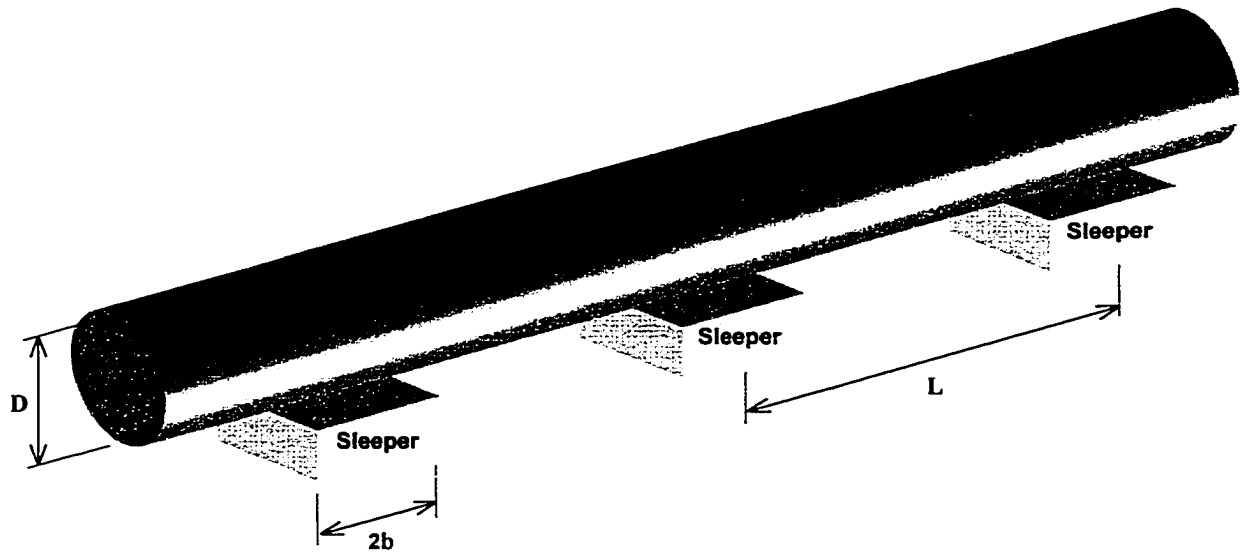


**Figure 1.2** Sleeper-supported pipe geometry

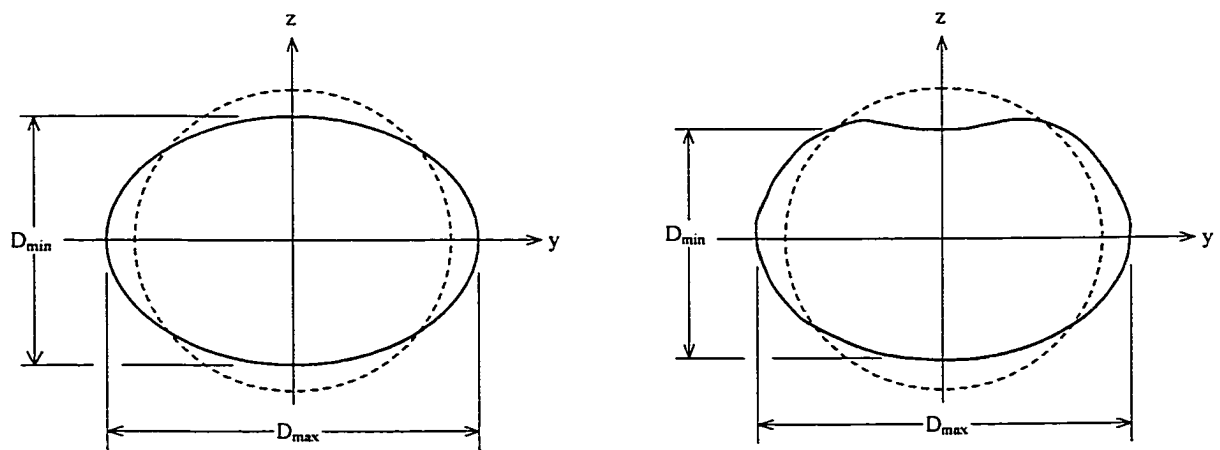


**Figure 1.3** Typical distorted cross-sectional shapes

## 2 EXPERIMENTAL PROGRAM

The primary objective of the experimental portion of the research program is to gain an overall understanding of sleeper-supported pipe behaviour. As a preliminary investigation, four laboratory tests of full-scale sleeper-supported pipes were conducted at the University of Alberta in 1995. This preliminary work allowed a basic understanding of the behaviour to be developed and permitted optimization of experimental procedures. With the information gained in the preliminary tests, seven more full-scale experiments were added to the research in 1996. The full-scale testing is also complemented by small-scale ancillary material tests. Descriptions of the experimental methods are presented in this chapter, and the results are presented in Chapter 4.

### 2.1 FULL-SCALE LABORATORY TESTS

A total of 11 full-sized line pipes (406 mm diameter and 762 mm diameter) were tested in such a way as to simulate field installations of sleeper-supported piping systems as closely as practicable. The goals of the experimental tests were to observe the overall deformational behaviour and stability characteristics of the specimens while monitoring variables such as load-carrying capacity and cross-sectional distortion. Ranges of external pipe diameter ( $D$ ), pipe wall thickness ( $t$ ), internal pressure ( $p$ ), grade ( $S$ ) and sleeper-support length ( $2b$ ) are considered in the testing parameters. Two methods of pipe manufacture—girth-welded and spiral-welded—are also encompassed by the specimens. All of the parameters used in each test are summarized in Table 2.1.

#### 2.1.1 Selection of Parameters

Seven specimens were chosen to have a nominal diameter of 762 mm and four specimens were selected to have a nominal diameter of 406 mm. Of the 11 specimens, three of the 762 mm diameter specimens were formed by spiral rolling, while all others had a single longitudinal seam weld. Grade 359 MPa and 483 MPa pipes were chosen, and the sleeper supports investigated ranged in length from 0.5 to 1.5 times the nominal diameter of the pipes. These parameters were selected to provide a representative sample of the type and geometry of pipes likely to be encountered in design applications.

### 2.1.2 Description of Specimens

The 11 full-scale test specimens were provided and fabricated by NOVA Gas Transmission Ltd. Fabrication procedures included sandblasting, cutting the pipes to length, welding of ellipsoidal end caps to those specimens that were pressurized, and girth welding of the 406 mm specimens. (The diameter of the 406 mm specimens was too small to allow access to the interior of the pipe at mid-length for mounting of testing instrumentation. Consequently, a segment of pipe was cut with a length short enough to allow one to reach inside to attach instrumentation. Additional segments were welded on to each end subsequently, thus forming the full-length test specimen.)

The spirally welded pipes used in the fabrication of specimens S5, S6, and S11 were manufactured by IPSCO Saskatchewan Inc. in Regina. In general, spirally welded pipe is formed from a coiled *skelp* (sheet of steel) that is of a particular width, and the rolling angle determines the diameter of the completed tube. For these specimens, the spiral weld was made with the Submerged Arc Welding (SAW) process, in which coalescence of the metals is achieved through heating with an electric arc between a bare wire consumable electrode and the workpiece. The arc is shielded by granular flux that melts into slag, which serves to add alloying elements and protect the weld pool from reacting chemically with the atmosphere. Usually, one weld pass is made on the inside and one on the outside of the pipe. For the specimens tested in this research, the skelp width is 1524 mm and the helical angle of forming is  $39.5^\circ$  (measured with respect to a plane transverse to the longitudinal axis of the pipe). Pipes S5, S6, and S11 were each made from continuous coils of steel, so no skelp end welds were present in any of these specimens. The forming technique for a typical spirally welded pipe is shown in Figure 2.1.

All other specimens were of the longitudinally welded type. These pipes are usually formed from a flat sheet or coil of steel by the 'U and O' process. This process is so named because the plate is first cold-rolled to have a U-shaped cross-section, and then the section is progressively rolled into a circular shape. Welding of the seam then forms a closed cross-section. A more detailed description is available in Shoemaker (1984). Figure 2.2 shows a typical process of forming pipe by the U and O method.

Based upon the appearance of the final weld bead, it is surmised that the SAW process was used for the seam-welded 762 mm specimens (S1, S2, S3, and S7). Because these specimens were not marked with identification when they were delivered to the University of Alberta, there is some doubt regarding their origin. (All specimens for the test program were donated by NOVA Gas Transmission Ltd. from excess material left over from various pipeline construction projects. Consequently, the origin of the materials was not well identified, since markings and trace numbers had oftentimes been removed by sandblasting.)

Of the 406 mm diameter pipes, S9 and S10 were manufactured by IPSCO. The origin of manufacture of the other two specimens, S4 and S8, is not clear. It is known that IPSCO uses the High-Frequency Resistance Seam Welding (RSEW-HF) technique for pipes of this size, a process that is commonly but imprecisely known as Electric Resistance Welding (ERW). In this process, the seam weld is formed as the edges are pressed together mechanically while heat is generated by the flow of high-frequency alternating electrical current on the surface of the pipe. The other 406 mm specimens also had a single longitudinal seam weld that appears to have been formed with the RSEW-HF process.

A useful overall description of various pipe forming and welding techniques is provided by Stelpipe (1993).

### **2.1.3 Test Set-up and Procedure**

The tests were performed in the I.F. Morrison Structural Laboratory at the University of Alberta with an MTS6000 universal testing machine equipped with a specially constructed loading head. Adjustable steel plates attached to the loading head simulated a sleeper support of variable size. In each test, the vertical displacement of the loading head was increased monotonically, thereby modelling the load transfer that occurs between a pipe and a sleeper support.

In field installations of sleeper supports, it is common practice to insert a thin layer of padding material (in the order of 13 mm thick) between the concrete sleeper and the pipe (Kormann and Zhou, 1995). This padding, usually wood, plastic, or neoprene, serves to protect the coating on the pipe. No attempt was made to represent this layer of

padding material in the experiments, however. The justification for this omission is that the contact interaction between a pipe and a steel plate in the tests is more serious than the true contact condition in which padding material is present. Direct steel-to-steel contact in the tests should result in loading conditions for the pipe that are conservatively severe. Additionally, modelling of such contact in subsequent finite element analyses is simpler than modelling of steel-to-concrete or steel-to-padding contact.

For ease of set-up, the orientation of the tests was inverted as compared to the normal orientation of a sleeper-supported pipe, that is, the loaded area in the test was on the top of the pipe. Each specimen was tested with the sleeper support located at mid-span and with a simple support at both end reactions. Figure 2.3 shows a schematic detail of the test set-up.

The loading head was stabilized by a system of stiff columns, upon which steel angles were allowed to slide on Teflon bearing pads (friction in the bearing pads was measured and was found to be negligibly small). This system ensured that the loading head remained level and true throughout each test. To verify this, electronic measurements of loading head deflection were taken along the longitudinal axis of the specimen and bubble-type levels were used in the transverse plane. No significant inclination was detected. Figure 2.4 illustrates the overall test arrangement, in which the specimen, the loading head, and the loading head stabilization system are shown.

A shallow steel saddle supported each end of the pipe in order to distribute the load more evenly over the cross-section. Each saddle was placed on a knife-edge and roller support so as to allow in-plane rotation and axial movement at the ends of the pipe. For those specimens that were unpressurized, a thick steel plate was welded to each end to act as a bearing stiffener, thereby limiting local cross-sectional distortion over the support. For the pressurized specimens, semicircular stiffeners were welded on the inside of the pipe over the support reactions. Ellipsoidal end caps were then welded to the pipe so as to form a pressure vessel. For all tests, horizontal stability of the system in the longitudinal direction and lateral stability were achieved through friction between the sleeper and the pipe surface.

All of the tests were conducted by controlling the displacement of the loading head rather than the loading force. The advantage of displacement control is that spontaneous collapse does not occur if a limit point (a condition of zero stiffness) is reached during loading. The full descending branch of the load-versus-displacement relationship can be obtained in this way, if desired.

#### **2.1.4 Instrumentation and Monitoring**

An extensive system of instrumentation was used to monitor the behaviour of each specimen. This included measurement of the total applied force, the forces at the reactions, sleeper displacement, strains in the region of contact (as measured by strain gauges), cross-sectional distortion, and level of internal pressure. A Fluke 2400B and its associated computer system provided data acquisition for all of the electronic measuring devices.

Instrumentation for the specimens was designed to provide redundancy of measurements wherever possible. Forces were monitored both through load cells at each supported end of the pipe and through the load measured by the testing machine. The sum of the reactions was nearly equal to the applied load—within about 2%—indicating that there was very little friction induced by the loading head stabilization system. The system of instrumentation for the specimens included longitudinal and circumferential strain gauges on the pipe walls, along with cable transducers to measure pipe deflections. A linear variable differential transformer that measures the stroke of the hydraulic piston and is part of the internal workings of the testing machine monitored sleeper displacement. Throughout each test, measurements necessary for characterizing the level of distortion were also taken manually at two cross-sections.

##### **2.1.4.1 Initial Measurements**

Initial geometric imperfections or misalignments will always be present in test specimens and *in situ* installations of piping. These imperfections have the potential to affect the behaviour and strength of members dramatically by promoting premature local or overall buckling. To obtain some feeling of the magnitude of initial imperfections in the specimens tested in this study, diametrical measurements were taken across the ends

of each specimen at several angles. These measurements do not vary significantly (variations of diameter are in the order of 1% or less). After gaining some experience with the tests, it was found that the specimens responded in a very stable fashion. Because of this stable behaviour, and since instability-induced failures are those most often affected by initial imperfections, it seems reasonable to neglect the initial imperfections for the sleeper-support problem. Consequently, in the numerical model that is described in Chapter 3, no attempt is made to represent these initial imperfections. This assumption was further substantiated when, after some trials with the finite element model, the solution results compared favourably with the test data.

#### **2.1.4.2 Strain Gauges**

The layout of the strain gauges was chosen so as to enable determination of specimen behaviour in the longitudinal and circumferential directions. The circumferential strain gauges were located at several cross-sections in the region of the sleeper. Gauges were affixed to the top of the pipe (designated 0 degrees), and at angles of 20, 40, 60, and 300 degrees. In order to monitor longitudinal bending effects, longitudinal gauges were placed at the 0 and 180 degree locations. Some of the longitudinal gauges were placed remotely from the sleeper supports where local effects should not influence the strains significantly. A typical strain gauge layout used for a test of 762 mm pipe is shown in Figure 2.5, and the layout for the 406 mm pipe is shown in Figure 2.6. Note that the gauge layout selected for a particular test depended upon the length of the sleeper support (2b) in that test. As described in Section 2.1.2, access to mount internal instrumentation for the 406 mm specimens was gained by cutting the pipe into sections. The sections were then rejoined by girth welds to form the completed specimen (the girth welds are shown in Figure 2.6).

A series of grooves, oriented transversely to the length of the pipe, were made in the sleeper so that the external gauges on the 0 and 20 degree lines were not crushed as the pipe deformed. Those specimens having internal pressure were equipped with waterproof internal strain gauges. Lead wires for these internal gauges penetrated the pipe wall at a specially designed waterproof fitting.

Each strain gauge gives information about the deformational behaviour of the pipe material in a single direction over a 10 mm length. Consequently, the data obtained are not particularly useful in the context of gaining an understanding of the overall behaviour of sleeper-supported line pipe. The strain gauge data were used principally as a means of determining whether each specimen was distorting symmetrically and as a secondary means of monitoring internal pressure.

#### ***2.1.4.3 Internal Pressure***

Specimens S3 and S9 were filled with water and pressurized to a level of 8450 kPa (gauge pressure), which corresponds to a hoop stress of 80% of the specified minimum yield strength in the circumferential direction. A manually controlled air-driven fluid pump was used to maintain the pressure at a constant value throughout these tests. The level of internal pressure was measured with an electronic transducer, and these values were recorded throughout the tests.

#### ***2.1.4.4 Displacement Measurements***

Cable transducers were mounted at several locations in order to monitor the vertical deflection of the pipes. The deflection at the bottom of the each pipe (180 degree location) was measured at sections 0 and 2, and the deflection at both the 0 and 180 degree positions were measured at sections 3, 4, 5, and 6 (see Figures 2.5 and 2.6 for typical section locations). Except for the pressurized specimens, cable transducers were mounted inside of the pipe to measure the change in diameter between the 0 and 180 degree locations at sections 0 and 2. This internal measurement is necessary for the calculation of cross-sectional distortion, described in detail below.

#### ***2.1.4.5 Cross-sectional Distortion***

Various measures of cross-sectional distortion are commonly used in the pipeline industry, as described in Chapter 1. Data relating to the distortion equations were obtained by taking measurements of vertical and horizontal pipe displacements throughout each test. These measurements were taken at two cross-sections: one at the centreline of the pipe, and one near the edge of the sleeper support (sections 0 and 2, respectively). The measurement of horizontal deformation was done manually, while

measurement of vertical deformations was part of the electronic data acquisition system. The horizontal measurements were made with respect to a steel frame that was attached rigidly to the loading head; the frame moved in the vertical direction with the loading head. A measuring square was then used to measure the horizontal distance from the frame to the point of maximum pipe width. The vertical co-ordinate of the point of maximum width, with respect to the steel frame, was also recorded.

## 2.2 ANCILLARY TESTS

In order to predict the behaviour of any structural system, it is necessary to have a thorough understanding of material properties for the members. For this project, the finite element analyses described in Chapter 3 are an attempt to replicate the results observed in the full-scale laboratory tests. In these analyses, the stress-strain relations for the pipes are used to develop the constitutive laws. Background information on the material properties of pipeline steels is discussed in this section, along with the tension coupon and hydraulic ring expansion test methods that were used for obtaining material stress-strain relations.

### 2.2.1 Material Properties of Pipeline Steels

Most line pipes, including the specimens tested in this study, are cold-rolled into shape. This process can alter the material properties of the finished pipe significantly as compared to those of the virgin steel coil or plate. Furthermore, pressure testing of the pipe to a level that causes some plastic straining is usually the last stage of the manufacturing process. (This step is necessary for satisfying manufacturing specifications and, in some cases, to size and round the pipe.) Consequently, pipeline steels often exhibit *anisotropic* behaviour, meaning that the material properties are not the same in every direction throughout the body.

It is well known that anisotropy arises partly from cold work effects in the forming process and partly from the *Bauschinger effect* (for example, see Lay, 1982). Cold working increases the yield strength of a ductile metal while the Bauschinger effect causes the tensile yield strength of a material to decrease as it is deformed plastically in compression (and vice versa). In addition, the magnitude and distribution of residual stresses may play a role in the behaviour of pipe specimens.

### **2.2.2 Tension Coupon Tests**

The most common method for obtaining the stress-strain properties of steel is to test a coupon of the material in uniaxial tension. The coupon is usually oriented parallel to the longitudinal axis of the pipe (axial direction) or transverse to this direction (hoop direction). For the work reported herein, tests of tension coupons were made for all 11 specimens, with two coupons taken from the longitudinal direction and two from the transverse direction of each specimen. The locations from which the coupons were taken corresponds to the regulations outlined in API Specification 5L (American Petroleum Institute, 1995). The dimensions of the coupons and the test procedures used correspond to the requirements of ASTM A370-94 (American Society for Testing and Materials, 1994).

Tension coupon testing is the most common means of obtaining the material characteristics of steel. The method is intended to provide information only about stress-strain properties; effects that originate from sources such as manufacturing-induced residual stresses can not be captured in the results of a tension coupon test. Residual stresses are, for the most part, released when the coupon is cut from the parent material. Consequently, the behaviour observed in a coupon test may differ from the behaviour that would have been exhibited by the parent material. For a coupon cut from the hoop direction of a pipe it is necessary to flatten the specimen prior to testing. This also changes the behaviour of the sample specimen, because it is likely that strain hardening and Bauschinger effects arise during the flattening process (see, for example, Llewellyn, 1992; Shoemaker, 1984). The flattening process also gives rise to residual stresses in the longitudinal direction of the coupon that vary through the thickness. These stresses also have an undesired influence the stress-strain behaviour of the flattened coupon. Because of the limitations associated with tension coupon tests, another method for the measurement of stress-strain material properties for pipes, known as hydraulic ring expansion testing, was also investigated in this work.

### 2.2.3 Hydraulic Ring Expansion Tests

In a hydraulic ring expansion test, a short ring of pipe (usually in the order of 75 mm in length) is cut from the parent pipe. This ring is machined to precise tolerances and is placed between two bulkheads with only a small amount of clearance between the specimen and the bulkheads. A rubber gasket prevents leaks at this gap, and fluid (usually oil or water) is placed inside the specimen. The fluid is then pressurized, which causes a uniaxial tensile stress around the circumference of the pipe. In this way, the material properties in the hoop direction can be evaluated directly. Unlike a transverse tension coupon test, there is no 'contamination' of the results by the flattening process. Consequently, ring expansion testing is believed to give a better representation of the initial portion of the stress-strain curve for the circumferential direction of circular tubular members. General procedures for hydraulic ring expansion testing can be found in ASTM A370-94 (American Society for Testing and Materials, 1994).

Ring expansion tests were carried out on samples taken from specimens S5 through S11. (Rings of material from specimens S1 through S4 were not available.) Because highly specialized equipment is required for this work, the testing was carried out using the facilities of the Research and Development division at IPSCO Saskatchewan Incorporated in Regina. The procedures used for the tests done at the IPSCO testing lab, which are slightly different from those described in ASTM A370-94, are outlined below.

The ring expansion testing apparatus used at IPSCO consists of two thick machined circular plates set a distance of 76.2 mm apart. When assembled, these two plates form a sandwich around the ring specimen. The plates are held together by a series of high-strength machine bolts. The testing process used is as follows:

1. Rings approximately 125 mm long are flame-cut from the parent pipe material. These rings are subsequently machined on a lathe to 76.0 mm in length.
2. The top plate is removed from the testing apparatus and a ring expansion specimen is centred on the lower plate (see Figure 2.7). A rubber gasket is

then installed inside of the ring (Figure 2.8), forming a seal at the ring-to-plate interfaces.

3. A layer of Teflon tape is wrapped around the ring specimen. A steel cable is wrapped once around the specimen on top of the Teflon, allowing the cable to slide with reduced friction. In order to measure circumferential expansion, and thereby strain, the cable is attached to a fixed point at one end and to an electronic cable transducer at the other end (see Figure 2.9).
4. The top plate is lowered into position and fixed to the lower plate using 38 mm bolts, which are tightened with an impact wrench (see Figure 2.10). Because the rings have a slightly smaller width than the gap between the plates, the ring should carry no compression when the bolts are tightened. The rubber gasket alone forms the sealed chamber inside the ring. Guards are also placed around the set-up.
5. Water is allowed to flow into the ring through a port in the lower plate and air is allowed to vent. Once filled, the vent is closed and the test can begin by increasing the internal pressure. The displacement of the cable transducer and level of hydraulic pressure are recorded during the tests, allowing calculation of the stress and strain in the hoop direction of the pipe wall.

The data obtained from the various ancillary test methods will be useful in the assessment and selection of an appropriate material model for use in the finite element analyses that are described in the next chapter.

**Table 2.1** Nominal specimen parameters

Specimen	Nominal Size $D \times t \times \ell$ (mm)	Grade (MPa)	Weld Type	p (kPa)	2b/D	D/t	$\ell/D$
S1	762 × 8.3 × 5600	483	Seam	0	1.5	91.8	7.35
S2	762 × 16.4 × 5600	483	Seam	0	1.5	46.5	7.35
S3	762 × 8.3 × 5600	483	Seam	8450	1.5	91.8	7.35
S4	406 × 6.0 × 3600	359	Seam	0	1.5	67.7	8.87
S5	762 × 8.3 × 5600	483	Spiral	0	1.0	91.8	7.35
S6	762 × 8.3 × 5600	483	Spiral	0	0.5	91.8	7.35
S7	762 × 16.4 × 5600	483	Seam	0	0.5	46.5	7.35
S8	406 × 8.0 × 3600	483	Seam	0	1.5	50.8	8.87
S9	406 × 6.0 × 3600	359	Seam	8450	1.5	67.7	8.87
S10	406 × 6.0 × 3600	359	Seam	0	0.5	67.7	8.87
S11	762 × 8.3 × 5600	483	Spiral	0	1.5	91.8	7.35

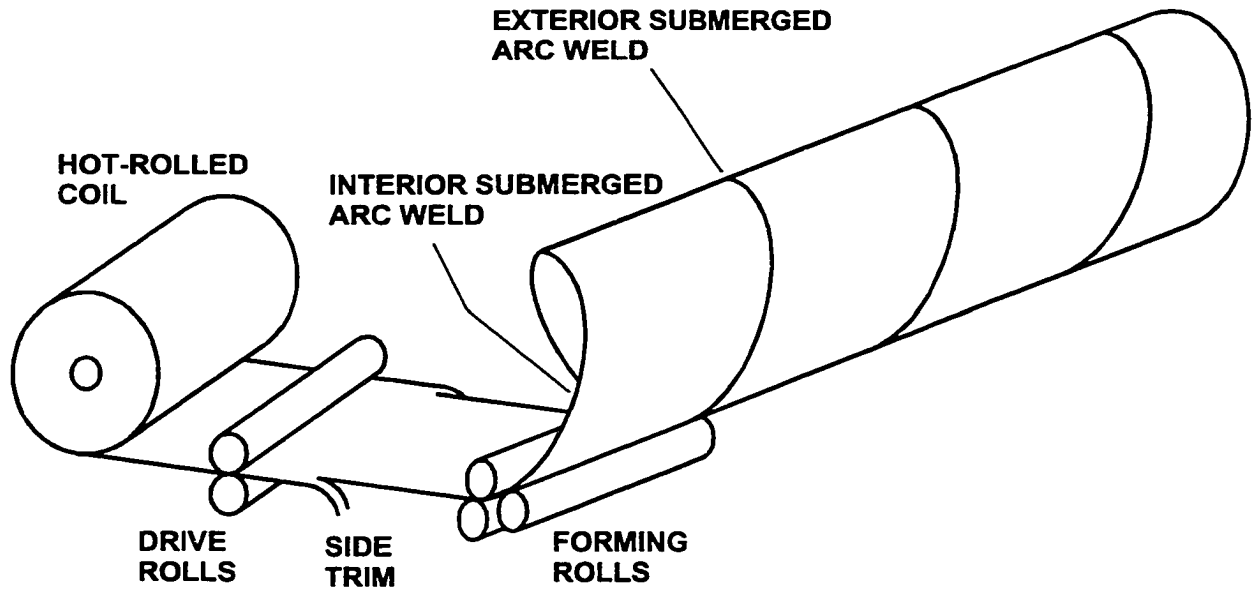


**Figure 2.1** Typical fabrication of spiral weld pipe

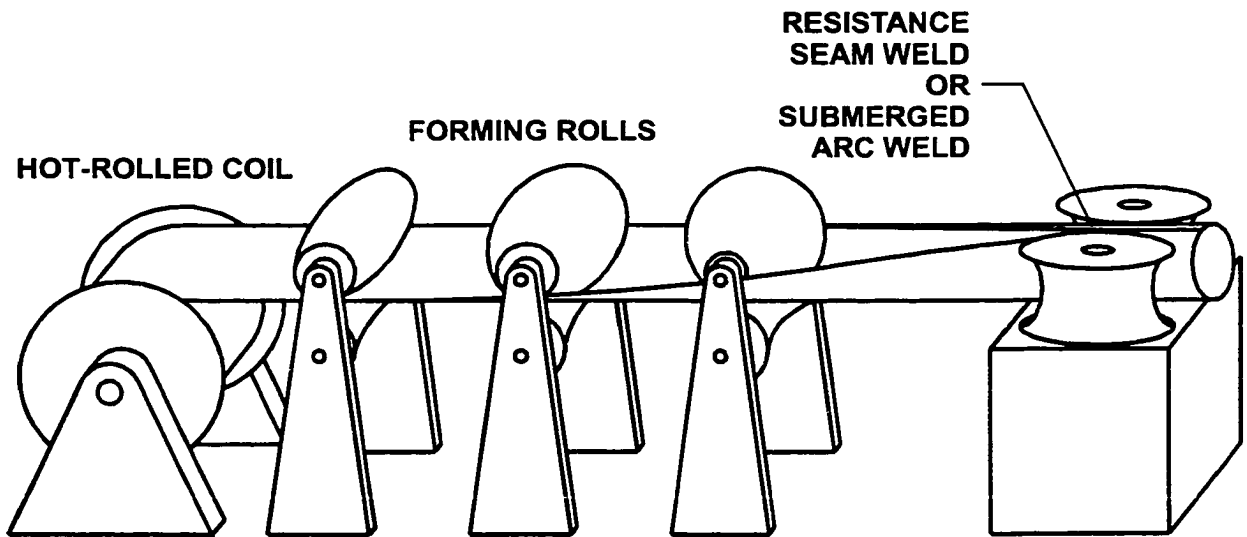


**Figure 2.2** Typical fabrication of pipe by the U and O method

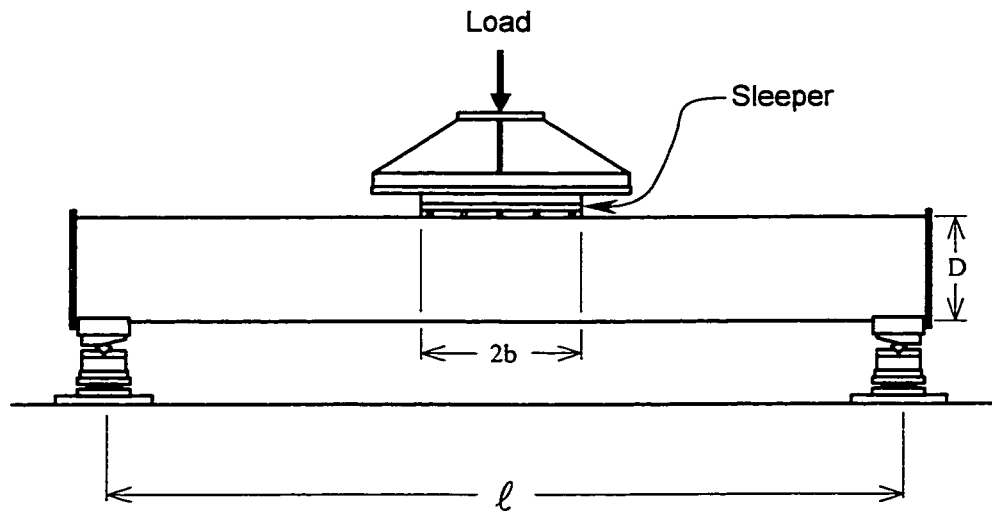


**Figure 2.3** Schematic of test set-up



**Figure 2.4** Typical test set-up

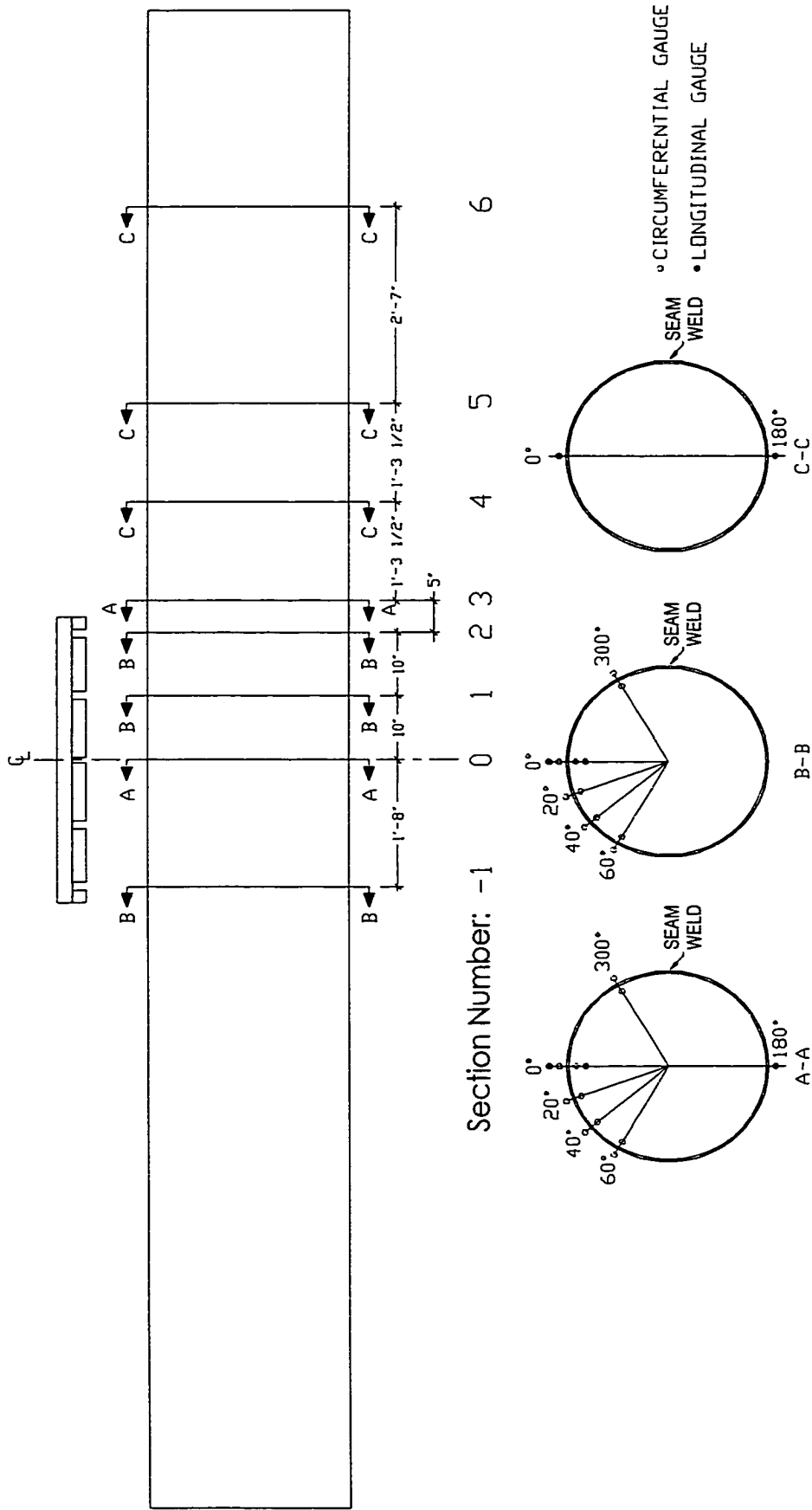
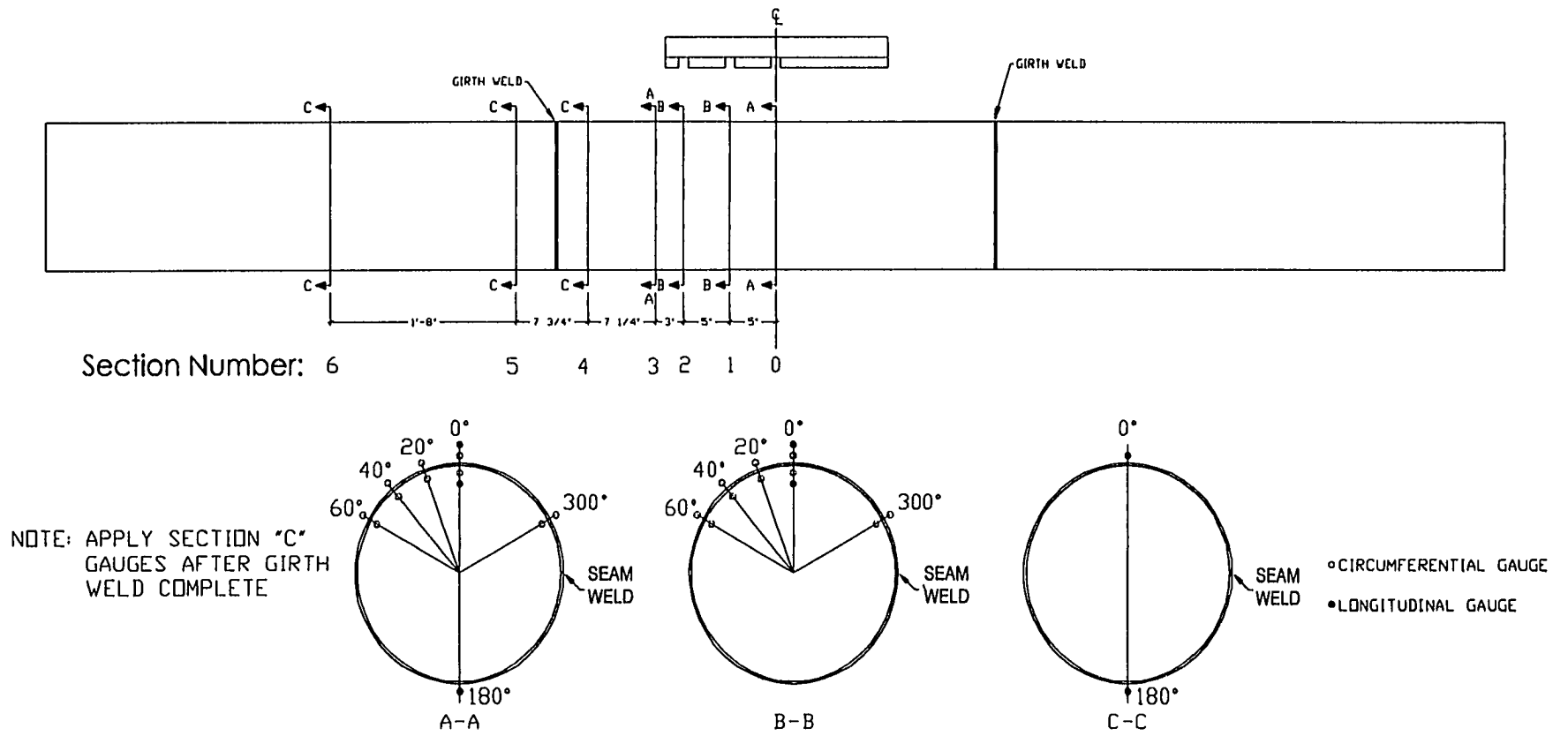
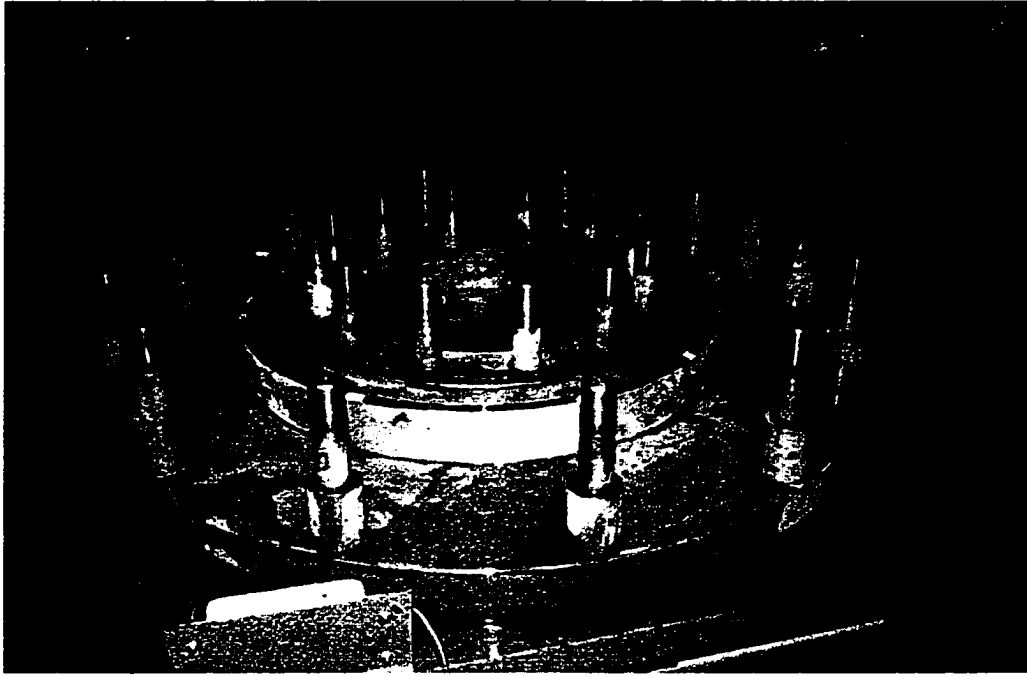


Figure 2.5 Typical strain gauge layout (762 mm specimen)



**Figure 2.6** Typical strain gauge layout (406 mm specimen)



**Figure 2.7** Ring specimen mounted in testing machine

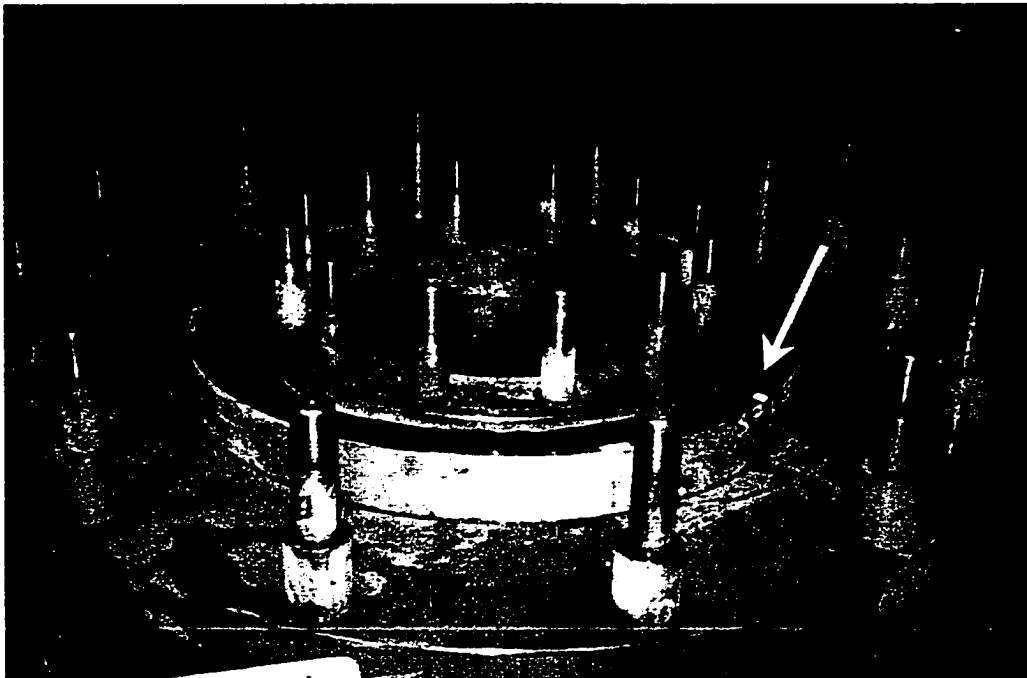


**Figure 2.8** Rubber gasket installed

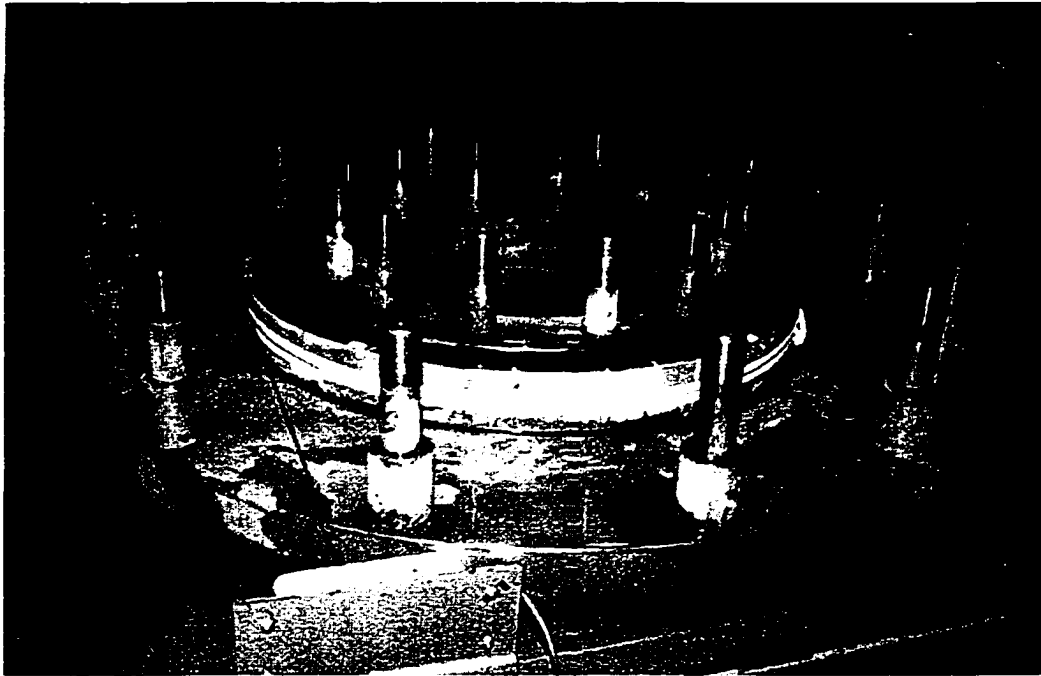


**Figure 2.9** Cable transducer mounted for strain measurement

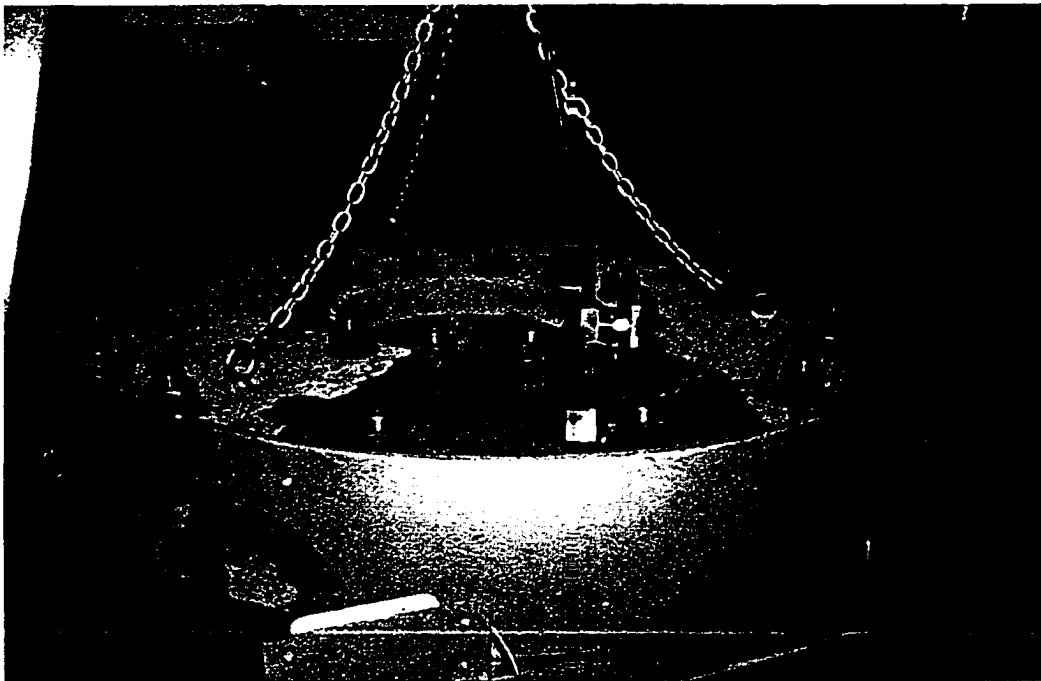


**Figure 2.10** Lid bolted into position and guards installed

### 3 FINITE ELEMENT ANALYSIS OF TEST SPECIMENS

#### 3.1 GOALS OF FINITE ELEMENT STUDY

The 11 tests that comprise the experimental program are a significant contribution towards the understanding of the behaviour of sleeper-supported line pipe. However, the specific parameters investigated in the laboratory tests do not encompass all of the scenarios that might be expected in field applications, nor are the loading conditions identical to *in situ* installations. Consequently, it is desirable to develop a means by which the behaviour of other pipe geometries and loading conditions can be predicted numerically, so as to avoid the large expense of performing additional tests. To make a numerical prediction of the behaviour, a non-linear finite element analysis modelling technique that simulates the interaction between a pipe and a sleeper support is developed in this chapter. Obtaining a good representation of the behaviour observed in the full-scale laboratory tests that are described in Chapter 2 is the primary objective of the numerical work.

As demonstrated in Chapter 1, it is necessary to consider both strength and serviceability criteria to make use of the limit states design philosophy. Therefore, the numerical model for sleeper-supported piping must be able to represent accurately both load-carrying capacity and deformational behaviour. It is known from the results of the laboratory tests that the material properties and the geometry of deformations are non-linear, so the process of modelling is expected to be complicated.

To perform the numerical analysis, the commercially available finite element analysis package ABAQUS/Standard Version 5.7-1 by Hibbitt, Karlsson & Sorenson, Inc. (HKS, 1997a) was chosen. This software is well suited for the solution of this problem because it offers a number of important features, including an appropriate contact formulation to describe the complicated sleeper-pipe interaction. Also available is a generic elastic-plastic material model that allows the constitutive law to be represented as a multi-linear curve with isotropic or kinematic hardening. The element library offers an efficient shell element that is suitable for modelling thin-walled pipes and allows for large displacements and finite membrane strains. The software can accommodate fluid pressure

inside the pipe as it undergoes large displacements and rotations (i.e., non-conservative loading), and the solution can use either load or displacement control. Finally, a post-processing package is available for data extraction and presentation.

All of the analyses were performed on Sun UltraSparc 1 workstations having 96 Mbytes of random access memory. On average, the analyses took several hours to perform, depending upon the number of variables in the problem and the tolerances necessary for convergence of the solution.

## **3.2 DESCRIPTION OF MODELS**

### **3.2.1 Finite Element Formulation**

The finite element method is a well-established procedure in many fields of engineering for the solution of complicated problems that would be unmanageable using closed-formed techniques. For the particular case of structural engineering, it is most often the principle of virtual work (which is a general statement of equilibrium) that is used to allow the differential equations of equilibrium to be transformed into algebraic equations. This is done by estimating the displacement field inside individual elements using shape functions. A complete description of the background of the finite element technique is beyond the scope of this report; Bathe (1996) describes this topic thoroughly.

Because of the non-linear nature of the analyses performed in this study, the software must use an incremental solution strategy to solve the equations of equilibrium. For the work reported herein, the formulation is of an incremental updated Lagrangian type. With this technique, the measures of stress and strain for an increment at time  $t+\Delta t$  are referred back to the configuration of the body at time  $t$ , the end of the previous increment. This is the most appropriate formulation because it allows non-linear geometric behaviour of the structure to take place at the same time as severe non-linear straining of the material.

Two issues related to incremental non-linear analysis are of particular interest: the technique that is used to solve the system of equilibrium equations at each increment, and the method by which increment size is chosen. The solution method employed by ABAQUS for the incremental equations of equilibrium is based upon Newton's

well-known approach. For non-linear problems with only static loads, which is the case for sleeper-supported pipes, the size of each increment must be controlled carefully in order to obtain an accurate solution. This careful control is necessary because, unlike dynamic analyses, there are no inertial or viscous effects present in a static problem to aid in the stabilization of the solution.

For the work described herein, the automatic step control algorithm available in ABAQUS was used to determine increment size. However, the magnitude of the first increment was often set manually at a small value to ensure the successful convergence of that increment. Because it is possible for a solution to converge along the wrong equilibrium path if excessively large increments are used in an analysis, it is necessary to check the effectiveness of the automatic incrementation scheme. This check is particularly important if the system under investigation might fail by instability. As a test of the automatic incrementation algorithm, several of the analyses described in this chapter were repeated with the increment size set manually to a small value. The results from these analyses do not differ significantly from those obtained using automatic incrementation. Consequently, the use of the automatic incrementation scheme in ABAQUS is judged to be appropriate. Additional details regarding solution procedures are beyond the scope of this report and are available in the documentation provided with the software (HKS, 1997b).

### **3.2.2 Elements**

The pipe is discretized in the finite element model using four-node doubly curved ‘shear flexible’ shell elements (ABAQUS element S4R), and the sleeper is represented by 8-node three-dimensional solid elements (ABAQUS element C3D8). With these elements it is possible to account for large deformations, non-linear material properties, and the sleeper-to-pipe contact conditions.

The particular shell element used in this study has been shown to be reliable and effective for modelling pipeline problems where large displacements and deformations occur (for example, see Souza and Murray, 1999). Each of the four nodes has six degrees of freedom, namely three translational ( $u_1, u_2, u_3$ ), and three rotational ( $\phi_1, \phi_2, \phi_3$ ). However, if the shell surface curves smoothly (as is the case for models of plain pipes),

only two of the rotational degrees of freedom are actively associated with stiffness. These are the out-of-plane rotations of the vector normal to the *reference surface*, which is defined as the mid-surface of the shell for all analyses described herein. The third component of the vector normal, rotation about its own axis (the ‘drill’ degree of freedom) is activated only when particular geometric criteria apply. Otherwise, a small artificial stiffness is assigned to this degree of freedom to avoid singularities in the stiffness matrix.

Membrane strains are those strains that do not contribute to bending of the element. For the S4R element, the membrane finite strain formulation allows the thickness of a shell element in the configuration at time  $t+\Delta t$  to be different from its value at time  $t$ , the beginning of the increment. In the through-thickness direction, which is normal to the reference surface, the strain has constant value. For plastic behaviour, Poisson’s ratio is assigned a value of 0.5 to account for the approximately incompressible behaviour of the material under these conditions. Strains that result from bending are assumed to be small and are derived from the derivatives of the normal to the reference surface.

The element has an isoparametric formulation, which means that the same interpolation functions are used for both the displacement field and for mapping to a natural co-ordinate system. The interpolation functions are  $C_0$  continuous. Translational degrees of freedom are interpolated independently from the components of the vector normal to the reference surface.

The element is formulated to be shear flexible, meaning that transverse shear deformation is allowed. The ability of the shell to deform in shear makes it useful for both thick and thin shell analyses. If the shell is thin, as in this study, shear deformation is negligible. In this case, the transverse shear stiffness constrains a material line normal to the reference surface to remain approximately normal to that surface throughout the deformation history. This behaviour is consistent with the Kirchhoff assumption in classical thin shell and plate theory.

To model the initial curvature of an element accurately, the user must specify the direction of the normal to the reference surface at each of the nodes. The program then

uses the shape functions to interpolate the initial reference surface gradient in accordance with the normal at each of the nodes. The element employs reduced numerical integration, which is performed using Simpson's rule. Five integration points through the thickness were chosen, which enables the non-linear behaviour of the material to be traced accurately.

### 3.2.3 Boundary Conditions

In the finite element models, two vertical planes of symmetry are utilized taken through the centrelines of the specimen—along with appropriate boundary conditions—so that only one quarter of the specimen is discretized (see Figure 3.1). In order to enforce these boundary conditions properly, displacement  $u_1$  and rotations  $\phi_2$  and  $\phi_3$  are restrained at nodes along the longitudinal plane of symmetry. On the transverse plane of symmetry, displacement  $u_3$  and rotations  $\phi_1$  and  $\phi_2$  are restrained. See Figure 3.2. Because the specimens in the laboratory tests did not show evidence of significant asymmetry, the use of these planes of symmetry in the numerical analysis is judged to be appropriate.

To match as closely as practicable the support reactions that were used in the laboratory tests, rigid beam elements in the model are built up so as to simulate the steel saddle support described in Chapter 2. This rigid body is linked by a rigid 'outrigger' to a node that represents the knife-edge support in the test set-up, at which only rotation  $\phi_1$  and displacement  $u_3$  are released (see Figure 3.2). Another rigid body joins all of the nodes at the end of the pipe to simulate the stiffener plate near the support. The sleeper, which is removed from Figure 3.2 for clarity, is constrained so that it can move only in the vertical ( $u_2$ ) direction. The displacement of the sleeper is controlled in the analyses in the same way that sleeper displacement was the controlling variable in the laboratory tests.

(For the models of the pressurized specimens, the layout of elements is somewhat different. Recall that each pressurized specimen had internal semicircular stiffeners welded over the supports. Ellipsoidal cap assemblies were also welded on the ends. These components were included in the finite element models of the pressurized specimens by modifying that model shown in Figure 3.2.)

### 3.2.4 Contact Formulation

When forces are transferred between a sleeper and a pipe, the geometry of the pipe in the region of contact changes as the level of force varies. To model the behaviour of such a system accurately, an analysis must account for the changing geometry of the contact interface between the two bodies throughout the loading history. There can be a transfer of surface traction—consisting of a compressive normal force and an in-plane shear force—only in those regions where the bodies touch. In the particular options chosen for the analysis of the test specimens, it is assumed that the coefficient of friction for contact is zero, that is, the in-plane component of surface traction is neglected. This simplifies the analysis and should result in conservative estimates of stresses and cross-sectional distortion for the pipe.

The sleeper-to-pipe contact problem can be modelled in ABAQUS using a ‘contact pair’ approach. In this option, the interaction between the surfaces is achieved using contact elements, whereby the sleeper is modelled as a ‘master’ surface and the nodes of the pipe are modelled as a ‘slave’ surface. In simple terms, the relative locations of the surfaces are monitored and a constraint is imposed so that slave nodes can not penetrate the master surface.

A particular contact problem may have to account for either small or finite relative sliding between the two surfaces. For the work described herein, the small-sliding contact formulation available in ABAQUS v5.7-1 is used. This approach allows the surfaces to experience arbitrarily large rotations, but, throughout the analysis, a particular node on the slave surface always interacts with the same local tangent plane on the master surface. More specifically, the master surface is defined initially by the directions of the normal vectors at the nodes, with the surface between nodes interpolated linearly. The normal vector field on the master surface will intersect the nodes on the slave surface at a discrete number of locations. *Anchor points* are then defined on the master surface representing the locations where the normal to the master surface intersects slave nodes. Each node on the slave surface is then considered to interact with a plane that is tangent to the master surface at the corresponding anchor point, not with the master surface itself. This plane rotates with the master surface as deformation occurs. The small-sliding formulation is

adequate for the analyses conducted in this study because the sleeper, which is the master surface, remains essentially planar at all times and the relative displacement of slave nodes is minimal in the direction parallel to the master surface. The primary advantage of a small sliding formulation is that it is less expensive computationally than a finite sliding formulation.

As stated Section 3.2.2, the reference surface is specified to be at the mid-surface of the shell elements, that is, halfway through their thickness. Therefore, contact occurs in the analyses between the sleeper and the *reference* surface of the shell rather than between the sleeper and the *outside* surface of the shell. A correction could be implemented to place the reference surface on the outside of the shell by means of an 'offset' command. However, if this were done, any internal fluid pressure present would act on the outside surface of the pipe rather than on the inside surface. This obvious violation of reality is also not desirable. Consequently, the reference surface chosen is located at the mid-surface of the shell, which represents a simplification of the analysis. The effects of the simplification are judged to be inconsequential: the geometry of the reference surface and that of the outside surface will be insignificantly different because the wall thickness is small as compared to the diameter of the pipe. This is the case for all of the specimens analyzed.

### **3.2.5 Material Model**

The constitutive relationship in all of the numerical analyses is based upon stress-strain properties obtained from tests of tension coupons taken from the longitudinal direction of the specimens. However, for the particular case of sleeper-supported pipe a significant portion of the deformation observed in the laboratory tests relates to strains in the transverse (hoop) direction of the pipe. Nevertheless, the results of longitudinal coupons were used in the numerical analysis. The reason for the selection of longitudinal coupon results is that the testing procedure for coupons of this type is the simplest and least expensive of the ancillary tests described in Chapter 2. Furthermore, no undesirable effects are introduced into the stress-strain results by the flattening process that is necessary for coupons taken from the hoop direction. Finally, although the hydraulic ring expansion tests are expected to provide the best estimate of the material properties in the

hoop direction, it will be shown in Chapter 4 that the stress-strain relationship in the hoop direction is not substantially different in most cases from that of the longitudinal direction. Regardless of the testing procedure used, the steel in all of the specimens exhibits the classical stress-strain behaviour of ductile steel, namely an initially linear elastic region followed by plastic flow with hardening.

The material model chosen for use with ABAQUS is founded on the well-known von Mises yield surface, which has the form of a cylinder that is centred on the hydrostatic stress axis in three-dimensional principal stress space. (Inherent in this choice of yield surface is the assumption that compressive stress-strain properties are identical to those in tension.) For any constitutive relation for steel, a hardening rule must also be chosen. For this work, the hardening rule used is isotropic, that is, the yield surface expands uniformly about the hydrostatic stress axis as plastic straining takes place. The expansion of the yield surface is described by a multi-linear approximation of the true stress versus true strain relationship from the tension coupon tests. To obtain the true values of stress and strain, the following transformations are applied to the tension coupon data:

$$\sigma_{\text{true}} = \sigma_{\text{nom}} (1 + \varepsilon_{\text{nom}}) \quad [3-1]$$

$$\varepsilon_{\text{ln}}^{\text{pl}} = \ln(1 + \varepsilon_{\text{nom}}) - \frac{\sigma_{\text{true}}}{E}$$

where:

$\sigma_{\text{true}}$	=	true stress (force per actual unit area)
$\sigma_{\text{nom}}$	=	engineering stress (force per initial unit area)
$\varepsilon_{\text{nom}}$	=	nominal strain (engineering strain)
$\varepsilon_{\text{ln}}^{\text{pl}}$	=	plastic component of the logarithmic strain
$E$	=	elastic modulus.

In reality, a kinematic or mixed hardening model in which the yield surface can move in stress space is usually more descriptive of the true behaviour of steel. However, it is well known that the benefits of using a kinematic hardening model are most influential when stress reversals are present in the loading. Because the loading in the finite element model in this study is essentially monotonic, the isotropic model was selected. It is recognized that there will be a limited amount of localized unloading and

reloading as the contact surface changes shape, but this effect is judged to be insignificant.

### **3.2.6 Initial Geometry and Residual Stresses**

For all of the analyses, measured values of pipe wall thickness were used in the definition of the shell elements. This information was obtained from the mean of wall thickness measurement data gathered from the tension coupon and ring expansion specimens. Nominal values of sleeper length, pipe length and pipe diameter were used in the analysis since it is known that these did not vary significantly from the actual dimensions.

Although initial geometric imperfections or misalignments will always be present in a real specimen, no attempt is made to represent these in the numerical models. The rationale for this decision is that the measured imperfections in the laboratory specimens were small, as reported in Chapter 2. In addition, it was found that the specimens responded in a very stable fashion in the laboratory tests. Because of this stable behaviour, and since instability-induced failures are those most often affected by initial imperfections, it seems reasonable to neglect the initial imperfections for modelling the sleeper-support problem.

Residual stresses are usually present in pipes as a result of the forming and welding processes. However, no direct attempt was made to measure the initial level of residual stress in the specimens: existing methods of assessing average residual stresses would involve destructive testing, such as by sectioning the material into strips. This is obviously not practicable for the experimental specimens, so residual stresses are not included in the finite element models. The decision to omit residual stresses is further substantiated by the ring expansion tests: those residual stresses in the hoop direction are included in the stress-strain results of the ring expansion tests. A ring expansion test is analogous to a stub column test of a structural steel member in that some measure of the level of residual stresses is made, but there is no indication of the distribution of these stresses. (It should be appreciated that the residual stresses may vary through the thickness of the pipe wall and that those stresses in the longitudinal direction are substantially released when the rings are cut from the parent material.) Since it is reported

in Chapter 4 that the behaviour of the ring expansion specimens is not appreciably different from that of the tensile coupons, the residual stresses are likely to be of little consequence.

For those specimens that were seam-welded, the weldment location in the tests was at 90 degrees to the sleeper. Therefore, it is expected that the effect of residual stresses arising from the welding process is negligible because of their physical distance from the loaded area. Additionally, since no significant asymmetric behaviour was observed in the full-scale laboratory tests it is reasonable to say that residual stresses arising from welding did not play an important role in the behaviour.

### **3.2.7 Mesh Selection and Refinement**

Several different finite element models with varying levels of mesh refinement were investigated prior to the selection of the 'optimal' mesh configuration (which is that mesh illustrated in Figures 3.1 and 3.2). The author judges the optimal finite element model to be the most economical model in terms of processor time costs while still maintaining very good solution accuracy.

To establish which configuration of mesh is the best, it is first useful to obtain the most numerically accurate solution possible. This solution can then serve as a benchmark by which other options can be judged. The mesh illustrated in Figure 3.3, termed the 'Refined Mesh' herein, contains nearly the maximum number of degrees of freedom that can be accommodated by the computer hardware available. Therefore, it is expected to provide the most accurate solution practicable.

In the Refined Mesh the element density is significantly greater in the region of contact than elsewhere. This is necessary in order to model the contact condition between the sleeper and the pipe accurately, as described in Section 3.2.4. The contact region, which is shaded in Figure 3.3, is 28 elements in the circumferential direction by 48 elements in the longitudinal direction. These elements sweep an arc of  $52.5^\circ$  in the 1-2 plane around the circumference, and their total length in the 3-direction is always  $1.4b$ , where  $b$  is the length of the portion of the sleeper that is modelled. To make the transition from low mesh density to higher mesh density, a linear constraint equation is used along the inter-element boundary. In this way the degrees of freedom at the central node, which

is a part of the higher density mesh, are interpolated linearly from the two adjacent nodes that bracket it.

Shown in Figure 3.4 is the ‘Coarse Mesh.’ This mesh was developed to determine an approximate lower limit on the amount of refinement that must be used in the discretization. Because this mesh is so coarse, especially in the region of contact, it is expected to give only marginally adequate results as compared to the Refined Mesh. Several other models having intermediary mesh densities were also investigated until one mesh was identified as optimal. For this mesh, the contact region is 14 elements in the circumferential direction by 24 elements in the longitudinal direction. The remainder of the mesh matches the Coarse Mesh in element density. The Optimal Mesh layout is illustrated in Figure 3.5.

Although it would be most accurate to use the Refined Mesh always, it is not practical for repeated analyses because of its excessive demands upon computer resources. On this basis it is deemed unacceptable. Other meshes can be compared with the Refined Mesh by examining the overall load-versus-displacement response of the system, as shown for specimen S1 in Figure 3.6. At early stages of the analyses, all of the models give approximately the same load-displacement response. However, later in the analysis the equilibrium path for the Coarse Mesh model becomes erratic. Such behaviour of a coarse mesh under similar loading conditions is also demonstrated in an example problem entitled “Crushing of a Pipe” provided in the software documentation (HKS, 1997d). This type of erraticism in the solution is attributed to the inability of the coarsely discretized contact region to assume the true, complicated, deflected shape of the pipe (because contact constraints are enforced only at the nodes). The Coarse Mesh was rejected for this reason. The equilibrium path for the Optimal Mesh is also slightly erratic at large levels of sleeper displacement, but its behaviour represents a significant improvement over that of the Coarse Mesh. Because the magnitude of the effect is small except at very severe displacements (far beyond those that would be considered allowable in field applications), the problem is judged not to affect the validity of the solutions, particularly at earlier stages of the analysis.

Cross-sectional distortion is also a limit state in the design process, so it is important to assess the three models in their relative ability to predict cross-sectional shape. Figure 3.7 demonstrates the relationship between sleeper displacement and out-of-roundness for the Refined, Coarse, and Optimal meshes. It is apparent that all of the models give similar results, so the level of mesh refinement does not seem to play a major role in the prediction of cross-sectional shape.

On the basis of the information presented in this section the Optimal Mesh was chosen for all finite element analyses of the full-scale laboratory specimens. The decision to use this mesh was further justified later when the analyses gave results that compared favourably with the test data. Results from the laboratory tests and from the numerical analyses are presented and discussed in Chapter 4.

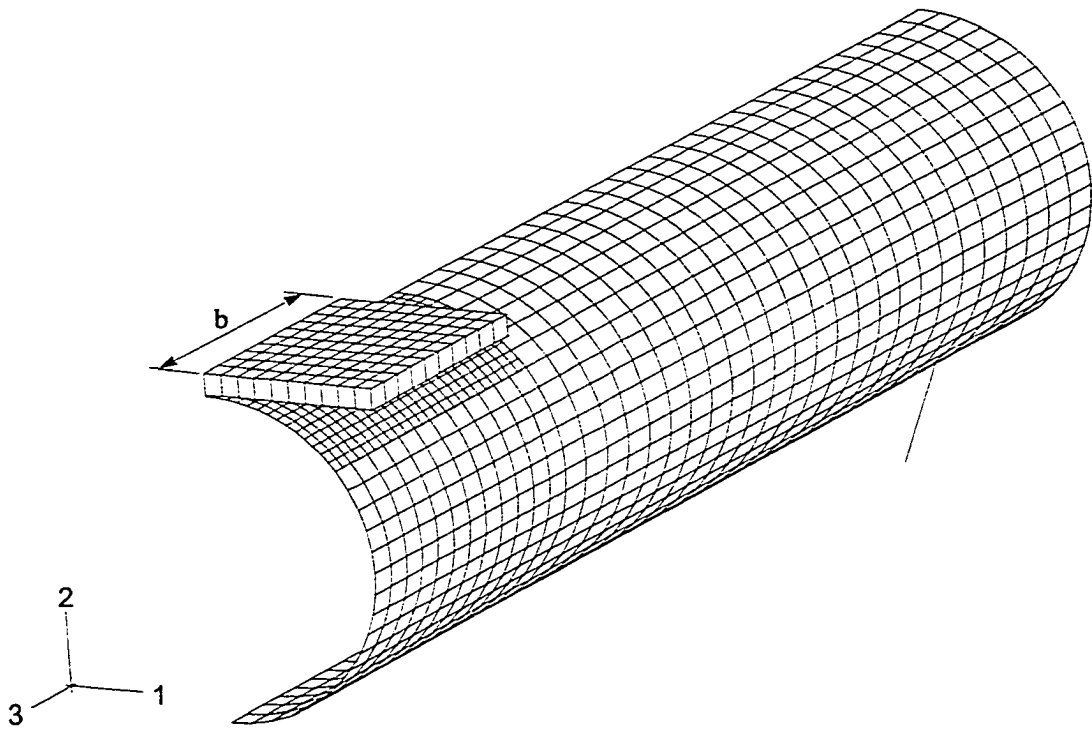


**Figure 3.1** Overall finite element mesh

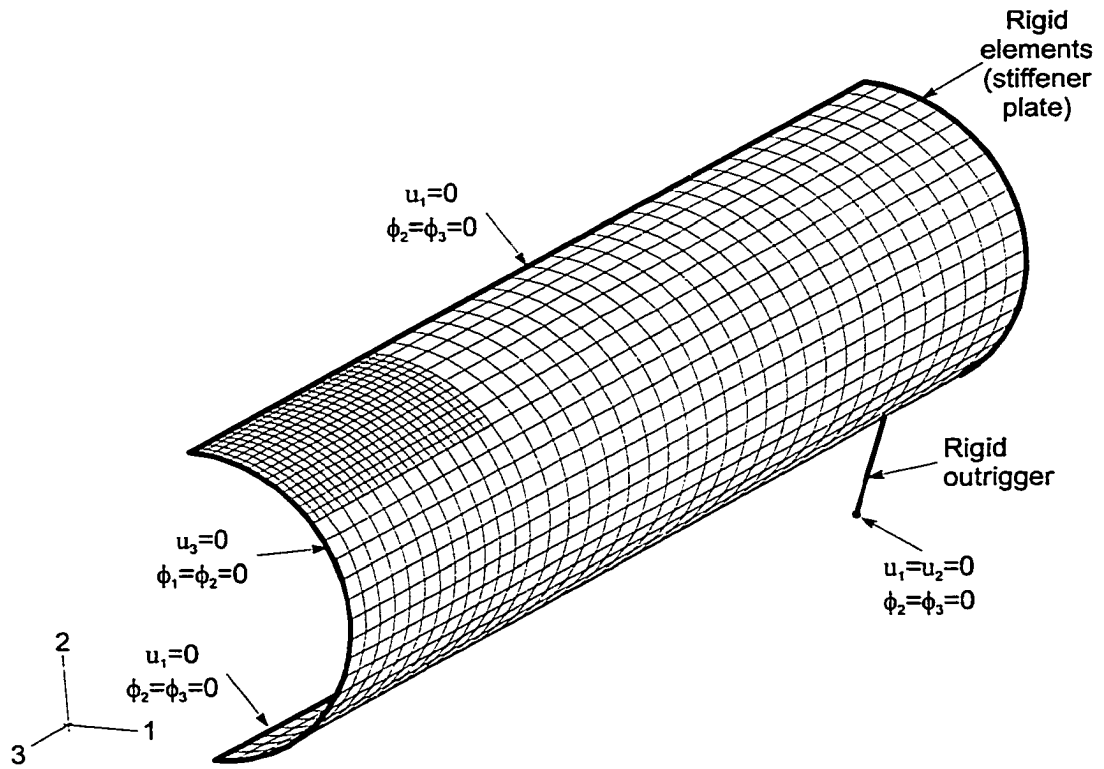


**Figure 3.2** Kinematic boundary conditions

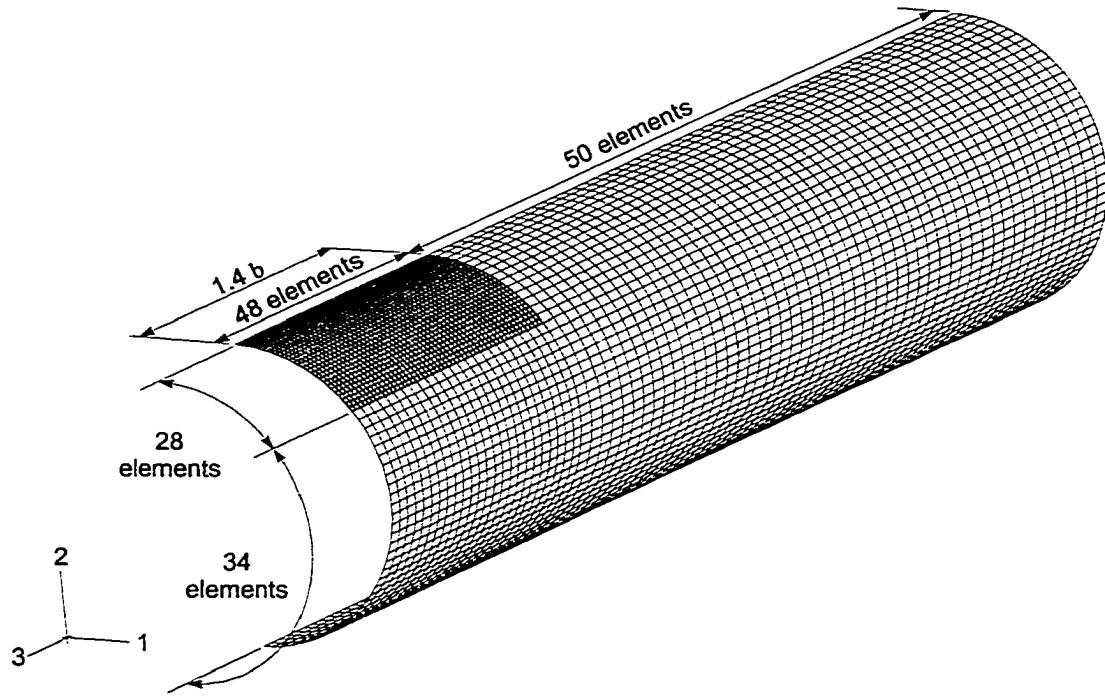


**Figure 3.3** Refined Mesh layout

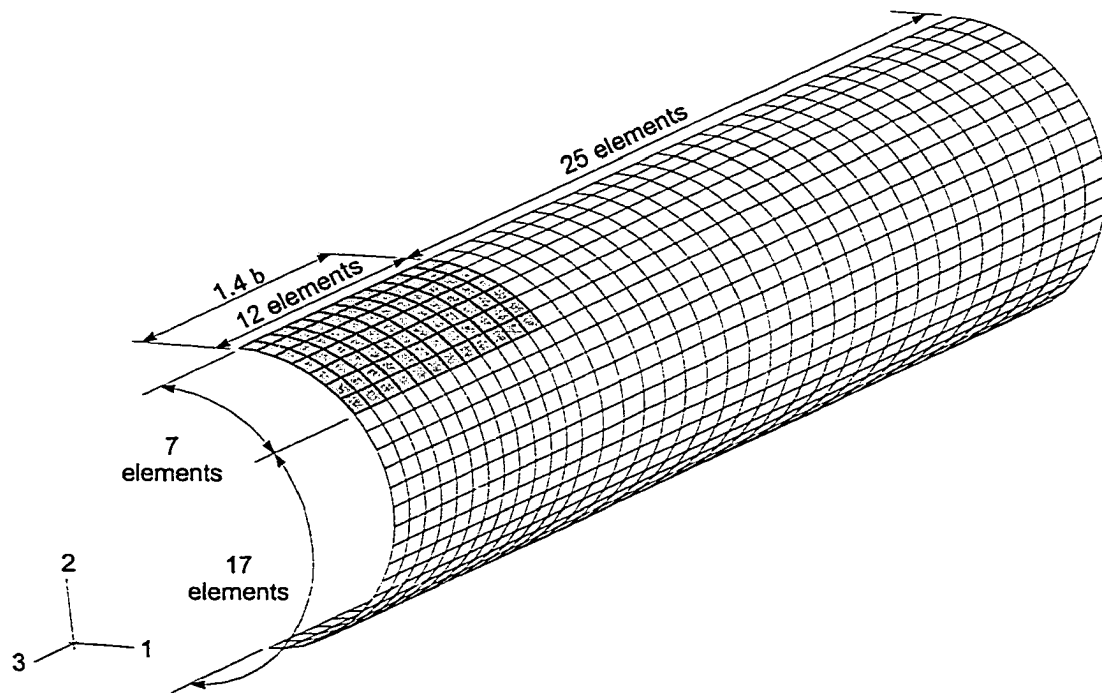


**Figure 3.4** Coarse Mesh layout

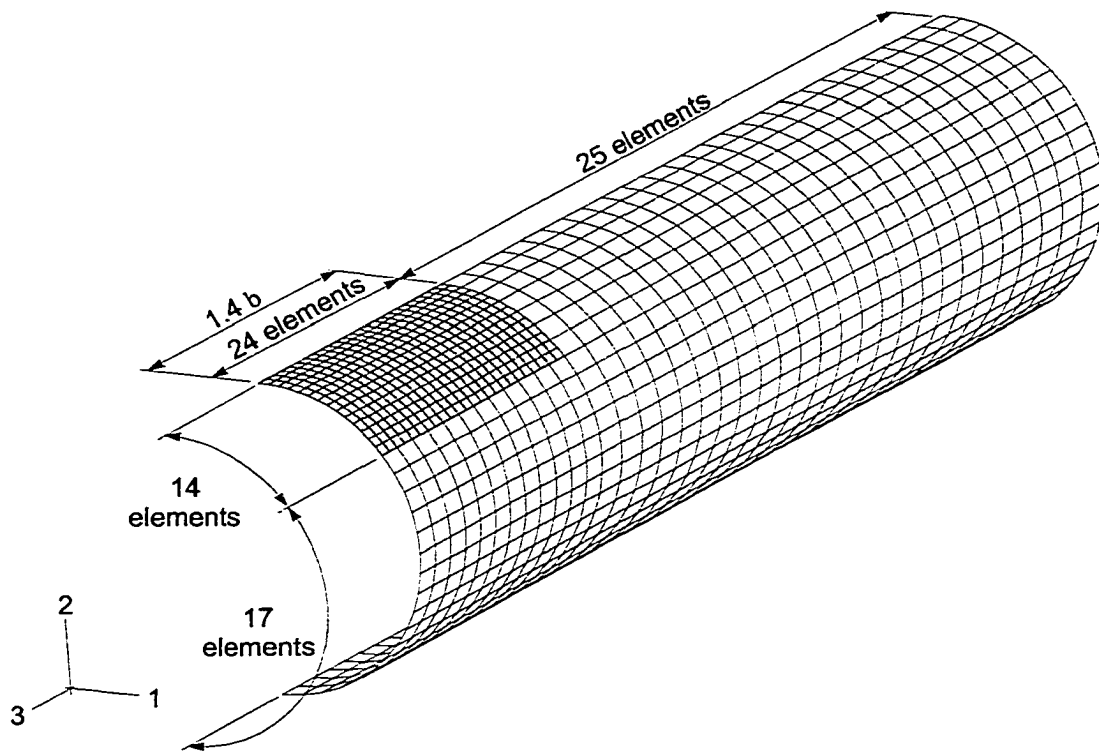


**Figure 3.5** Optimal Mesh layout

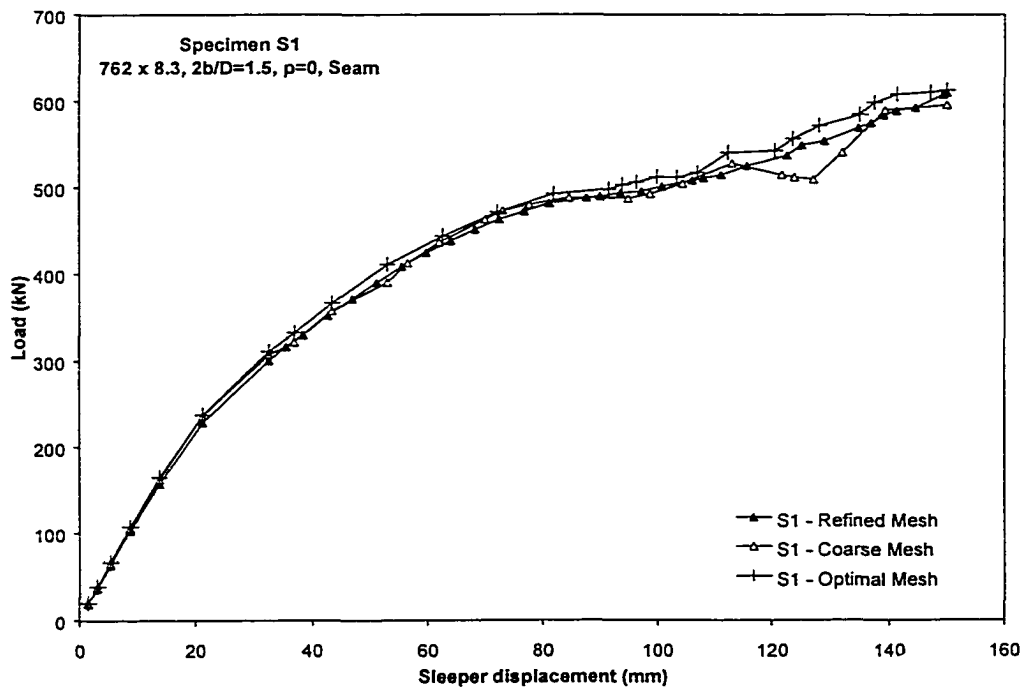


**Figure 3.6** Correlation of strength behaviour

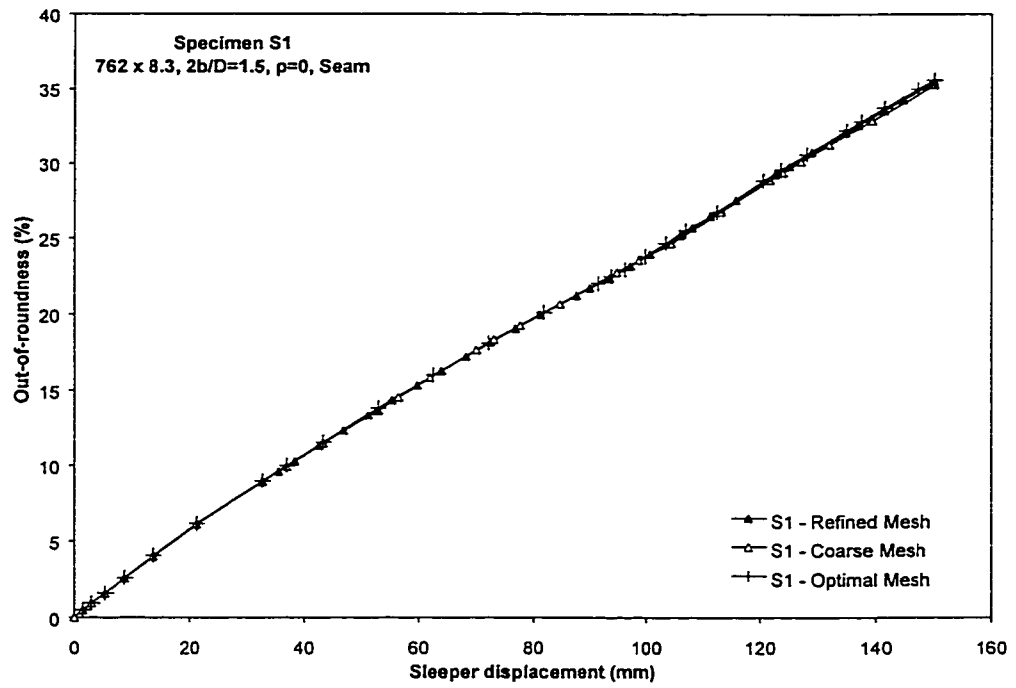


**Figure 3.7** Correlation of distortional behaviour

## **4 DISCUSSION OF EXPERIMENTAL AND NUMERICAL RESULTS**

This chapter reports and characterizes the results from the full-scale tests of sleeper-supported pipes along with the associated ancillary material tests. Numerical analyses of the full-scale test specimens were described in Chapter 3, and the findings from these analyses are discussed in this chapter. Comparisons of the numerical results with those results obtained from the laboratory tests are also presented. Throughout the chapter, postulations are made regarding the underlying fundamental mechanisms that control the behaviour of the sleeper-supported pipes.

### **4.1 RESULTS: FULL-SCALE LABORATORY TESTS**

#### **4.1.1 Qualitative Observations**

In the 11 full-scale tests of sleeper-supported line pipes the response of all specimens can be characterized as both extremely stable and ductile. All tests were carried out to a level of sleeper displacement in excess of 100 mm, which should represent a case at least as severe as any that might realistically be expected in field conditions. At no time during the loading history was there any indication of material distress that would threaten the pressure integrity of the base metal or weld metal of any specimen. However, the magnitude of cross-sectional distortion was considerable.

The region of contact between the sleeper and the pipe is initially a straight line in the longitudinal direction of the specimen. As the sleeper is displaced, the pipe cross-section begins to distort, particularly by flattening in the region of contact. The effects of internal pressure begin to control the behaviour at this stage: unpressurized specimens respond in a different manner than those that are pressurized. For the unpressurized specimens, the pipe deforms next in such a way that a pair of contact lines develops separated by a gap where the pipe moves away from the sleeper along the centreline of the bearing area. During this process, the top of the pipe reverses in curvature or ‘snaps through’ to reach a new equilibrium configuration. This deformed configuration is stable, and the load-carrying capacity of the pipe is maintained indefinitely as the sleeper support displacement increases. In Figure 4.1(a) the gap is

clearly evident along the centreline, and Figure 4.1(b) illustrates how the contact region changed during the course of the test.

For specimens S3 and S9 the presence of internal pressure prevented the pipe wall from reversing in curvature along its centreline of contact with the sleeper. A different mechanism of displacement takes place for these specimens: as the sleeper displacement becomes large, bulges develop in the pipe wall at the edges of the sleeper support. These bulges can be observed visually; one is illustrated in Figure 4.2. Driving the formation of the bulges are a combination of localized sleeper-to-pipe contact stresses, the high level of tensile circumferential stress induced by internal pressure, and the axial compressive bending stresses. These stresses result in inelastic behaviour in the region of the bulge, which effectively decreases the stiffness of the pipe wall. With the reduced level of stiffness locally, the pipe wall is no longer able carry the longitudinal compressive bending stress and it begins to buckle outwardly, forming a bulge. As expected, the magnitude of the bulges increases approximately in proportion with the displacement of the sleeper support. In turn, the bulges reduce the overall bending stiffness of the pipe in its role as a beam between the support reactions. Subsequent displacement of the sleeper principally causes overall bending deflection rather than further cross-sectional distortion.

#### **4.1.2 Quantitative Observations**

##### ***4.1.2.1 Consideration of Random Errors***

A variety of sources of error can affect the results of any type of experiment. Errors can be categorized as blunders, random errors, or systematic errors (see, for example, Sabnis et al., 1983). Blunders are outright mistakes that must be avoided; random errors manifest themselves as the statistical variation of measured quantities as a result of some, possibly unknown, underlying controlling mechanism; a systematic error always has the same algebraic sign, causing a measured quantity to be shifted from the true (or desired) value. While it is not the intention of the author to provide an in-depth description of error analysis, it is obvious that prudence dictates a discussion be made of the influences that such errors might have on the experimentation reported herein.

Every reasonable effort has been made to ensure that no blunders exist in the experimental program, and, to the author's knowledge, all systematic errors of constant

magnitude have been removed by subtracting initial measurement values from final measurement values. Other systematic errors, such as those caused by inaccurate calibration of a measuring device, are difficult to detect and should be treated as blunders.

The effects of random errors, which can be controlled by selecting measuring devices with appropriate accuracy, can also be estimated and tracked in a meaningful way. To do this, an estimate of the random error of each measuring device must be made based upon information provided by the manufacturer, or through engineering judgement, or both. It is then necessary to track the influence of these random errors as the measurements are used in subsequent calculations. The equation for propagation of random error through calculations is derived from the well-known theory of least squares (see, for example, Davis et al., 1982):

$$e_G = \sqrt{\left(\frac{\partial G}{\partial a} e_a\right)^2 + \left(\frac{\partial G}{\partial b} e_b\right)^2 + \left(\frac{\partial G}{\partial c} e_c\right)^2 + \dots} \quad [4-1]$$

where:

G	=	a function of measurement variables a, b, c...
a, b, c...	=	independent measurement variables
e <sub>G</sub>	=	error associated with the resultant of the function G
e <sub>a</sub> , e <sub>b</sub> , e <sub>c</sub> ...	=	error associated with each measurement variable.

Estimates of error for the various measuring devices used in the experimentation are presented in Appendix A along with sample calculations for the error associated with parameters such as out-of-roundness.

For most of the work reported herein, the measurements taken during the tests have small error relative to their magnitude. This was accomplished by selecting appropriate measuring instruments for the task at hand. For these cases, the influence of random errors is minimal and can be neglected. However, there are some instances in which random errors become significant even when the accuracy of the measuring devices is acceptable. For example, relative errors can become unacceptably great when one large measurement value is subtracted from another: the resulting residual can be quite small as compared to the accuracy of the measuring device. For the test results reported in the following sections, a discussion of error is provided whenever its influence is deemed to be of significance.

#### **4.1.2.2 Load versus Sleeper Displacement**

The most useful measure of the overall behaviour of the specimens is the relationship between the applied load and sleeper displacement, as shown in Figures 4.3 through 4.13. (Note that different scales are used in each of the charts in Figures 4.3 through 4.13. Results from the finite element analyses are also shown in these charts and are discussed in Section 4.3.) Sleeper displacement was controlled in the tests and is thus considered to be the independent variable in the figures. Even at magnitudes of sleeper displacement far beyond those that would be expected in a field installation, the unpressurized specimens did not reach a limit point (a point of zero stiffness) on the load-displacement curve. However, limit points would surely have been identified if the loading apparatus were capable of accommodating larger sleeper displacements.

An idealized load-displacement relationship developed from the observed experimental and numerical results for a typical unpressurized specimen is illustrated in Figure 4.14. In the first region shown in the figure the pipe behaves in an elastic manner and the magnitudes of the displacements are small. Consequently, the load-displacement relationship is approximately linear. As the magnitude of sleeper displacement increases, localized inelastic behaviour begins to reduce the overall stiffness of the system, which is represented by Region 2 in the figure. This postulation is supported by the level of strain measured by strain gauges in the laboratory tests and also by the strains computed in the finite element analyses. The loss of stiffness exhibited in Region 2 is compounded by a reduction of the moment of inertia as a result of cross-sectional distortion. Eventually, a plateau on the load-displacement curve develops that represents a condition of essentially zero stiffness of the system. This is Region 3 in Figure 4.14. Experimental measurements show that this plateau begins approximately at the same time as the initiation of reversal of pipe wall curvature, that is, when the gap opens between the pipe and the sleeper along the longitudinal centreline of contact. This effect is most pronounced for specimen S5. In Figure 4.15, the load versus sleeper displacement behaviour for specimen S5 is shown along with the corresponding size of the gap that opens between the sleeper and the pipe at mid-span. It is evident that the rapid increase in gap size occurs concurrently with the plateau of reduced stiffness. This is true both for the experimental and the numerical results. In the figure, vertical error bars are shown for the measured values of gap size

because the error associated with these measurements is estimated to be  $\pm 1.5$  mm, which is large in proportion to the size of the gap. Calculations of this error are given in Appendix A. After the plateau, stiffness begins to increase again as the rate of increase of gap size decreases (see Figure 4.15). Therefore, it is hypothesized that the pipe undergoes a form of local inelastic snap-through, where stiffness is lost during the snap-through process (Region 3). Stiffness is then regained once the top of the pipe reaches the more stable snapped-through configuration (Region 4).

For the unpressurized specimens, there is only one exception to the idealized load-displacement relationship illustrated in Figure 4.14: specimen S2, which is a 762 mm diameter pipe with a nominal wall thickness of 16.4 mm. For this specimen, there is no discernible plateau on the load-displacement curve (see Figure 4.4). The specific causes for the unique behaviour of specimen S2 are not clear, but it is believed that its particular geometric parameters—the wall thickness is great and the sleeper size is large—are such that a plateau does not develop. Results from subsequent finite element modelling of this specimen also do not show evidence of a plateau, even with a maximum sleeper displacement of 300 mm.

Two of the unpressurized specimens, S4 and S10, were unloaded after the behaviour was well into the non-linear range. These specimens were then reloaded. This was done in order to assess the behaviour during a full cycle of loading and unloading. Upon reloading, the load-displacement equilibrium path for each specimen appears to have resumed its original course. The cycle of loading and unloading is clearly evident in Figures 4.6 and 4.12.

For the pressurized specimens, S3 and S9, the load-displacement behaviour is influenced drastically by the presence of the internal pressure. Load-carrying capacity is enhanced significantly, as is the overall stiffness of the system. However, a limit point on the load versus sleeper deflection curve is evident for specimen S3, and specimen S9 appears to be approaching a condition of zero stiffness (see Figures 4.5 and 4.11, respectively). The loss of stiffness is attributable to the formation of the bulges at the edges of the sleeper support, as described in Section 4.1.1. The limit point is reached only at values of deformation far beyond those that would be considered allowable in a field

installation, however. This suggests that serviceability limits states rather than ultimate limit states govern the design of sleeper-supported pipeline systems.

After the load carried by the specimen ceased to increase, the internal pressure in each of specimens S3 and S9 was reduced to zero while sleeper displacement was held constant. This was done in order to assess the influence that depressurization has on the behaviour. Upon returning the internal pressure to its full original value (8450 kPa), the displacement of the sleeper was again increased. The cycle of releasing and restoring internal pressure is evident as a vertical line in each of Figures 4.5 and 4.11. For each case, it appears that the equilibrium path resumed its original course after the pipe was repressurized to its initial value.

#### ***4.1.2.3 Out-of-Roundness versus Sleeper Displacement***

Before assessing the cross-sectional distortion of the specimens, it is necessary to choose a means of describing that distortion. Throughout the remainder of this report out-of-roundness is used as the criterion. The reason for this selection is multi-faceted: out-of-roundness is a useful descriptor of the likelihood of cross sectional collapse; standards such as Det Norske Veritas (1996) use the out-of-roundness equation [1-12] exclusively; in industrial practice, out-of-roundness is often used as the primary distortion criterion in the design process.

To assess the deformational behaviour of the specimens, it is useful to consider the relationship between out-of-roundness and sleeper displacement, as shown in Figures 4.16 through 4.26. (Out-of-roundness measurements are not available for specimens S4 and S8 because of instrumentation failure. However, the results obtained from the finite element analyses for these specimens, which will be discussed in Section 4.3, are shown.) The measurements of out-of-roundness are taken from a cross-section at mid-span of the pipe: out-of-roundness has maximum value at this section because the magnitude of the gap that forms along the centreline is greatest at this location. Where error is judged to be significant, appropriate error bars are shown for the out-of-roundness data in the figures.

In general, the relationship between out-of-roundness and the magnitude of the sleeper displacement is linear. This suggests that the level of out-of-roundness is controlled principally by the magnitude of sleeper displacement rather than by the

amount of load transferred, as it is clear from Figures 4.3 through 4.13 that load is not related linearly to sleeper displacement after yielding begins.

For the two pressurized specimens, S3 (Figure 4.18) and S9 (Figure 4.24), the relationship between out-of-roundness and sleeper displacement can be characterized as bi-linear. Initially, out-of-roundness increases rapidly with sleeper displacement, although the magnitude of the distortion is considerably less than that for the unpressurized specimens. As inelastic material behaviour becomes significant (at a displacement of about 50 mm for Specimen S3 and 25 mm for S9), the rate of change of out-of-roundness with respect to sleeper displacement decreases substantially. The formation of the bulges at the edges of the sleeper, which is described in Section 4.1.1, is believed to cause the decreased rate of out-of-roundness. As the bulges form, the ability of pipe wall to carry compressive stresses in the vicinity of the bulge is compromised, decreasing the stiffness locally. This effect leads to a corresponding decrease in the overall flexural stiffness of the member so that subsequent vertical displacement of the sleeper results primarily in overall pipe bending rather than local cross-sectional deformation. The rate of cross-sectional distortion is thereby reduced.

It is clear that pressure-induced stiffening of the pipe plays an important role in preventing cross-sectional distortion, as seen in the results for specimens S3 and S9. The slopes of the initial portion of the out-of-roundness versus sleeper displacement curves are much less steep than those for the unpressurized specimens. Maximum out-of-roundness for these specimens has a value less than 10%, whereas all other specimens exceed this value by at least a factor of two.

## **4.2 RESULTS: ANCILLARY MATERIAL TESTS**

As discussed in Chapter 2, most line pipes, including the specimens tested in this study, are cold-rolled into shape. This process and other aspects of their manufacture can alter the material properties of the finished pipe significantly as compared to those of the virgin steel coil or plate. Of particular interest in this study is the initial portion of the stress-strain curve, which is of primary importance in the definition of the isotropic hardening material model used in the numerical analyses. The engineering stress-strain curves, up to a level of 2.5% strain, from all of the ancillary tests are presented in Appendix B.

#### 4.2.1 Tension Coupon Test Results

Four tension coupons were taken from each specimen: two aligned with the longitudinal direction of the pipe, and two with the transverse direction. Those taken from the transverse direction were flattened prior to testing.

None of the flattened tension coupons exhibit a well-defined yield point or yield plateau. Instead, a sweeping curve joins the linear elastic region to the hardening region on the stress-strain curve. This behaviour is consistent with those results reported in the literature for flattened tensile coupons (see, for example, Saikaly et al., 1996). Because such a curve does not exhibit a well-defined yield plateau, it is standard practice in the pipeline industry to choose the stress corresponding to a strain of 0.5% as the yield strength. This value is not of particular scientific interest, but it does provide a simple characterization of the material behaviour.

It is likely that the lack of a well-defined yield plateau is primarily a result of the flattening process. During flattening, the level of inelastic deformation induced varies through the thickness of the coupon. This gives rise to different levels of axial residual stresses through the thickness. When the coupon is loaded in tension, those portions of the cross-section that contain tensile residual stresses begin to yield first. In turn, other portions of the cross-section yield as the tensile load increases. The varied onset of yielding manifests itself as the loss of a well-defined yield plateau on the stress-strain curve. For the flattened coupons, the Bauschinger effect might reduce the tensile yield strength of those areas of the cross-section that were yielded in compression during the flattening process. Taking into consideration all of these factors, it is judged that results from transverse coupon tests should not be used in the development of a finite element constitutive model because they are not representative of the actual stress-strain relationship for the material.

A well-defined yield point is observed on the stress-strain curves for most of the longitudinal tension coupons, but there is a gradual curve joining the elastic and inelastic regions in some cases. The author believes that different pipe manufacturing processes—alloying elements, rolling method, pressurization for quality assurance, etc.—are the source of the difference in behaviour among specimens. Because no flattening is

required, the longitudinal coupons are believed to give a representative description of material behaviour.

#### **4.2.2 Hydraulic Ring Expansion Tests**

The fluid pressure in a hydraulic ring expansion test causes a uniaxial tensile stress to develop around the circumference of the pipe. In this way, the material properties in the hoop direction can be evaluated directly. Unlike a transverse tension coupon test, no flattening process is required. Consequently, ring expansion testing is the preferred method for obtaining unbiased material properties for the hoop direction of circular tubular members.

It appears, at first glance, that the ring expansion method is vastly superior to the flattened tension coupon approach, but there are practical disadvantages. For example, the entire stress-strain curve can not be obtained when using the hydraulic ring expansion method: if radial expansion becomes too great, lateral contraction of the ring caused by Poisson's ratio effects can result in fluid leakage. Although friction between the rubber gasket and the plates should be minimal, it is not possible to assess the magnitude of any effect that might be present. Furthermore, the problem of friction will be compounded if the machining of a ring is not done within specifications or if there are other alignment problems: there may be direct steel-to-steel friction between the ring and the plates.

In addition to these systemic disadvantages of the method, it must be recognized that the data acquisition and control systems for ring expansion testing used at IPSCO are not well suited for scientific research. Given that the equipment was loaned, the author was not at liberty to make modifications to it. Consequently, limitations exist in the hydraulic ring expansion test results obtained in this study, as described below.

Because the strength of steel increases significantly with the rate of plastic straining, it is essential in a material test that 'static' stress values be recorded. This is done by holding the rate of straining in the steel at zero until the load, and thus the stresses, reach a minimum value. Dynamic stress values can be up to 15% greater than the static values, depending on the strain rate and the type of steel (Galambos, 1998). Because the static stress represents the minimum strength of the material, it is obvious that this value must be used to describe material strength in a static structural analysis. However, the IPSCO hydraulic ring expansion testing system is controlled by hydraulic

pressure alone, and there is no electronic feedback system by which displacement can be the controlling variable. Consequently, it was not possible to hold the level of strain in the ring at a constant value periodically throughout the test in order to record static stress values. Because the hydraulic pressure is controlled by manual adjustment of the air supply to an air-driven water pump, it was also not possible to establish a consistent rate of straining in the ring. This means that the influence of strain rate is not of constant magnitude throughout a particular test. In order to limit the severity of these effects, the tests were conducted at the slowest strain rate practicable. However, the rate was still too great to allow its influence to be neglected. These limitations severely hamper the usefulness of the data for scientific applications.

The results for the ring expansion tests taken from specimens S5 through S11 are presented in Appendix B. (Recall that rings of material from specimens S1 through S4 were not available.) With the limitations of the method in mind, it is reasonable to say that the hydraulic ring expansion tests give results that are, in most cases, similar to those of the longitudinal tension coupons. Because of this similarity, the stress-strain curves obtained from the longitudinal tension coupons were selected for use in the finite element analysis models. The advantage of using the longitudinal coupon results is that there is confidence that controlled and consistent testing methods were used that provide clearly defined static stress values.

As an aside, it is often reported in the literature that the yield stress obtained for a particular pipe specimen in a hydraulic ring expansion test is greater than that obtained using a flattened coupon. The difference between the results of flattened transverse tensile coupons and hydraulic ring expansion testing is most often attributed solely to the Bauschinger effect, with no consideration given to the testing procedure itself or the influence of residual stresses that develop during the flattening process (Llewellyn, 1992; Mak and Tyson, 1998; Saikaly et al., 1996; Shoemaker, 1984; Streisselberger et al., 1992). However, as stated previously, the author contends that the residual stresses that develop in the longitudinal direction of the tension coupon during the flattening process will have a significant influence on the observed behaviour and should not be ignored. Furthermore, a number of factors may influence the results of hydraulic ring expansion tests that would tend to cause an overestimate of material strength, such as the presence

of friction between the ring and the sandwich plates. The author believes that much valuable information about the fundamental characteristics of pipeline steels can be gained through ring expansion tests in a study that is conducted properly. Unfortunately, the development of the required testing regimen and apparatus is beyond the scope of this research. In such a study, the test procedures could be improved over those reported herein by using an electronic feedback loop to a control system that operates a servovalve on the hydraulic pressure supply. This would allow the rate of straining to be controlled and enable the user to obtain static yield stress measurements. Further research in this area is recommended.

### **4.3 RESULTS OF MODELLING AND COMPARISON WITH LABORATORY TESTS**

To assess the accuracy of the results provided by a finite element model, it is instructive to make a visual comparison of the deformed shape of the model with that of the actual test specimens. Such a visual comparison indicates whether the overall deformational mechanism predicted by the model matches reality. Additionally, it is necessary to select certain measures by which the performance of the model can be measured quantitatively. For this work, load versus sleeper displacement and out-of-roundness versus sleeper displacement are useful relationships that measure of the overall performance of the numerical model. Using these relationships, criteria related to both strength and deformational behaviour of the finite element model can be assessed.

#### **4.3.1 Qualitative Observations**

Illustrated in Figures 4.27 and 4.28 is the progression of deformation predicted by the finite element model for typical unpressurized and pressurized specimens, respectively. In qualitative terms, the models account appropriately for the change in contact conditions that were observed in the laboratory tests. For the unpressurized systems, a gap opens between the sleeper and the pipe along the longitudinal centreline, which is the same deformational mechanism observed in the laboratory. This gap is illustrated best in a cross-sectional view taken from the finite element analysis results, as shown in Figure 4.29. The similarities in the overall deformed shape are clearly evident when one compares Figure 4.29 with the photographs shown in Figure 4.1. Furthermore, for specimen S5, the size of the gap predicted by the analysis corresponds reasonably

well with that measured in the experiment (see Figure 4.15), which also supports the validity of the numerical results.

For the pressurized specimens the fluid forces the pipe to remain in contact with the sleeper over a large area. Consequently, a gap does not form. The outward bulge at the edge of the sleeper that developed in laboratory specimen S3 (Figure 4.2) also appears in the finite element model (Figure 4.30). Similar behaviour was observed for the other pressurized specimen, S9.

### **4.3.2 Quantitative Observations**

Finite element predictions of the behaviour for all 11 specimens are presented graphically in terms of load versus sleeper displacement in Figures 4.3 through 4.13. It is evident that the predicted load-versus-displacement characteristics correlate very well with those obtained from the laboratory. Some differences are noted, however, particularly for those unpressurized specimens that have a large value of  $D/t$  (see Table 2.1). In these cases, the finite element model is somewhat stiffer than the actual specimen, but not to a great extent. The finite element solutions for the unpressurized specimens show evidence of the four distinct regions of behaviour that are apparent in the laboratory tests: linear elasticity, initial yielding, snap-through, and post snap-through stiffening (see Figure 4.14). Specimen S2 is an exception to this trend, as described in Section 4.1.2.2.

The equilibrium path is somewhat erratic for a few of the analyses, due in part to the incremental iterative nature of the solutions and also to the complicated geometry in the region of contact between the sleeper and the pipe. For example, in Figure 4.12 the equilibrium path for specimen S10 becomes slightly erratic as nodes either touch or lose contact with the sleeper surface. Confirmation that the nodal density is the underlying cause of this effect was demonstrated in Section 3.2.7. An erratic equilibrium path is also evident to some degree for most of the other unpressurized specimens, but is judged not to have an adverse affect on the validity of the results. For the pressurized specimens, the correlation between test and numerical results is good, as shown in Figures 4.5 and 4.11. The presence of internal pressure tends to make the system more stable and decreases the complexity of the deformed shape in the contact region, which results in a smoother equilibrium path.

The ability of the numerical analyses to predict distortion is also very good, as shown in Figures 4.16 through 4.26. For the unpressurized specimens, the finite element model is able to reproduce both the linear relationship between out-of-roundness and sleeper displacement as well as an appropriate slope for the line. The approximately bi-linear relationship that is observed in the laboratory results of the pressurized specimens is also represented well by the finite element models, as demonstrated in Figures 4.18 and 4.24.

Based upon the information presented in this section, it is reasonable to conclude that the behaviour of the actual specimens and that predicted by the numerical models are very similar. This is true from the point of view of both overall strength and cross-sectional distortion criteria. Therefore, the methods described herein are judged to form the basis of a general modelling technique that appropriately predicts the behaviour of sleeper-supported pipes in the laboratory. At the same time, the need for accurate solutions is balanced with the processor-time costs of the analysis. The author believes that the method has proved itself to an extent that it is reasonable to extrapolate beyond the existing test data so that other piping and sleeper configurations can be examined. This is done in Chapter 5, in which an idealized *in situ* model for sleeper-supported piping is developed.

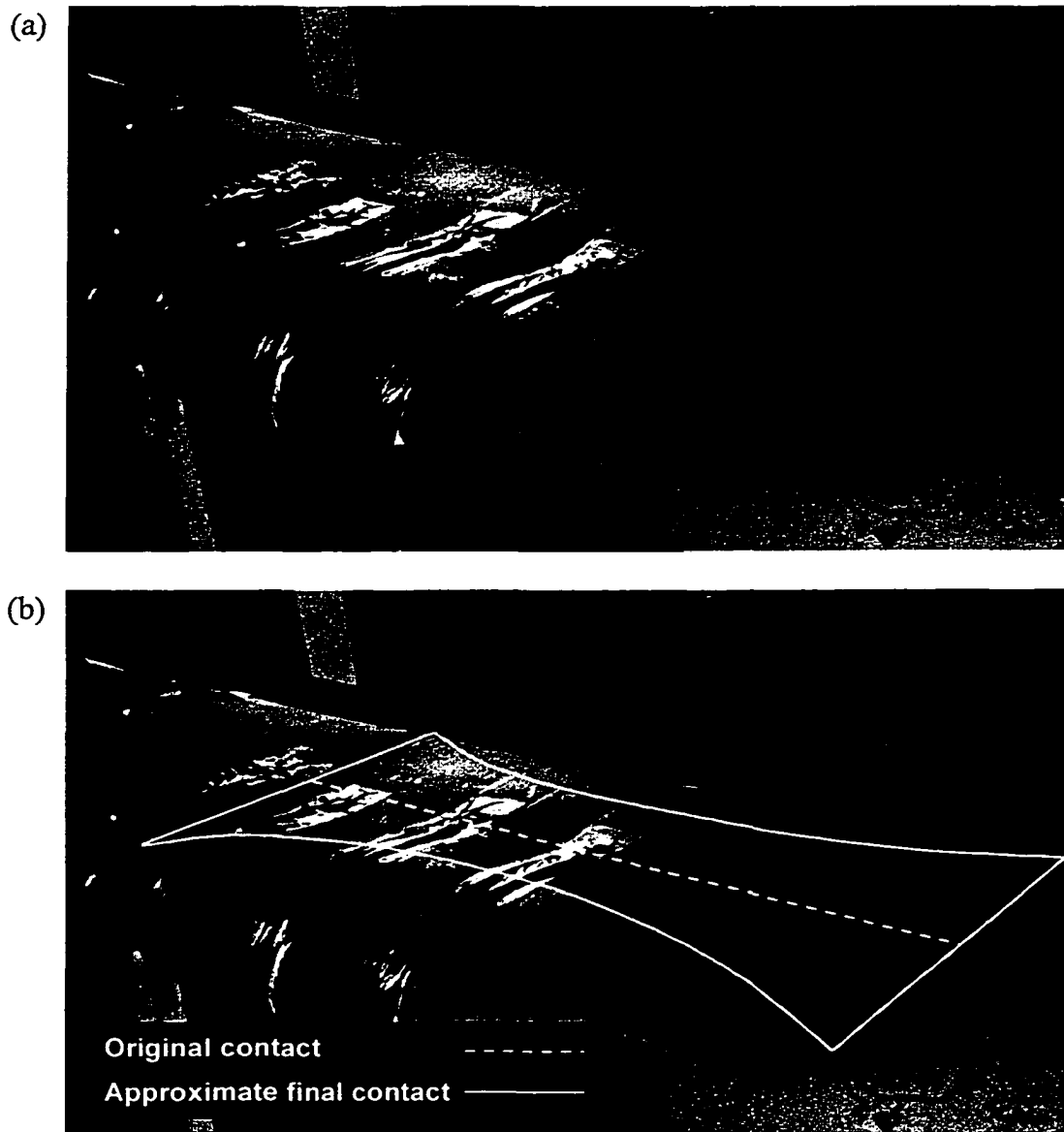


**Figure 4.1** Typical deformation of sleeper-to-pipe contact region, unpressurized specimen

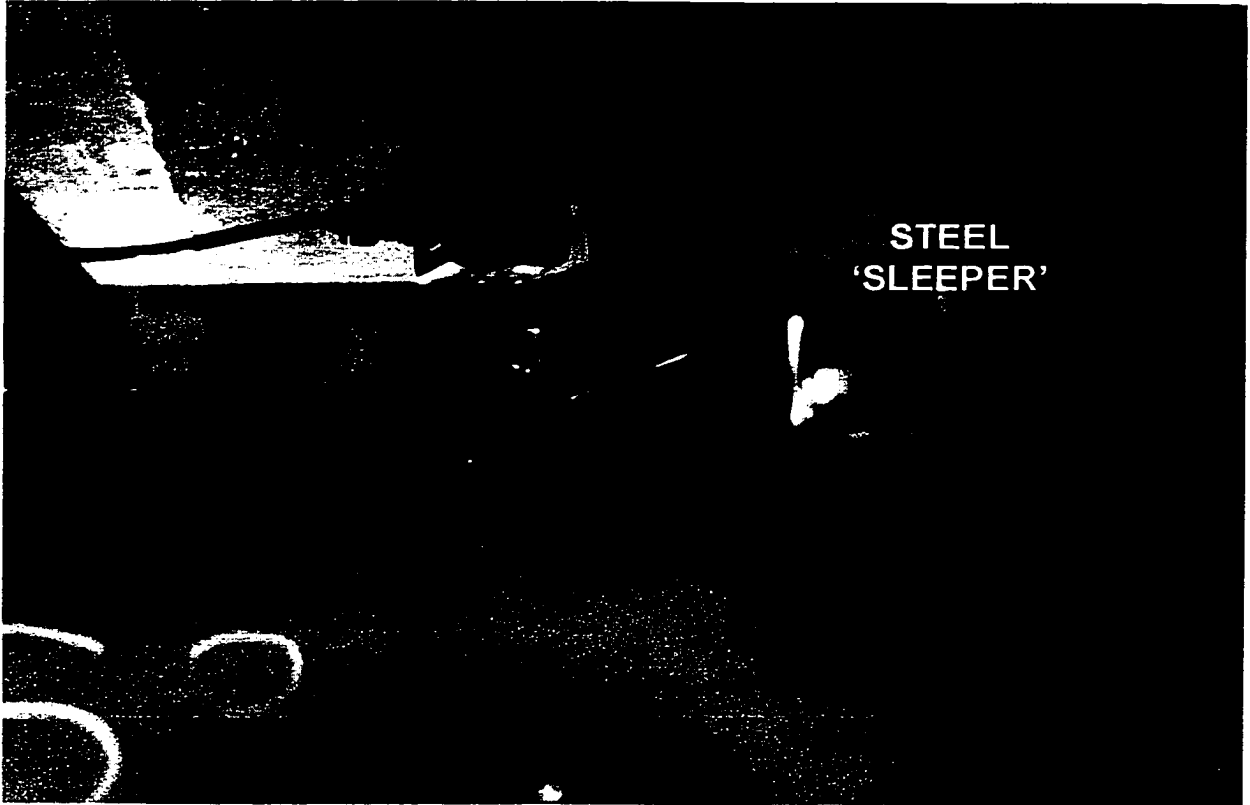


**Figure 4.2** Typical deformation of pressurized pipe showing bulge at edge of sleeper

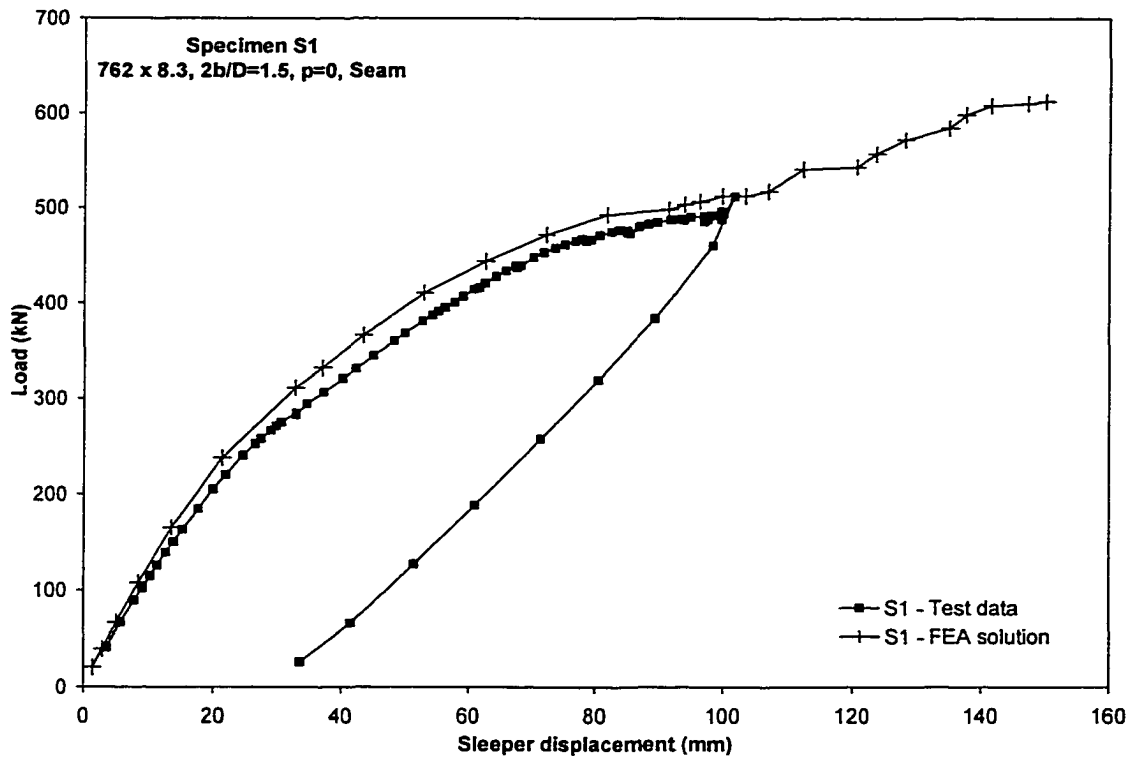


**Figure 4.3** Load vs. sleeper displacement, Specimen S1

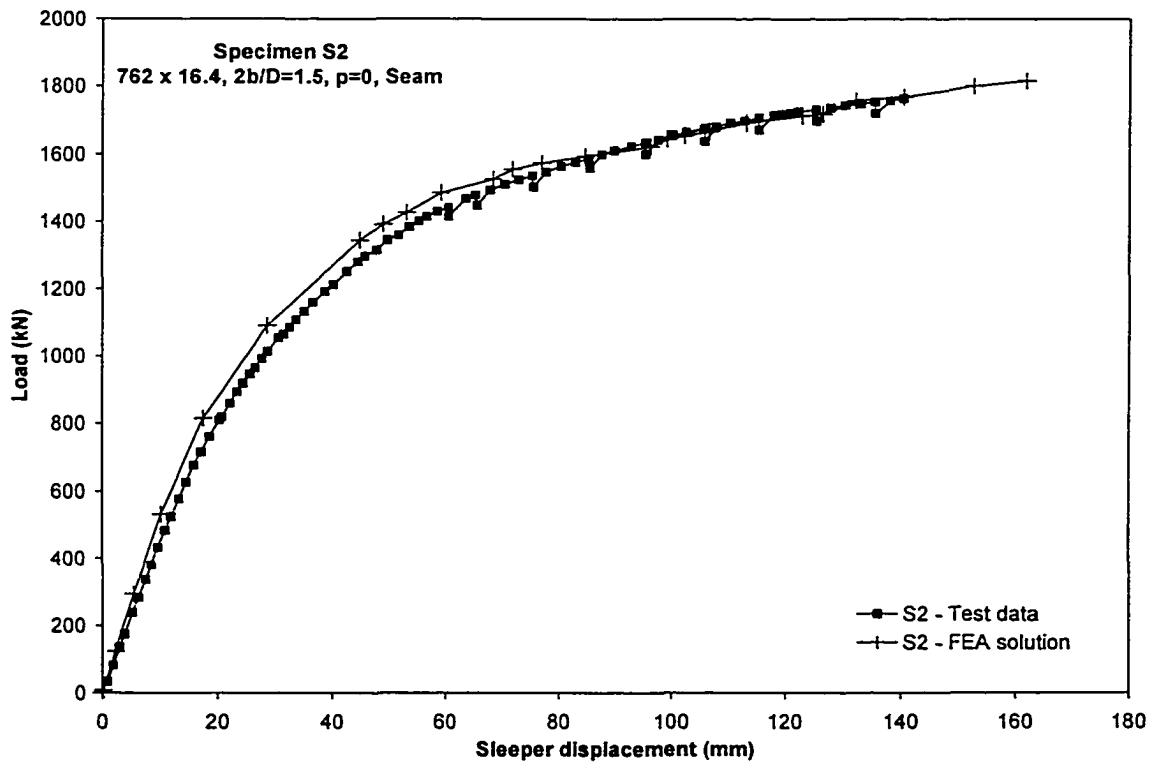


**Figure 4.4** Load vs. sleeper displacement, Specimen S2

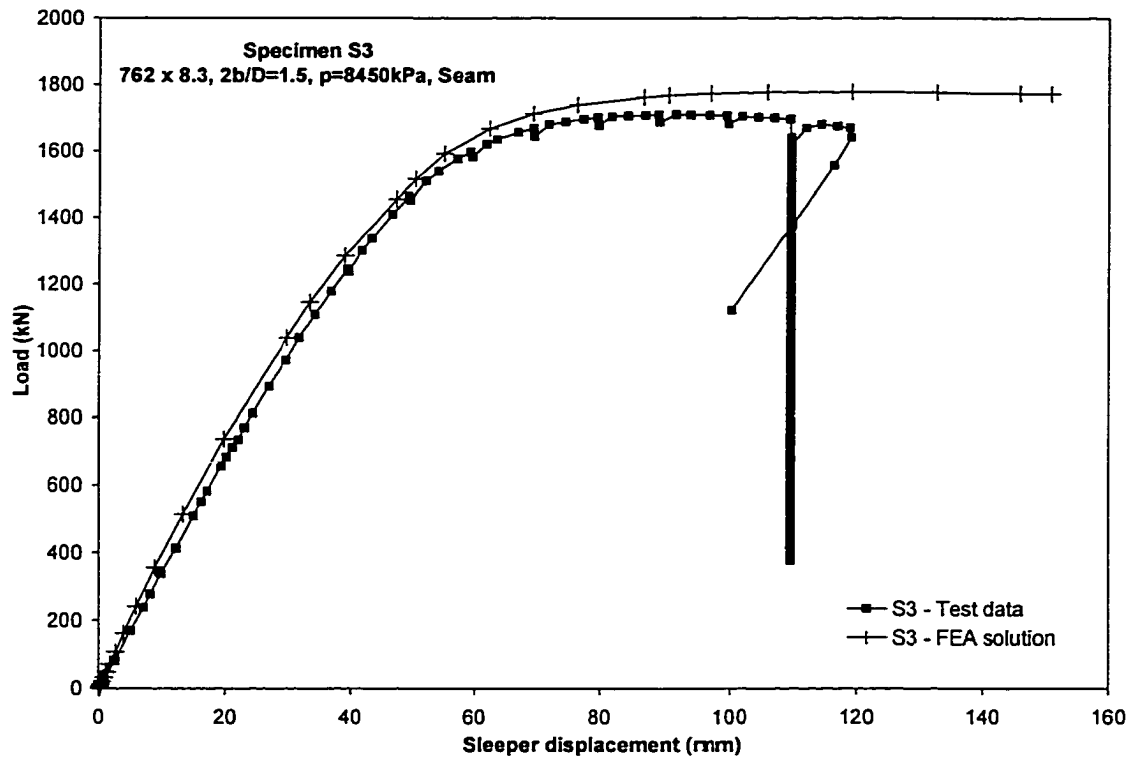


**Figure 4.5** Load vs. sleeper displacement, Specimen S3

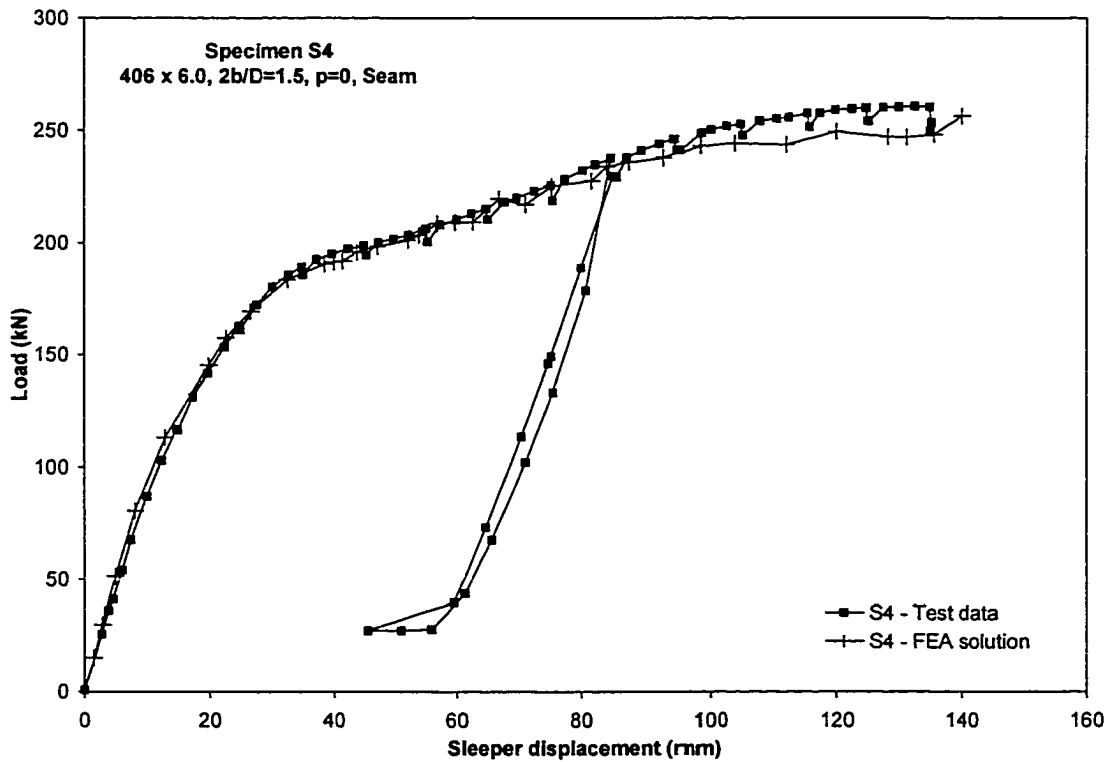


**Figure 4.6** Load vs. sleeper displacement, Specimen S4

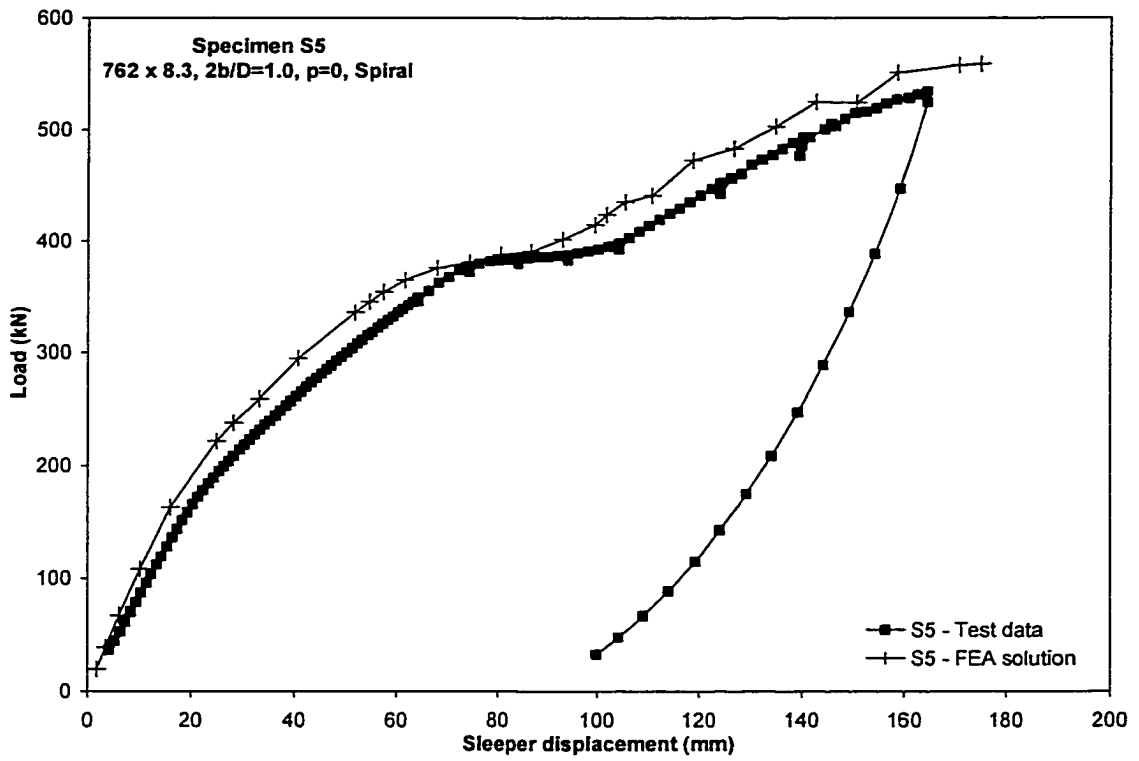


**Figure 4.7** Load vs. sleeper displacement, Specimen S5

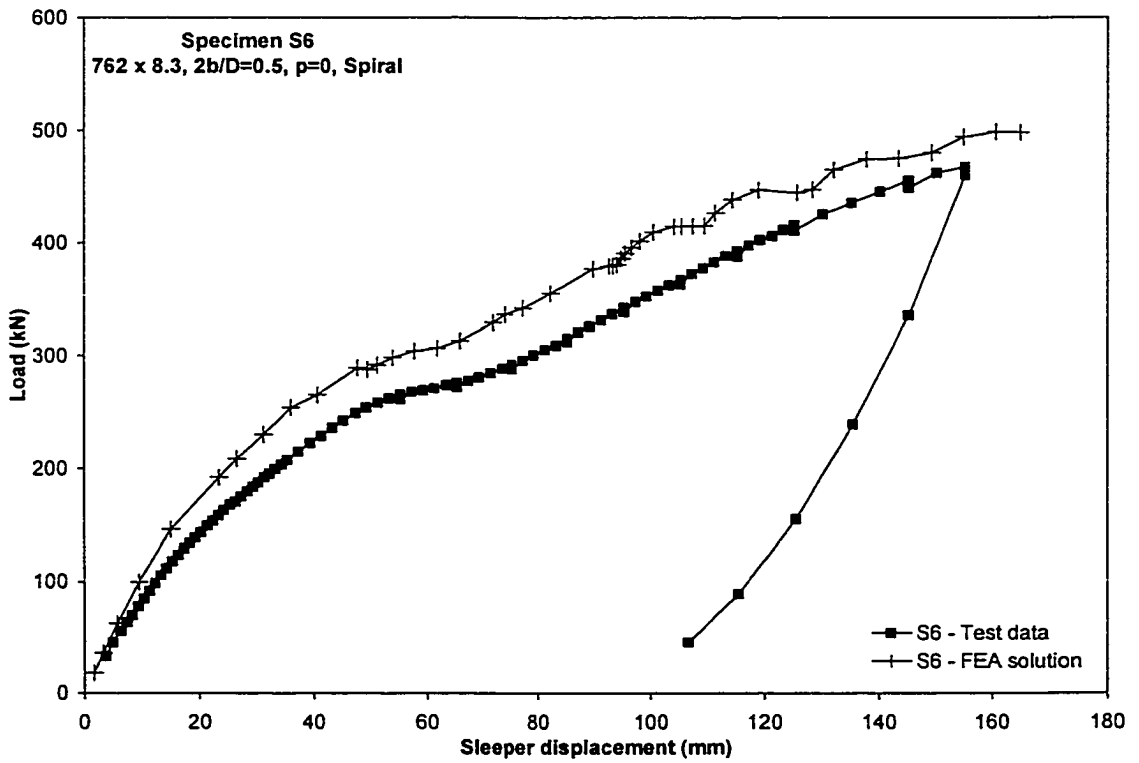


**Figure 4.8** Load vs. sleeper displacement, Specimen S6

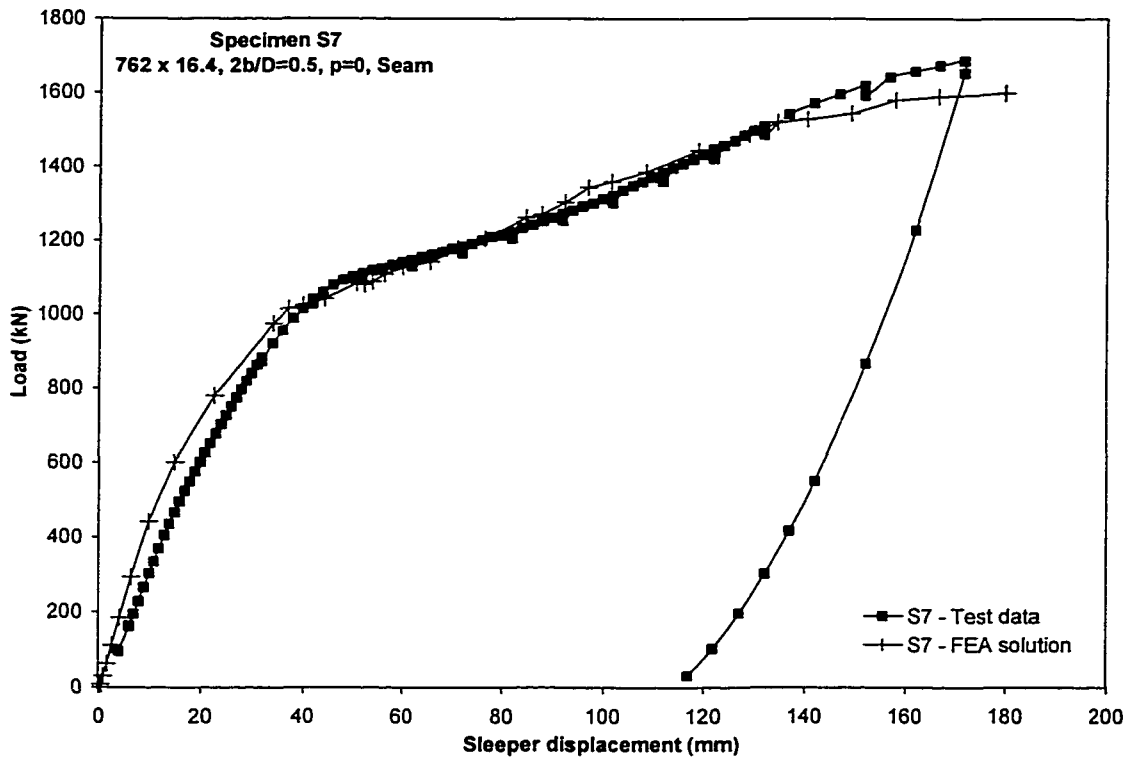


**Figure 4.9** Load vs. sleeper displacement, Specimen S7

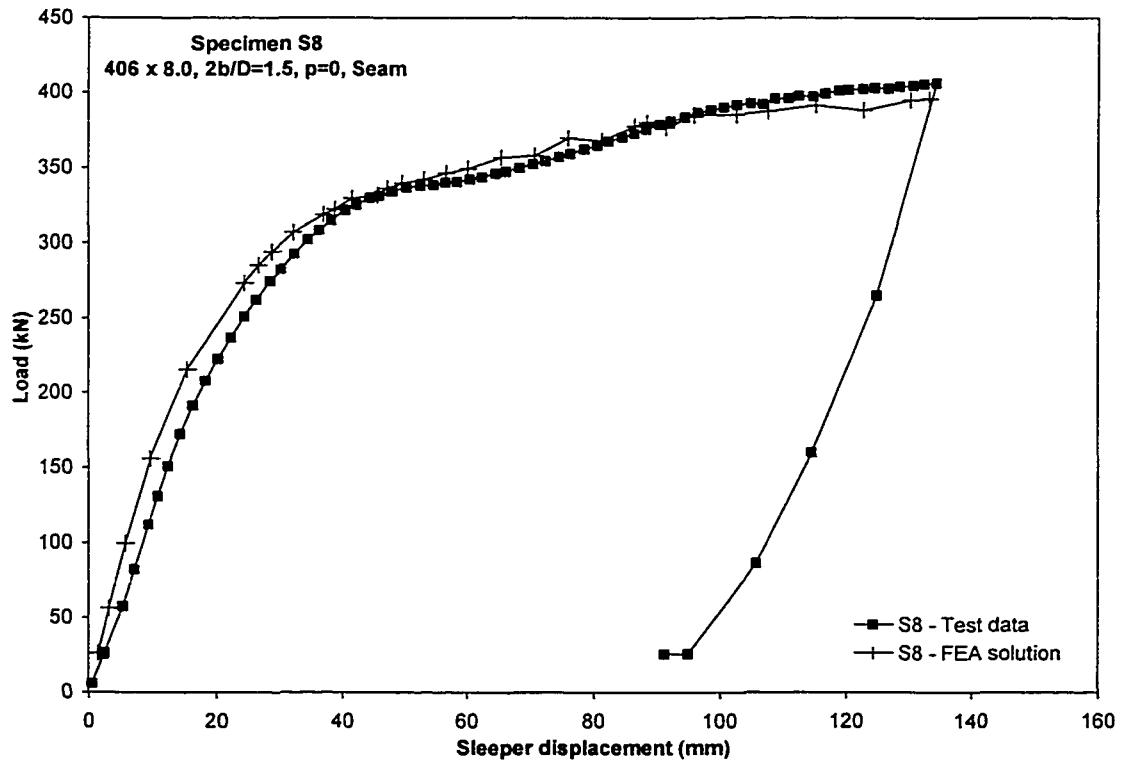


**Figure 4.10** Load vs. sleeper displacement, Specimen S8

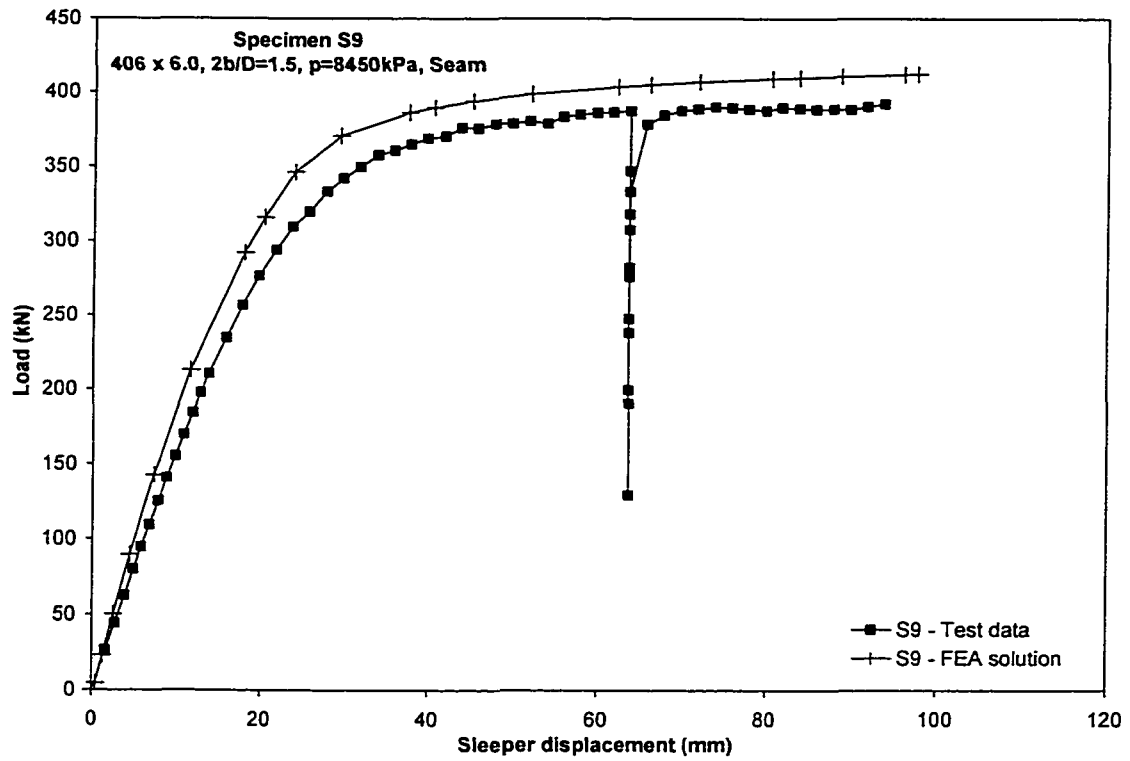


Figure 4.11 Load vs. sleeper displacement, Specimen S9

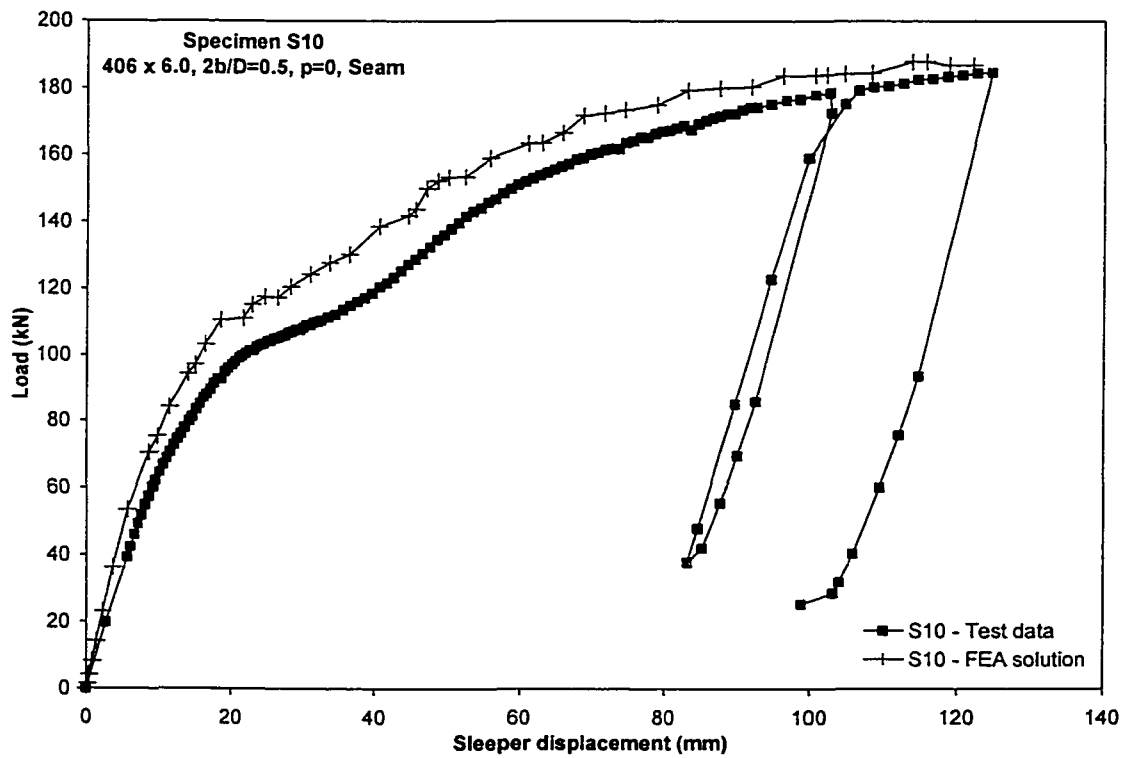
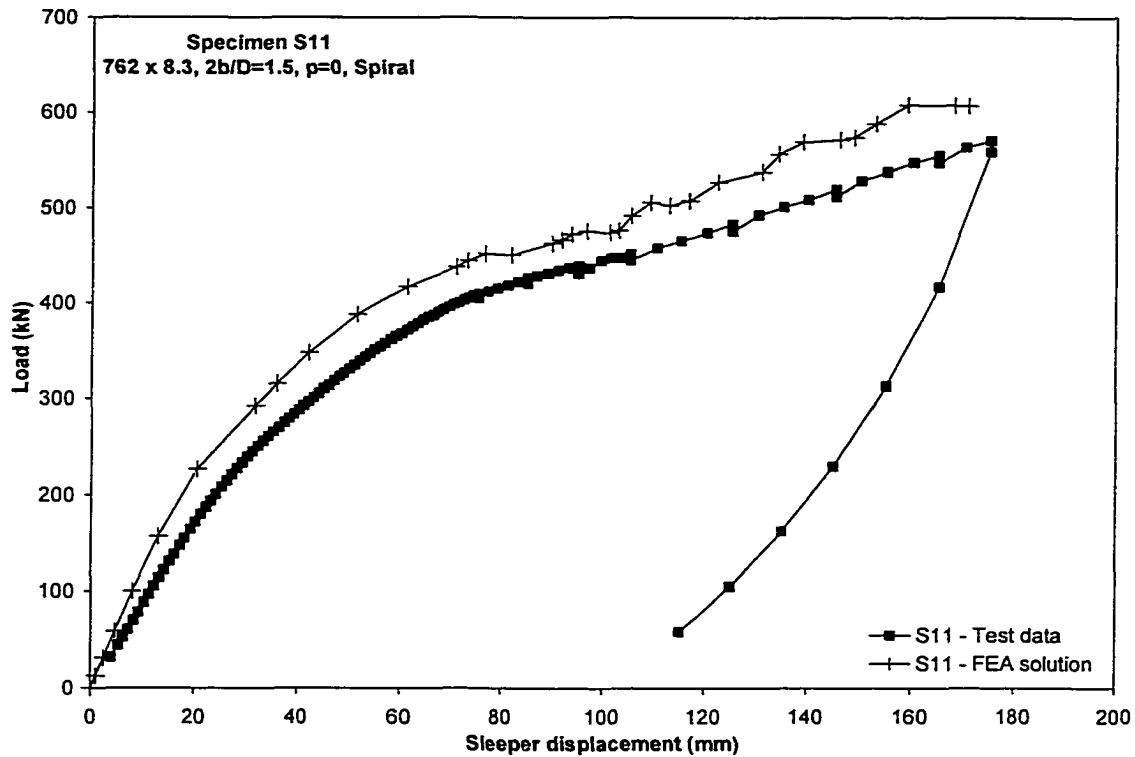
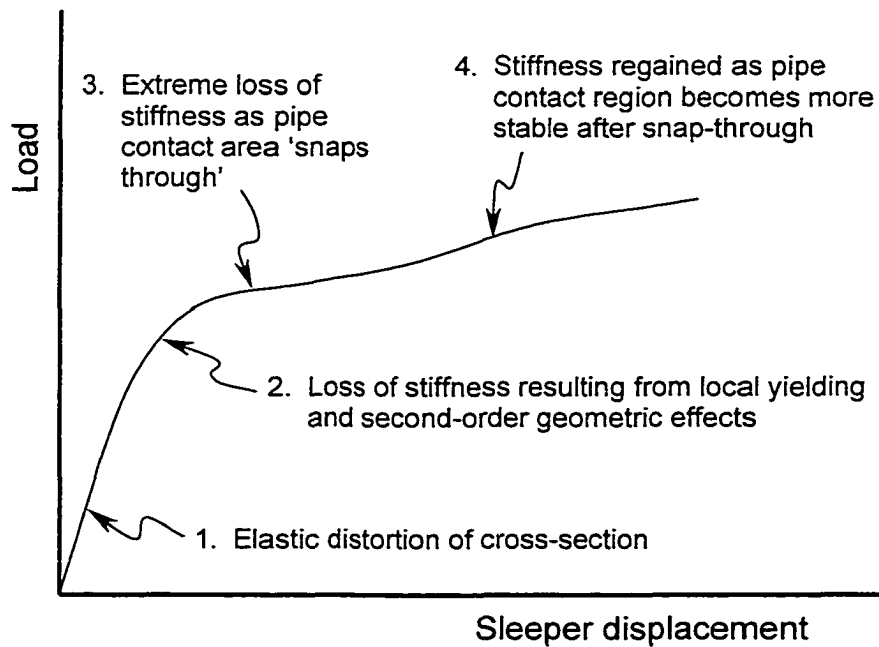


Figure 4.12 Load vs. sleeper displacement, Specimen S10



**Figure 4.13** Load vs. sleeper displacement, Specimen S11



**Figure 4.14** Idealized load vs. sleeper displacement relationship, unpressurized specimens

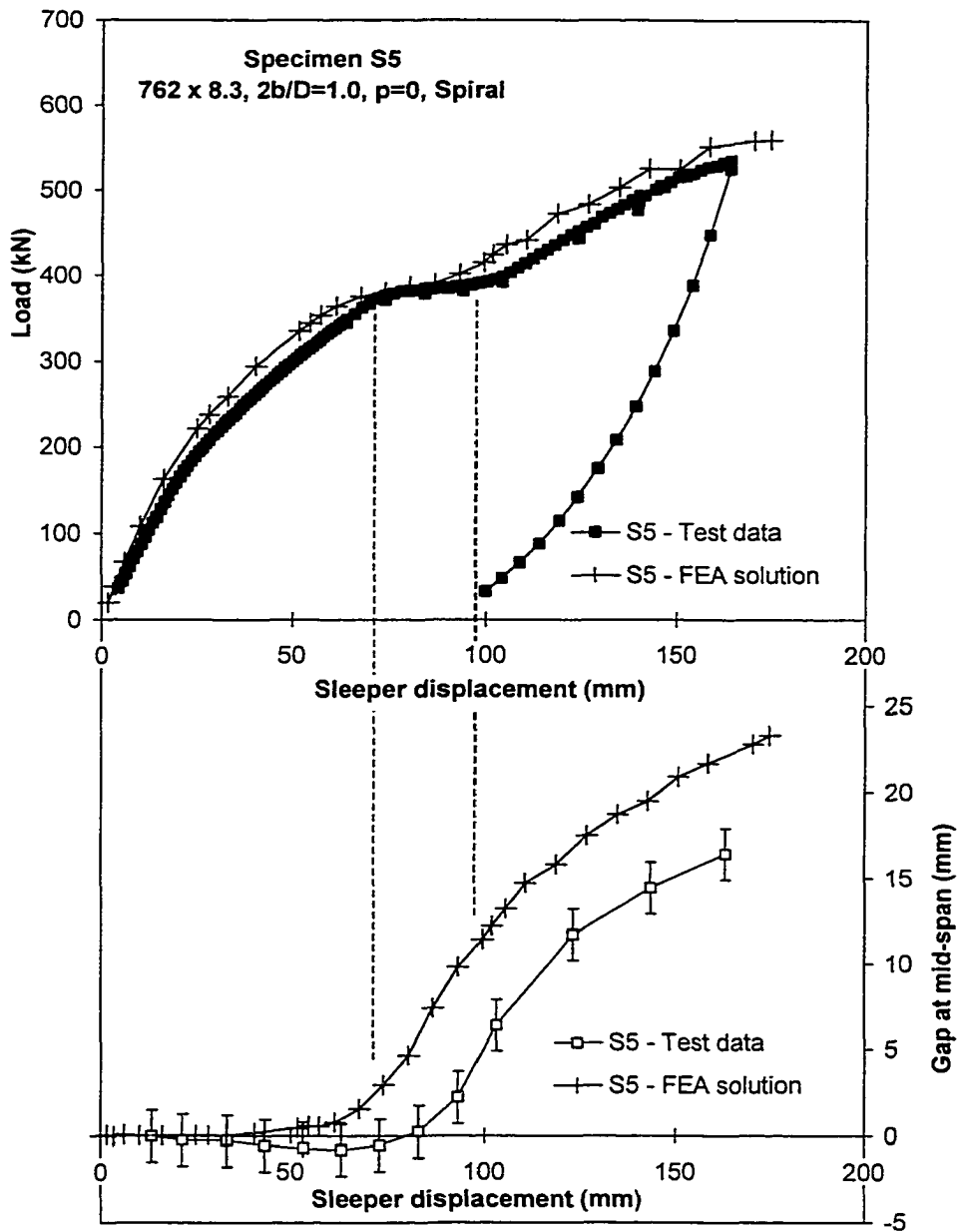


**Figure 4.15** Decreased stiffness evident as the pipe wall reverses in curvature along the centreline of contact, Specimen S5

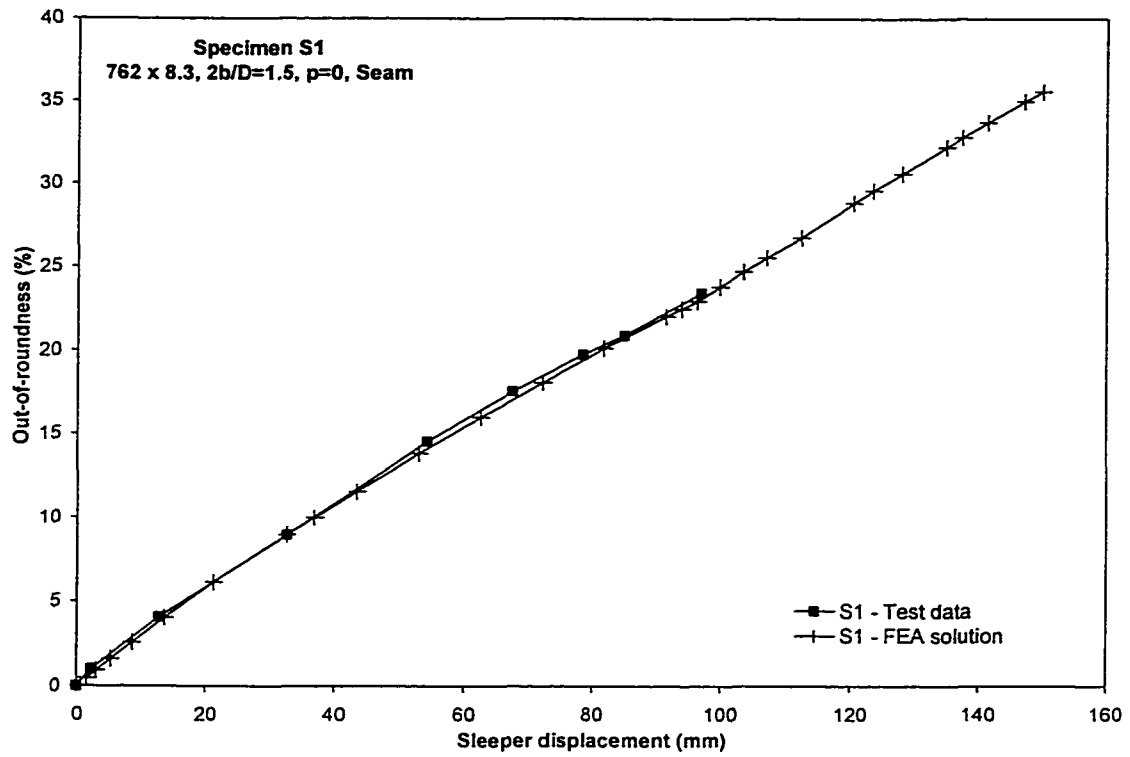


**Figure 4.16** Mid-span out-of-roundness vs. sleeper displacement, Specimen S1

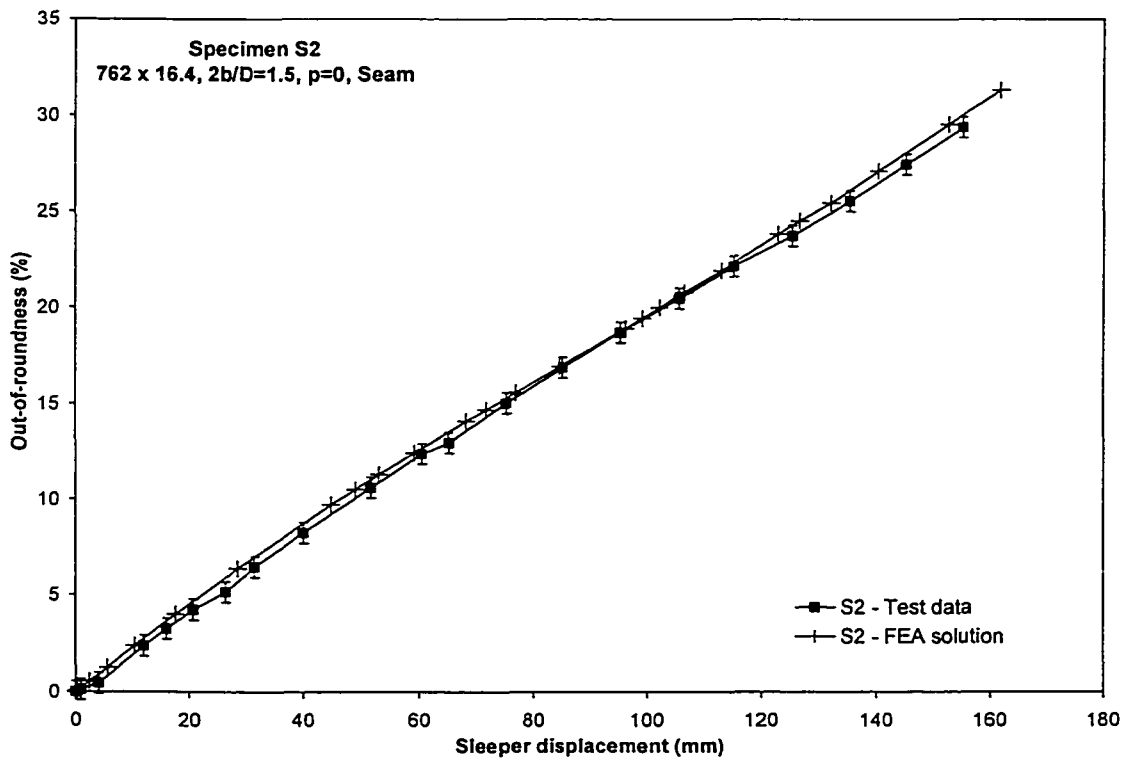


**Figure 4.17** Mid-span out-of-roundness vs. sleeper displacement, Specimen S2

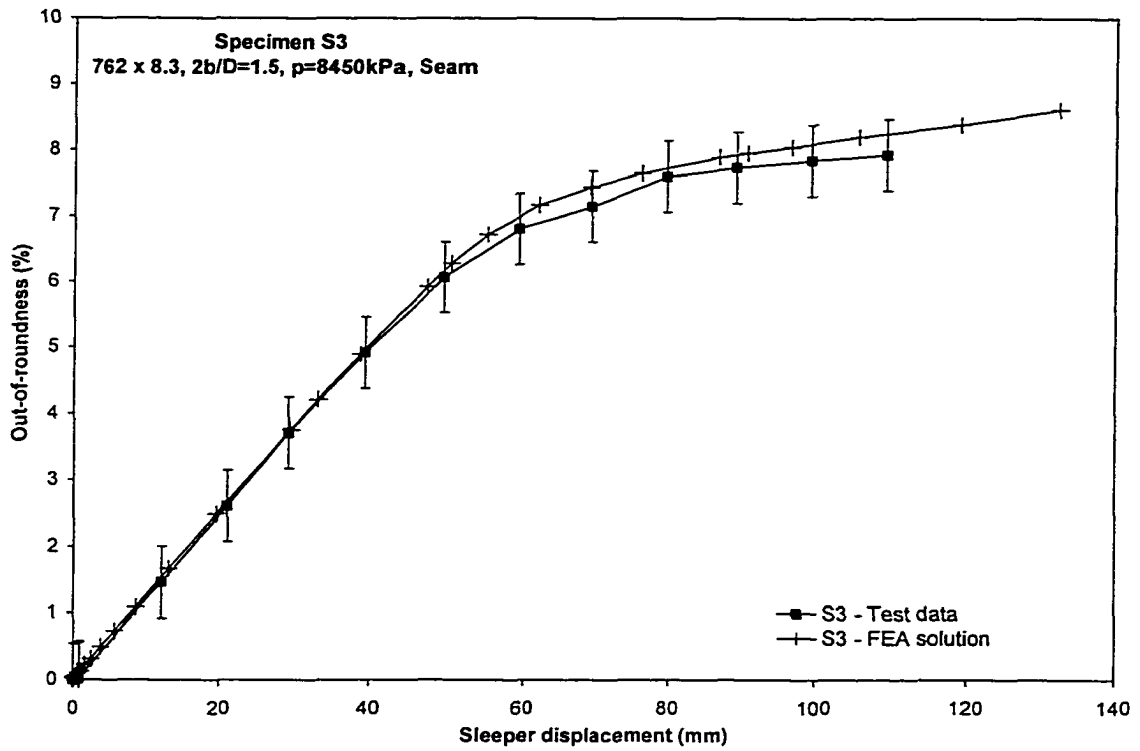


**Figure 4.18** Mid-span out-of-roundness vs. sleeper displacement, Specimen S3

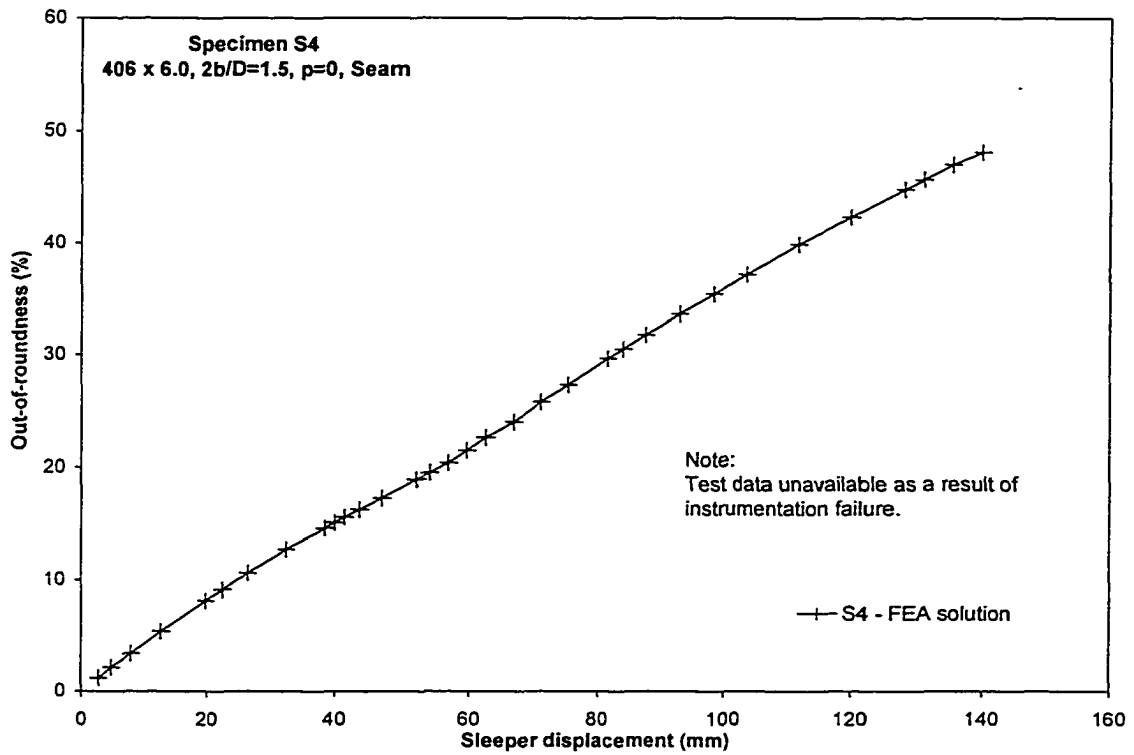


**Figure 4.19** Mid-span out-of-roundness vs. sleeper displacement, Specimen S4

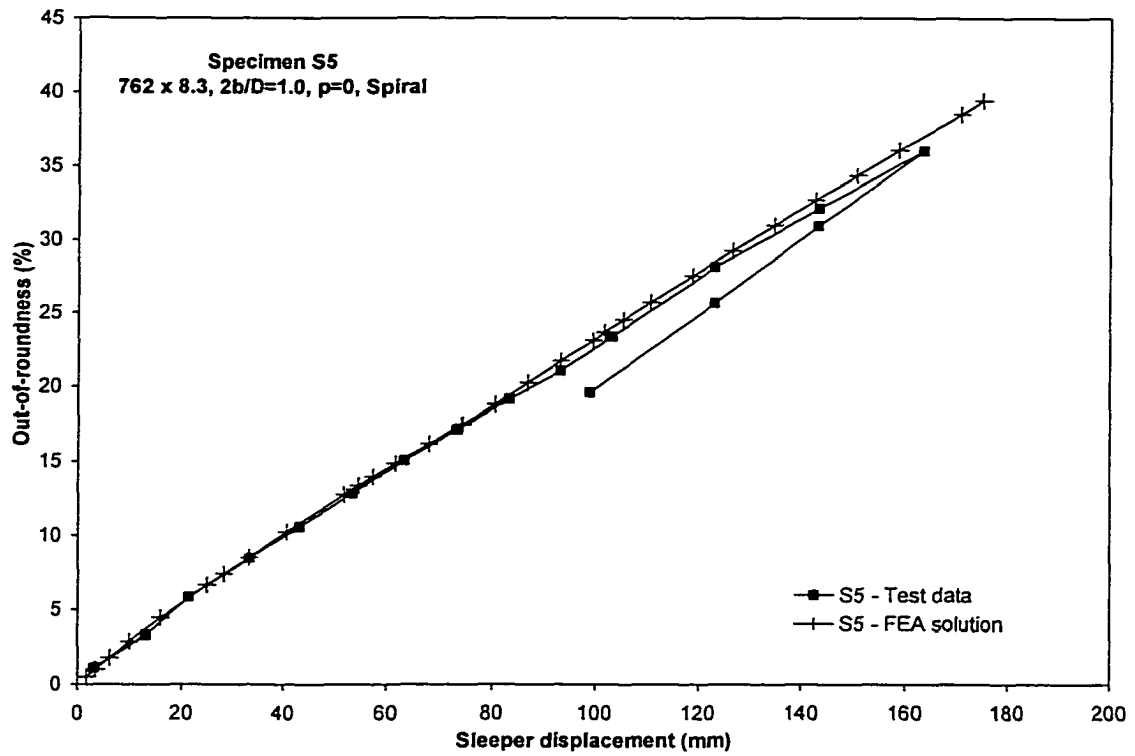


**Figure 4.20** Mid-span out-of-roundness vs. sleeper displacement, Specimen S5

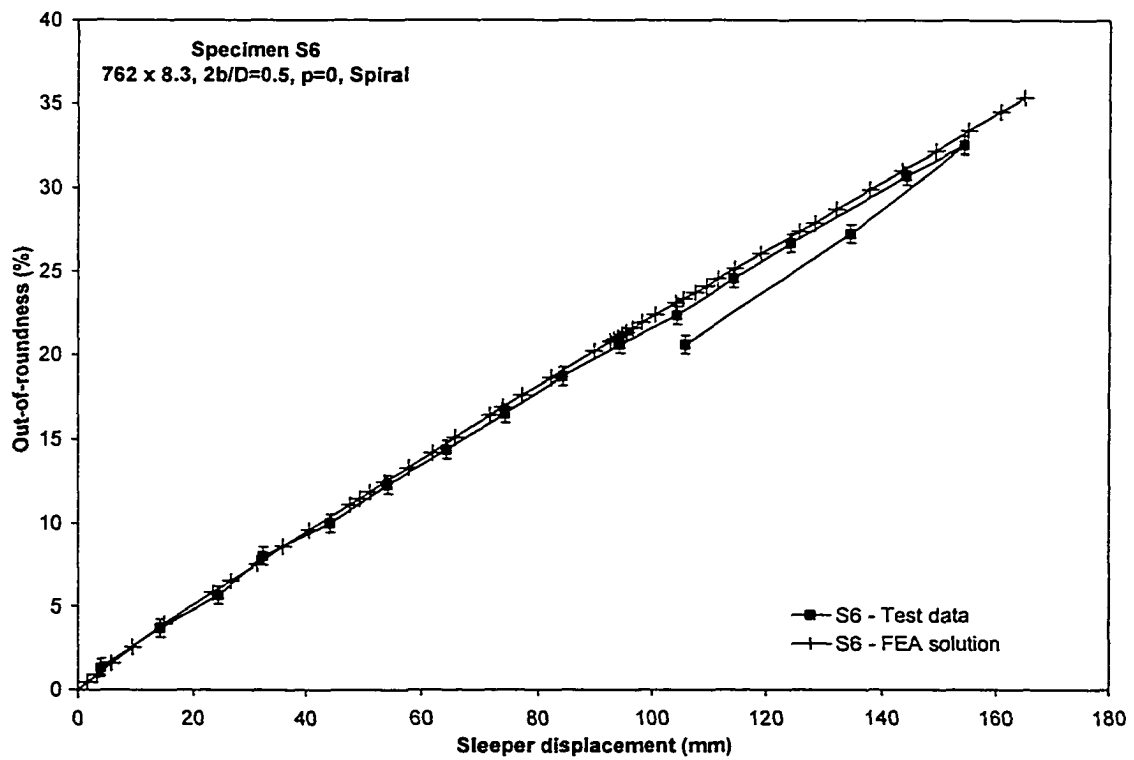


**Figure 4.21** Mid-span out-of-roundness vs. sleeper displacement, Specimen S6

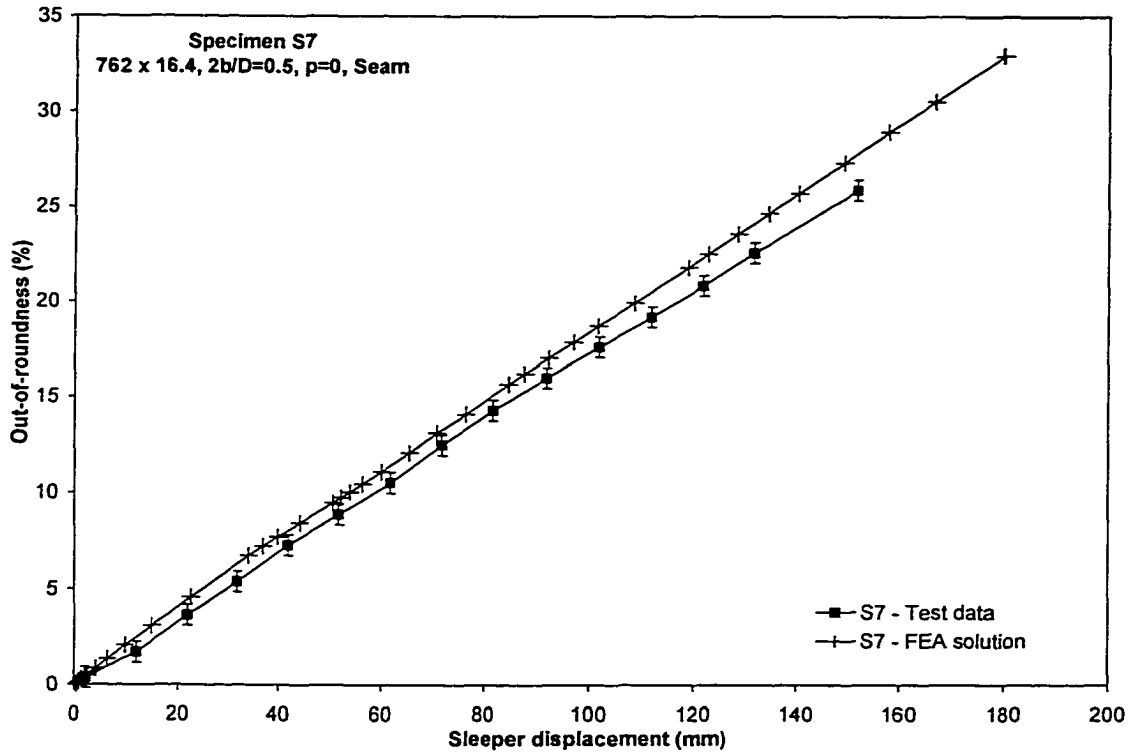


**Figure 4.22** Mid-span out-of-roundness vs. sleeper displacement, Specimen S7

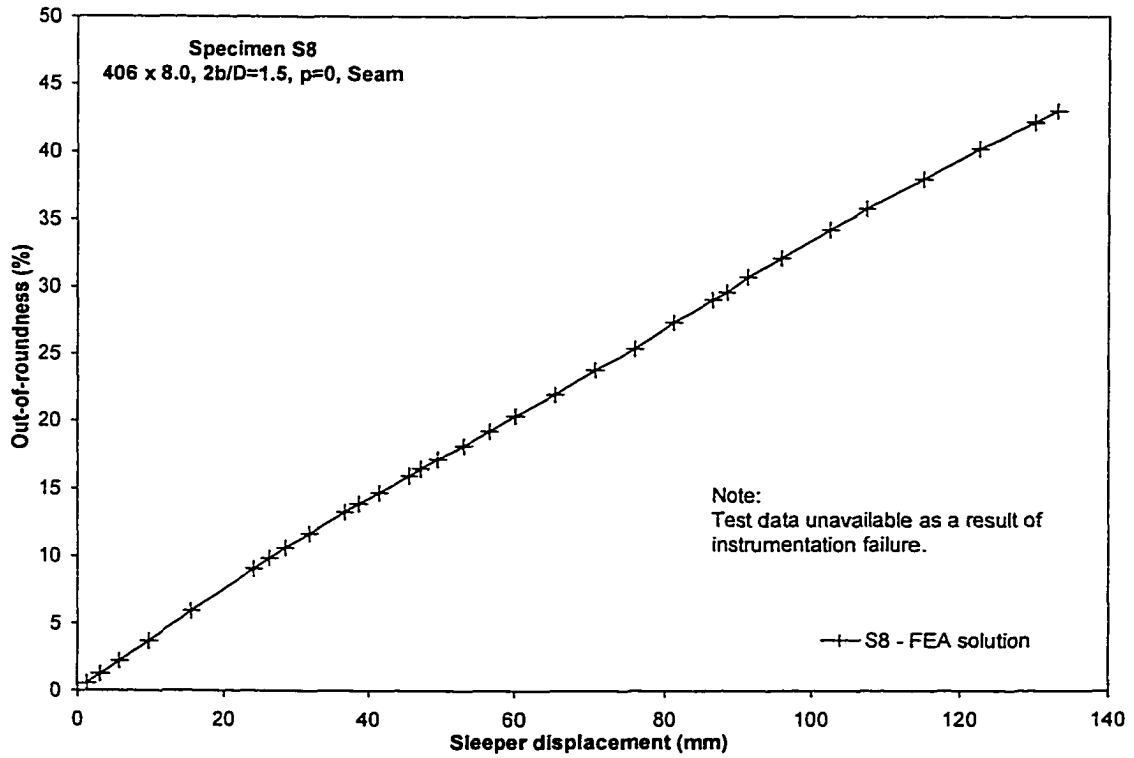


**Figure 4.23** Mid-span out-of-roundness vs. sleeper displacement, Specimen S8

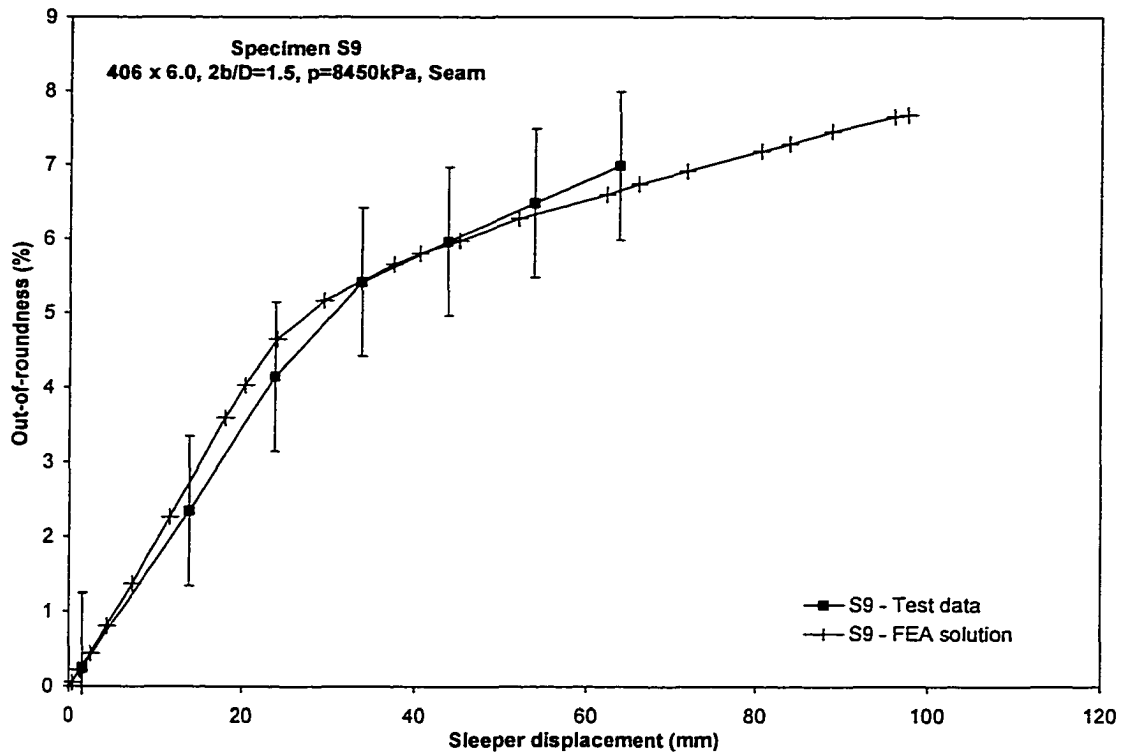


**Figure 4.24** Mid-span out-of-roundness vs. sleeper displacement, Specimen S9

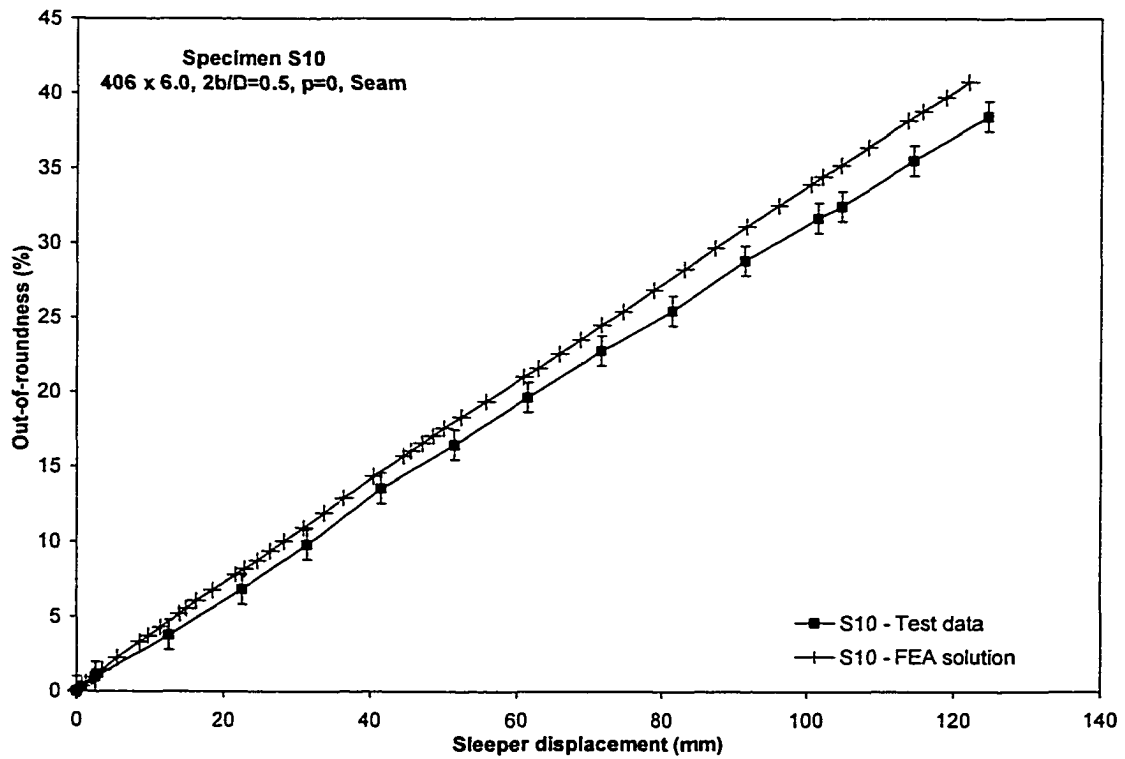


**Figure 4.25** Mid-span out-of-roundness vs. sleeper displacement, Specimen S10

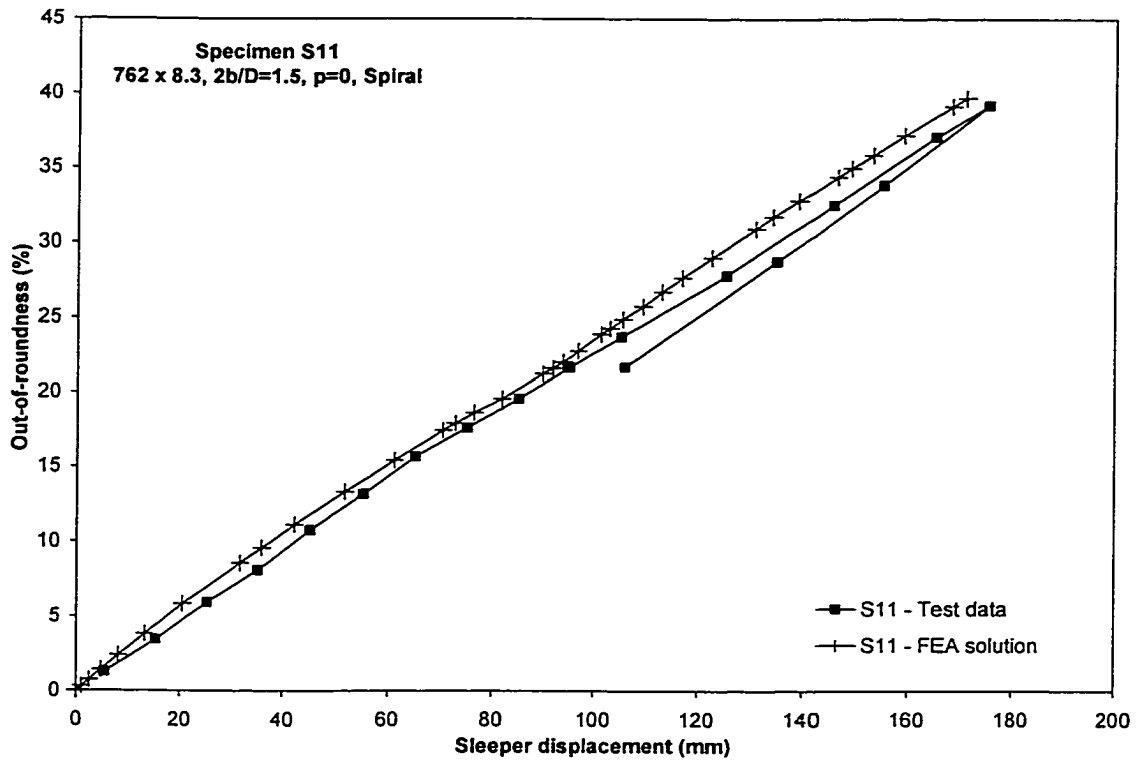
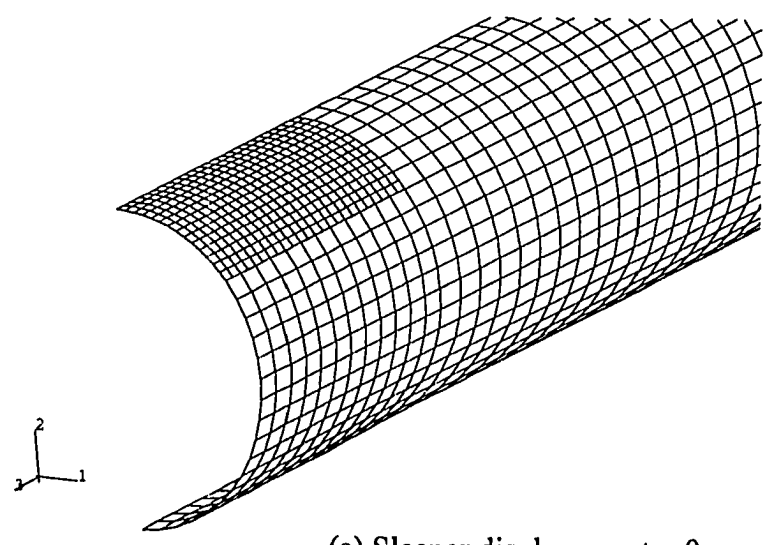
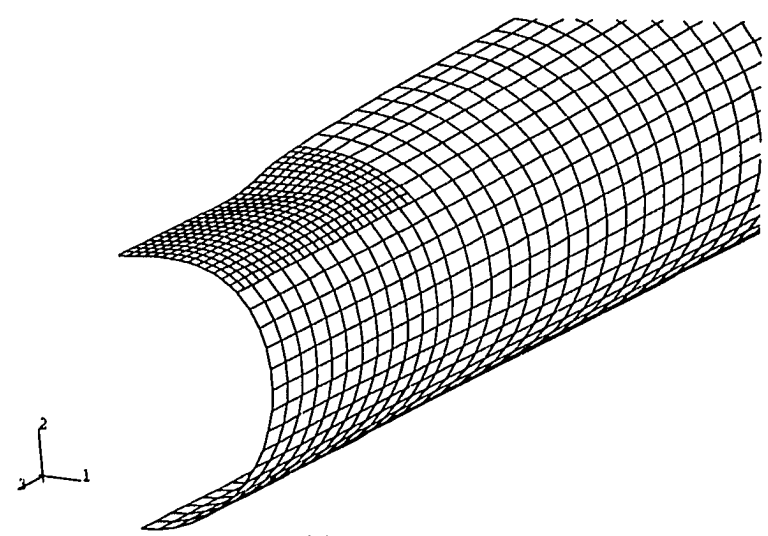


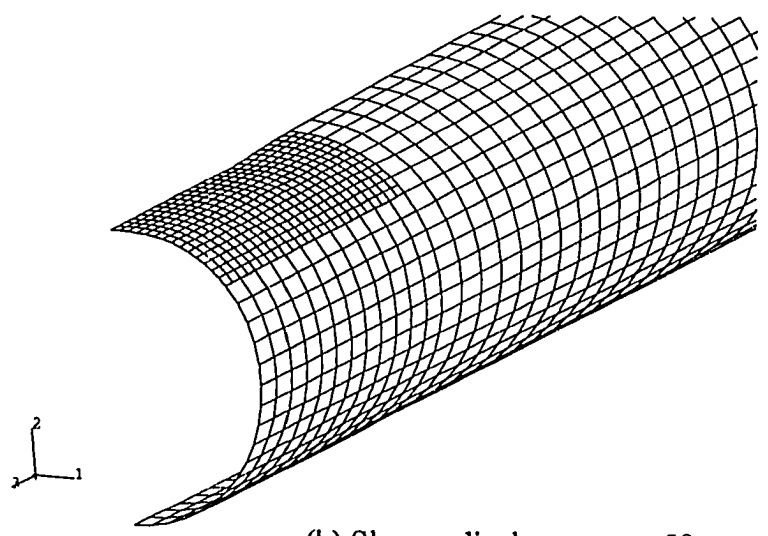
**Figure 4.26** Mid-span out-of-roundness vs. sleeper displacement, Specimen S11



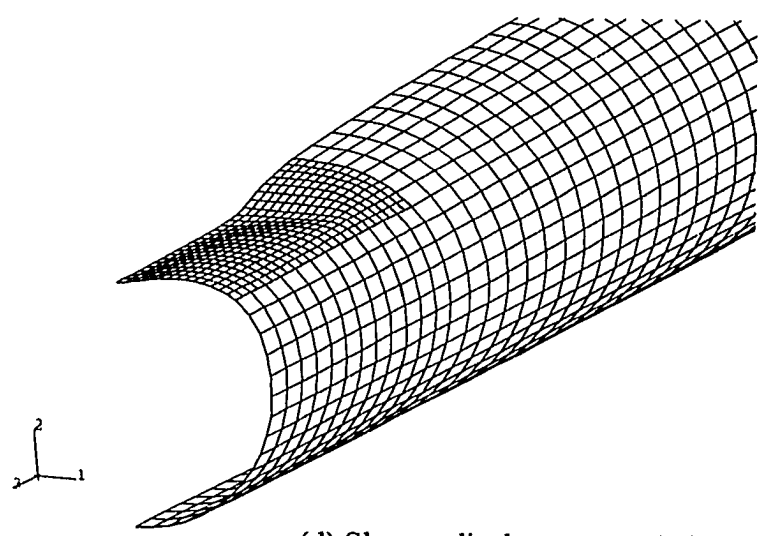
(a) Sleeper displacement = 0 mm



(c) Sleeper displacement = 100 mm

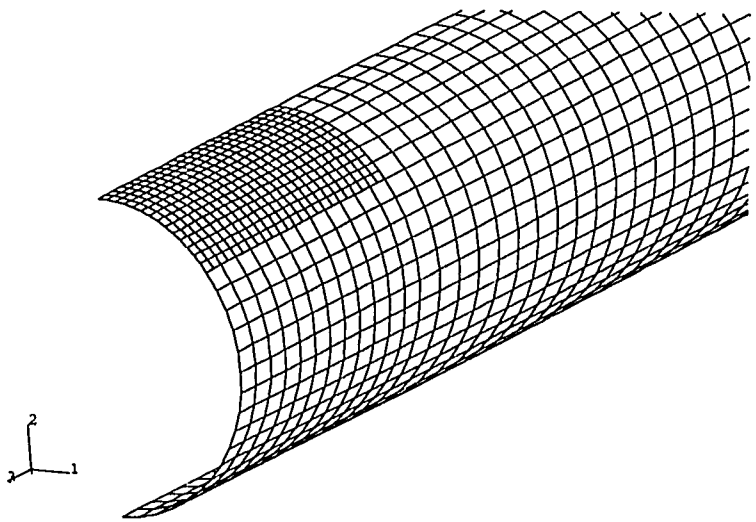


(b) Sleeper displacement = 50 mm

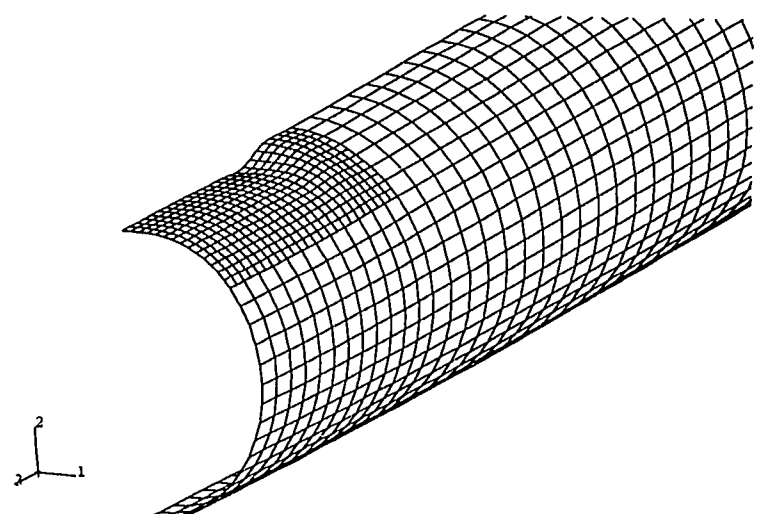


(d) Sleeper displacement = 150 mm

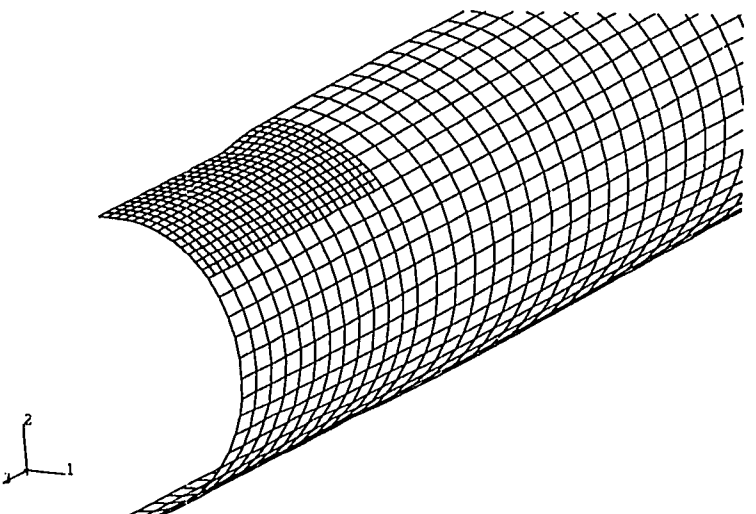
**Figure 4.27** Typical progression of deformation, unpressurized specimen (S1)



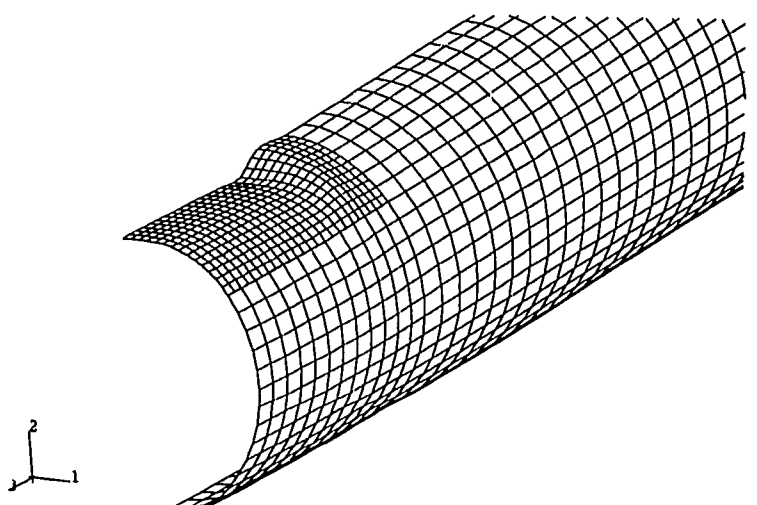
(a) Sleeper displacement = 0 mm



(c) Sleeper displacement = 100 mm



(b) Sleeper displacement = 50 mm



(d) Sleeper displacement = 150 mm

**Figure 4.28** Typical progression of deformation, pressurized specimen (S3)

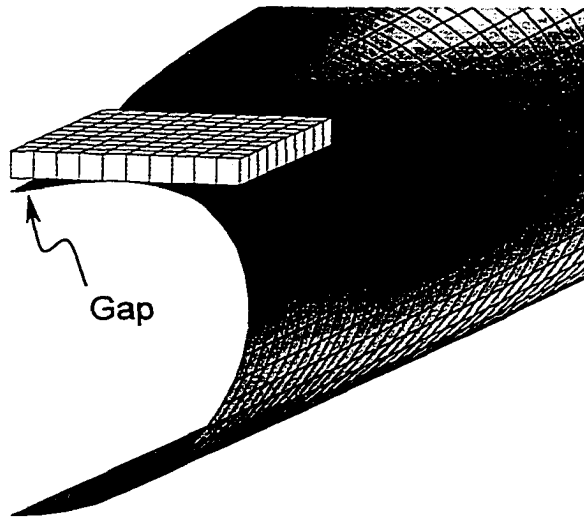


**Figure 4.29** Deformed configuration from finite element model, Specimen S1 (unpressurized)

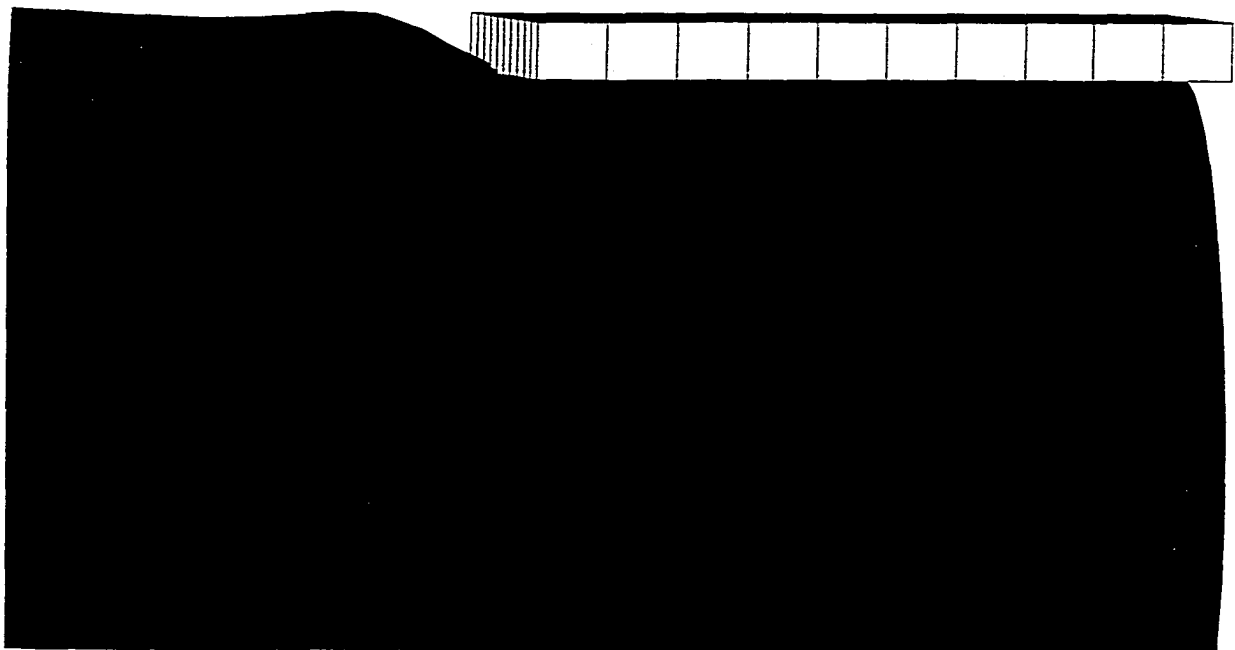


**Figure 4.30** Deformed configuration from finite element model, Specimen S3 (pressurized)

## 5 FINITE ELEMENT MODELLING OF *IN SITU* CONDITIONS

In Chapter 1 it was established that the existing method for the design of sleeper-supported pipes is not adequate. Consequently, a fundamental goal of this study is to improve basic knowledge about the behaviour of sleeper-supported piping systems so as to aid in the development of a new method for their design. This is to be accomplished through a numerical study of sleeper-supported piping systems that have dimensional, material, and operational parameters that range across a spectrum of realistic situations. Specifically, the influences of various sleeper sizes and spacings, pipe specifications, and levels of internal pressure are investigated.

The numerical study is undertaken using finite element analysis techniques that are essentially the same as those developed in Chapter 3 for the models of the full-scale test specimens. Because the modelling of the test specimens was successful, it would not be reasonable to make substantive changes to the finite element procedures. However, modifications to some of the boundary conditions, the loading method, and the solution strategy are necessary in order to simulate field installations of sleeper-supported piping more realistically. This chapter outlines the development of a finite element model that represents idealized *in situ* conditions for sleeper-support pipes. Data generated from this model are used in Chapter 6 for the development of a simplified empirical model that predicts the behaviour of *in situ* sleeper-supported piping systems.

### 5.1 IDEALIZATION OF *IN SITU* SLEEPER-SUPPORTED PIPING

There are two fundamental questions that must be addressed in a performance assessment of sleeper-supported pipelines: What are the loads that act on the line, and what is the behaviour of the pipe as it acts to resist those loads? Obviously, the nature and magnitude of the loads must be resolved before an attempt can be made to predict the response by numerical means. For sleeper-supported pipes, both soil pressure and sleeper-to-pipe contact impart the loads. The primary focus of this investigation is specifically on the interaction between pipe and sleeper supports rather than between the pipe and the surrounding soil. However, it is still necessary to consider how the soil imparts load to the system and to appreciate that the strength of the pipe is not

independent of the soil loads: interaction of soil with the pipe affects the behaviour of the pipe, and vice versa.

Consideration of an infinitely long pipe supported on a series of uniformly spaced sleepers is a useful starting point in the development of rational loading and boundary conditions for the *in situ* finite element model. The pipe is buried in soil at constant depth, as shown in Figure 5.1(a), and the material properties of the soil are assumed to be constant along any line parallel with the longitudinal axis of the pipe. Using this simplification, the detailed development of the idealized model is discussed in the following sections.

### **5.1.1 Soil Loads on Pipelines**

For any buried pipeline system, the assessment of forces that are transferred between the soil medium and the pipe is an integral part of the design process. In general terms, forces from soil-structure interaction can arise as a result of primary loads, secondary loads, or both. As discussed in Chapter 1, primary loads are those for which a specific level of force must be maintained in order to sustain static equilibrium. This loading condition is often referred to as ‘load-control’ in the literature. The weight of soil overburden on a pipe is an example of a primary load. Secondary (or ‘displacement-controlled’) soil loads result from relative movement between the pipe and the surrounding soil. Slope failures, earthquake fault slips, frost heave, and, in certain circumstances, permafrost thaw settlement are examples of secondary soil loads. In these cases, the pipe and the soil around the pipe must deform sufficiently to accommodate whatever overall movement occurs in the soil medium; the stresses that arise in the pipe depend only on its stiffness properties and on the amount of deformation imposed.

For sleeper-supported pipe, it is obvious that surface loads and the weight of soil overburden must always be considered in the design process. These are primary loads. By their very nature, secondary loads tend to be more site-specific, and must be assessed depending upon the likelihood that they may arise at a particular installation. For example, it is unlikely that sleeper-supported pipes would ever be subjected to severe ground fault movement or slope instability; compressor stations, where sleepers are most often used, would probably not be built near these hazards (NOVA Gas Transmission Ltd., 1999). Frost heave and settlements from permafrost thaw or other sources might

also be issues in the design process. However, these loads would depend greatly on local soil and climatic conditions and the operating temperature of the line. Furthermore, the loads imposed on the pipe from such movements would be limited to the weight of soil overburden and surface loads, so it is questionable whether this load type should be considered as displacement-controlled. Taking into account all of these factors, the author judges that only primary soil loads need to be considered in the *in situ* model.

### **5.1.2 Selection of a Soil Model**

A wide variety of soil modelling techniques are available for the assessment of soil-pipeline interaction forces, but these can be grouped into two general categories: those most appropriate for primary loads, and those most appropriate for secondary loads. For those cases in which primary loads, such as the weight of soil overburden, are dominant, empirical and semi-empirical equations are available to estimate soil pressures that act on the pipe (see, for example, Spangler and Handy, 1973). These formulas are widely used by pipeline designers, and their application is reasonably simple. However, if secondary loads, such as earthquake fault movements, are to be considered, it becomes significantly more difficult to estimate soil-pipeline interaction: the load-deformation behaviour of the soil medium and of the pipe itself should be considered explicitly. To do this, it is most common to model the soil itself using the finite element method, either by discretizing the soil medium with two-dimensional or three-dimension finite elements or, alternatively, by representing the soil medium as a series of non-linear springs.

The author has chosen the first option for the *in situ* model, that is, soil pressures are applied directly to the pipe and the soil itself is not modelled discretely. This selection was made for a variety of reasons. First, the predominant loads are expected to be primary, as identified in Section 5.1.1, and these can be estimated using common empirical methods. Second, a large number of parameters (pipe size, thickness, and grade, sleeper size and spacing, and level of internal pressure) are already considered in the study. This requires the analysis of a large number of finite element models. If discrete modelling of the soil were added to the study, consideration of its cohesive properties, time-dependent behaviour, and other factors would make it necessary to increase the total number of parametric combinations to an unmanageable extent. Third, the sequence of installation and backfilling, the degree of compaction obtained, the type

of trench, and a number of other practical aspects of the construction process all influence the behaviour of the soil. None of these factors can be estimated with confidence by the author, since they will be site-specific. Consequently, the designer of a sleeper-supported pipe installation will be in the best position to make accurate judgements related to the soil conditions at that site. On this basis, the model chosen for use in the *in situ* model should be compatible with techniques that the design engineer is likely to use for the estimation of soil pressures. All of these factors contributed to the decision to apply soil pressures directly to the pipe without modelling the soil itself.

### **5.1.3 Empirical and Semi-empirical Estimation of Soil Pressures**

Any assessment of soil forces, even by means of empirical formulas, is by no means simple and a great deal of engineering judgement is required to make appropriate choices. A number of options are available in common practice that depend upon the specific type of soil, the type of pipe, and installation procedures (trench geometry, degree of backfill compaction, etc.). Many researchers report work in this field; Prevost and Kienow (1994) provide a useful literature review. In general terms, soil pressures that act on the line can be grouped into three categories: vertical downward soil pressure on the crown of the pipe that results from gravity forces, vertical upward soil pressure on the invert of the pipe that resists the downward forces, and transverse passive soil forces that act on the pipe as it distorts laterally (Spangler and Handy, 1973).

#### **5.1.3.1 Vertical Downward Soil Pressure**

Several methods are available for the estimation of downward soil pressures exerted on a pipe as a result of soil self-weight. One of the most common is the well-known *Marston Theory of Loads on Underground Conduits* (see, for example, Spangler and Handy, 1973). In simple terms, this method is based upon equilibrium of the backfill above the pipe, including the effects of consolidation and settlement. As settlement occurs in the backfill, lateral earth pressure is mobilized between the backfill and the sides of the trench. This gives rise to frictional shearing stresses in the vertical upward direction in proportion to the angle of internal friction of the soil. Therefore, for equilibrium, the pipe must carry the weight of soil that is not carried by friction or by the backfill in the trench around the pipe. In other words, the pipe may carry the weight of

the soil directly above itself and also some soil that is located over the side-fills. The forces are a function of the type of soil, the depth of cover, the width and shape of the trench, the quality of compaction of the backfill, and the stiffness of the pipe.

For flexible pipes, such as those considered in this study, the similarity in stiffness between the pipe and the side fills is such that they can both be considered to carry the mass of soil that is located directly above themselves. Consequently, the vertical soil pressure can be estimated conservatively by considering only the self-weight of the soil in a block taken directly above of the pipe. This is generally known as a prism load in literature on flexible pipe culverts. The use of the prism load method is much simpler than the Marston approach, but is probably less accurate. It is the method that is used in the derivation of the design equation developed by Kormann and Zhou (1995) that was described in Chapter 1, and it is also an "...acceptable conservative method of determining the soil pressure..." according to the Australian pipeline design standard (Standards Australia, 1997).

In addition to the self-weight of the soil, live loads on the ground surface can also affect the downward soil pressure that a pipe must resist. Near installations of sleeper-supported pipes, heavy trucks or other equipment are the most likely sources of these surface loads. To estimate the soil pressures induced on a pipe, analytical methods such as the well-known *Boussinesq Stress Distribution* are available (see, for example, McCarthy, 1988). For a particular surface load, this method provides an estimate of how the sub-surface stresses disperse with depth in a homogeneous, isotropic, semi-infinite soil medium. A number of modifications to the original Boussinesq method are also available to account for a variety of practical on-site conditions.

It is obvious that many variables have influence on the vertical downward soil pressure. As stated previously, a designer of a sleeper-supported pipe project will be in the best position to make accurate judgements related to the soil conditions for a particular site. On this basis, the soil model used in the development of a simplified design method should be reasonably generic so that a variety of conditions can be represented. To allow wide applicability, a simple soil model that consists only of a uniform downward soil pressure has been chosen for the *in situ* model. This pressure acts on the area obtained when the pipe is projected onto a plane that is parallel with a level

ground surface. It remains the responsibility of the engineer to use the Marston, Boussinesq, or similar methods to choose an appropriate value of the downward soil pressure to reflect site conditions. This value should include the effects of soil self-weight, surface loadings, and any other site-specific design loads.

### ***5.1.3.2 Vertical Upward and Lateral Soil Pressures***

It is obvious that, in order to maintain equilibrium conditions, equal upward forces must resist any downward soil forces that act on a pipe. At first glance, one might assume that the pipe material itself should be capable of carrying all of these vertical compressive forces that tend to collapse the cross-section. However, if the pipe is pressurized, the internal pressure itself carries a portion of the load. Furthermore, interaction with the soil may prove to be beneficial to the strength (see, for example, Spangler and Handy, 1973). To a large extent, the interaction of a pipe with the surrounding soil is governed by the rigidity of the pipe itself. Rigid pipe (such as concrete or clay pipe) is not able to deform sufficiently to develop significant lateral earth pressures, and must carry the entire vertical load itself. Conversely, lateral deformation of a flexible pipe allows the development of radial thrust from passive earth pressure. If the soil fill is of good quality and is compacted well, this lateral pressure adds significant stiffness to the soil-pipeline system. The deflection of the pipe is reduced considerably as compared to its deflection if it acted alone to resist the soil forces. Structurally, the maximum bending moments carried in the pipe walls are also reduced by the presence of lateral soil forces, thus enhancing the load-carrying capacity.

For a sleeper-supported piping system, the pipe is supported vertically both by the soil bedding between sleeper supports and by the sleepers themselves. In most cases, the sleepers, which are essentially spread footings on virgin soil, are likely to settle much less than the backfill under the pipe. Because the sleepers elevate the pipe above the bottom of the trench during the installation process (see Figure 1.1), earth must be placed directly beneath the pipe during backfilling. Consequently, the ability to achieve any reasonable degree of compaction in this region is suspect, at best, and settlement of soil under the pipe in the region between sleepers is likely to be relatively great. With these facts in mind, it is most reasonable to assume for the *in situ* model that the sleepers alone carry all of the vertical forces—the soil bedding beneath the pipe between sleeper supports carries

no load. This assumption is realistic and also conservative: only the sleepers carry all of the gravity forces, which should maximize local stress and deformation effects in the pipe near the sleeper supports.

Because line pipes are flexible (particularly under conditions of low internal pressure), it can be expected that some degree of lateral passive soil pressure develops that acts to provide additional stiffness and strength. However, because soil types vary widely depending on geographical location, it is difficult to approximate any contribution that might be present. Furthermore, one of the purposes of using sleepers to support pipes in compressor station yards is to reduce the need for careful compaction of the fill around the pipes. It would not be reasonable for the designer to assume the presence of well-compacted material unless it is explicitly specified as part of the design. As a result, the author judges that it is appropriate to ignore the contributions of lateral passive soil pressure in the idealized model of sleeper-supported pipes that is developed in this chapter. This decision is conservative: the predicted pipe strength should be less than the true strength and the predicted deflection should be greater than the true deflection. Neglecting lateral soil pressure also simplifies the finite element analyses.

#### **5.1.4 Equilibrium of the Idealized System**

Based upon the decisions made in the previous sections, a free-body diagram of the idealized system is shown in Figure 5.1(b). In this figure, the uniformly distributed downward soil pressure resulting from the combined effects of all gravity loads is designated as  $w$ . The upward reaction on the pipe,  $q$ , at the location of the sleepers is shown as a uniformly distributed load for simplicity. Based upon this assumption, the shear force, bending moment, and deflected shape diagrams are shown in Figures 5.1(c) through (e), respectively. (It is important to appreciate that the actual upward load distribution at the sleepers is not necessarily uniform—it depends upon the nature of the contact interaction between the sleeper and the pipe. However, the uniform representation is a reasonable estimate of the true distribution for the purposes of visualizing equilibrium of the system.)

Consider next the free-body diagram of the pipe segment shown in Figure 5.1(f) that spans from the centreline of a sleeper (section  $a$ ) to a point halfway between sleepers (section  $b$ ). Axial force and bending moment may act on each end of the segment, but

there is no net vertical shear force at these locations. On the basis of symmetry of the deflected shape it can be seen that all points on each end of the segment must remain in a vertical plane of symmetry as deformation occurs. Furthermore, a longitudinal tangent to the surface of the pipe taken at either end of the segment must remain normal to the vertical plane. At the same time, the cross-section must be free to distort in this plane. Because the pipe is infinitely long, the vertical plane is not free to move in the axial direction. All of these factors must be considered in the development of appropriate boundary conditions for the finite element model of *in situ* conditions.

### 5.1.5 Critical Examination of the Idealization

One assumption in particular made in the development of the idealized sleeper-supported piping system is clearly not realistic: in a real compressor station the pipes are not infinitely long. For a pipe segment taken from a line having a reasonably short length, it is expected that the ends of the segment are not restrained axially to any significant degree. This is contrary to the idealization developed above. Despite this fact, consideration of an infinitely long pipe is judged to be the most appropriate means of modelling the problem, as described below.

The primary factor governing whether a finite or infinite length of pipe should be modelled is the level of longitudinal tensile stress that develops in the pipe wall. Tensile stresses, in general, stiffen the pipe: their presence reduces the severity of local compressive stresses, thereby stabilizing the pipe and delaying the onset of local buckling or wrinkling. Consequently, the modelling technique (finite pipe length or infinite pipe length) that results in lower longitudinal tensile stresses should be chosen.

For a pipe of finite length, internal pressure causes tensile stresses to develop in the pipe wall in the longitudinal as well as circumferential directions. The longitudinal stress is induced directly by the internal pressure acting on the ends of the pipe (or on elbows). For this case, the longitudinal tensile stress,  $\sigma_\ell$ , is approximately equal to one half of the circumferential tensile stress,  $\sigma_h$ . This level of longitudinal tension may be reduced somewhat by axial restraint provided along the length of the pipe by the soil. However, it is difficult to quantify this contribution and it is likely to be insignificant if

the pipe is short. Because pressure is a primary load, the level of tensile stress is maintained even if yielding of the material occurs.

The longitudinal tensile stresses that develop in an infinitely long buried pipe are less than one half of the hoop stress,  $\sigma_h$ . In this case, internal pressure does not directly give rise to a component of longitudinal tension because of the axial restraint provided by the soil. Instead, Poisson effects cause longitudinal tension to develop as circumferential strain increases, as follows:

$$\varepsilon_\ell = \frac{\sigma_\ell}{E} - \frac{\nu\sigma_h}{E} = 0 \quad [5-1]$$

because of axial restraint, from which

$$\begin{aligned} \sigma_\ell &= \nu\sigma_h \quad \text{and, for } \nu = 0.3, \\ \sigma_\ell &= 0.3\sigma_h \end{aligned} \quad [5-2]$$

where,

$$\begin{aligned} \nu &= \text{Poisson's ratio (0.3 for elastic behaviour of steel)} \\ \varepsilon_\ell &= \text{longitudinal strain.} \end{aligned}$$

It is clear, therefore, that the level of longitudinal tensile stress induced in the pipe wall is lower for the case of an infinitely long pipe. Recalling that tensile stresses usually stiffen and stabilize the pipe, the use of the infinitely long pipe in the analyses is judged to be more conservative. Furthermore, the longitudinal stresses in the infinitely long pipe are secondary in nature, and would be diminished as yielding occurs in the material.

Another observation regarding the use of an infinitely long pipe is that the axial restraint of both ends of pipe segment *a-b* gives rise to a component of direct tension in the pipe if it acts as a catenary between sleeper supports. However, trial finite element analyses showed that these tensile forces are negligibly small as compared to those described by equation [5-2], and the effect is deemed to be inconsequential.

Finally, the soil model used in this work is greatly simplified, and the beneficial effects of lateral soil pressure have been intentionally neglected. The potential exists to improve the *in situ* idealization to reflect the interaction between the pipe and the soil more realistically. However, because the soil model used in this work should always provide conservative estimates of the behaviour, refinement of the soil-structure interaction model is not deemed necessary at this time.

## 5.2 FINITE ELEMENT MODELLING OF IDEALIZED SLEEPER-SUPPORTED PIPING

Loading and boundary conditions for the *in situ* finite element model are developed from the idealization presented in Section 5.1. Based upon the isolated segment *a-b* from Figure 5.1(f), the geometry of the finite element mesh is that shown in Figure 5.2. In this mesh, the geometry and the level of refinement match the models of the laboratory specimens reported in Chapter 3, except that the sleeper is now located beneath the pipe to match its orientation in field installations. A vertical plane of symmetry is again used along the longitudinal centreline of the segment. As in Chapter 3, all of the analyses described in this chapter make use of ABAQUS/Standard v5.7-1 (HKS, 1997a).

### 5.2.1 Kinematic Boundary Conditions

The nature of the idealized *in situ* conditions described in Section 5.1 require that displacement component  $u_3$  and rotational components  $\phi_1$  and  $\phi_2$  must be restrained at nodes on both ends of the modelled segment. The vertical plane of longitudinal symmetry is achieved by setting displacement  $u_1$  and rotations  $\phi_2$  and  $\phi_3$  to zero for nodes on that plane. Only the sleeper is restrained in the  $u_2$  direction, so it carries all of the vertical forces applied to the model. All kinematic boundary conditions used in the *in situ* finite element model are summarized in Figure 5.3.

Interaction between the sleeper and the pipe is modelled with the same contact formulation as that used for the models of the laboratory specimens. The sleeper-to-pipe contact surfaces provide the only restraint for the pipe in the negative 2-direction. Because there is no restraint of the pipe in the positive 2-direction, the assembled stiffness matrix can develop problems related to numerical instability. In order to overcome this effect, the self-weight of the steel pipe, which is small in relation to the forces induced by external loads, is considered in the analysis. This ensures that sleeper-to-pipe contact is initiated immediately, thereby providing numerical stability to the system.

### 5.2.2 Loads

The only external loads to be applied to the *in situ* finite element model are self-weight, internal pressure, and uniform soil pressure in the negative 2-direction.

Self-weight and internal pressure are accommodated easily using the available software options, but the unidirectional soil pressure is not: for shell elements, surface pressure can act only in a direction normal to the reference surface. To overcome this difficulty, the soil pressure is projected instead onto the pipe and distributed as a set of equivalent internal body forces. To determine the distribution, the body force per unit volume for each element is set at a value that is proportional to the area,  $A_p$ , obtained when that element is projected onto a horizontal plane. In turn, the software distributes these body forces into work-equivalent forces applied at the nodes. A cross-section of the pipe that shows the resulting nodal force distribution is shown in Figure 5.4.

As the pipe is loaded with soil pressure, its width increases. The tributary area of the pipe exposed to vertical soil pressure thereby enlarges, which, in turn, causes the loads to increase. The shaded region in Figure 5.5 represents that portion of the overall load that is attributable to this second-order effect. These second-order loads exacerbate distortion of the cross-section and hasten collapse, so it is not conservative to neglect their effect in an analysis. Consequently, the influence of the second-order loads has also been investigated. Because there is not a built-in function in ABAQUS that enables the user to model unidirectional pressure on shell elements, it is also not possible to account directly for second-order effects that result from such loading. However, the usefulness of the software is enhanced by its capability to accept external FORTRAN algorithms written by the user. For this work, the author developed a subroutine that reads the list of nodal displacements that is generated after an increment of the solution. Using these values, it calculates for each element the change in area,  $\Delta A_p$ , of its projection on the horizontal plane. The non-linear component of the load is set at a level directly proportional to this change in area. Therefore, the total body force that acts in the negative 2-direction on a particular element consists of a linear and a non-linear component. The first-order component is proportional to the initial projected area,  $A_p$ , and the second-order component is proportional to the change of this projected area,  $\Delta A_p$ , as shown in Figure 5.6.

At early stages of an analysis, the deformations, and thus the second-order loads, are not significant. For the design of a sleeper-supported pipe, which is likely to be governed by limiting cross-sectional distortion to a reasonable level (probably less than

$\sigma=15\%$ ), the second-order effect will be small if the distortion is within the acceptable range. Therefore, it may be possible to neglect the second-order effect. However, it was found that the additional computational effort required to incorporate the second-order effect into the solution does not increase processor time significantly. Consequently, it is included in all analyses performed in the parametric study. An example illustrating the influence of the second-order effect is presented in Section 5.4.3.

### 5.2.3 Selection of a Solution Technique

For the finite element analyses described in Chapter 3, load was introduced onto the pipe by means of an imposed displacement of the sleeper. This matched conditions in the laboratory and allowed the solutions to accommodate potential non-linear geometric and material instability of the structure. However, the idealized loads for the *in situ* model are imposed directly by soil pressure, and the sleeper must provide equal and opposite reactive forces. Consequently, load rather than displacement must be the controlling variable in these analyses, and this requires that modifications be made to the solution technique. As before, non-linear geometry and material properties must be taken into account in the problem, and the generalized load-displacement equilibrium path may not always have a positive slope. A special solution procedure is required in order to track the behaviour of a structure through regions of zero stiffness or where it is necessary for the structure to release strain energy to remain in static equilibrium. This section describes the options that were reviewed as potential solution strategies for the finite element analyses of *in situ* conditions.

The basic approach taken in ABAQUS for the solution of the non-linear equations of equilibrium is the well-known load-controlled Newton (or Newton-Raphson) iterative method. Although modifications to the Newton approach are available, ABAQUS makes use of the standard (or full) Newton method as the default solver (HKS, 1997b). However, any type of Newton solution technique, either standard or modified, only works up to the limit load—it can follow only an equilibrium path that has positive slope. In other words, the Newton method diverges once the limit point is reached, because the tangent stiffness matrix becomes singular (see, for example, Bathe, 1996). The solution path followed in a standard Newton analysis is illustrated in Figure 5.7.

Because the intention is to use distortion as the governing criterion in the new design method for sleeper-supported pipes, it is not essential for the finite element models to be able to predict the collapse load or behaviour during collapse. However, it is still of academic interest to do this. Consequently, so-called *arc length control* methods for overcoming limit points by means of indirect load control were explored. The technique was first developed by Riks (1972; 1979) with subsequent improvements by others (for example, Ramm, 1980). The arc length method is similar to displacement control in that the load level is an unknown in the system of equations. In simple terms, an arc length method uses an iteration path that starts initially in a direction normal to a tangent plane taken on the equilibrium surface at the previously converged point. In this context the geometry is the space of the nodal displacement variables and a scalar load parameter. Because the iteration path follows the normal to the tangent, the solution usually converges at the limit point and beyond.

The so-called modified Riks method, which is an available solution option in ABAQUS (HKS, 1997b; HKS, 1997c), is a type of arc length control. Because the Riks method should allow the behaviour during collapse to be obtained, it was deemed to be the solution strategy of choice for the *in situ* finite element model. However, after performing some trial runs with the model, it was discovered that the Riks method of solution could not be relied upon to provide a solution for the portion of the response beyond the limit point. Investigation of this problem revealed that the use of contact surfaces (in this case the region of sleeper-to-pipe interaction) in a Riks solution is not reliable if loss of contact occurs (HKS, 1997c). This problem seems to be a limitation of the software itself.

The only other means of obtaining the behaviour during collapse for the particular loading scenario used in the *in situ* model would be to add viscous damping or inertial effects to the problem. The resulting dynamic forces would serve to stabilize the structure during collapse. To implement such an analysis would be difficult and the solutions would likely have considerable computational expense, so it is judged not to be a practical option.

As a result, it is necessary to use the default Newton solution method in ABAQUS for the finite element analyses of *in situ* conditions. This technique does not

allow the behaviour during collapse of the structure to be modelled, but gives a sufficient amount of the solution to be useful in the range of interest.

#### **5.2.4 Material Representation, Residual Stresses, and Initial Geometry**

The material model used in the *in situ* model is the same as that used in Chapter 3, except that the stress-strain curve is now assumed to be elastoplastic. The yield surface is a circular cylinder centred on the hydrostatic stress axis, and it changes neither size nor shape as inelastic behaviour occurs. More simply, it can be said that strain hardening is neglected and that plastic flow occurs once the shear stress in the material reaches a critical value. The plastic strain increment takes place in a direction normal to the yield surface. This representation is a conservative approximation of the true material behaviour, which would exhibit strain hardening. The elastic modulus is set at 207 000 MPa, which is that value recommended in CSA Z662-96 for the numerical analysis of pipelines (Canadian Standards Association, 1996). Poisson's ratio is assigned a value of 0.3 in the elastic range and 0.5 for plastic straining.

Residual stresses are not represented in the *in situ* model because, in the experimental tests, they were found not to have a significant influence on the behaviour. As in the analyses of the laboratory specimens, the finite element meshes for all of the *in situ* models have perfectly cylindrical initial geometry.

### **5.3 SELECTION OF REPRESENTATIVE MODEL PARAMETERS**

To develop a new design method for sleeper-supported pipes it is necessary to study a set of parameters representative of standard practice. These should reflect a variety of realistic loading conditions and geometric configurations for sleeper-supported pipes. The following parameters are likely to be of the most interest to the designer, and are judged to comprise all of the fundamental variables that govern the behaviour of the idealized sleeper-supported piping system:

- $w$             downward soil pressure
- $p$             actual level of internal pressure ( $\leq$  design pressure)
- $o$             out-of-roundness
- $D$             pipe diameter
- $2b$            sleeper support length

- $t$  pipe wall thickness
- $L$  sleeper support spacing (o/c)
- $\sigma_y$  static yield strength
- $E$  modulus of elasticity
- $G$  shear modulus
- $\nu$  Poisson's ratio

Shear modulus,  $G$ , will not play a major role in the behaviour because shear deformation is negligible in the analysis of thin-walled pressure vessels; it need not be considered in the parametric study. Poisson's ratio,  $\nu$ , which is a dimensionless measure, has nearly a constant value for all types of steel and can also be deleted from the parametric study.

The location and contents of the line, and thus the specific design rules that must be followed, are clearly also parts of the design process. The type of pipe manufacture, spiral or seam welded, is not listed as a parameter because no discernible difference in behaviour between these two types of pipe was evident in the laboratory tests.

### 5.3.1 Simplification of the Parametric Study—Dimensional Analysis

Based upon the foregoing discussion, a total of nine variables will be investigated in the parametric finite element study:  $w$ ,  $p$ ,  $o$ ,  $D$ ,  $2b$ ,  $t$ ,  $L$ ,  $\sigma_y$ , and  $E$ . To study these factors in combination would require the analysis of an unmanageable number of models. To reduce the complexity of the parametric study, it is useful to implement methods of dimensional analysis, which is a process by which extraneous information is eliminated from a relation between quantities. The dimensional analysis approach is described in brief below; Taylor (1974) provides a complete description of dimensional analysis methods.

Consider any physical problem, the behaviour of which is governed by a set of  $n$  quantities,  $A_1, A_2, \dots, A_n$ , that comprise all of the variables essential to the solution of the mechanics of the system. It is reasonable to assume that the solution can be expressed in terms of a homogeneous function:

$$F(A_1, A_2, \dots, A_n) = 0 \quad [5-3]$$

If one wishes to establish the form of this function by means of physical or numerical modelling, it is necessary to vary all of the quantities in order to examine their influences on the solution. For reasons of practicality, it would be advantageous to cast the function in another form so as to reduce the number of parameters that must be investigated. This can be done by means of the Buckingham Pi theorem, which is stated in simple terms by Langhaar (1951) as follows:

*If an equation is dimensionally homogeneous, it can be reduced to a relationship among a complete set of dimensionless products.*

For a set of dimensionless products to be complete, each product in the set must be independent of the others, and every other dimensionless product of the variables is a product of powers of dimensionless products in the set. It can be shown that the number of dimensionless products formed in a complete set is  $n-r$ , in which  $r$  is the rank of the dimensional matrix of the variables  $A_1, A_2, \dots, A_n$ . (The rank of a matrix is the largest order of any square sub-matrix that has a non-zero determinant. Note also that an often-used rule of thumb is that  $r$  is the total number of dimensions (mass, length, time, etc.) encompassed by the variables  $A_1, A_2, \dots, A_n$ . While often correct, this guideline is not rigorously accurate and can lead to incorrect answers.) As consequence of the Pi theorem, the function [5-3] can be recast in terms of dimensionless independent  $\pi$ -parameters:

$$F(\pi_1, \pi_2, \dots, \pi_{n-r}) = 0 \quad [5-4]$$

The importance of this transformation is that scale effects can be controlled in an experimental or numerical modelling program and the number of parameters that must be considered is reduced by  $r$ , which can result in a significant saving of cost and effort.

### **5.3.2 Application of Dimensional Analysis to Sleeper-supported Pipe Problem**

Using fundamental units of mass (M), length (L), and time (T), the dimensional matrix for the variables encompassed by the sleeper-support problem has the following form:

	w	p	o	D	2b	t	L	$\sigma_y$	E
M	1	1	0	0	0	0	0	1	1
L	-1	-1	0	1	1	1	1	-1	-1
T	-2	-2	0	0	0	0	0	-2	-2

This matrix has rank two. Consequently, seven independent non-dimensional  $\pi$ -terms must be formed. Wherever possible, it is advantageous to choose terms that are commonly used in the pipeline industry, such as  $D/t$ . The parameters chosen are:

$$\begin{aligned}
\pi_1 &= \frac{D}{t} \\
\pi_2 &= \frac{p}{\left(\frac{2 \times \sigma_y \times t}{D}\right)} = \frac{p}{p_y} \\
\pi_3 &= \frac{2b}{D} \\
\pi_4 &= \frac{L}{D} \\
\pi_5 &= \frac{\sigma_y}{E} = \varepsilon_y \\
\pi_6 &= \frac{w}{\sigma_y} \\
\pi_7 &= o
\end{aligned}
\tag{5-5}$$

where,

$p_y$  = pressure at which the hoop stress equals the yield strength  
 $\varepsilon_y$  = strain at which yielding begins.

The first five  $\pi$ -parameters are necessary as input to the *in situ* finite element model,  $\pi_6$  is related directly to the loading variable in the model, and  $\pi_7$  is obtained as output. In terms of limit states design, the ultimate limit state is described by the maximum value of  $\pi_6$  obtained in the analysis (assuming that the solution is able to reach the limit point). The serviceability limit state can be described in terms of  $\pi_7$ , the level of out-of-roundness.

### 5.3.3 Representative Ranges of the $\pi$ -Parameters

In typical practice, the maximum allowable operating pressure for a natural gas pipeline lies between about 7 000 and 10 000 kPa. Common grades of pipe are 359 MPa, 483 MPa, and 550 MPa, and the most common manufacturing processes make use of high-frequency resistance seam welding or submerged arc welding. (Grade 550 pipes, which were not tested in the experimental program, are included in the parametric study because grade 550 material has recently become standard for the construction of many major new Canadian pipeline systems (Glover et al., 1999)). Using these figures, representative values of  $D/t$  for typical Canadian practice can be calculated using the requirements of Clause 4.3.3.1.1 in CSA Z662-96:

$$t = P \times \frac{D}{2} \times \frac{1}{S} \times \frac{1}{F} \times \frac{1}{L} \times \frac{1}{J} \times \frac{1}{T} \quad [5-6]$$

where,

- P = design pressure (usually maximum allowable operating pressure)
- S = specified minimum yield strength
- F = design factor (taken as 0.8 for steel).
- L = location factor
- J = joint factor (taken as 1.0 for seamless, electric welded and submerged arc welded pipe)
- T = temperature derating factor (taken as 1.0 except when operating temperature exceeds 120°C).

Considering usual conditions, this formula can be rewritten as:

$$\frac{D}{t} = \frac{1.6}{P} \times S \times L \quad [5-7]$$

According to the CSA Z662-96 rules, the location factor,  $L$ , is taken as 1.0 for general installations that carry non-sour gas if there is minimal human habitation in proximity (Class Location 1). However, in compressor station yards where sleeper supports are most commonly used, the location factor is to be taken as 0.625. This is done to increase the level of safety within the station, which is a critical component of the system. Using the typical values for pressure and grade in equation [5-7],  $D/t$  for yard piping ranges from about 40 to 80. For mainline piping, values of  $D/t$  in the range from 60 to 120 are common. The difference between yard piping and mainline piping reflects the fact that equation [5-7] effectively limits the allowable hoop stress to 50% of the specified minimum yield strength for yard piping and 80% of the specified minimum

yield strength for line piping. These factors establish ranges for  $\pi_1$  that should be considered in the parametric study.

The *actual* level of internal pressure in a line at a particular time can vary between zero and full pressure, with the most common level of pressure at a given location depending on, among other factors, its location relative to compressor stations. Therefore, the engineer should, as a minimum, consider the two extremes in the design process, namely operation at zero pressure ( $p/p_y=0$ ) and also at full pressure ( $p/p_y=0.5$  or  $p/p_y=0.8$ , depending on whether the location is a compressor station yard or mainline, respectively). This establishes bounds for the second  $\pi$ -parameter.

In general, sleeper supports currently used in practice have a length of  $1.5D$  (Kormann and Zhou, 1995), or, in equivalent non-dimensional terms,  $2b/D=1.5$ . However, in certain circumstances where space constraints are severe it may be necessary to use smaller sleepers or to support the pipe on horizontal steel beams mounted on piles. Consequently, the values of  $\pi_3$  that will be considered in the parametric study are  $2b/D=1.5$ ,  $2b/D=1.0$ , and  $2b/D=0.5$ . This is consistent with the sizes that were investigated in the experimental test program.

Sleeper spacing is described by the fourth  $\pi$ -parameter. To establish reasonable bounds on  $\pi_4$ , it is instructive to consider the existing design method for sleepers given in equation [1-3]. This equation prescribes the spacing to be in the order of  $2D$  to  $4D$  for pipes with typical embedment depths (about 1.5 to 3 m). This is evident in Figure 5.8, which represents equation [1-3] graphically for several common sizes of pipe. Because one goal of this research is to establish specifically whether greater support spacings are possible, the parametric investigation will include  $L/D$  ratios of 5, 7, and 9.

The fifth  $\pi$ -parameter describes the yield strain of the material. Because  $E$  is essentially constant at 207 000 MPa for all grades of carbon and high-strength low-alloy steel, this parameter will vary directly with the yield strength,  $\sigma_y$ , of the material. Yield strengths of 359 MPa, 483 MPa, and 550 MPa are considered in the analyses to correspond to grades that are in common use.

The final two dimensionless parameters,  $\pi_6$  and  $\pi_7$ , are obtained directly from the analyses. To reiterate, the downward soil pressure,  $w$ , is the control variable in the analyses, and is made non-dimensional by dividing by the yield strength to obtain  $\pi_6$ . The

seventh  $\pi$ -parameter is the level of out-of-roundness,  $o$ , which is calculated from nodal displacements obtained from the analyses.

#### 5.4 PERFORMANCE ASSESSMENT OF THE *IN SITU* MODEL

It was shown in Chapter 4 that the finite element models of the test specimens provide good predictions of the behaviour observed in the experiments. However, validity of the results from the idealized finite element model of *in situ* conditions that are developed in this chapter can not be assessed directly—no *in situ* test data are available. Because the essence of the finite element modelling techniques used in Chapter 3 have been preserved in the models of *in situ* conditions, it is reasonable to assume that the results are valid. Other aspects of the *in situ* finite element model must also be assessed by proving that the Buckingham Pi theorem is implemented properly, by examining the influence of second-order loads, and by testing the ability of the model to be numerically stable for all of the many possible combinations of input parameters.

##### 5.4.1 Suitability of Non-dimensional Parameters

One of the requirements of the Buckingham Pi theorem is that all of the fundamental variables necessary to describe the mechanics of the problem must be included in the set of  $A_n$  quantities. For the idealized sleeper-supported pipe problem, these variables were identified as  $w$ ,  $p$ ,  $o$ ,  $D$ ,  $2b$ ,  $t$ ,  $L$ ,  $\sigma_y$ , and  $E$ . To assess whether all of the essential variables that play a role in the behaviour are represented in this set, a preliminary investigation was carried out on pipes having identical  $\pi$ -parameters but different scales. If the set contains all of the essential quantities, then the results from these analyses will be unaffected by changes in scale.

To test whether all important variables are taken into account, five analyses of pipes each having identical  $\pi$ -parameters of  $D/t=80$ ,  $p/p_y=0$ ,  $2b/D=1.0$ ,  $L/D=7$ , and  $\varepsilon_y=2.33 \times 10^{-3}$  are considered. Choosing pipe diameters and grades to range across a spectrum of typical values varies the scale. As detailed in Table 5.1, the first model considers a pipe of small diameter made of low strength material, the second a small pipe with high strength material, and so on. Each model in the table is designated in the form  $\pi_1-\pi_2-\pi_3-\pi_4-\pi_5$ , with an additional letter to indicate the scale of the model. Once  $D$  and  $\sigma_y$  are selected, values of  $t$ ,  $2b$ ,  $L$ ,  $E$ , and  $p$  are chosen so that the five  $\pi$ -parameters remain

constant. These are also shown in Table 5.1. Note that the specific values of the individual variables in these five analyses are not necessarily representative of real steel pipelines: the only intent is to demonstrate that the effect of model scale has been controlled appropriately.

To reiterate, if no significant differences are identified between analyses that have identical  $\pi$ -parameters but different scales, then it can be said that appropriate account has been made of all variables that govern the mechanics of the problem. A comparison of the models described in Table 5.1 is presented graphically in Figure 5.9 in terms of non-dimensional soil pressure ( $\pi_6$ ) versus out-of-roundness ( $\pi_7$ ). Examination of the figure reveals that large changes of scale evoke no change in response, even when comparing extreme cases (e.g., the difference between a small pipe with low material strength and a large pipe with great strength). A similar procedure can be followed to show that the same is true for those cases in which internal pressure is present. Therefore, one must conclude that all of the variables that play a major role in the behaviour are accounted for appropriately in the set of seven  $\pi$ -parameters listed in [5-5].

As an aside, it is worthwhile to examine an error that is sometimes made by structural researchers who employ the Buckingham Pi theorem. An incorrect assumption is easily made that  $E$ , the modulus of elasticity, can be omitted from the set of variables that govern the problem. This is usually done because  $E$  is approximately constant for a particular type of material; for example, virtually all types of steel have  $E \approx 207\,000$  MPa. However, this assumption will often lead to an incorrect assessment of system behaviour, particularly if there is geometric or material non-linearity. In the following paragraphs it will be demonstrated that the inclusion of  $E$  as a parameter is essential in order to control the effect of model scale.

Let us assume for a moment that  $E$  is omitted from the list of variables that govern the behaviour of sleeper-supported pipelines so that only  $w$ ,  $p$ ,  $o$ ,  $D$ ,  $2b$ ,  $t$ ,  $L$ , and  $\sigma_y$  remain. For this case  $n$  is eight and  $r$  is two, so that the number of non-dimensional  $\pi$ -parameters required is six. One might choose the following:

$$\begin{aligned}
\pi_i &= \frac{D}{t} \\
\pi_{ii} &= \frac{p}{\left(\frac{2 \times \sigma_y \times t}{D}\right)} = \frac{p}{p_y} \\
\pi_{iii} &= \frac{2b}{D} \\
\pi_{iv} &= \frac{L}{D} \\
\pi_v &= \frac{w}{\sigma_y} \\
\pi_{vi} &= 0
\end{aligned}
\tag{5-8}$$

This is the same set of  $\pi$ -parameters as presented in equation [5-5], except that  $\varepsilon_y$  is now absent. Implicit in the assumption to neglect  $E$ , and therefore  $\varepsilon_y$ , is that the behaviour of the system is not affected by this parameter when the scale of the model is changed. Let us use the same values presented in Table 5.1, except that  $E$  is now held constant, that is, the assumption is made that  $E=207\,000$  MPa in all cases because the pipes are steel. These values are shown in Table 5.2. When analyses are made of these five pipes, it is hoped that the response of all five will be identical because parameters  $\pi_i$  through  $\pi_{iv}$  are held constant. However, the results are not identical. Figure 5.10 shows the responses obtained from the analyses for these five models, making it clear that the response is not independent of model scale if  $E$  is held constant. Consequently, it is essential to include  $E$  among the group of system variables so that the effect of yield strain can be assessed in a parametric study. To omit this variable will lead to incorrect predictions of the behaviour.

#### 5.4.2 Examination of the Deformed Shape

It is instructive to look at the overall deflected shape of a typical pipe in order to determine whether all kinematic boundary conditions are implemented properly and to judge whether the solution is giving results that are consistent with expectations. In Figure 5.11, the progression of deformation is shown for a pipe having of  $D/t=80$ ,  $p/p_y=0.5$ ,  $2b/D=1.0$ ,  $L/D=7$ , and  $\varepsilon_y=2.33 \times 10^{-3}$ . These represent middle values in the range

of interest for each parameter. The mechanism observed is similar to that seen in the experimental tests, and all of the kinematic boundary conditions are satisfied correctly.

### **5.4.3 Influence of the Second-order Soil Loads**

As stated in Section 5.2.2, the soil loads on the finite element model consists of both a linear component and a non-linear component. Now that the problem has been arranged in non-dimensional form, an assessment can be made of the magnitude of the second-order effect. To make this assessment, unpressurized pipes having  $D/t=120$  are examined. Pipes with these properties are expected to exhibit second-order effects most severely, because they undergo the greatest amount of distortion for a given load. Figure 5.12 shows the finite element analysis results for a pipe having parameters 120-0-1.0-7-2.33, both including and excluding the second-order effect. Even for this extreme case, the second-order effect results only in a reasonably minor decrease in performance, particularly at 'acceptable' levels of out-of-roundness. Although the second-order effect is included for all analyses performed herein, it would probably be reasonable to neglect this effect in any future study.

### **5.4.4 Numerical Stability of the Model**

It is necessary for the finite element model to perform reliably for all of the diverse ranges of parameters outlined in Section 5.3.3. As a test of the numerical stability of the model, a number of combinations of the various  $\pi$ -parameters were tried in order to identify potential difficulties. During these trial runs it was discovered that certain combinations of the input variables caused numerical instability and, as a consequence, premature termination of the solution. Unpressurized pipes having  $D/t=40$  caused the most difficulty. The failure of the solution to converge reliably in these cases is attributed to the sudden violation of contact constraints between the sleeper and the pipe. For pressurized pipes, the presence of internal pressure serves to stabilize the system, so it is not surprising that the lack of convergence appeared only in analyses of unpressurized systems. Those pipes having  $D/t=40$  are the most stiff and, for a given load, deform less than those having greater values of  $D/t$ . Recalling that contact is defined only at the nodes of the pipe, any local violations of contact constraints that occur are more severe for a heavy-walled pipe. The violations lead to the difficulties related to convergence.

Several options are available to stabilize the solution numerically. One choice is to refine the finite element mesh within the contact area to provide more nodes. However, refinement of the mesh for just a few analyses is undesirable, since homogeneity of modelling techniques throughout the study is preferred. Customization of the mesh would also make the reduction of the output data more difficult. Instead, a more elegant solution is available that involves adding viscous damping to the contact interface. The viscous damping allows some pressure to be transmitted between the contact surfaces before they touch, which smoothes violations of the contact constraints and helps the software to obtain a solution. Pressures arising from damping develop in proportion to the clearance between surfaces and their relative 'velocity.' In this context, velocity is not measured in real time, but rather in the solution time used by the software's automatic incrementation scheme. Viscous pressure is transmitted only when the surfaces are within a critical distance of each other,  $c_0$ . As the surfaces become closer, the damping coefficient,  $\mu$ , also increases, up to a maximum value,  $\mu_0$ , when the surfaces are in contact. Additional details are available in the software documentation (HKS, 1997c).

The objective is to add sufficient damping to stabilize the system, but not so much that the solution is altered significantly by its presence. The clearance at which damping begins,  $c_0$ , was selected to be 1 mm, so that the transfer of pressure begins only when the surfaces are within close proximity. A reasonable value of  $\mu_0$  was chosen by trial and error: a large value of damping was imposed in a first attempt, and progressively smaller values were used until the numerical instabilities reappeared. Eventually,  $\mu_0=0.01$  MPa/(mm/s) was chosen, which is sufficient to stabilize the system but does not affect the solution adversely. When comparing the results of this analysis with that portion of the solution available from the undamped analysis, no significant differences are present. Consequently, the method is judged to be appropriate. In Chapter 6, which describes the parametric finite element study, viscous damping is used for all unpressurized cases in which  $D/t \leq 80$ . Damping is also added in the few other cases in which convergence problems related to violation of contact constraints arose.

**Table 5.1** Parameters for investigation of potential scale effects

Designation	D (mm)	t (mm)	$\sigma_y$ (MPa)	2b (mm)	L (mm)	$p_y$ (MPa)	p (MPa)	E (MPa)
80-0-1.0-7-2.33a	406	5.08	359	406	2842	8.98	0	153 857
80-0-1.0-7-2.33b	406	5.08	550	406	2842	13.75	0	235 714
80-0-1.0-7-2.33c	762	9.53	483	762	5334	12.08	0	207 000
80-0-1.0-7-2.33d	1219	15.24	359	1219	8533	8.98	0	153 857
80-0-1.0-7-2.33e	1219	15.24	550	1219	8533	13.75	0	235 714

$$\text{Designation: } \frac{D}{t} - \frac{p}{p_y} - \frac{2b}{D} - \frac{L}{D} - \epsilon_y$$

**Table 5.2** Parameters for investigation of potential scale effects if E is considered to be a constant

Designation	D (mm)	t (mm)	$\sigma_y$ (MPa)	2b (mm)	L (mm)	$p_y$ (MPa)	p (MPa)	E (MPa)
80-0-1.0-7a	406	5.08	359	406	2842	8.98	0	207 000
80-0-1.0-7b	406	5.08	550	406	2842	13.75	0	207 000
80-0-1.0-7c	762	9.53	483	762	5334	12.08	0	207 000
80-0-1.0-7d	1219	15.24	359	1219	8533	8.98	0	207 000
80-0-1.0-7e	1219	15.24	550	1219	8533	13.75	0	207 000

$$\text{Designation: } \frac{D}{t} - \frac{p}{p_y} - \frac{2b}{D} - \frac{L}{D}$$

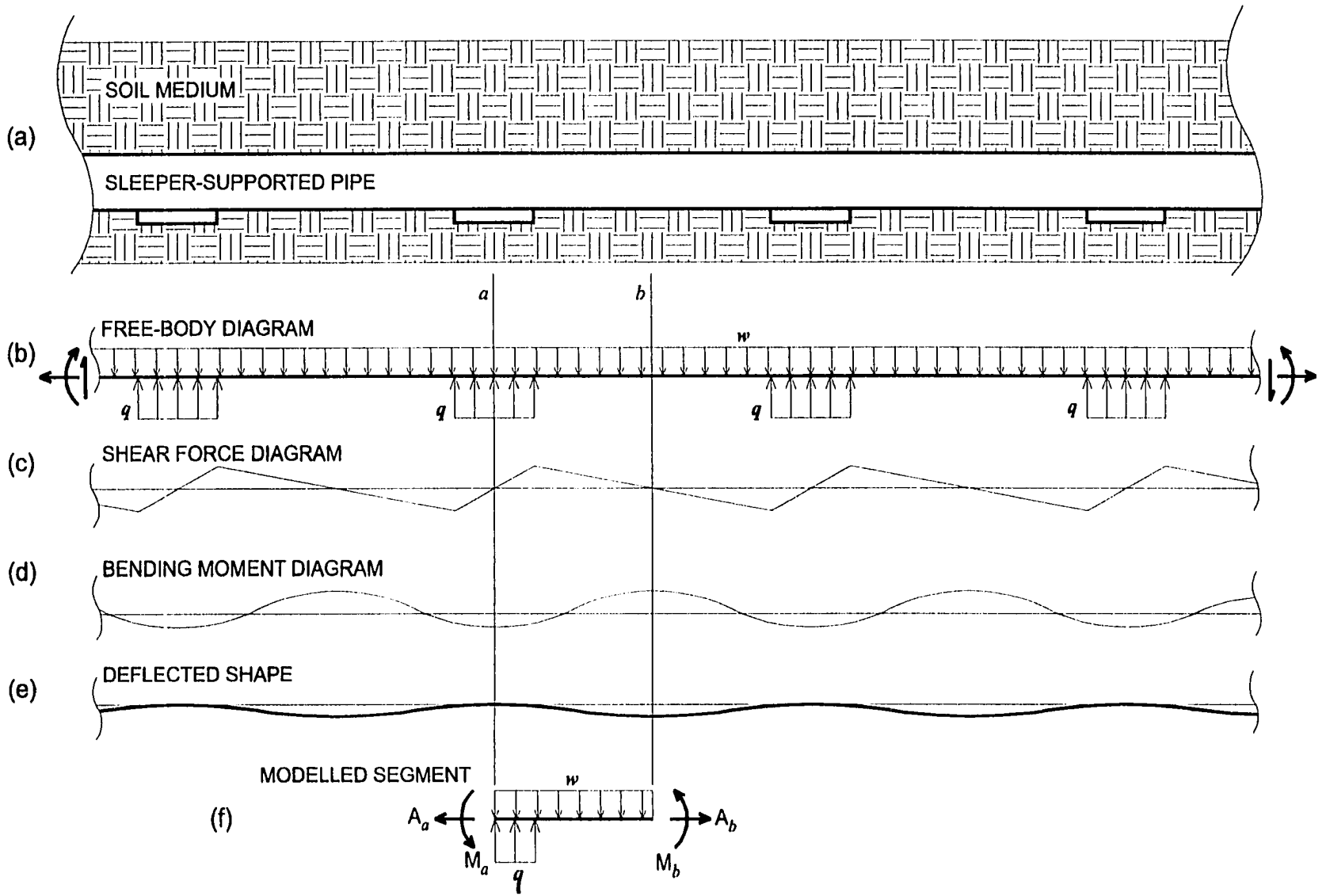


**Figure 5.1** Idealization of *in situ* sleeper-supported piping

Figure 5.3 Kinematic boundary conditions for *in situ* model

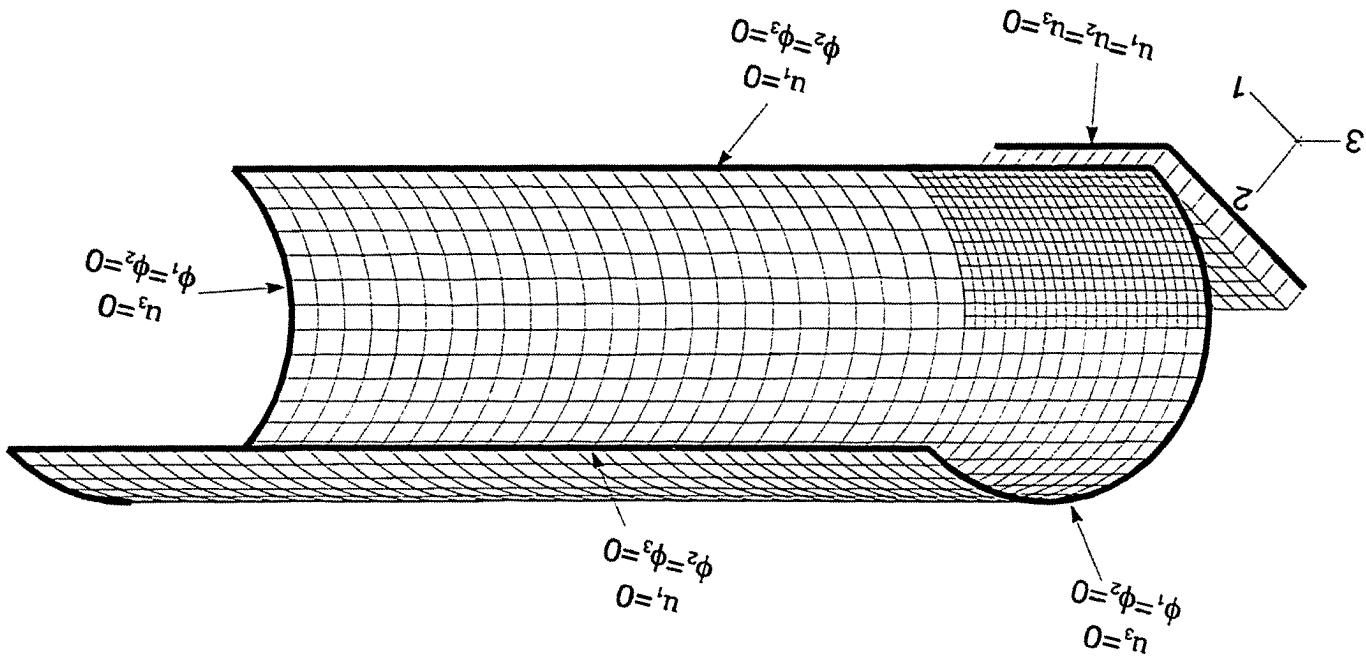
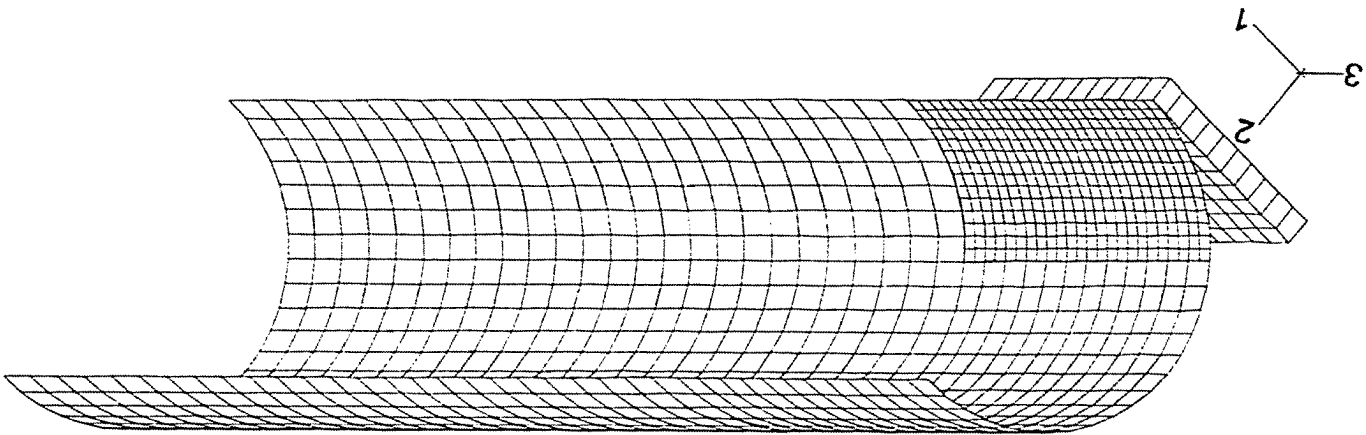
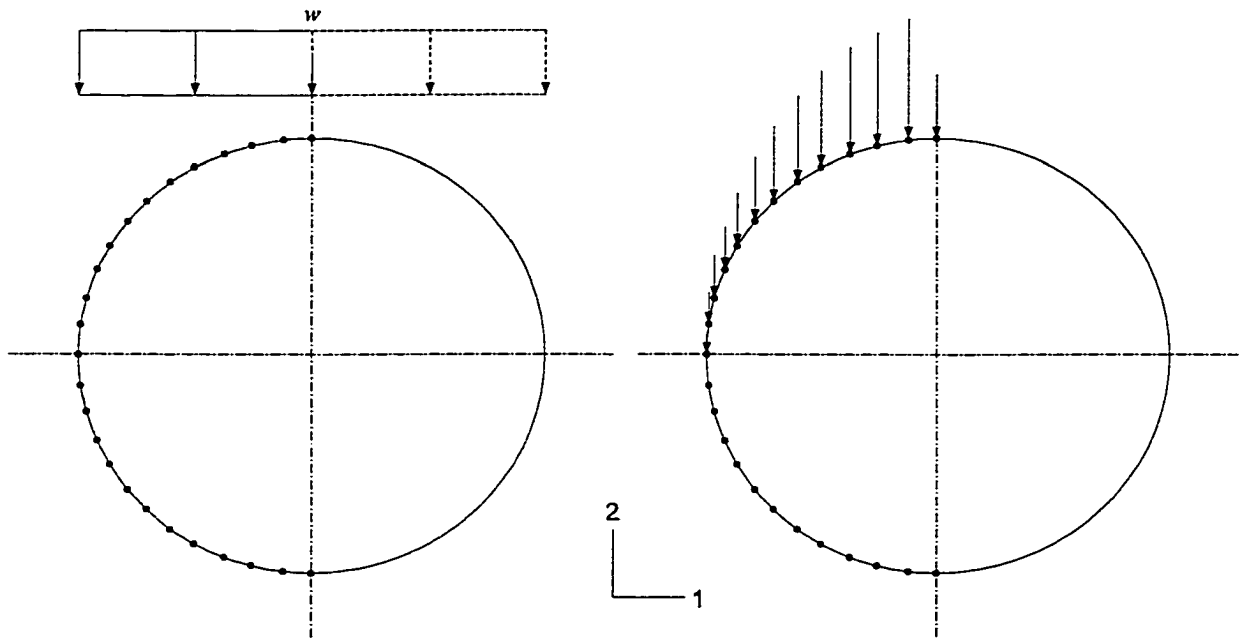
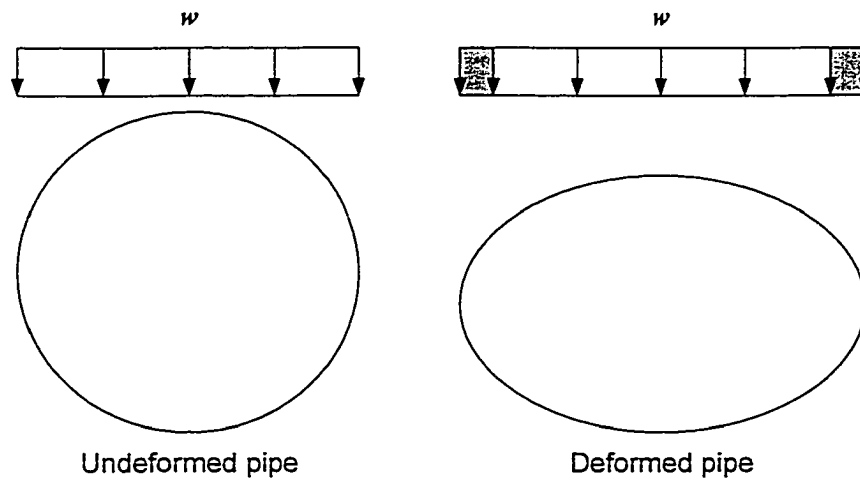


Figure 5.2 Finite element mesh for *in situ* model





**Figure 5.4** Uniform soil pressure distributed as work-equivalent nodal forces



**Figure 5.5** Second-order loads resulting from distortion

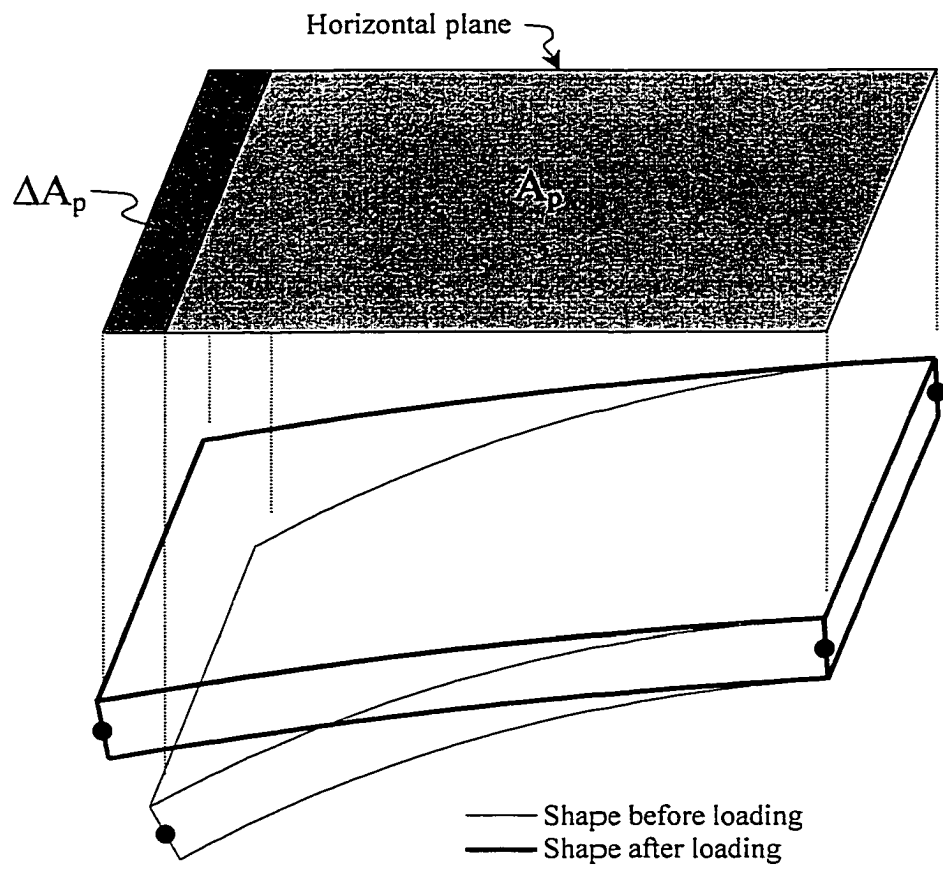


**Figure 5.6** Second-order effect for an individual element

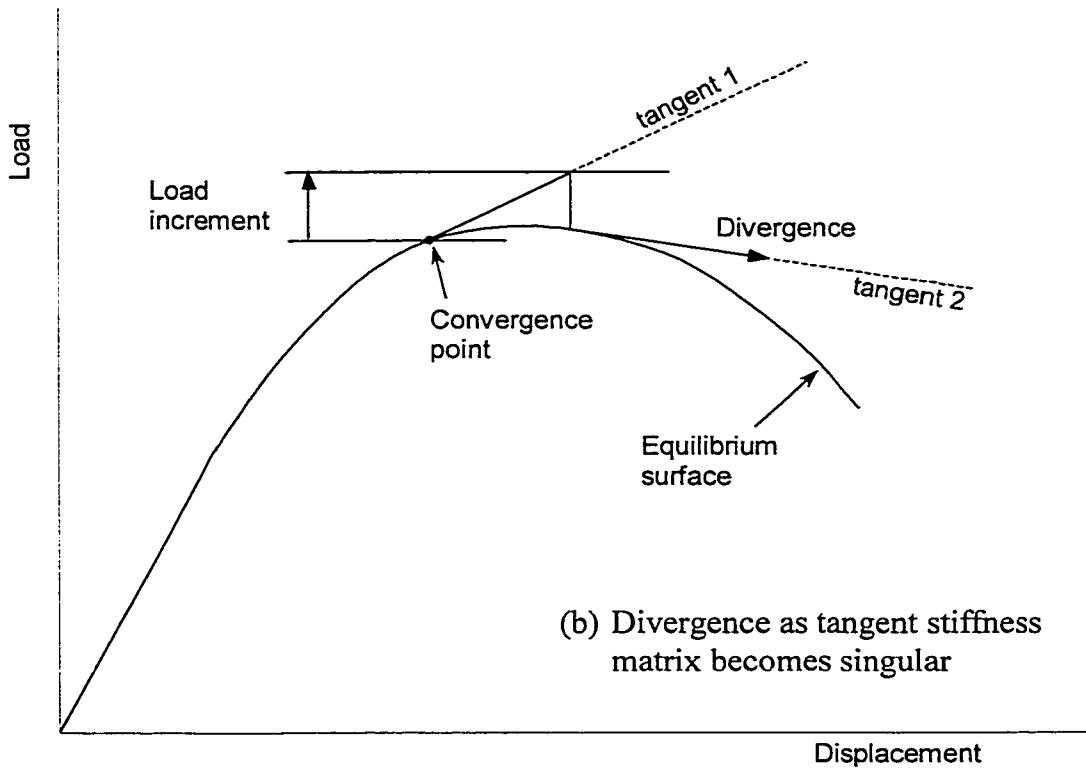
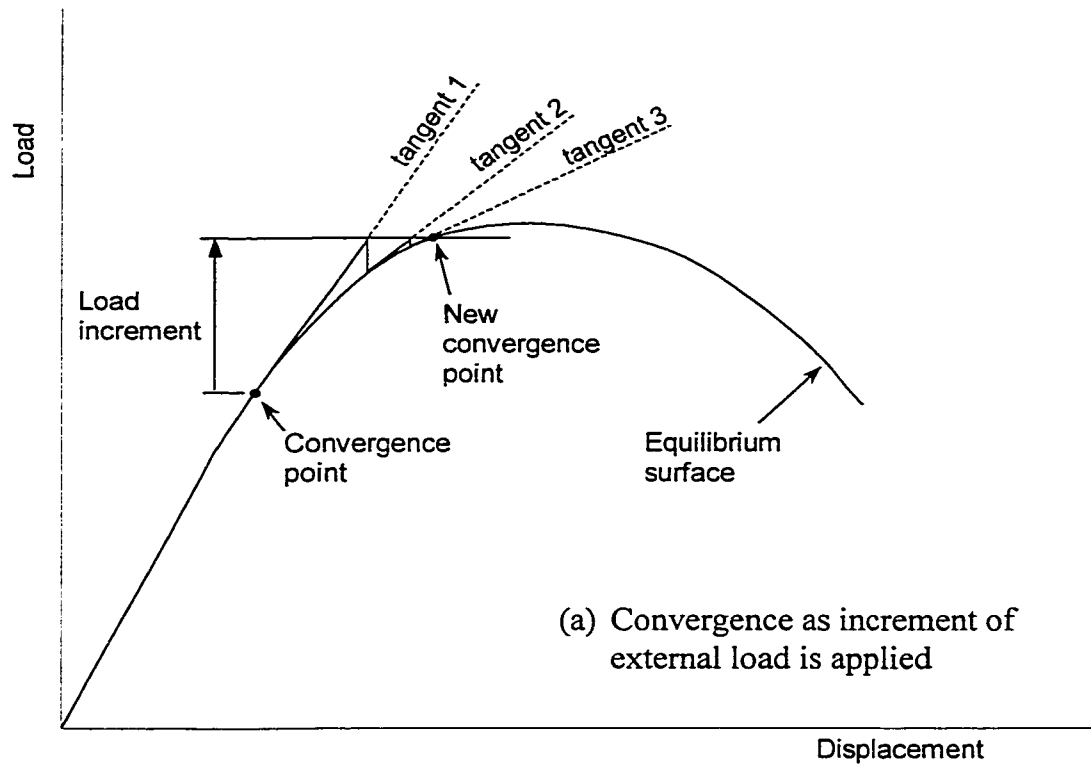


**Figure 5.7** Standard Newton solution approach

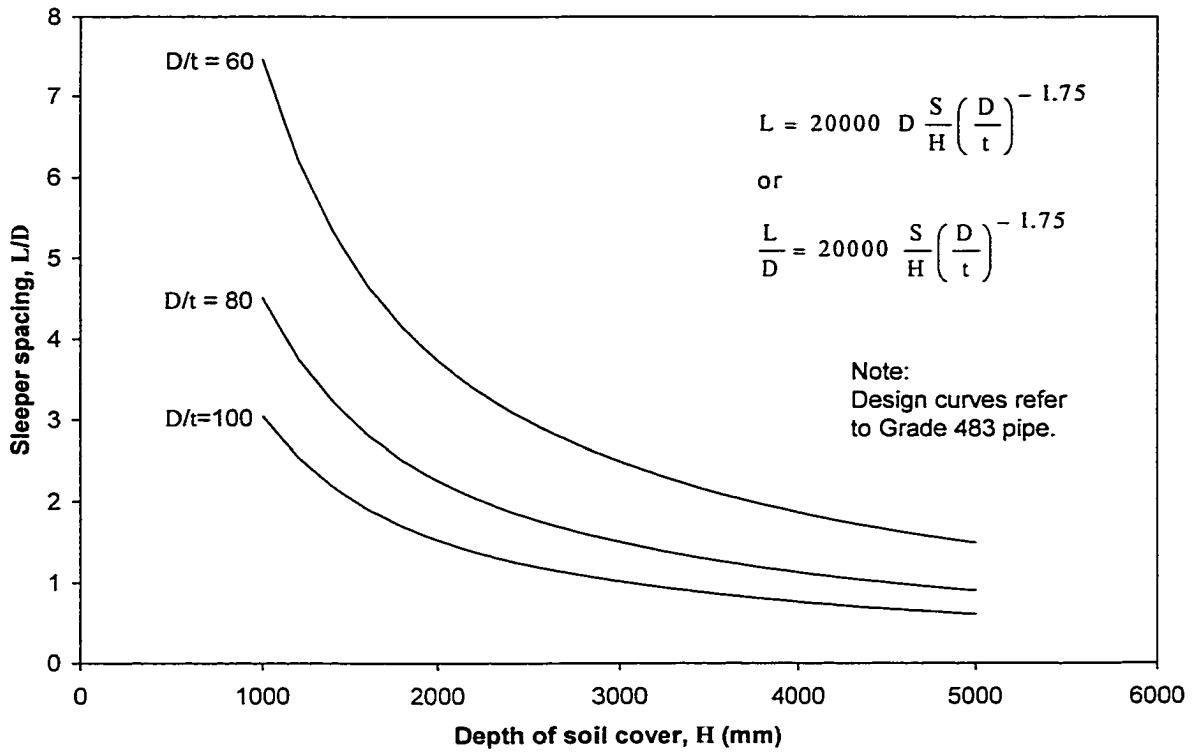


**Figure 5.8** Sleeper spacing for typical parameters based upon design equation by Kormann and Zhou (1995)

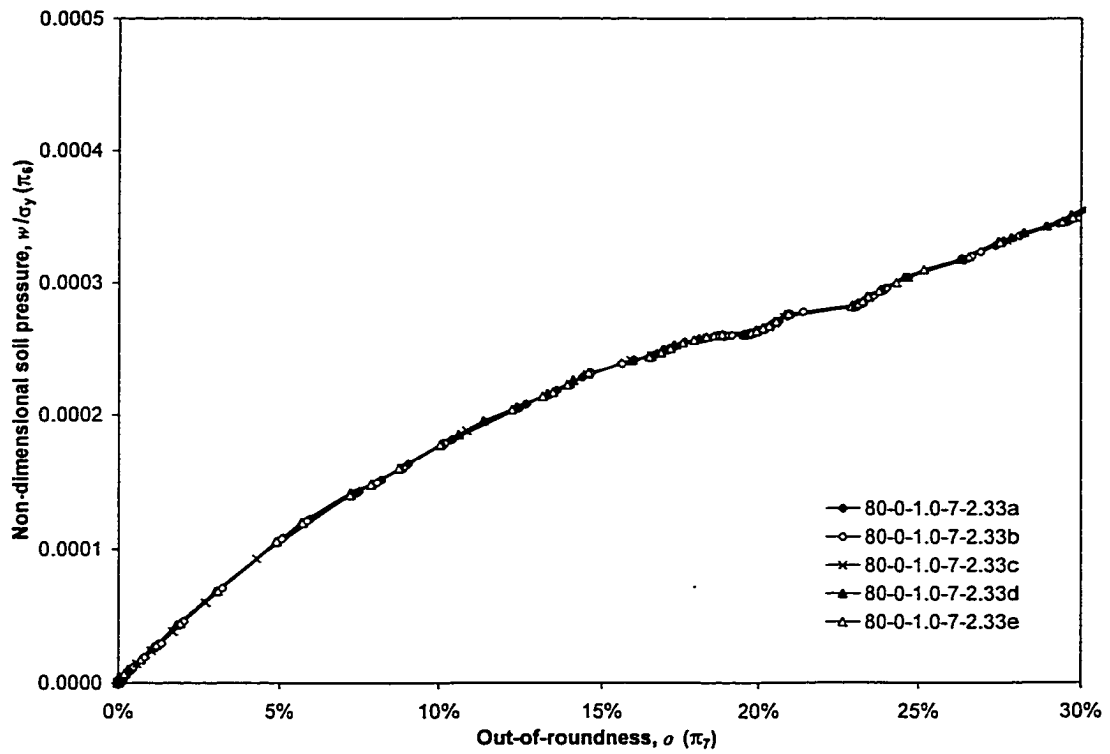


**Figure 5.9** Effect of varying model scale while maintaining  $\pi$ -parameters as constants

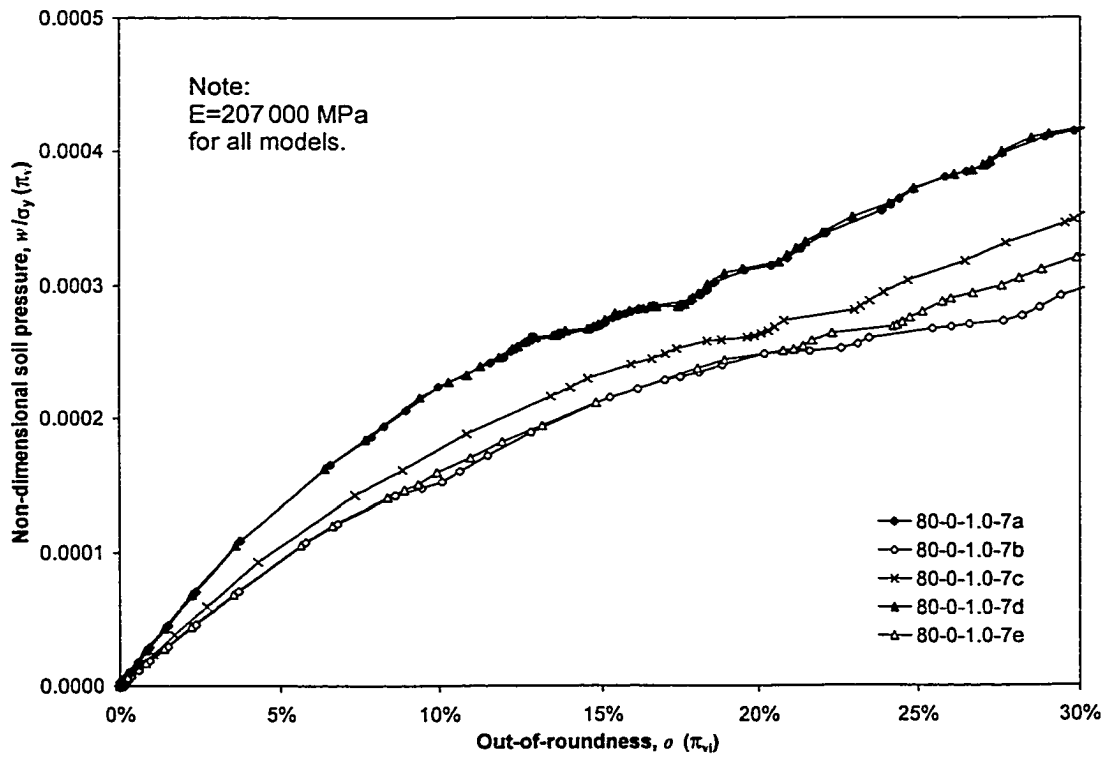


**Figure 5.10** Effect of varying model scale while maintaining  $E=207\,000$  MPa

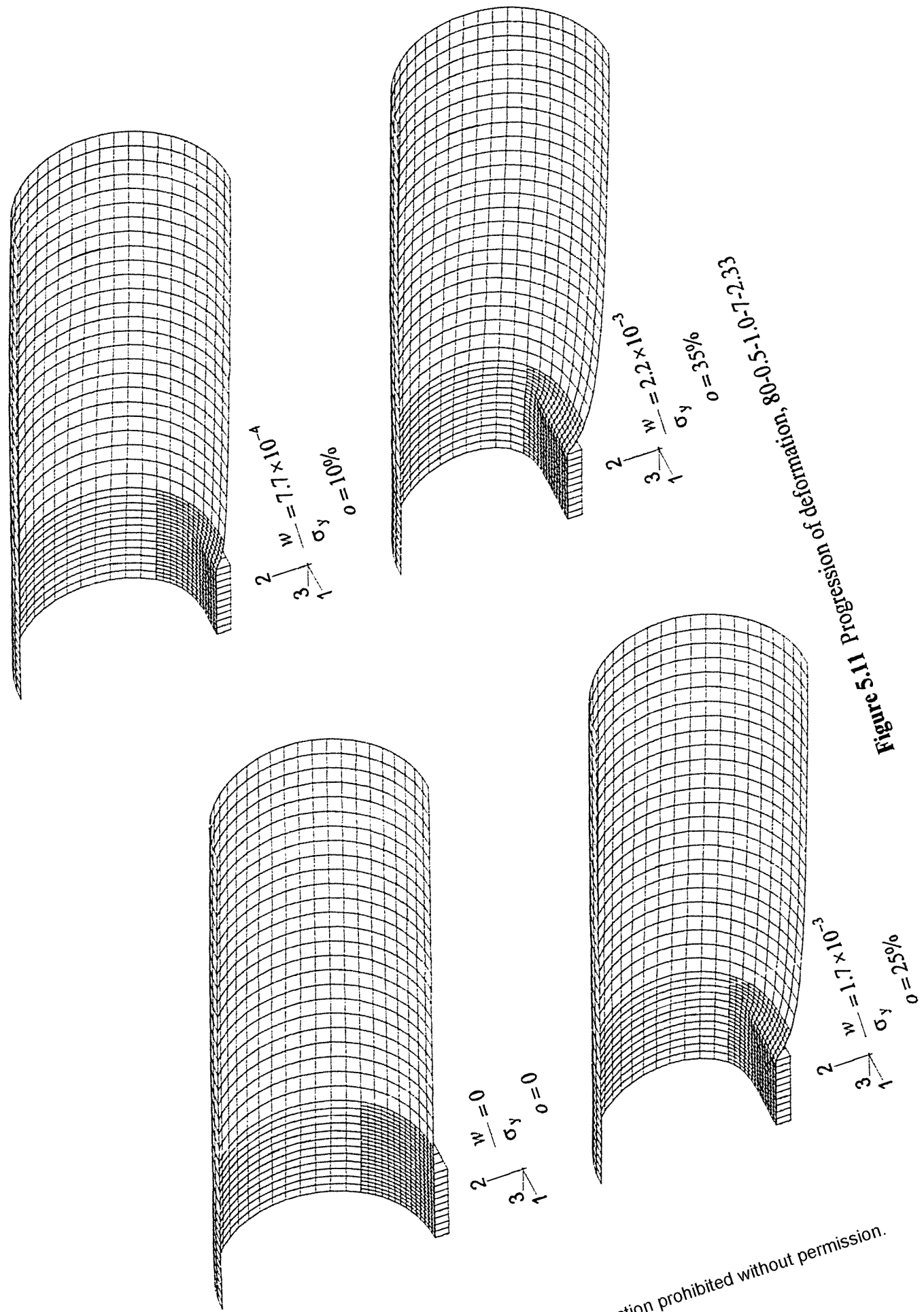


Figure 5.11 Progression of deformation, 80-0-S-1-0-1-0-1-0-3

Reproduced with permission of the copyright owner. Further reproduction prohibited without permission.

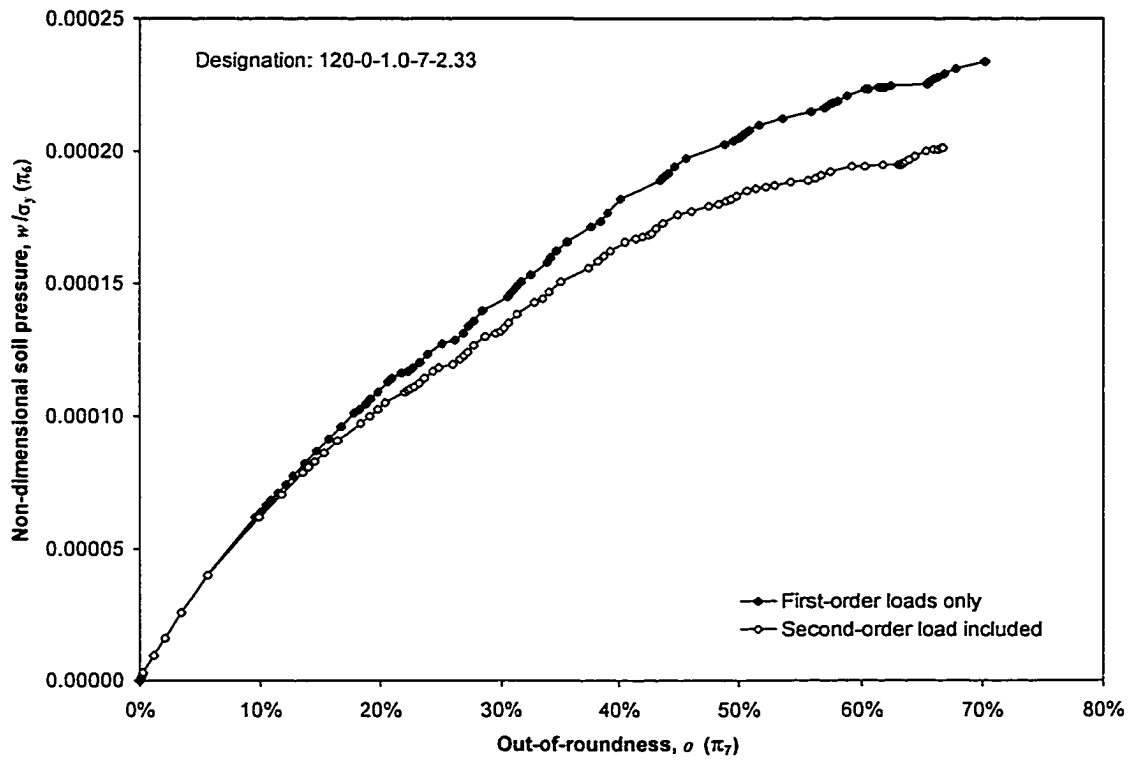


Figure 5.12 Influence of second-order soil loads

## 6 DEVELOPMENT OF SIMPLIFIED DESIGN EQUATIONS

A primary goal of this research is to develop a new method for the design of typical sleeper-supported pipe installations that provides acceptable levels of safety, serviceability, and economy. At the same time, the method should be reasonably simple for the designer to use. In this chapter, new design equations are formulated by making use of the foundation of knowledge developed in the first five chapters.

In any attempt to describe the behaviour of a real system mathematically, it is generally preferable to derive an equation that has a well-founded theoretical basis. The equation developed by such an approach is known as a *mechanistic* model. It is now known that the structural mechanics of sleeper-supported piping systems are not straightforward: many variables influence their behaviour, and non-linearities in geometry and in material response compound the degree of complexity. Several attempts to predict the behaviour of these systems based solely upon structural mechanics failed to produce a useful model. Consequently, it appears to be impossible to derive a mechanistic model that adequately describes the behaviour of *in situ* sleeper-supported pipes. Instead, an *empirical* approach becomes necessary: data are collected and analysed, and a model is developed that closely approximates the observed behaviour.

The objective of this chapter is to develop an empirical model that describes the behaviour of sleeper-supported pipes. The model will focus on the prediction of cross-sectional distortion, which is believed to be the governing variable in most cases among the design limit states for sleeper-supported pipes. So-called *response surface methodology* techniques, which make up a structured approach to mathematical model building, are used for the development of the empirical model. The data from which the model is derived are generated using the finite element model of *in situ* conditions that was described in Chapter 5.

### 6.1 RESPONSE SURFACE METHODOLOGY

In order to develop an empirical description of the behaviour of idealized sleeper-supported piping systems it is useful to employ response surface methodology techniques. In general terms, response surface methodology is a set of statistical procedures that can be used to obtain a better understanding of the set of variables that

influence the behaviour of any system. Based on a description given by Khuri and Cornell (1996), the steps involved in response surface methodology can be summarized as:

1. the design of a set of experiments that yield adequate and reliable measurements of the response of interest;
2. the determination, by means of regression analysis, of a mathematical model that best fits the data collected from the experiments;
3. optimization of the experimental factors to produce the maximum (or minimum) value of the response.

The *response* is a dependent variable that is influenced by independent variables known as *factors*. Factors are those variables that can be controlled by the experimenter, which, when changed in value, will cause the value of the response to change as well. For the sleeper-support problem only the first two steps in the preceding list need to be performed: an appropriate set of experiments (finite element analyses) must be designed, and empirical mathematical models that describe the behaviour of sleeper-supported pipes must be developed.

The overall process of response surface methodology is not structured rigidly. The method is intended to be adaptive and flexible, allowing the experimental design to evolve in an efficient way as the researcher's understanding of the system develops (Box et al., 1978). Khuri and Cornell (1996) provide a useful model that describes the sequential nature of conjecture, design, experimentation, and analysis that is followed when employing response surface methodology to learn about any system. This process, which is illustrated in Figure 6.1, is a useful guideline and the actual steps employed will depend upon the nature of the task at hand. In this chapter, an iterative approach of this type is used for the study of the sleeper-supported pipe problem.

### 6.1.1 Mathematical Description of a Response Surface

The mathematical relationship between the response and the factors is known as a *response function*. The true value of the response,  $\eta$ , depends upon  $k$  factors,  $X_1, X_2, \dots, X_k$ , such that:

$$\eta = \phi(X_1, X_2, \dots, X_k) \quad [6-1]$$

where,

$\phi$  = true response function.

The form of the true response function is not usually known, so it is often convenient to cast the function in another form. If the true response function is continuous and smooth, it can be represented locally to any required level of accuracy as a polynomial by means of a Taylor series expansion. For example, if  $\eta$  is assumed to depend on two factors,  $X_1$  and  $X_2$ , the function would have the form:

$$\eta = \phi(X_1, X_2) = \beta_0 + \beta_1 X_1 + \beta_2 X_2 + \beta_{11} X_1^2 + \beta_{22} X_2^2 + \beta_{12} X_1 X_2 + \dots \quad [6-2]$$

where,

$\beta_0, \beta_1, \beta_2, \dots$  = coefficients of the true response function.

It is, however, obvious that only a finite number of terms can be used in the expansion. The deletion of higher-order terms from the expansion usually introduces error into the prediction of the response. If only the first three terms are taken from equation [6-2], the model is referred to as *first-order* or *linear*—the simplest type that can be used. If the next three terms are added, the model is considered to be *second-order*, and so on. If additional accuracy is desired, more and more terms can be added to the polynomial until, in theory, the exact solution is obtained. In practice, however, other sources of error will prevent us from obtaining the exact solution, as described below.

With the selection of an appropriate number of terms from the Taylor series expansion, the values of the coefficients remain to be calculated. This must be done by obtaining data and evaluating the constants using the well known *least squares* or similar error minimization techniques (see, for example, Box et al., 1978). Because experimental errors and other factors beyond the understanding or control of the experimenter will always affect the data, true values of  $\beta_0, \beta_1, \beta_2$ , etc., can not be obtained. Instead, estimated values of the coefficients are calculated based upon the particular set of data employed. This introduces a second source of error and leads to the conclusion that it is not possible to determine the true response function for any real system, only an estimate of it. Such an estimate is called a *predicted response function* or a *prediction equation*. For example, if a second-order model is used as a subset of equation [6-2], the following prediction equation is obtained:

$$\hat{Y} = b_0 + b_1X_1 + b_2X_2 + b_{11}X_1^2 + b_{22}X_2^2 + b_{12}X_1X_2 \quad [6-3]$$

where,

$$\begin{aligned} \hat{Y} &= \text{predicted value of the response} \\ b_0, b_1, b_2, \dots &= \text{estimated regression coefficients.} \end{aligned}$$

For a general case, the prediction equation represents a line in two-dimensional space if the predicted response depends on one factor; if it depends on two factors, the equation represents a surface in three-dimensional space; if it depends on  $k$  factors, it represents a hypersurface in  $(k+1)$ -dimensional space.

Using a polynomial expression for the prediction equation is useful because it can approximate any smooth, continuous function to any required degree of accuracy if a sufficient number of terms are added. Consequently, there is no need for the analyst to have any knowledge of the true form of the response equation. Furthermore, to obtain estimates of the coefficients, the system of equations that must be solved is linear. This can be done easily, adding to the convenience of the technique. However, the method has a number of disadvantages, as described below.

If a polynomial is used, it may be necessary to include many terms in the prediction equation to make a reasonable representation of the response surface, especially if there are a large number of factors. The number of coefficients in a complete second-order prediction equation is given by the following relation (see, for example, Khuri and Cornell, 1996):

$$p = \frac{(k+1)(k+2)}{2} \quad [6-4]$$

where,

$$\begin{aligned} p &= \text{number of regression coefficients} \\ k &= \text{number of factors.} \end{aligned}$$

For example, with six factors—as is the case for the sleeper-support problem—a complete second-order polynomial regression equation would contain 28 coefficients. This is obviously not a desirable form for an engineering design equation. Instead, non-linear regression analysis techniques may be more appropriate.

Non-linear regression techniques, in which the system of equations for the unknown coefficients is not linear, usually allow a more compact form of the prediction

equation to be developed. This is particularly so if one has some insight into an appropriate form of the equation based on physical or mechanical arguments. For the sleeper-support problem, this is possible to some extent. The disadvantage of non-linear regression analysis is that the solution is more difficult because the system of equations for the coefficients is non-linear. However, with the power and convenience of today's personal computers, such non-linear regression analysis is reasonably simple to execute and is becoming commonplace. To solve the system of non-linear equations, an incremental iterative solver must be used, much the same as that used in non-linear structural analysis.

Regardless of whether the regression is to be linear or non-linear, it is first necessary to design and perform experiments to obtain the data that will be analysed. Important aspects of how an experimental program should be developed are described in the next section.

### **6.1.2 Design of Experiments: An Overview**

The objective of any experiment is to learn about the system being considered. The experiment, however, must inevitably be performed within physical, temporal, budgetary, and other constraints. Consequently, it is necessary to design experiments to meet these constraints while still satisfying the objectives. Experimental design is a process that combines expert knowledge of the subject area with appropriate statistical techniques to allow an optimal amount of useful data to be obtained in the most efficient manner possible (Box et al., 1978). The statistical aspects of experimental design as related to the sleeper-support problem are described in this section.

As demonstrated in Figure 6.1, the experimental process should be iterative, evolving as the experimenter's understanding of the system grows. At the same time, the particular experimental design employed must be compatible with the type of prediction equation used to describe the response surface. However, before an experimental design can be constructed, the experimenter must assess which variables should be considered as factors and what bounds should be placed on their levels. For the sleeper-supported pipe problem, the factors were identified in Section 5.3.3 along with realistic limits on their ranges. These bounds identify the so-called *region of interest* in the  $k$ -dimensional space of all possible combinations of the factors. Within this space, each different combination

of factors represents a unique *design point*, or, in other words, a separate experiment that has different values of the independent variables.

Oftentimes, before a thorough experimental design is undertaken, it is advisable to conduct a so-called *screening experiment*. This involves performing the experiment at a small number of design points in order to gain a basic understanding of the system. A screening experiment often gives insights into whether the response is linearly or non-linearly related to a particular factor. In some cases, the screening experiment might indicate that a particular factor has negligible influence on the response. If so, there is the potential to reduce significantly the complexity and expense of the remaining experimental work.

The simplest type of experimental design is ‘first-order,’ which is generally used in conjunction with first-order regression. In this case, only two levels of each factor are required, because the resulting prediction equation is planar. Of course, such a design is useful only for problems in which the response surface is approximately planar within the region of interest. For this class of experiment the most common form is a  $2^k$  *factorial* design. The name stems from the fact that a total of  $2^k$  design points are required, where  $k$  is the number of factors. Many variations of this approach are also available (see, for example, Box et al., 1978).

To reiterate, the objective of regression analysis is always to identify the approximate shape of the response function within the region of interest. To identify the shape, an adequate number of design points within this region must be considered. A first-order design may not be able to accomplish this objective: each factor is sampled at only two levels, so it is not possible to establish any curvature that may be present in the response surface.

If significant curvature is present in the response surface, at least three levels of the factors must be sampled and the response equation must be at least second-order. With three levels, the most common approach is to use a so-called  $3^k$  *factorial* experimental design. It is obvious that the required number of experiments grows rapidly with the number of levels of the factors. For example, for  $k=5$ , 243 design points and, therefore, 243 experiments, are required to consider all possible combinations of the factors. This would be the case for a  $3^k$  factorial design for the sleeper-supported pipe

problem. It is fortunate that it is not always necessary to explore all possible combinations of the factors, but rather only a representative subset thereof. This is known as a *fractional factorial* experimental design. However, it is not usually known in advance what a representative subset might be. Two options are possible for the selection of a representative subset of design points: a purely statistical approach to the experimental design can be followed, or specific design points can be chosen using expert knowledge and judgement. In either case, it is best to perform a screening study to obtain results at a few design points to gain some knowledge of the underlying system, which is consistent with the overall response surface methodology approach presented in Figure 6.1. Consequently, a screening study is the first step undertaken in the experimental design for the sleeper-supported piping problem.

## **6.2 APPLICATION OF RESPONSE SURFACE METHODOLOGY TO THE SLEEPER-SUPPORTED PIPE PROBLEM: SCREENING STUDY**

The first step in the application of response surface methodology is to identify the response variable and the factors on which the response is likely to depend. In the context of the sleeper-supported piping problem the non-dimensional distortion,  $\pi_7$ , is the response variable. The distortion criterion used to represent  $\pi_7$  is out-of-roundness,  $o$ , measured at the transverse centreline of the sleeper. This value, which is defined in equation [1-12], is to be obtained from experiments (the finite element analysis models developed in Chapter 5) for a given set of input factors,  $\pi_1$  through  $\pi_6$  ( $D/t$ ,  $p/p_y$ ,  $2b/D$ ,  $L/D$ ,  $\epsilon_y$ , and  $w/\sigma_y$ , respectively). The first five factors are specified directly by the analyst in the finite element input file. Nominally, the non-dimensional soil pressure,  $w/\sigma_y$ , is also a factor. However, it is not known *a priori* whether a solution will exist for a particular preselected value of  $w/\sigma_y$ : the maximum possible value of  $w/\sigma_y$  is limited to the load-carrying capacity of the system. As a result, the analyst does not have direct control over  $w/\sigma_y$  and it can not be treated as a factor in the experimental design. Special consideration of  $w/\sigma_y$  is required before it can be used in subsequent regression analyses; this problem is discussed in full detail later in this chapter.

The finite element model of *in situ* conditions for sleeper-supported piping systems that was developed in Chapter 5 fulfills the role of the experiment. As such, it is

necessary to perform an experimental design to choose those models that will be analysed as part of the response surface methodology procedures. A screening study is performed in this section to address this problem.

### 6.2.1 Combinations of $\pi$ -Parameters for the Screening Study

In Section 5.3.3, realistic bounds were placed on the ranges for factors  $\pi_1$  through  $\pi_5$ , and discrete values of interest were identified based on practical considerations. These values set the framework for the experimental design of the screening study. Specifically, the factor levels selected are:

$$\begin{array}{llll}
 \pi_1: & D/t & = & 40, 80, \text{ and } 120 \\
 \pi_2: & p/p_y & = & 0, 0.5, \text{ and } 0.8 \\
 \pi_3: & 2b/D & = & 0.5, 1.0, \text{ and } 1.5 \\
 \pi_4: & L/D & = & 5, 7, \text{ and } 9 \\
 \pi_5: & \varepsilon_y & = & 1.73 \times 10^{-3}, 2.33 \times 10^{-3}, \text{ and } 2.66 \times 10^{-3}.
 \end{array} \quad [6-5]$$

These values demarcate the boundaries of the region of interest in the 5-dimensional space of all possible combinations of  $\pi_1$  through  $\pi_5$ . Consequently, a preliminary set of models involving each of the five factors will be investigated. Since it is expected that at least some of the factors have a non-linear effect on the response, three levels of each factor are needed in the screening study.

The goal of the screening study is to obtain some feeling for the shape of the response surface. To do this, 11 finite element models are analysed, with the factor levels based upon the classical *one-factor-at-a-time* method of experimental design. In this method, each factor is varied through all of its levels while all other factors are maintained as constants (see, for example, Box et al., 1978). While the relevance of this approach is limited to those instances in which the variables act additively, it does provide a useful first estimate of the behaviour. Using the one-factor-at-a-time method, the corresponding parameters for the finite element analysis models of the screening study are shown in Table 6.1. The first model listed is 80-0.5-1.0-7-2.33, which is a 'base' model that has intermediate values of all of the factors:  $D/t=80$ ,  $p/p_y=0.5$ ,  $2b/D=1.0$ ,  $L/D=7$ , and  $\varepsilon_y=2.33 \times 10^{-3}$ . In statistical terminology, such an experiment is known as the *design centrepoint*, because all of the factors are set at the intermediate value. Varying only one  $\pi$ -parameter at a time in the base model forms the other models.

For example, in the next two models listed in Table 6.1,  $D/t$  takes on values of 40 and 120, respectively, while maintaining  $p/p_y=0.5$ ,  $2b/D=1.0$ ,  $L/D=7$ , and  $\epsilon_y=2.33 \times 10^{-3}$ . Repeating this process with the other  $\pi$ -parameters completes the experimental design.

### 6.2.2 Results and Discussion of Screening Study

Finite element models for the screening study that correspond to the parameters listed in Table 6.1 were analysed using ABAQUS. Results from the 11 analyses are presented graphically as plots of  $\sigma$  versus  $w/\sigma_y$  in Figures 6.2 through 6.6. Because  $\sigma$  is the dependent variable, it is plotted on the vertical axis in each case. Each graph shows the results for the design centrepoint, 80-0.5-1.0-7-2.33, along with the results for extreme values of the particular factor under consideration. By examining the results of each analysis with respect to the design centrepoint, an assessment can be made of the significance and the influence of each factor. For ease of comparison, Figures 6.2 through 6.6 are all plotted to the same scale.

In Figure 6.2 it is evident that  $D/t$  ( $\pi_1$ ) has significant influence on the behaviour. As expected, the greater the value of  $D/t$ , the greater the amount of distortion for a given load. Furthermore, the response is clearly non-linear, that is, if  $D/t$  is increased by a certain multiple, the amount of distortion for a given load increases by a greater multiple. This suggests curvature in the response surface with respect to this variable, implying that at least three levels of  $D/t$  must be investigated. From a practical standpoint, this parameter is judged to be of primary importance and it should be investigated further at a significant number of design points.

The value of parameter  $p/p_y$  ( $\pi_2$ ) also has a major effect on the behaviour and must be considered to be of primary importance. Figure 6.3 shows that the presence of internal pressure reduces the amount of distortion considerably and also serves to strengthen the pipe. Because the behaviour is influenced so drastically by internal pressure, it may be difficult to account for this effect in regression equations that will be developed at later stages of the work. Consequently, it is judged that the experimental design for the main body of the parametric study should evolve as three separate experiments, one at each level of internal pressure ( $p/p_y=0$ , 0.5, and 0.8). Similarly, in subsequent regression analyses, a separate predicted response function will be developed

for each level of pressure. Subject to limitations that are considered in Chapter 7, interpolation between the results given by these three equations can be used to predict the behaviour at other levels of pressure. This approach should simplify the process of equation development and provide economy in the experimental design: an optimal number of design points can be used for each of the three separate experiments.

It appears that out-of-roundness varies in a reasonably linear way with  $2b/D$  ( $\pi_3$ ), as illustrated in Figure 6.4. As compared to  $D/t$  and  $p/p_y$ , the influence of  $2b/D$  is less important. These facts suggest that relatively fewer design points can be explored for this parameter.

For a given soil pressure,  $w/\sigma_y$ , the amount of out-of-roundness,  $o$ , is almost directly proportional to  $L/D$  ( $\pi_4$ ), as shown in Figure 6.5. Because the distortion over a sleeper support is localized, it is reasonable, from engineering judgement, to expect the amount of distortion to be related linearly to the amount of soil load carried by the sleeper. Multiplying the non-dimensional soil pressure,  $w/\sigma_y$ , by  $L/D$  provides a value that is directly proportional to the soil load. When out-of-roundness is plotted versus soil load, it is apparent that no significant difference in behaviour is exhibited by systems that have different values of  $L/D$  (see Figure 6.7). Consequently,  $L/D$  can appear as a linear term in prediction equations for the behaviour of pressurized sleeper-supported piping systems, and there is no need to include  $L/D$  as a factor in the experimental design. It must be recognized, however, that the mechanics of a piping system are influenced significantly by internal pressure; for systems in which the level of internal pressure is low,  $L/D$  may not have a linear influence on the response. This possibility is explored in an additional screening study, reported in Section 6.3.3.1, specifically for the case of zero internal pressure.

Yield strain,  $\varepsilon_y$  ( $\pi_5$ ), has little influence on the behaviour of those models considered in the screening study (see Figure 6.6). Arguments can be made based upon structural mechanics why this should be so. For two otherwise identical sleeper-supported piping systems that have different yield stresses (and, therefore, different yield strains), the behaviour would be identical if the material remains completely elastic. Because the onset of yielding would occur at different levels of strain, differences in the post-yield behaviour are inevitable. However, for sleeper-supported pipes, yielding begins only in

local regions that gradually increase in size as soil pressure increases. Unless the yielded regions are large in size, the loss of stiffness from inelastic behaviour is expected to be negligibly small as compared to the effect of stiffness induced by internal pressure. Consequently, the effect of  $\varepsilon_y$  is expected to be minor, at least for pressurized pipes. The possibility of deleting this factor from the study of pressurized pipes appears to be justified.

The downward soil pressure,  $w/\sigma_y$ , is an independent variable that is controlled exclusively by the finite element software. Figures 6.2 through 6.6 show clearly that distortion,  $o$ , always increases with soil pressure, as expected. Further detailed discussion of  $w/\sigma_y$  is required in order to ensure that the data set is compatible with the regression techniques that are used subsequently.

### 6.2.3 Establishing Consistency in the Data Set for Use in Regression Analyses

The data presented in Figures 6.2 through 6.6, along with additional data that are reported later, are eventually used in regression analyses to estimate the response function for sleeper-supported pipes. Consequently, it is necessary to examine the data set to ensure that it is compatible with the statistical techniques involved in regression analysis. In particular, to meet the needs of the experimental design, all factors must be set at a specific number of preselected values. Upon examination of the data, two shortcomings are apparent: 1) the behaviour is not defined at all values of factor  $w/\sigma_y$ ; and 2) the number and the location of equilibrium points, given as output by ABAQUS, is not the same from one analysis to the next.

#### 6.2.3.1 Special Consideration of Factor $w/\sigma_y$ ( $\pi_6$ )

The final objective of this work is to develop an equation that predicts distortion,  $\pi_7$ , in terms of factors  $\pi_1$  through  $\pi_6$ . This can be expressed in mathematical terms as:

$$\begin{aligned} \pi_7 &= f(\pi_1, \pi_2, \pi_3, \pi_4, \pi_5, \pi_6) \\ &\text{or, equivalently,} \\ o &= f(D/t, p/p_y, 2b/D, L/D, \varepsilon_y, w/\sigma_y). \end{aligned} \tag{6-6}$$

To establish the form of this function, experiments must be performed that involve varying the levels of each factor through the range of interest. For example,  $D/t$  is to be investigated at levels of 40, 80, and 120, as shown in equation [6-5]. However, a problem

arises with the non-dimensional soil pressure,  $w/\sigma_y$ : in some cases, its value is not defined. For example, the behaviour when the factor  $w/\sigma_y$  takes on the discrete values 0.000, 0.002, and 0.004 might be of particular interest. Consider next the pool of data consisting only of those curves shown in Figure 6.2. In this figure, each curve approaches a limit—the maximum load-carrying capacity of the system. Consequently, all three curves are defined at  $w/\sigma_y=0.000$ , but only two are defined at  $w/\sigma_y=0.002$ , and only one is defined at  $w/\sigma_y=0.004$ . Physically, this is simply a reflection of the fact that a thin-walled pipe can never carry a load as great as a comparatively thick-walled pipe. However, it means that the researcher can not choose specific arbitrary levels for factor  $w/\sigma_y$  for the experimental design, because it is not known *a priori* whether a solution will exist for each chosen value.

Although this problem may at first appear intractable, it can be resolved simply: treat  $w/\sigma_y$  as the response variable and  $o$  as a factor. Such a switch of the dependent variable with an independent variable will not have any significant effect in subsequent regression analyses. Mathematically this can be expressed as:

$$w/\sigma_y = g(D/t, p/p_y, 2b/D, L/D, \varepsilon_y, o) \quad [6-7]$$

This approach is useful because  $w/\sigma_y$  will always exist when a value of  $o$  is specified, at least up to the maximum value of practical interest, which is about  $o=25\%$ . Therefore, in the experimental design, one can specify values of distortion that are of interest and be confident that a solution will always exist. Consequently, the data from all finite element models should be defined at  $o=0\%$ , at  $o=25\%$ , and at a number of intermediate levels. However, the solution provided by the finite element software is given only at particular discrete values that can not be controlled by the experimenter. The data set must be made more uniform, as described below.

### 6.2.3.2 Ensuring Uniformity of the Output Data

Typical data for three finite element analyses are shown in Figure 6.8. These data are the same as those presented in Figure 6.2, but the axes have been switched in accordance with the decision to make  $w/\sigma_y$  the dependent variable. If these data are to be used in a regression analysis, two limitations are apparent: the number of points on each curve is not the same, nor are the curves defined at the same discrete values of  $o$ . If the

number of points on each curve is not the same, then those curves for which more points are defined will exert excess influence on the outcome of the least squares regression calculation. Consequently, it is desirable to make the data uniform so that each curve is defined at the same number of points, and, further, to define the set of points for each curve at equal values of  $o$ . In order to ensure that sufficient resolution is maintained, 11 data pairs  $(w/\sigma_y, o)$  are taken from each finite element analysis. The levels of  $o$  considered are 0% to 25%, in increments of 2.5%. To obtain these specific points, linear interpolation is used.

After applying these techniques to the data in Figure 6.8, it has the appearance shown in Figure 6.9. Data sets with such uniformity are used throughout the remainder of this work.

### **6.3 EXPERIMENTAL DESIGN AND THE DEVELOPMENT OF PREDICTION EQUATIONS**

The screening experiment reported in Section 6.2 indicates that it is advantageous to pursue the parametric study in the form of three separate experiments, one for each of  $p/p_y=0$ ,  $p/p_y=0.5$ , and  $p/p_y=0.8$ . The process followed in the execution of these three studies is shown in Figure 6.10, a full description of which is made in this section. Using the results from the numerical parametric studies, empirical equations are developed to predict the behaviour of *in situ* sleeper-supported piping systems.

For all finite element models described in this section, the pipes are 762 mm in diameter and have a modulus of elasticity of 207 000 MPa. All other dimensions and material specifications are chosen to give appropriate values of the dimensionless  $\pi$ -parameters. Because the scale effect is controlled completely in the models, as shown in Section 5.4.1, the results are applicable to pipes of any size or material that have identical  $\pi$ -parameters.

#### **6.3.1 Parametric Study of $p/p_y=0.5$**

##### **6.3.1.1 Experimental Design, $p/p_y=0.5$**

The screening study described in Section 6.2 considered three levels of each factor  $\pi_1$  through  $\pi_5$ . Because 80-0.5-1.0-7-2.33 is the design centrepnt for the screening study, nine of the eleven analyses had factor  $p/p_y$  set at a value of 0.5. It is

logical to focus first on the parametric study of  $p/p_y=0.5$ , since a considerable amount of data is already available for this case.

For the parametric study of  $p/p_y=0.5$ , the specific points that make up the experimental design must be selected by using the information gathered in the screening study. The screening study shows that factors  $D/t$  and  $2b/D$  have a significant influence on the behaviour. Consequently, both of these factors must be considered in the parametric study. It is judged that three levels of each of these factors should be considered, namely those given in equation [6-5], so that curvature in the response surface can be estimated.

The other two input factors,  $L/D$  and  $\epsilon_y$ , have a predictable effect on the behaviour observed in the screening study. Specifically,  $L/D$  has a correlation with  $o$  that is almost linear. As a result, it is judged that  $L/D$  can appear in the prediction equation as a linear term, and no further investigation of this variable is deemed necessary:  $L/D$  is deleted from the parametric study for the case when  $p/p_y=0.5$ . Similarly,  $\epsilon_y$  is deleted because its effect in the screening study is judged to be insignificant.

As a result of these decisions, only two factors,  $D/t$  and  $2b/D$ , need to be investigated at each of three levels. Consequently, a  $3^2$  experimental design is employed. This gives a total of nine design points, and, therefore, nine finite element analyses, that must be performed to investigate the case when  $p/p_y=0.5$ . This experimental design is shown in the centre column of Figure 6.10.

### **6.3.1.2 Results of Parametric Study and Prediction Equation Development, $p/p_y=0.5$**

The results from the nine analyses for the case of  $p/p_y=0.5$  are presented in Figure 6.11 in the form of graphs of  $w/\sigma_y$  versus  $o$ . All of the data are presented in accordance with the uniform standards detailed in Section 6.2.3. In all cases the results are similar to those obtained in the screening study: for a given level of  $o$ ,  $w/\sigma_y$  decreases with  $D/t$  and increases with  $2b/D$ .

To reiterate, the objective is to develop a reasonably simple and accurate empirical equation to predict  $w/\sigma_y$  in the curves shown in Figure 6.11. Because the response surface is clearly not planar and because there are three factors to be included in the prediction equation, it is expected that the use of linear regression analysis techniques

would not be appropriate: too many terms would be required in the polynomial equation. Consequently, non-linear regression analysis is used for all of the work reported herein, which will likely allow equations of more compact form to be developed. The commercially available statistical software SigmaPlot 4.0 (SPSS, 1997) is used to perform the non-linear regression.

With any type of regression analysis, the form of the prediction equation must be chosen first and optimal values of the unknown coefficients must be calculated. In SigmaPlot the coefficients are found by minimizing the *residual errors* using the well-known least squares technique. A residual error is the difference between the observed value of the response and the value given by the prediction equation:

$$\begin{aligned} r_i &= Y_i - \hat{Y}_i \\ r_i &= Y_i - \hat{Y}_i \end{aligned} \quad [6-8]$$

where,

$$\begin{aligned} r_i &= \text{residual error } i \\ Y_i &= \textit{i} \text{th observed value of the response variable} \\ \hat{Y}_i &= \textit{i} \text{th predicted value of the response variable.} \end{aligned}$$

Subject to certain limitations that are described later, this technique provides an equation with optimal predictive ability. However, the particular form of the equation chosen may not be the most suitable, and several equations having different forms are usually tried. Consequently, means are required by which to compare the predictive ability of equations that have different forms. The *coefficient of multiple determination* is one quantitative measure of the predictive ability of a regression equation (see, for example, Devore, 1991):

$$R^2 = 1 - \frac{\text{SSE}}{\text{SST}} = 1 - \frac{\sum_{i=1}^n (Y_i - \hat{Y}_i)^2}{\sum_{i=1}^n (Y_i - \bar{Y})^2} \quad [6-9]$$

where,

$$\begin{aligned} R^2 &= \text{coefficient of multiple determination} \\ \text{SSE} &= \text{error sum of squares: sum of squared residual errors} \\ \text{SST} &= \text{total sum of squares: sum of squared deviations of the observed values about the sample mean} \\ \bar{Y} &= \text{mean of observed values of the response variable} \end{aligned}$$

$n$  = number of observed values of the response variable.

The coefficient of multiple determination describes the proportion of the variation in the response that is described by the prediction equation. If  $R^2=1$ , the equation describes all variation of the response perfectly; in practice, this is usually impossible to achieve, so the equation that gives the value of  $R^2$  closest to unity is usually judged to be the best model. (Because the objective is to find a model that provides good fit but is reasonably simple, the model that has the greatest value of  $R^2$  is not necessarily the best. Strictly speaking, the *adjusted coefficient of multiple determination* should be used as the measure of predictive ability: it takes into account the cost of adding additional unknown coefficients to the prediction equation (see, for example, Devore, 1991). Because all equations reported in this work have the same number of unknown coefficients, the use of  $R^2$  as the basis of comparison is sufficient.)

Several prediction equations, each having a different form, were proposed as models for the case when  $p/p_y=0.5$ . After several trials, an equation having the following form was found to give the greatest value of  $R^2$ :

$$\hat{Y} = a(X_1)^b(X_2)^d(X_3)(X_4)^g$$

or, using the notation of the problem at hand, [6-10]

$$\frac{w}{\sigma_y} = a\left(\frac{D}{t}\right)^b\left(\frac{2b}{D}\right)^d\left(\frac{L}{D}\right)^{-1}(o)^g$$

where,

$X_1, X_2, \dots$  = independent factors  
 $a, b, d, g$  = regression coefficients.

Recall that the exponent of  $L/D$  in this equation is set to -1 manually because of the linearity demonstrated by this term, as described in Section 6.2.2. This equation also satisfies the physical requirement that the level of soil pressure must be zero when out-of-roundness is zero. Performing non-linear regression analysis to obtain optimal values for the coefficients gives:

$$\frac{w}{\sigma_y} = 5.5425\left(\frac{D}{t}\right)^{-1.1445}\left(\frac{2b}{D}\right)^{0.3019}\left(\frac{L}{D}\right)^{-1}(o)^{0.7877} \quad [6-11]$$

For this equation  $R^2=0.9986$ , which indicates an excellent degree of predictive ability. This predictive ability, of course, is corroborated only within the range of each factor considered in the analysis. Figure 6.12 shows the predicted behaviour (hollow symbols) obtained using equation [6-11] along with the finite element data (solid symbols) upon which the equation was developed. The quality of the correlation is apparent in these figures, but this method of presentation of the data is rather cumbersome. A clearer illustration of the difference between the data and the regression predictions is obtained in a graph of predicted response versus the response given by the finite element model. This is shown in Figure 6.13, which contains all of the data points from Figure 6.12. The diagonal line in Figure 6.13 represents perfect correlation between the observed and predicted values; a particular point lies above the line if the predicted value is greater than the value obtained from finite element analysis, and vice versa. The vertical distance between a data point and the diagonal line represents the magnitude of the residual error for that point. Bounds representing an error of 10% in the prediction are also shown; almost all of the points lie within these bounds, with the exception of some near the origin.

Despite its good correlation with the observed behaviour, some criticisms can be made of equation [6-11]. It is known that the piping system idealized in the finite element model must have an out-of-roundness,  $o$ , of zero if the soil pressure,  $w/\sigma_y$ , is zero. It is clear that equation [6-11] satisfies this condition. However, the mechanics of the idealized piping system dictate that the slope of the response surface with respect to  $o$  must be finite. This is simply a reflection of the fact that the pipe can not be infinitely stiff. However, if one evaluates the slope of regression equation [6-11] with respect to  $o$ , it is clear that the slope is infinite when  $o$  is zero:

$$\frac{\partial \left( \frac{w}{\sigma_y} \right)}{\partial o} = 4.3658 \left( \frac{D}{t} \right)^{-1.1445} \left( \frac{2b}{D} \right)^{0.3019} \left( \frac{L}{D} \right)^{-1} (o)^{-0.2123}$$

and, with  $o = 0$ ,

$$\frac{\partial \left( \frac{w}{\sigma_y} \right)}{\partial o} \rightarrow \infty.$$

[6-12]

Consequently, it is expected that the regression equation given in [6-11] will overestimate the amount of soil pressure that is carried when the level of out-of-roundness is small. This postulation is substantiated by the results shown in Figure 6.13: all points lie within the 10% errors bands except for some points near the origin, for which the predicted values are slightly too great.

In an attempt to correct this shortcoming, a reasonably small change in the form of the proposed equation is made to allow the slope to be finite when  $o$  equals zero:

$$\frac{w}{\sigma_y} = a \left( \frac{D}{t} \right)^b \left( \frac{2b}{D} \right)^d \left( \frac{L}{D} \right)^{-1} \left( 1 - g^{(100 \times o)} \right)$$

[6-13]

and, after regression,

$$\frac{w}{\sigma_y} = 3.3505 \left( \frac{D}{t} \right)^{-1.1443} \left( \frac{2b}{D} \right)^{0.3021} \left( \frac{L}{D} \right)^{-1} \left( 1 - 0.9689^{(100 \times o)} \right).$$

This modified equation provides  $R^2=0.9980$ —approximately the same value of  $R^2$  as equation [6-11]—but the tendency for the prediction to be too great when  $o$  is small is improved noticeably. This is apparent in the graphs of the predicted and finite element responses in Figure 6.14, and also in Figure 6.15, which shows the predicted response versus finite element response for equation [6-13]. In both figures, those points that lie near the origin have been shifted downward slightly, giving a more conservative estimate of the behaviour.

### 6.3.2 Parametric Study of $p/p_y=0.8$

#### 6.3.2.1 Screening Study and Experimental Design, $p/p_y=0.8$

The case for which  $p/p_y=0.8$  is considered next because it is expected that the behaviour of these pipes is not fundamentally different from those pressurized at a level  $p/p_y=0.5$ . Because the screening study carried out in Section 6.2 considered only one case for which  $p/p_y=0.8$ , it is necessary to perform an additional screening study to consider more cases having this pressure condition. The one-factor-at-a-time method is used in the development of this screening study; the design points considered are shown in the rightmost column in Figure 6.10.

The results of the screening study for the case when  $p/p_y=0.8$  are presented in Figures 6.16 through 6.19. Examination of these figures provides guidance in the selection of the specific design points that should be included in the parametric study. Figures 6.16 and 6.17 reveal that factors  $D/t$  and  $2b/D$  have significant influence on the behaviour, so both of these factors must be considered in the parametric study. It is judged that three levels of each of these factors should be considered so that curvature in the response surface can be estimated. Note that this same approach was used for the case of  $p/p_y=0.5$ .

The influence of factor  $L/D$  is shown in Figure 6.18. In a manner similar to the case when  $p/p_y=0.5$ , the effect of  $L/D$  on the response is almost linear. This linearity is evident when a value that is proportional to the soil load,  $w/\sigma_y \times L/D$ , is plotted versus  $\phi$  (see Figure 6.20). Consequently,  $L/D$  can appear in the prediction equation for  $p/p_y=0.8$  as a linear term, and it is deemed that no further investigation of this variable is necessary.

Figure 6.19 shows that the influence of  $\varepsilon_y$  on the response is small compared to those influences of the other factors. Consequently,  $\varepsilon_y$  is deleted from the parametric study of  $p/p_y=0.8$ . This is consistent with the course of action taken for the case of  $p/p_y=0.5$ .

Because the same trends are shown in the data for both  $p/p_y=0.8$  and  $p/p_y=0.5$ , a  $3^2$  experimental design is implemented again: two factors,  $D/t$  and  $2b/D$ , are investigated at each of three levels. As before, this gives a total of nine design points, and, therefore, nine finite element analyses. The experimental design for the parametric study of  $p/p_y=0.8$  is shown at the bottom of the rightmost column in Figure 6.10.

### **6.3.2.2 Results of Parametric Study and Prediction Equation Development, $p/p_y=0.8$**

Results from the parametric study of  $p/p_y=0.8$  are presented in Figure 6.21 in the form of graphs of  $w/\sigma_y$  versus  $\phi$ . The results are similar in form to those demonstrated in Figure 6.11 for the case where  $p/p_y=0.5$ .

Because of the similarity in behaviour between the cases where  $p/p_y=0.5$  and  $p/p_y=0.8$ , it is reasonable to propose a prediction equation having the same form as [6-13]. To reiterate, this equation is desirable because it takes into account the fact that

$w/\sigma_y=0$  when  $o=0$  and that  $\partial(w/\sigma_y)/\partial o < \infty$  when  $o=0$ . Performing non-linear regression analysis on the data presented in Figure 6.21, the following regression equation is obtained for  $p/p_y=0.8$ :

$$\frac{w}{\sigma_y} = 3.2793 \left( \frac{D}{t} \right)^{-1.0759} \left( \frac{2b}{D} \right)^{0.3473} \left( \frac{L}{D} \right)^{-1} (1 - 0.9689^{(100 \times o)}) \quad [6-14]$$

This equation provides  $R^2=0.9989$ , which indicates an excellent degree of predictive ability. A comparison of the prediction equation with the finite element data is presented in Figure 6.22; the finite element data are shown with solid symbols and the predicted values are shown with hollow symbols. A graphical summary of the correlation is shown in Figure 6.23 in terms of predicted soil pressure versus the soil pressure obtained from the finite element analyses. The quality of the correlation is very good, with only a few points lying outside of the 10% error bands.

### 6.3.3 Parametric Study of $p/p_y=0$

#### 6.3.3.1 Screening Study and Experimental Design, $p/p_y=0$

Because it is expected that the behaviour of unpressurized systems may be significantly different from those that have internal pressure, the last case to be considered in the parametric study is  $p/p_y=0$ . In order to make an assessment of which experimental design points should be examined, a screening study that focuses on the behaviour of unpressurized systems is performed. The experimental design of this screening study is based upon the one-factor-at-a-time method, which gives the design points that are shown in the leftmost column of Figure 6.10. Finite element analyses of models corresponding to these design points were performed and the resulting data are presented in Figures 6.24 through 6.27. All of these figures are plotted to the same scale for ease of comparison.

Examination of Figure 6.24 shows that  $D/t$  has a significant non-linear influence on the behaviour of unpressurized piping systems. In fact, as compared to the influences of  $2b/D$ ,  $L/D$ , and  $\varepsilon_y$  (see Figures 6.25, 6.26, and 6.27, respectively), the influence of  $D/t$  is vastly dominant. The dominance of  $D/t$  and its non-linear effect on the response give rise to some doubt whether the examination of  $D/t$  at only three levels (40, 80, and 120)

in the parametric study is sufficient to provide an adequate representation of the response surface. Consequently, it is judged that two additional levels of  $D/t$ , 60 and 100, should also be examined to ensure that the data set has sufficient resolution.

The screening study shows that the influences of all other factors are small as compared to  $D/t$ . It is, however, not necessarily reasonable to neglect their influences on the response. Because the effect of  $2b/D$  plays a small but significant role in the response of pressurized piping systems, it would not be reasonable to exclude this factor from the parametric study of unpressurized systems. Consequently,  $2b/D$  at levels of 0.5, 1.0, and 1.5 are examined.

Whereas  $L/D$  contributed a linear effect to the behaviour of the pressurized piping systems, the influence of  $L/D$  on the behaviour of unpressurized systems is not linear. This non-linearity is evident in Figure 6.28, which shows non-dimensional soil load plotted versus out-of-roundness: the lines are not co-linear. Therefore,  $L/D$  must be included in the parametric study of unpressurized systems.

In Figure 6.27, it is apparent that the influence of  $\epsilon_y$  on the response is of a magnitude similar to the influences of factors  $2b/D$  and  $L/D$  in Figures 6.25 and 6.26, respectively. This differs from the case of pressurized systems, for which the effect of yield strain was found to be negligible (because the contribution of elastic stiffness was small as compared to stiffness induced by internal pressure). For the unpressurized systems, the material itself provides the only stiffness and, therefore, yield strain is significant. As a result,  $\epsilon_y$  is considered in the parametric study of  $p/p_y=0$ .

Because  $D/t$  is to be examined at five levels and  $2b/D$ ,  $L/D$ , and  $\epsilon_y$  are each to be investigated at three levels, 135 design points are needed to make up a factorial experimental design for the parametric study ( $5 \times 3^3 = 135$ ). Such a large number of design points would require a significant expenditure of resources in the execution of the finite element analyses. Consequently, it is desirable to reduce the number of design points somewhat in order to save both cost and effort. As described above, it is not possible to reduce the number of design points on the basis of engineering judgement: all of the factors seem to play a significant role in the behaviour. However, the number of design points can be reduced to a manageable number by making use of a fractional factorial experimental design. One such option is to use a  $3^{3-1}$  fractional factorial design

instead of a  $3^3$  approach, thereby reducing the number of design points by two-thirds. The final design obtained in this case is a  $5 \times 3^{3-1}$  hybrid—comprising only 45 design points—that is much more manageable than a full factorial design.

In any  $3^{3-1}$  design only nine points are taken from the 27 points that make up a  $3^3$  design. The question of which particular design points should make up the subset of nine remains to be solved. Montgomery (1976) provides useful guidance regarding appropriate selections. In simple terms, the objective is to choose a subset for which the centre of mass of the nine points lies at the design centrepoint. In practice, twelve such sets are possible, and there is no statistical reason to choose one set rather than another. Using a  $3^{3-1}$  subset given by Montgomery (1976), the design for the parametric study of  $p/p_y=0$  becomes that shown in the leftmost column of Figure 6.10.

As with any fractional design, the results from a  $3^{3-1}$  design are not as informative as the results from a  $3^3$  design: fewer cases are studied, so the pool of data gathered is smaller. Consequently, a ‘penalty’ must be paid in the accuracy of the final prediction equation. This penalty is that the effects of some higher-order interaction terms are not discernible from the main effects when a fractional design is used (Montgomery, 1976). For the work reported herein, adverse effects are not expected to arise from the fractional design: the fractional component of the study involves only those factors that do not have a large influence on the response.

Finite element models were analysed corresponding to the 45 design points for  $p/p_y=0$  that are detailed in Figure 6.10. For practicality, because there are so many analyses, the results are presented in Appendix C. The data from the graphs in Appendix C are used to develop an equation to predict the behaviour of unpressurized sleeper-supported piping systems. Given the success of the equations developed for  $p/p_y=0.5$  and  $p/p_y=0.8$ , an equation of similar form is proposed for the case when  $p/p_y=0$ :

$$\frac{w}{\sigma_y} = a \left( \frac{D}{t} \right)^b \left( \frac{2b}{D} \right)^d \left( \frac{L}{D} \right)^e (\epsilon_y)^f (1 - g^{(100 \times o)}) \quad [6-15]$$

where,

**a, b, d, e, f, g** = regression coefficients.

This equation differs from [6-13] and [6-14] only in that  $L/D$  and  $\varepsilon_y$  are now included. Using equation [6-15], all data in Appendix C, and performing non-linear least-squares regression, the following prediction equation is obtained:

$$\frac{w}{\sigma_y} = 1.4017 \left(\frac{D}{t}\right)^{-2.2045} \left(\frac{2b}{D}\right)^{0.1468} \left(\frac{L}{D}\right)^{-0.9144} (\varepsilon_y)^{0.4891} (1 - 0.9040^{(100 \times \varepsilon)}) \quad [6-16]$$

The  $R^2$  value for this equation is 0.9932, which indicates a very good level of predictive ability. Because the response in equation [6-16] depends on five factors, prediction of the behaviour is expected to be somewhat more difficult than in equations [6-13] and [6-14], which depend on only three factors. This complication is reflected in the nominally lower value of  $R^2$  for equation [6-16].

Figure 6.29, which illustrates predicted soil pressure versus the soil pressure obtained by finite element analysis, allows one to judge whether [6-15] is an appropriate form for the prediction equation. Because most of the points shown in the figure lie between the 10% error bands, it is reasonable to conclude that [6-16] is an appropriate representation of the behaviour of unpressurized piping systems. Most of those points that lie outside of the bands fall below the diagonal line, which means that the greatest errors made by the prediction equation tend to underestimate the strength that is calculated by the finite element model.

#### 6.4 DISCUSSION OF REGRESSION TECHNIQUES

Equations [6-13], [6-14], and [6-16] give predictions that agree very well with the results from the finite element analyses of *in situ* sleeper-supported piping systems. However, it is prudent to examine the statistical methods used in the regression analyses to identify any potentially significant limitations or shortcomings. Such an examination is done by performing a series of diagnostic checks.

If shortcomings were present in the regression analyses, they would most likely arise because of a violation of one or more of the three fundamental assumptions upon which the least squares approach to regression analysis is derived. These assumptions are *independence*, *normality*, and *homoscedasticity*.

The assumption of independence means that the values within the set of residual errors,  $r_i$ , are not correlated with each other. For the work performed herein, this

assumption should be satisfied because the factors  $\pi_1, \pi_2, \pi_3, \pi_4, \pi_5,$  and  $\pi_7$  are themselves independent. Furthermore, the most common source of correlation among residual errors arises from influences related to the sequence in which data are collected. Because all of the data in this study are from computer simulations, the same results are always obtained regardless of the order in which the simulations are executed. Consequently, the assumption of independence is satisfied in this work.

The assumption of normality means that the source data are normally distributed around the regression surface, or, equivalently, that the residual errors have a normal distribution. In this work, the source data for the regression come from finite element models—a deterministic method of analysis—so it is known that the data originate from a population that does not have random error. Consequently, the residual errors of the regression equation are not expected to have a normal distribution, and the data may violate the normality assumption.

Plotting each residual,  $r_i$ , versus its *cumulative probability*,  $P_i$ , acts as a test of normality (Khuri and Cornell, 1996). The cumulative probability, which represents the likelihood that any given residual will be less than a particular value, is calculated as:

$$P_i = \left[ \frac{100(i - 0.5)}{n} \right]. \quad [6-17]$$

To make this calculation, the set of residuals must be ordered so that residual  $i$  is the  $i$ th smallest in magnitude, where  $i=1, 2, \dots, n$ . If the residuals are normally distributed, the plot should appear as an approximately straight line when a linear scale is used on the vertical axis and a normal probability scale is used on the horizontal axis. Such plots are shown in Figure 6.30 for the residuals from equations [6-13], [6-14], and [6-16]. These three plots can be characterized as somewhat linear, except for a few points at each end. Gunst and Mason (1980) indicate that scatter of the points near the ends is a common occurrence, even for those cases in which the data are truly normally distributed: these last few points can be ignored. Because the judgement of normality is somewhat subjective, it is probably best to conclude that the residuals are not normally distributed in this case. Fortunately, the consequences of failing the test of normality are not necessarily severe, especially if the non-linearity is not excessive. A failed normality test means that least-squares regression estimates are still valid, although any statistical tests

of significance that might be done would generally be erroneous. Consequently, the fact that the residual errors are not quite normally distributed is judged to have no adverse effect on the regression equations developed in Section 6.3.

Homoscedasticity means that the variance of the residual errors is approximately constant for all values of the factors and for all values of the predicted response. If the errors are homoscedastic, it is expected that the regression equation will provide approximately the same magnitude of error in its estimate regardless of the values of the factors. If the residuals are *heteroscedastic*, that is, they do not have constant variance, it may indicate that a significant factor has been overlooked or that a transformation should be applied to one of the factors, that is, the form of the regression equation should be modified. Significant heteroscedasticity can also prevent a least squares analysis from obtaining optimal values of the regression coefficients (Box et al., 1978).

To detect heteroscedasticity, it is useful to examine so-called *residual plots*. A residual plot is a graph of the residual errors versus one of the factors or versus the predicted response,  $\hat{Y}$ . For multiple regression analysis, as performed in this study, it is customary to plot the residuals against  $\hat{Y}$  (Devore, 1991). If the scatter of the points about the horizontal axis remains at approximately the same width for all values of  $\hat{Y}$ , the residuals can usually be judged to be homoscedastic. Residual plots for each of equations [6-13], [6-14], and [6-16] are presented in Figure 6.31. Examination of these plots shows that the data is heteroscedastic: in each case, the cloud of data points is very narrow at the origin and generally widens with increasing  $w/\sigma_y$  (i.e.,  $\hat{Y}$ ). Such heteroscedasticity is not surprising, because the data are obtained from finite element analyses: the errors are generally systematic, not random. In all cases the error in the finite element solution is zero when the loads are zero, and the error increases in magnitude as the loads increase.

The fact that the residuals are heteroscedastic does not invalidate the regression analyses, but it does reduce the quality of the prediction somewhat (Tabachnick and Fidell, 1996). However, recalling the excellent predictive ability of each of equations [6-13], [6-14], and [6-16], there is little room for improvement in the correlation. The value of  $R^2$  exceeds 0.99 in each case, and there is little to be gained by modifying the form of the regression equations or by employing the method of weighted residuals (Box

et al., 1978) to enhance the predictive ability of the equations. Consequently, it is judged that the heteroscedasticity of residual errors has no adverse affect on the prediction equations.

In conclusion, it appears that the simplified equations developed in this chapter for the behaviour of sleeper-supported piping systems are valid in their ability to predict the behaviour that is given by the finite element analyses of *in situ* conditions. As a caveat, it must be appreciated that this predictive ability has been demonstrated only within the factor ranges considered in this study. It is also necessary to assess a number of practical considerations before the equations can be implemented for design. This assessment is reported in the next chapter, along with comparisons of the newly developed equations with the existing design equation [1-3].

**Table 6.1** Set of variables for screening study of all parameters

Designation	D (mm)	t (mm)	$\sigma_y$ (MPa)	2b (mm)	L (mm)	$p_y$ (MPa)	p (MPa)	E (MPa)
<b>80-0.5-1.0-7-2.33</b>	<b>762</b>	<b>9.53</b>	<b>483</b>	<b>762</b>	<b>5334</b>	<b>12.08</b>	<b>6.04</b>	<b>207 000</b>
40-0.5-1.0-7-2.33	762	19.05	483	762	5334	24.15	12.08	207 000
120-0.5-1.0-7-2.33	762	6.35	483	762	5334	8.05	4.03	207 000
80-0.0-1.0-7-2.33	762	9.53	483	762	5334	12.08	0.00	207 000
80-0.8-1.0-7-2.33	762	9.53	483	762	5334	12.08	9.66	207 000
80-0.5-0.5-7-2.33	762	9.53	483	381	5334	12.08	6.04	207 000
80-0.5-1.5-7-2.33	762	9.53	483	1143	5334	12.08	6.04	207 000
80-0.5-1.0-5-2.33	762	9.53	483	762	3810	12.08	6.04	207 000
80-0.5-1.0-9-2.33	762	9.53	483	762	6858	12.08	6.04	207 000
80-0.5-1.0-7-1.73	762	9.53	359	762	5334	8.98	4.49	207 000
80-0.5-1.0-7-2.66	762	9.53	550	762	5334	13.76	6.88	207 000

Designation:  $\frac{D}{t} - \frac{p}{p_y} - \frac{2b}{D} - \frac{L}{D} - \epsilon_y$

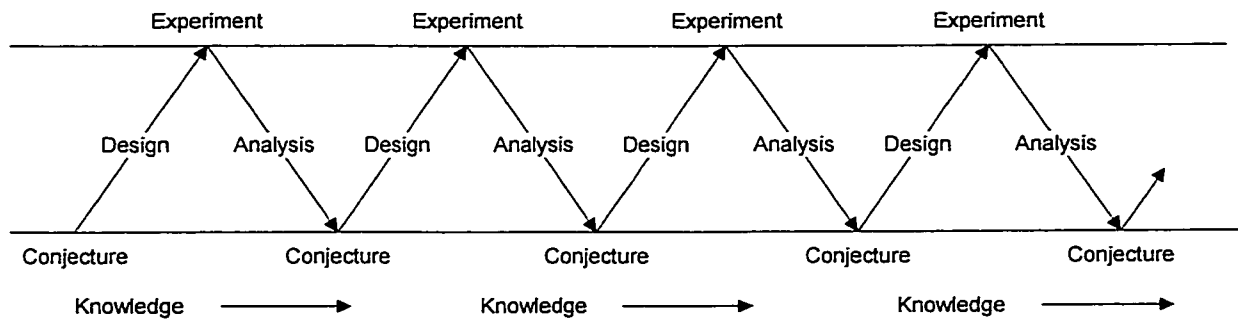


**Figure 6.1** Flow chart of the development of knowledge used as part of response surface methodology proposed by Khuri and Cornell (1996)

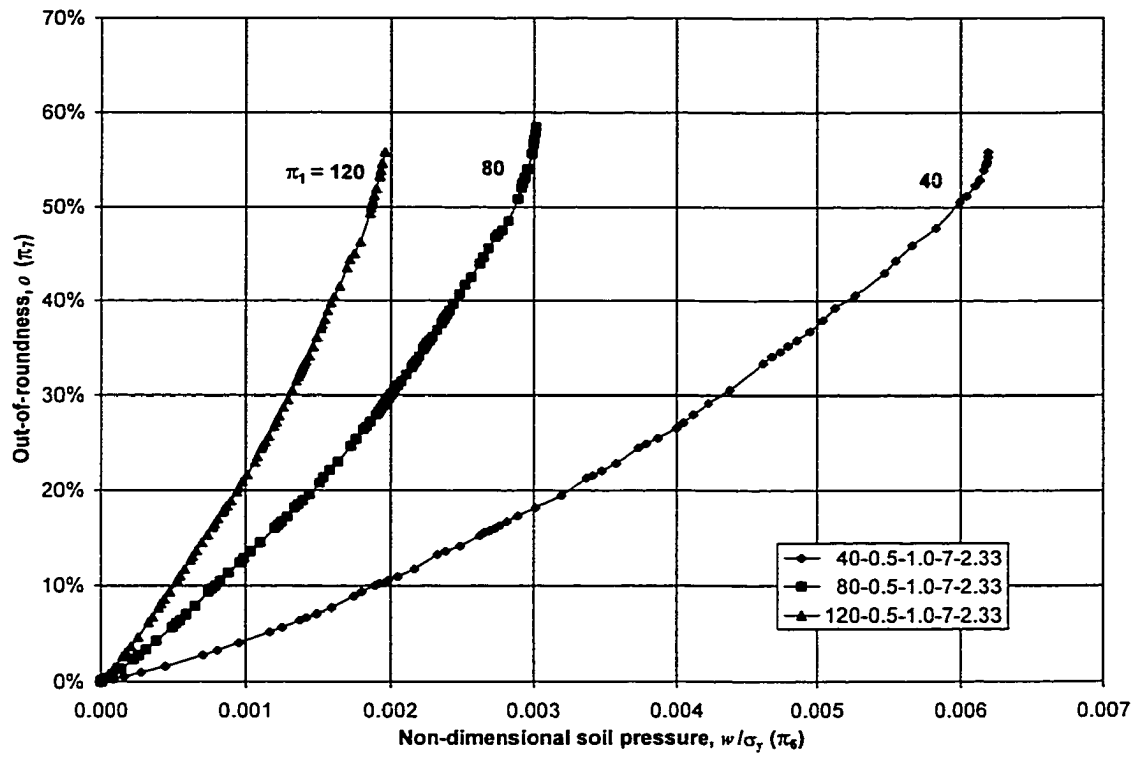


**Figure 6.2** Effect of variation of  $D/t$  ( $\pi_1$ )

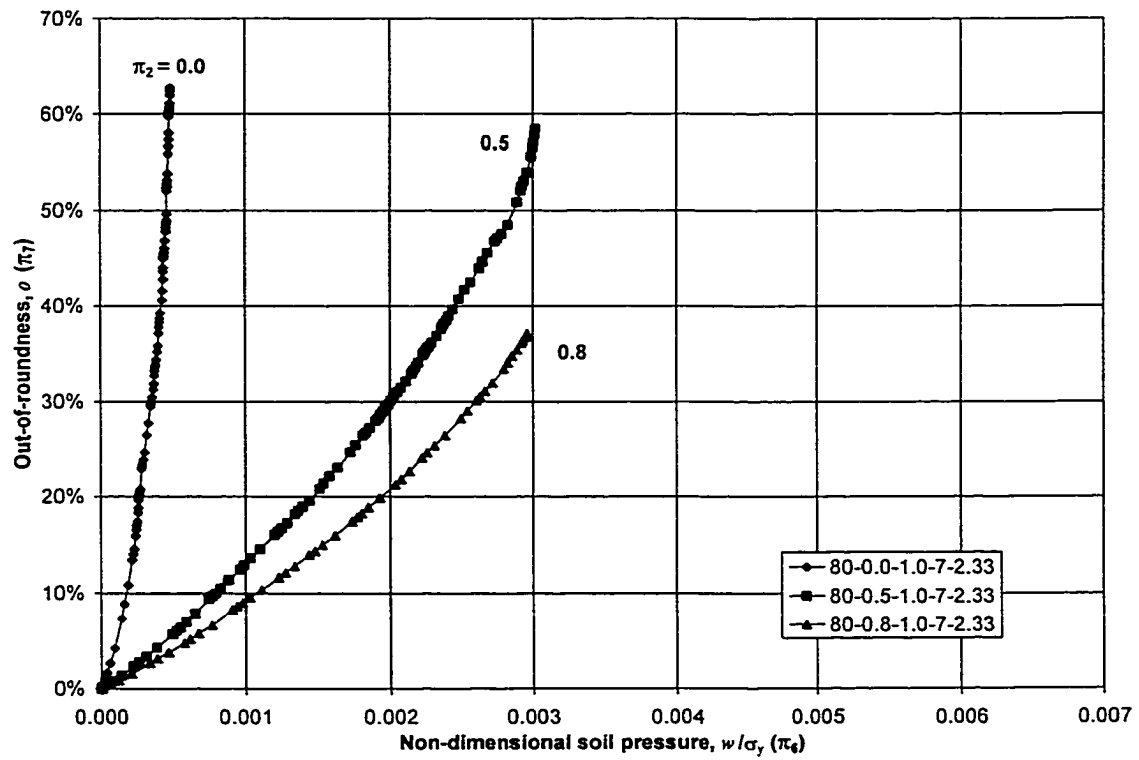


**Figure 6.3** Effect of variation of  $p/p_y$  ( $\pi_2$ )

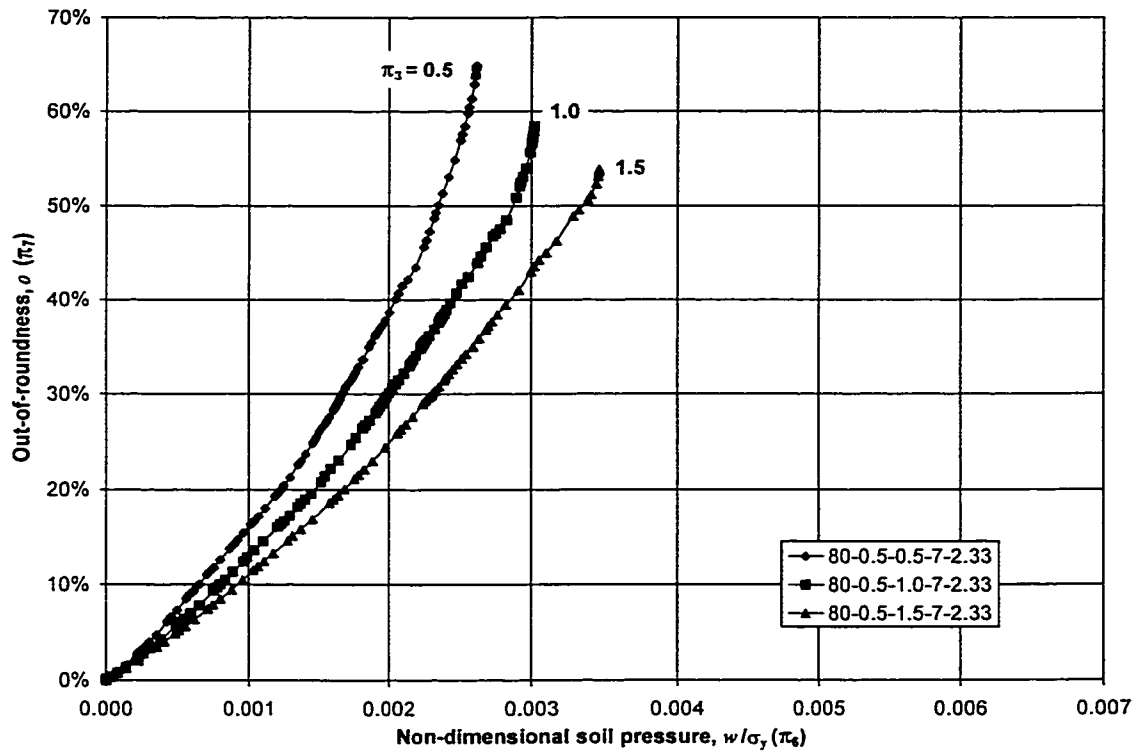


**Figure 6.4** Effect of variation of  $2b/D$  ( $\pi_3$ )

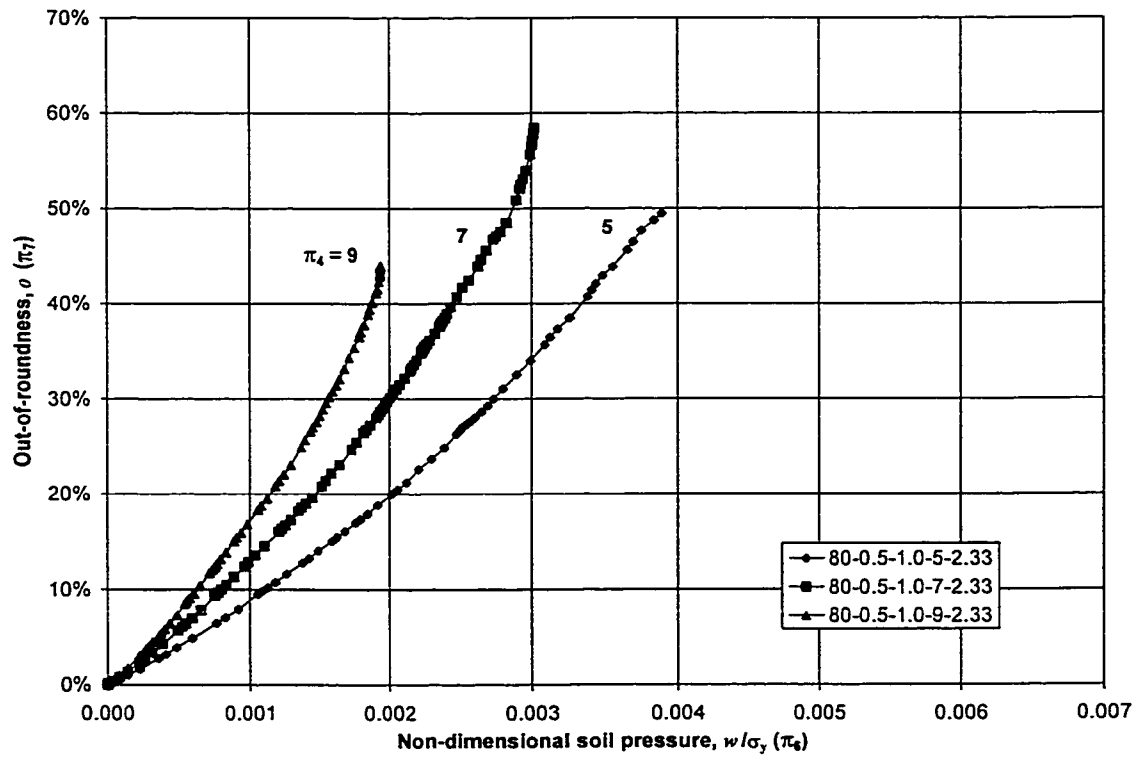


**Figure 6.5** Effect of variation of  $L/D$  ( $\pi_4$ )

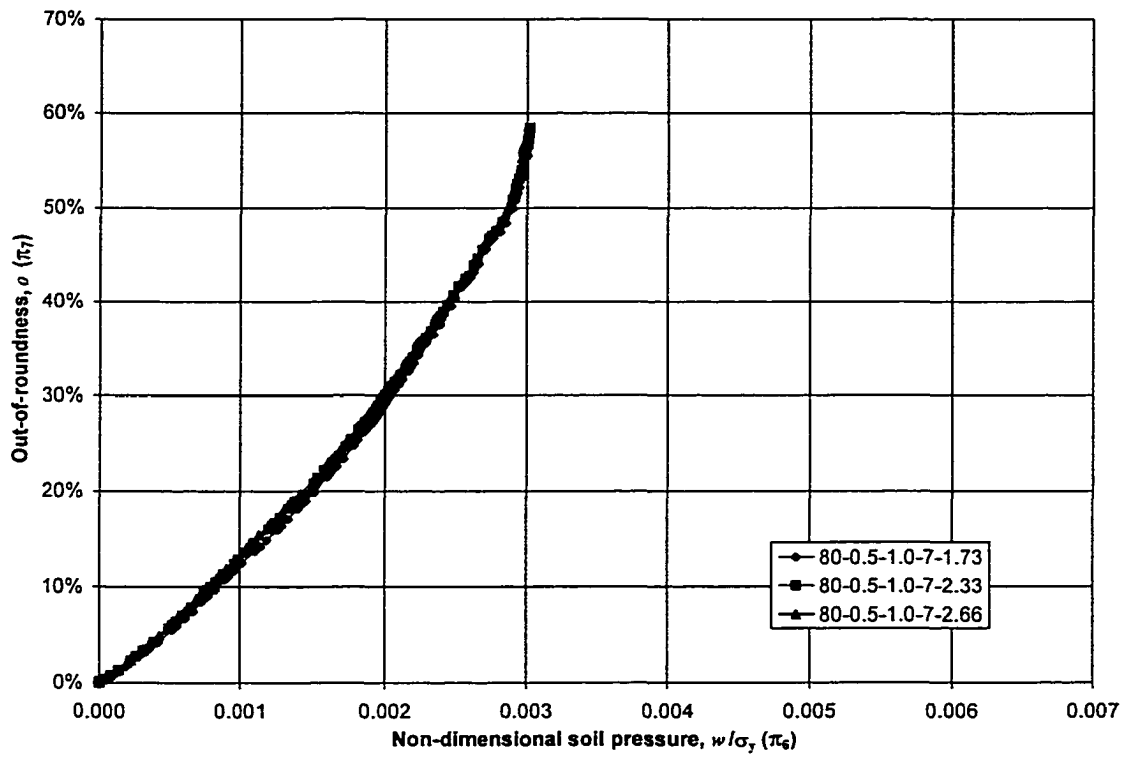


**Figure 6.6** Effect of variation of  $\epsilon_y$  ( $\pi_5$ )

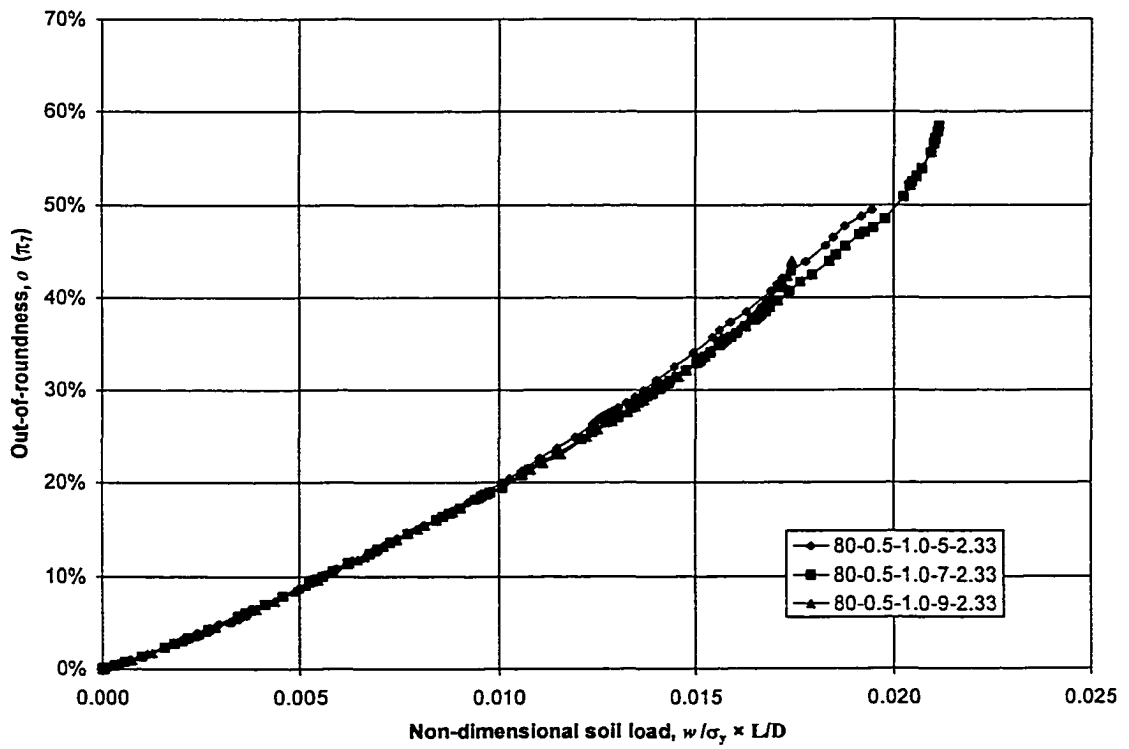


**Figure 6.7** Variation of response with soil load

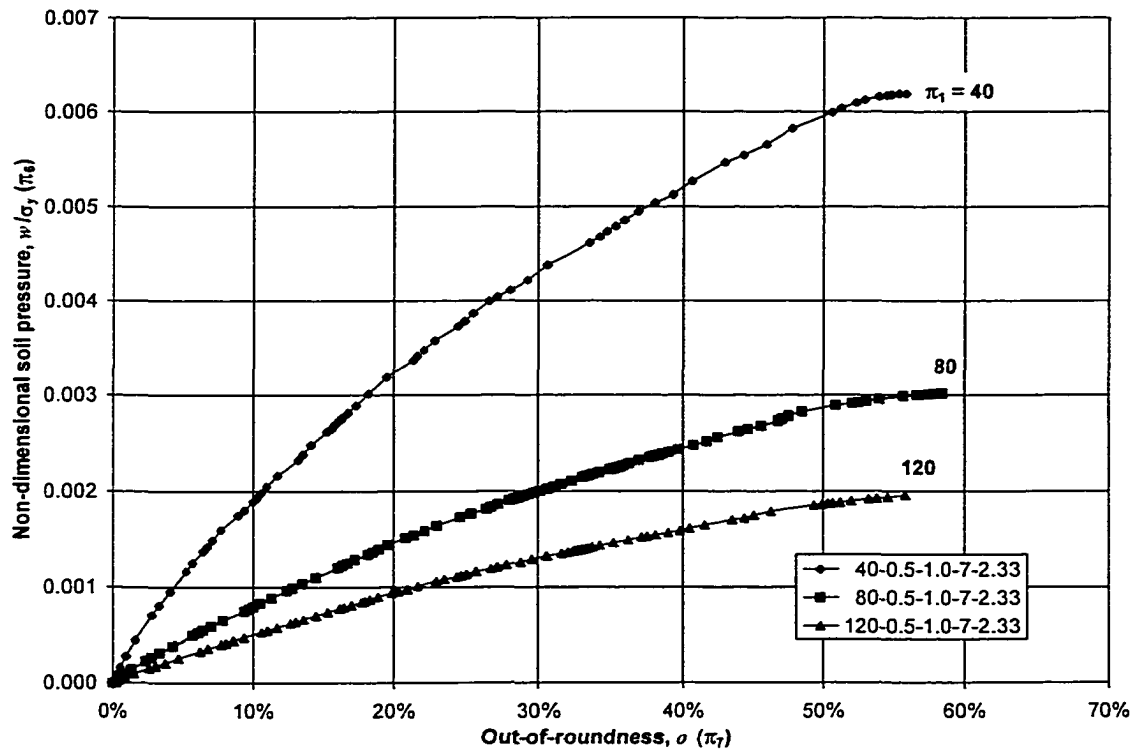


**Figure 6.8**  $w/\sigma_y$  redefined as the response variable,  $\sigma$  as a factor

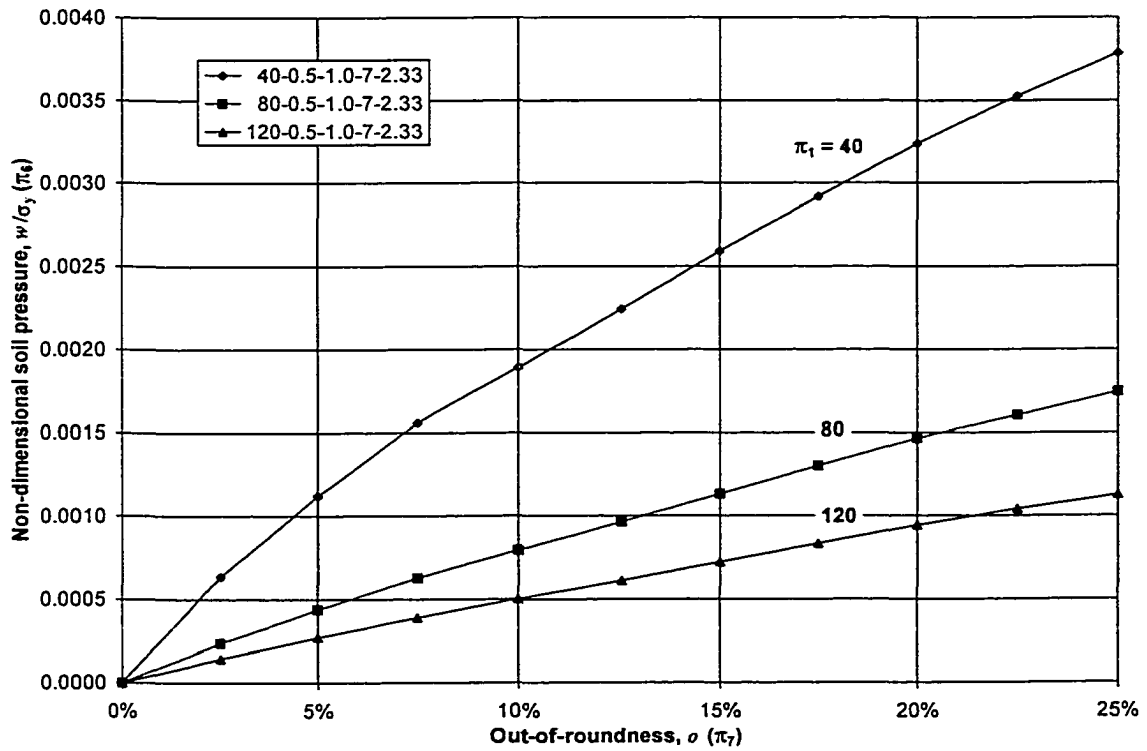


**Figure 6.9** Data redefined at 2.5% increments of  $\sigma$  to provide uniformity in the data set

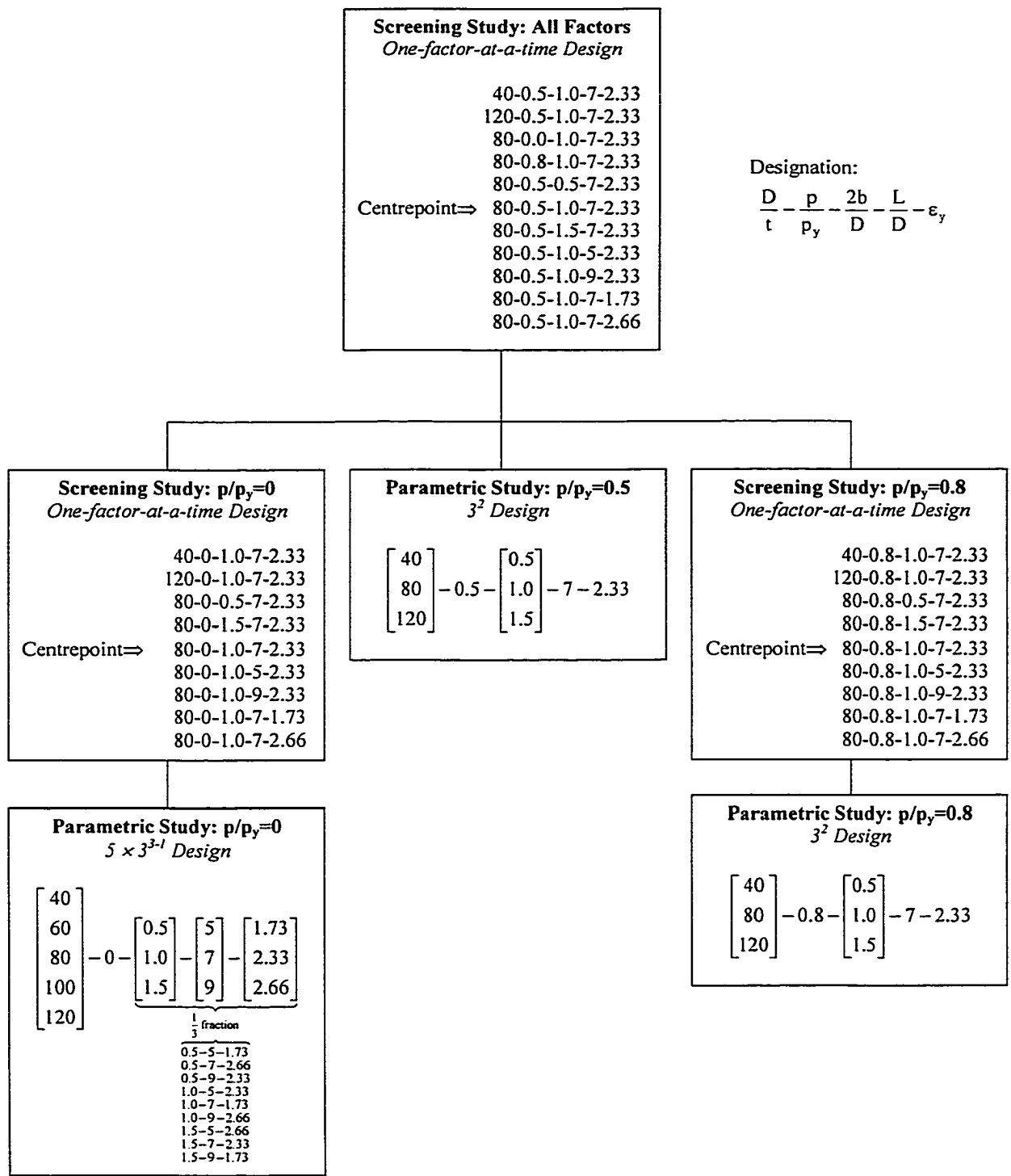


**Figure 6.10** Overall layout of parametric finite element analysis study

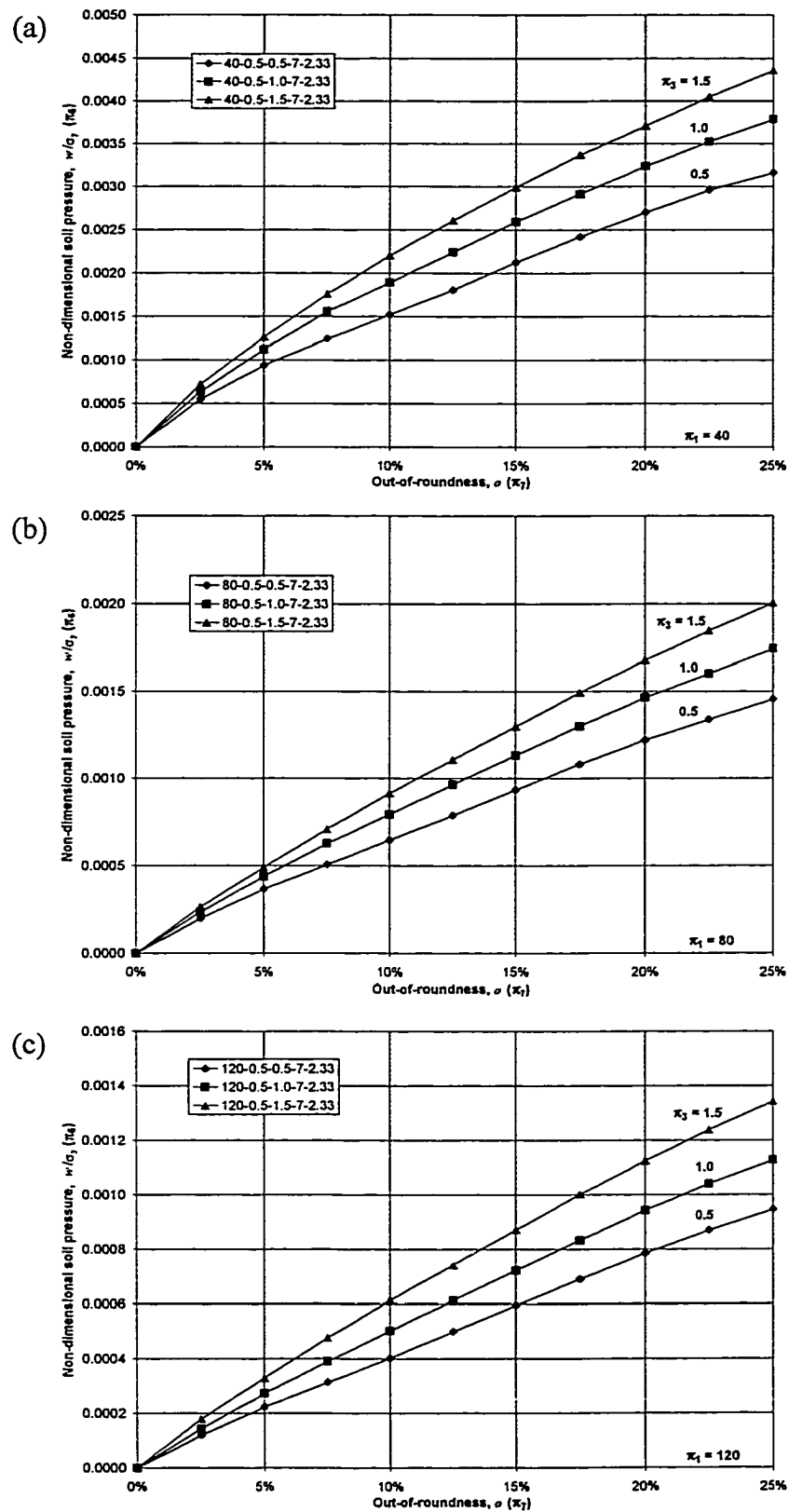


**Figure 6.11** Results from finite element analyses for parametric study at  $p/p_y=0.5$

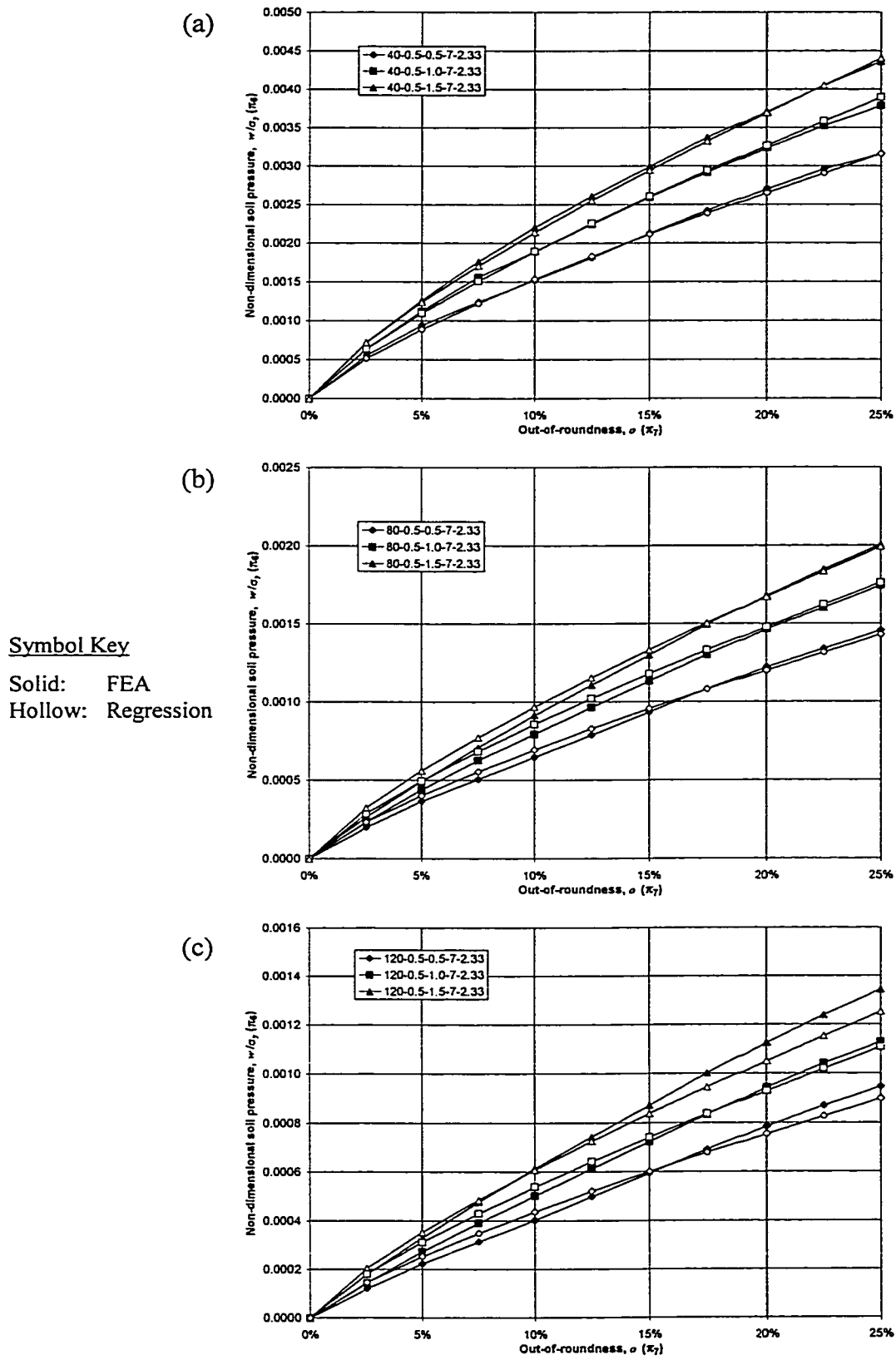


**Figure 6.12** Comparison of predicted response by equation [6-11] with finite element data for  $p/p_y=0.5$

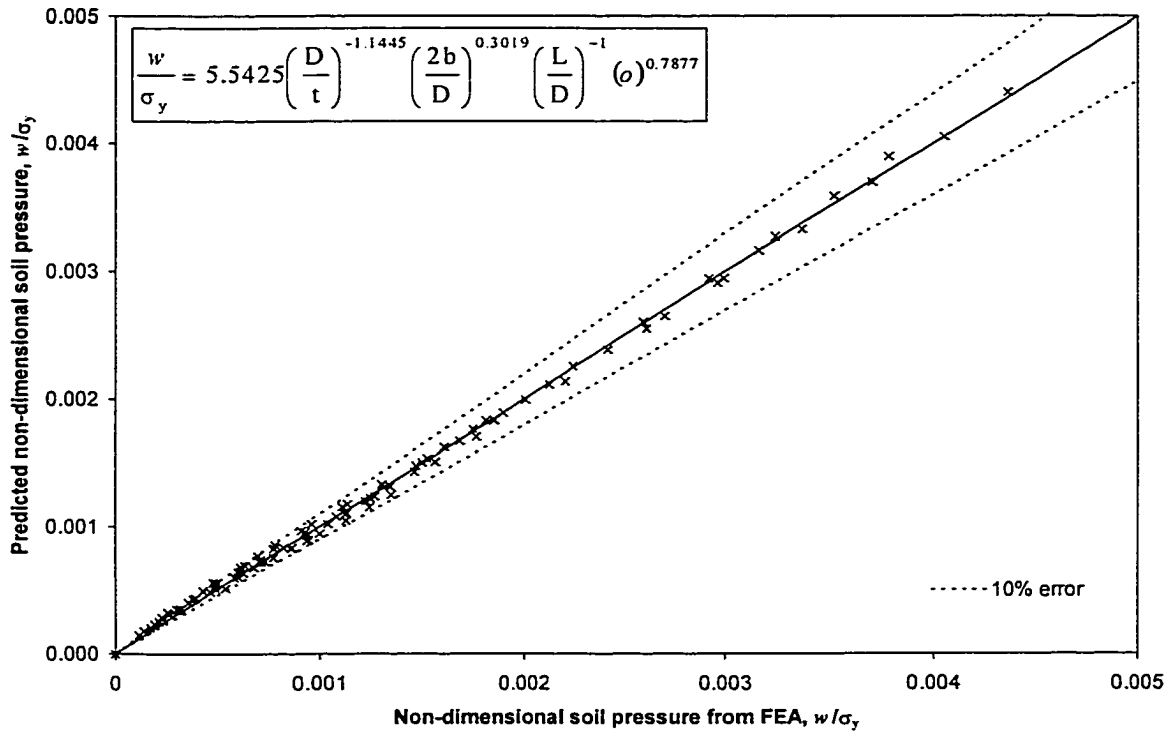


**Figure 6.13** Predicted response by equation [6-11] versus finite element response for  $p/p_y=0.5$

Symbol Key  
 Solid: FEA  
 Hollow: Regression

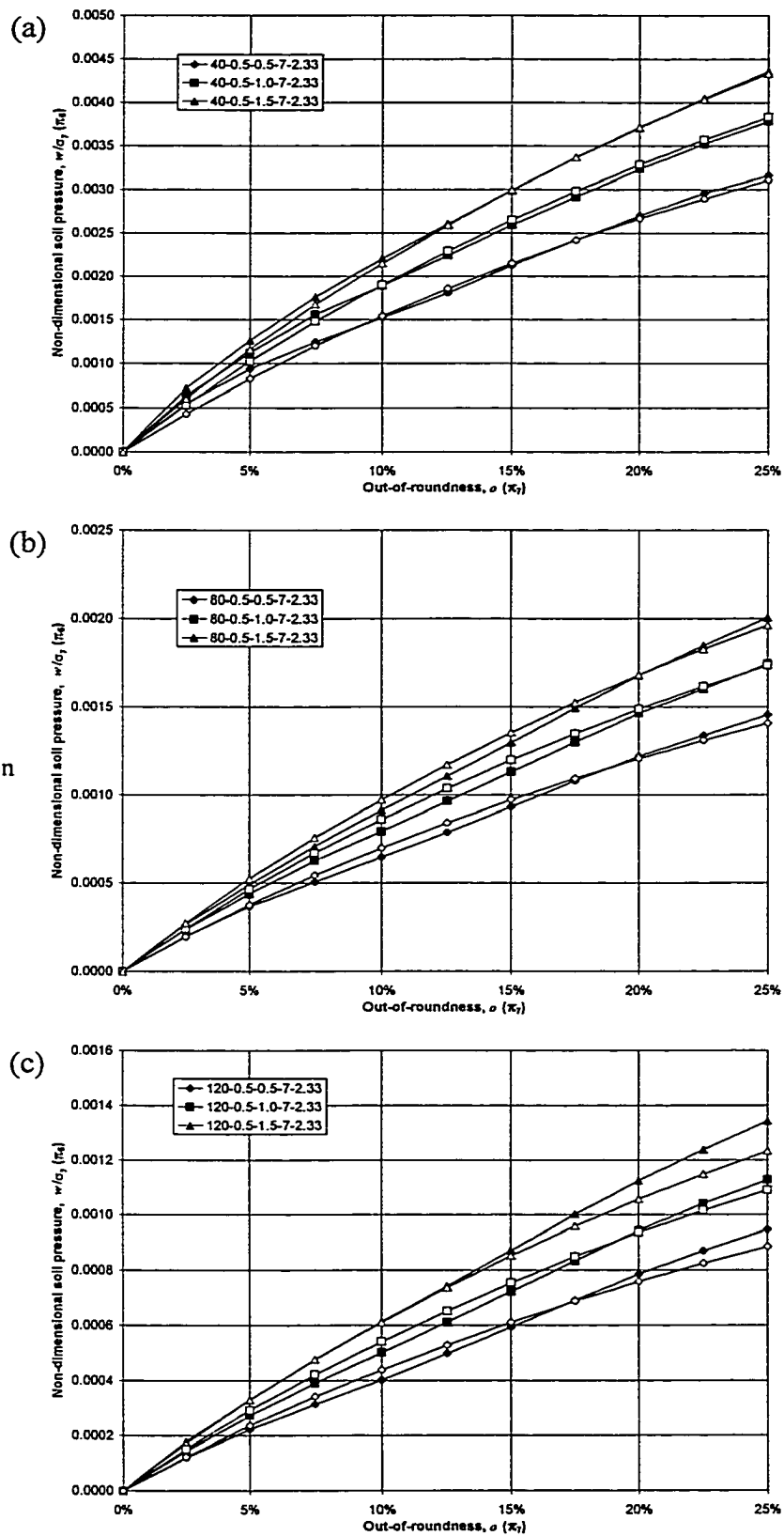


**Figure 6.14** Comparison of predicted response by equation [6-13] with finite element data for  $p/p_y=0.5$

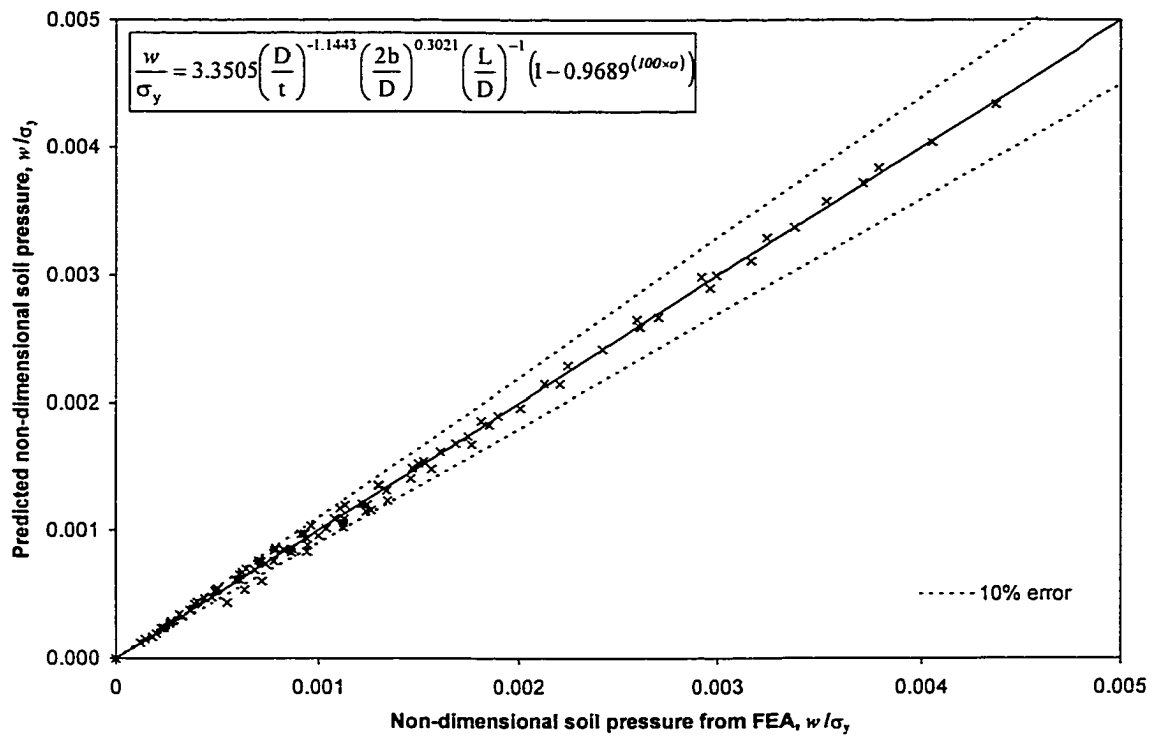


**Figure 6.15** Predicted response by equation [6-13] versus finite element response for  $p/p_y=0.5$

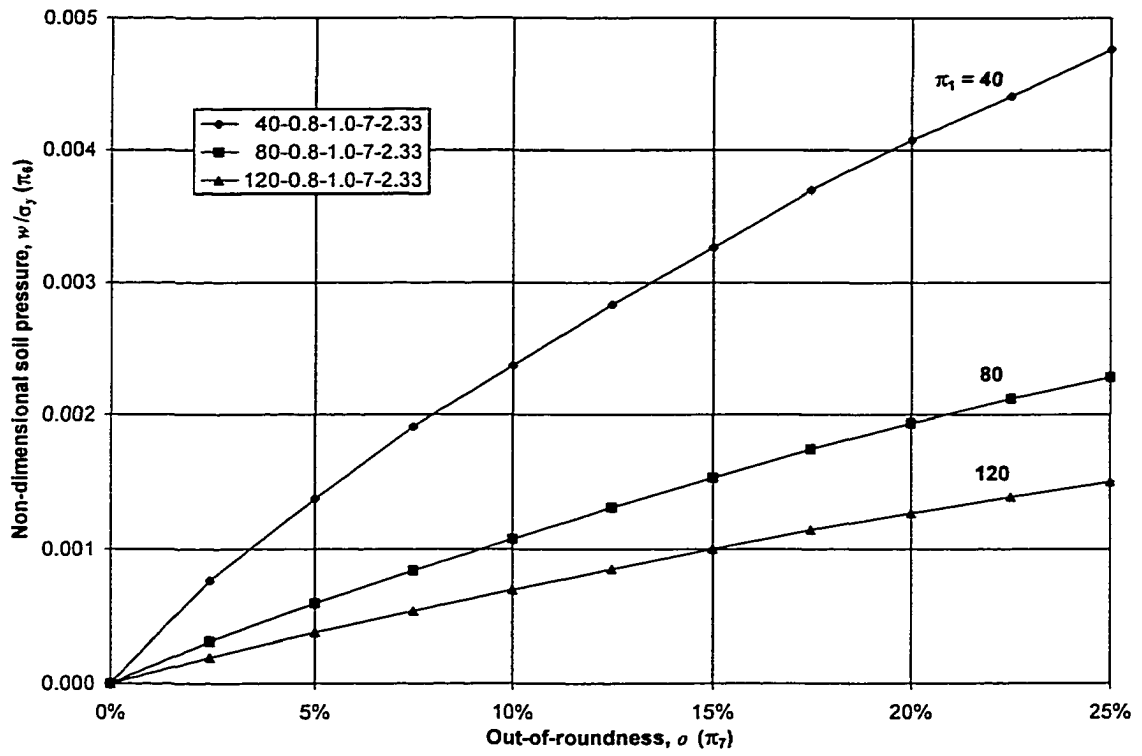


**Figure 6.16** Effect of variation of  $D/t$  ( $\pi_1$ ) when  $p/p_y=0.8$

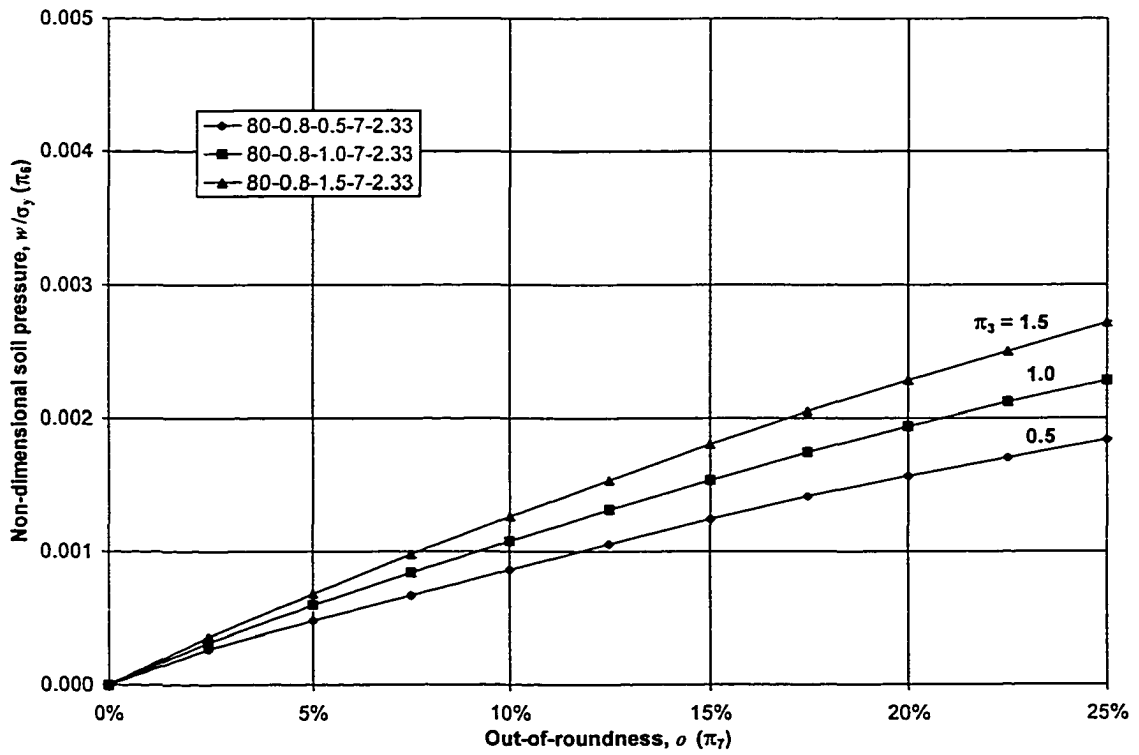


**Figure 6.17** Effect of variation of  $2b/D$  ( $\pi_3$ ) when  $p/p_y=0.8$

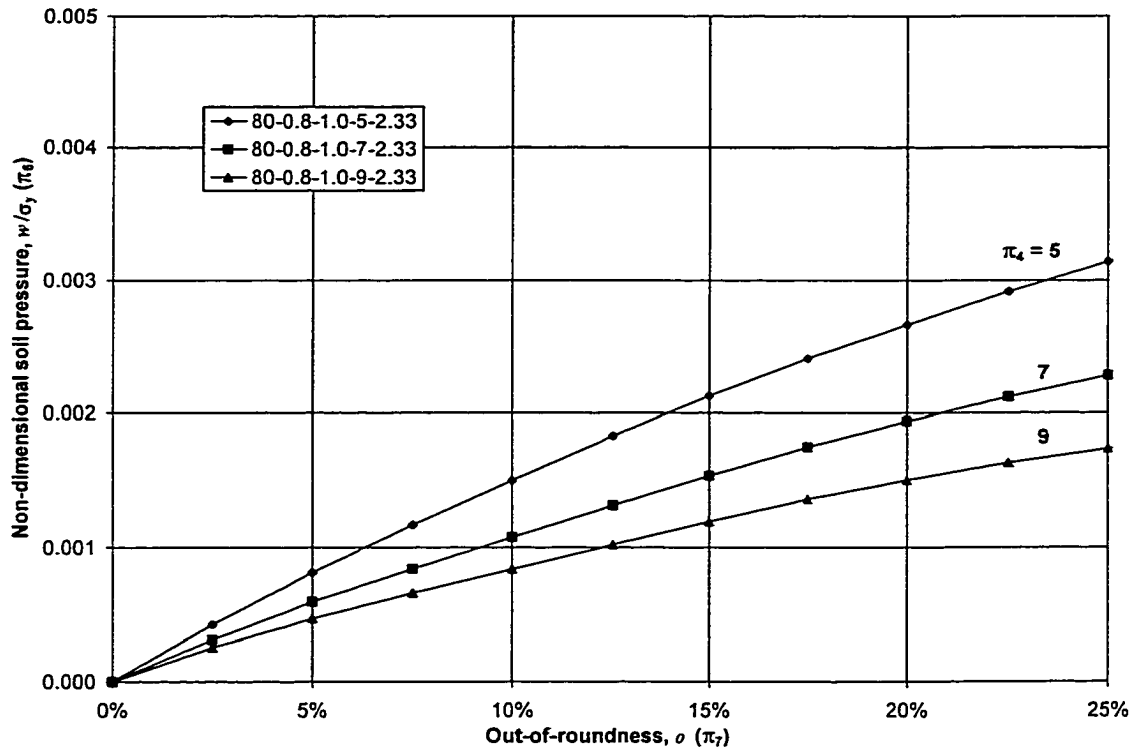


**Figure 6.18** Effect of variation of  $L/D$  ( $\pi_4$ ) when  $p/p_y=0.8$

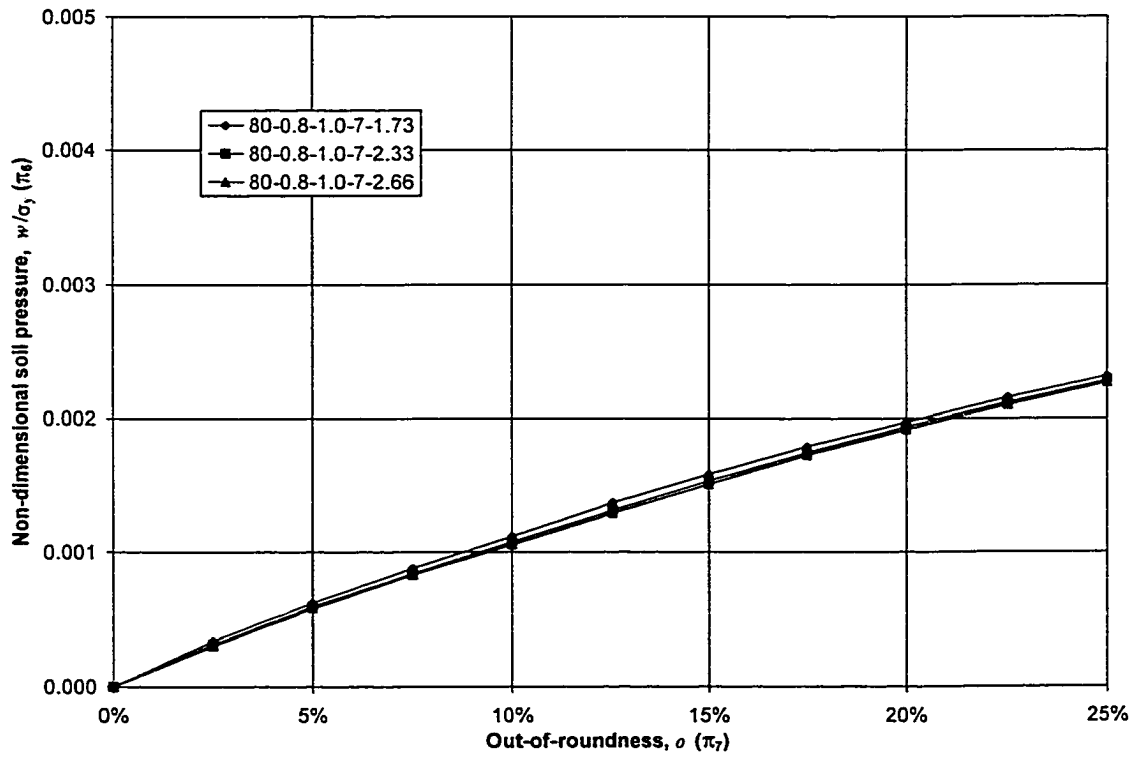


**Figure 6.19** Effect of variation of  $\epsilon_y$  ( $\pi_5$ ) when  $p/p_y=0.8$

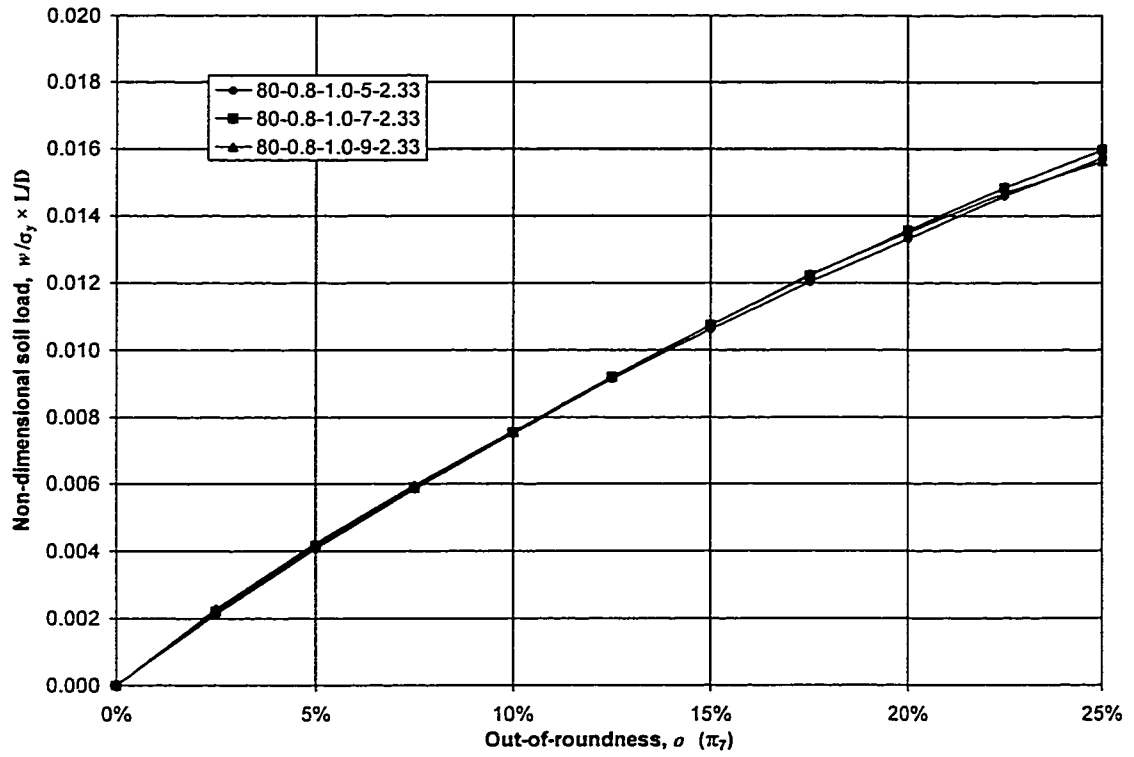


**Figure 6.20** Variation of response with soil load when  $p/p_y=0.8$

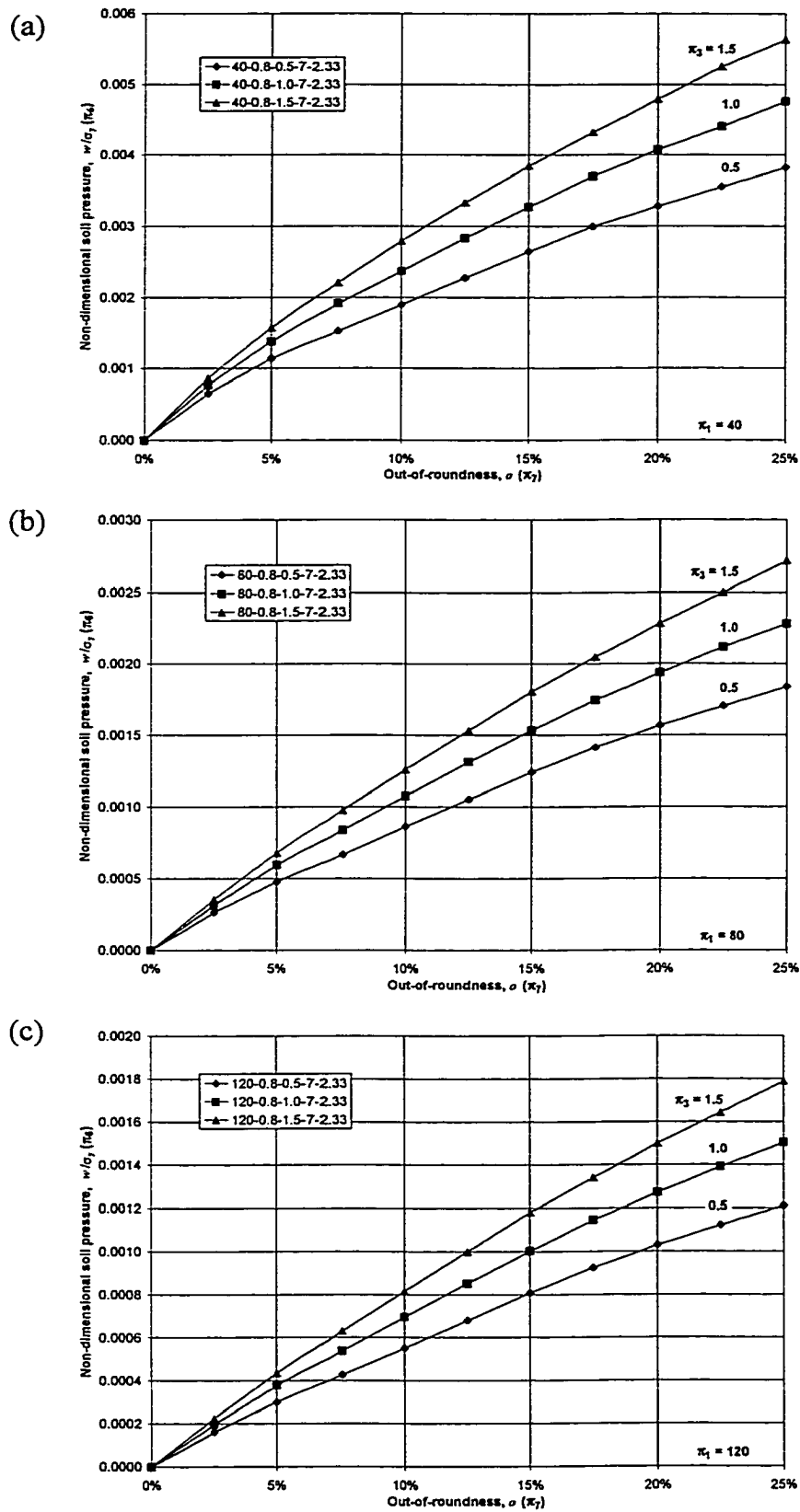
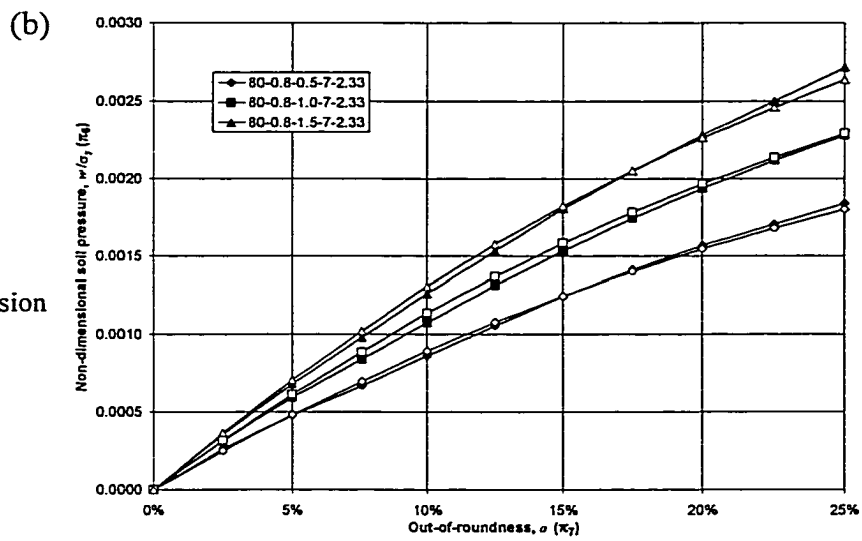
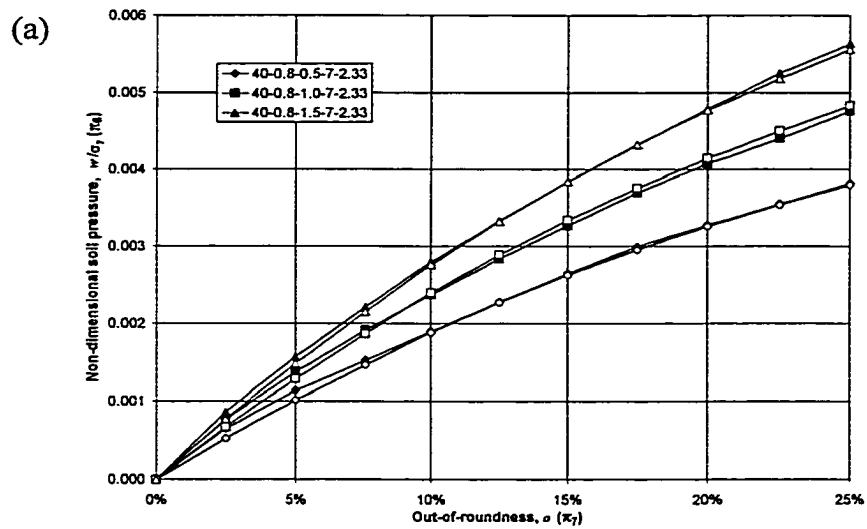


**Figure 6.21** Results from finite element analysis for parametric study at  $p/p_y=0.8$



Symbol Key

Solid: FEA

Hollow: Regression

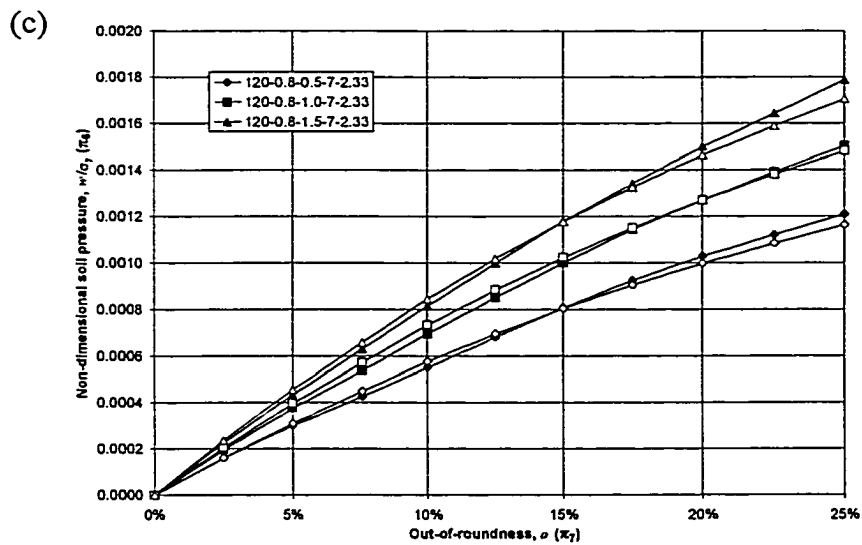


**Figure 6.22** Comparison of predicted response by equation [6-14] with finite element data for  $p/p_y=0.8$

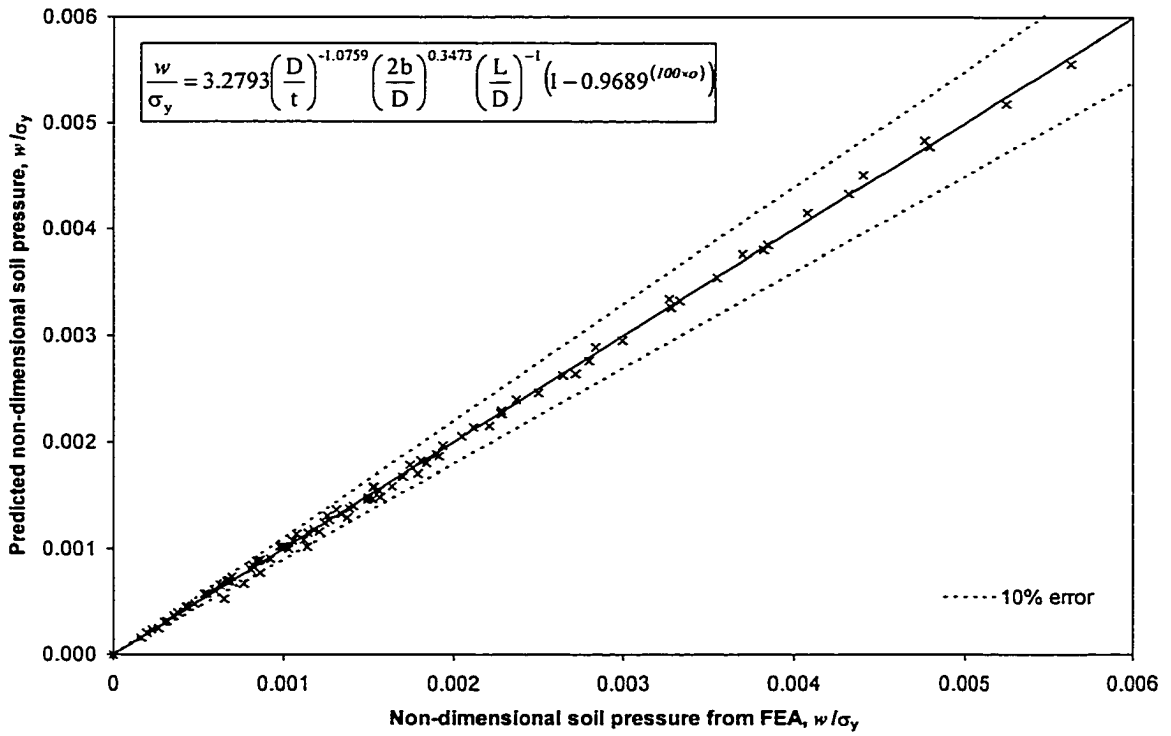


**Figure 6.23** Predicted response by equation [6-14] versus finite element response for  $p/p_y=0.8$

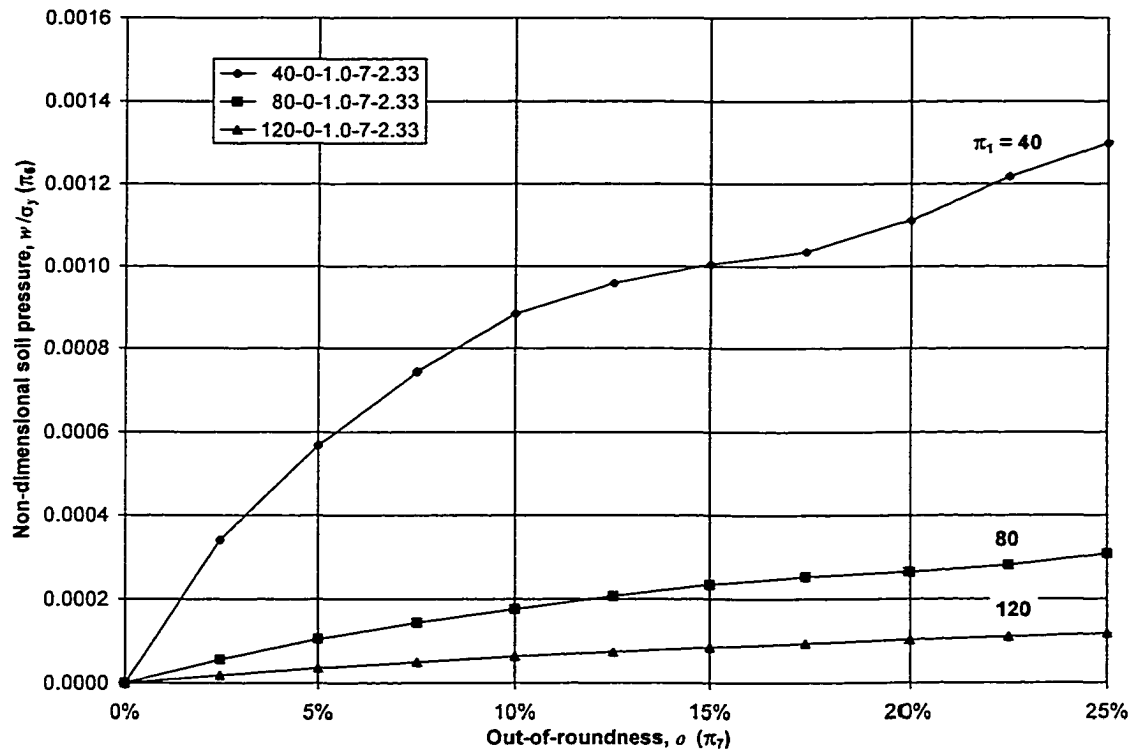


Figure 6.24 Effect of variation of  $D/t$  ( $\pi_1$ ) when  $p/p_y=0$

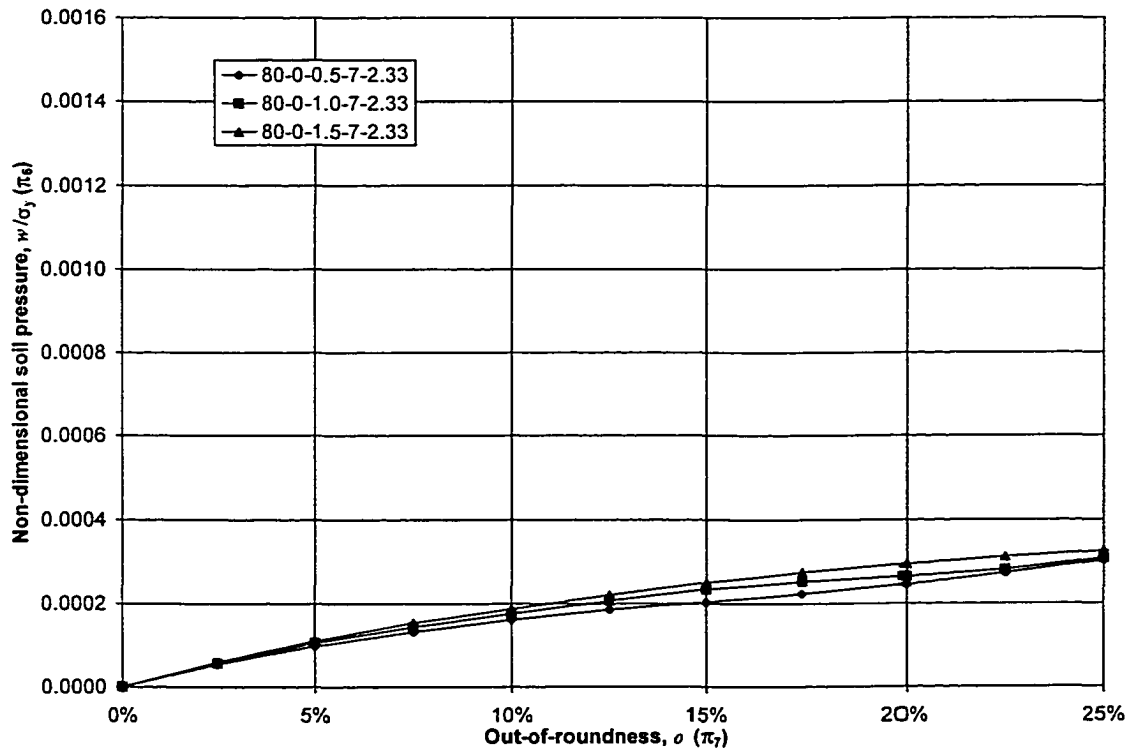
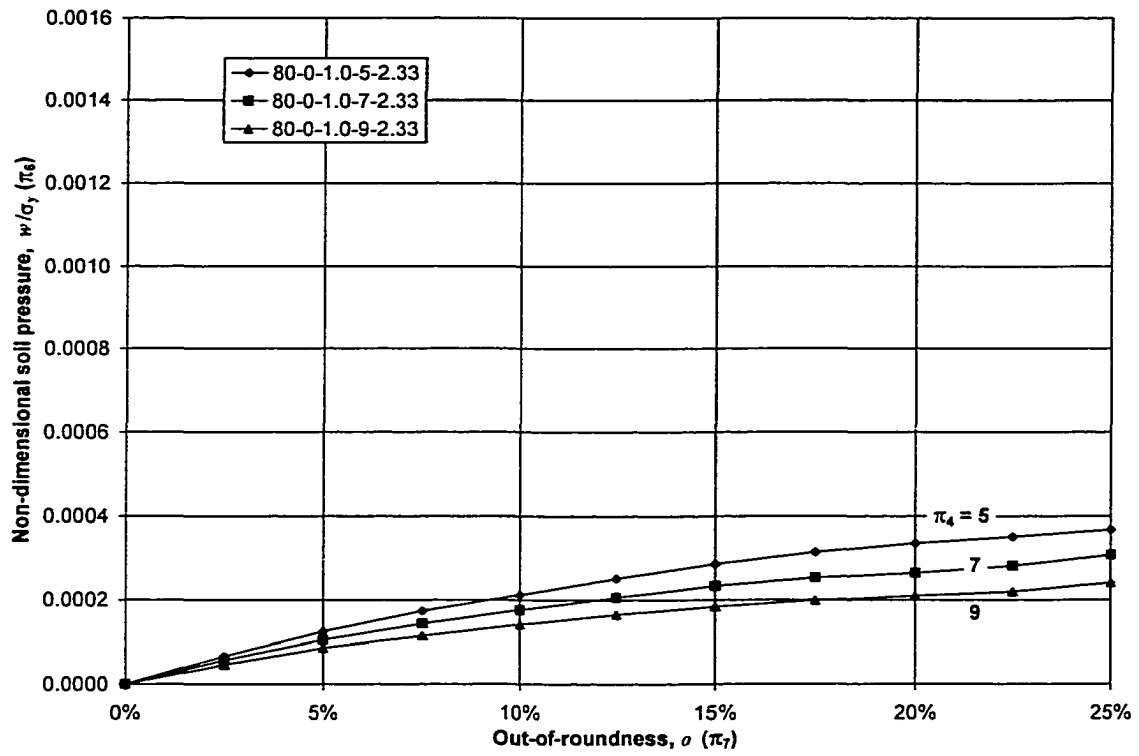
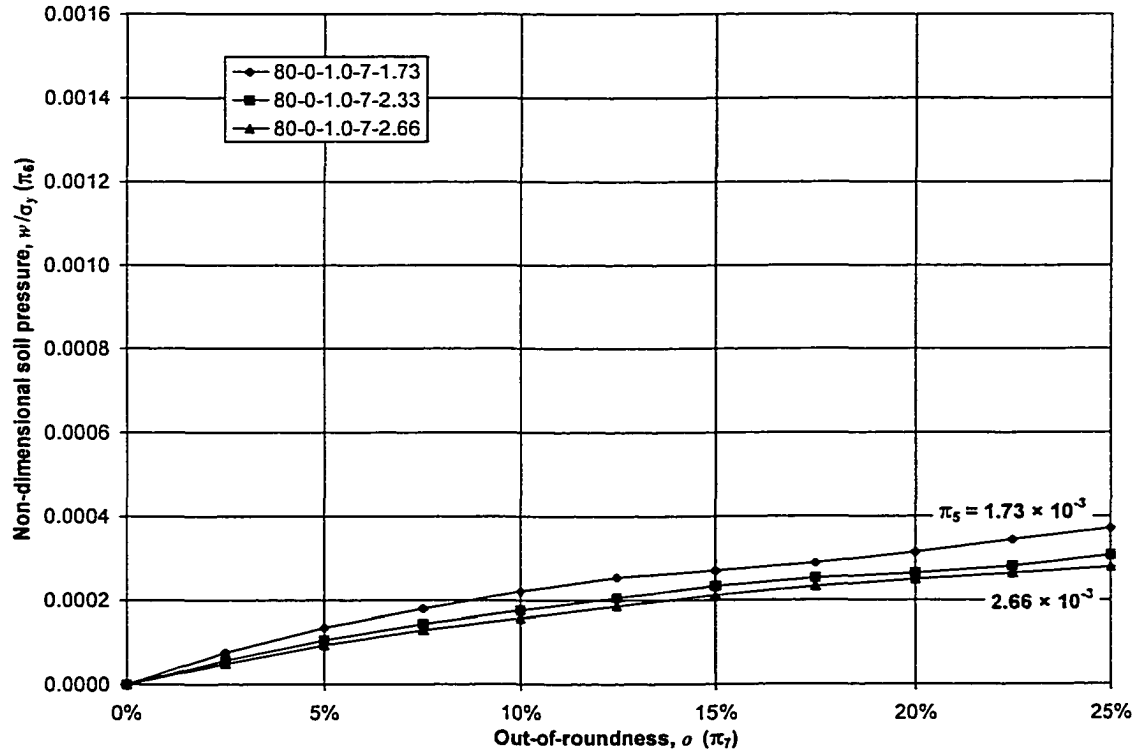


Figure 6.25 Effect of variation of  $2b/D$  ( $\pi_3$ ) when  $p/p_y=0$



**Figure 6.26** Effect of variation of  $L/D$  ( $\pi_4$ ) when  $p/p_y=0$



**Figure 6.27** Effect of variation of  $\epsilon_y$  ( $\pi_5$ ) when  $p/p_y=0$

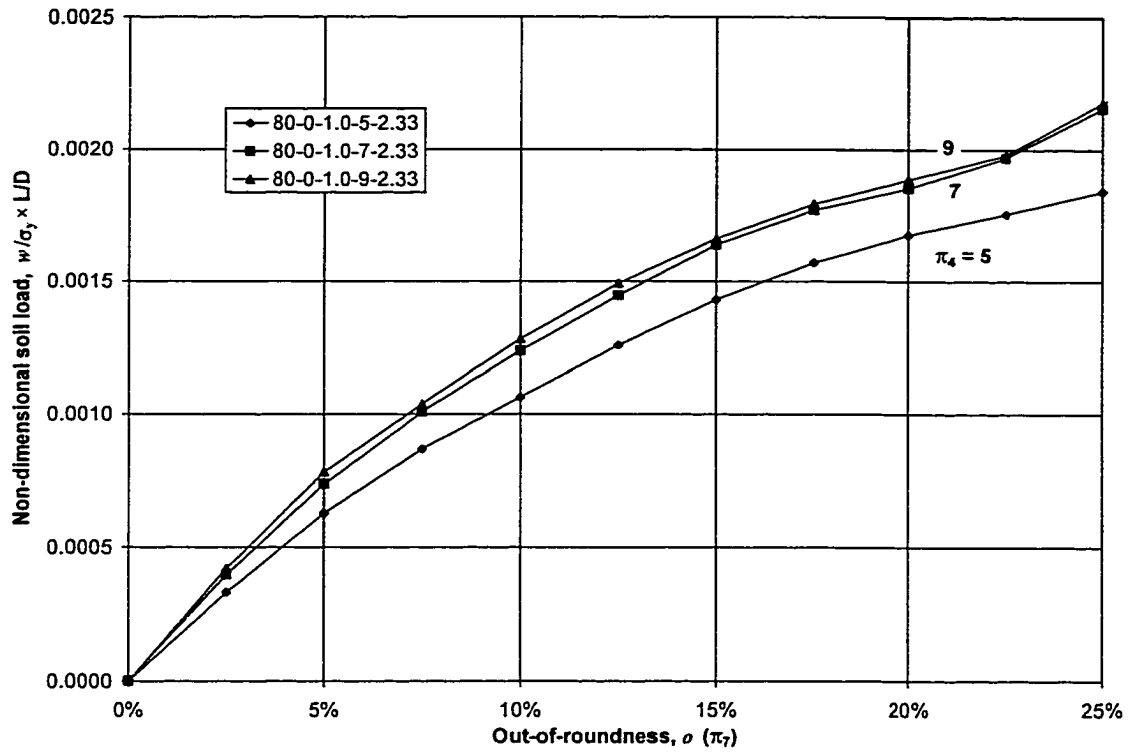


**Figure 6.28** Variation of response with soil load when  $p/p_y=0$

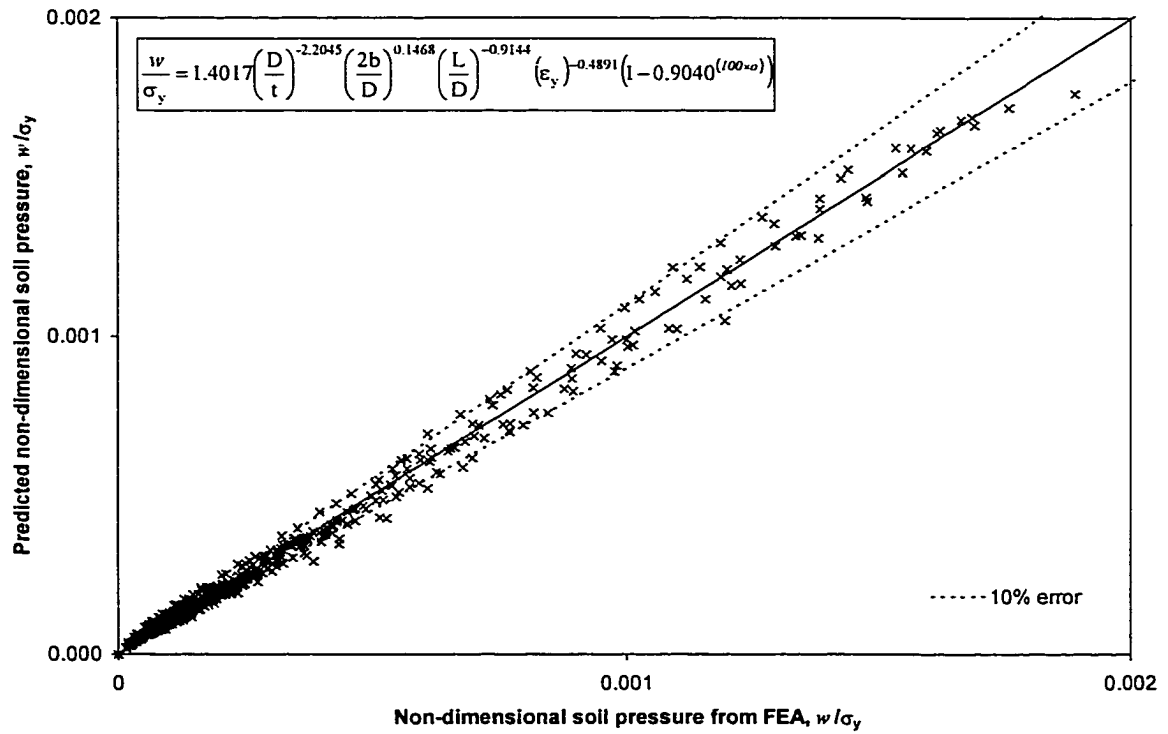


**Figure 6.29** Predicted response by equation [6-16] versus finite element response for  $p/p_y=0$

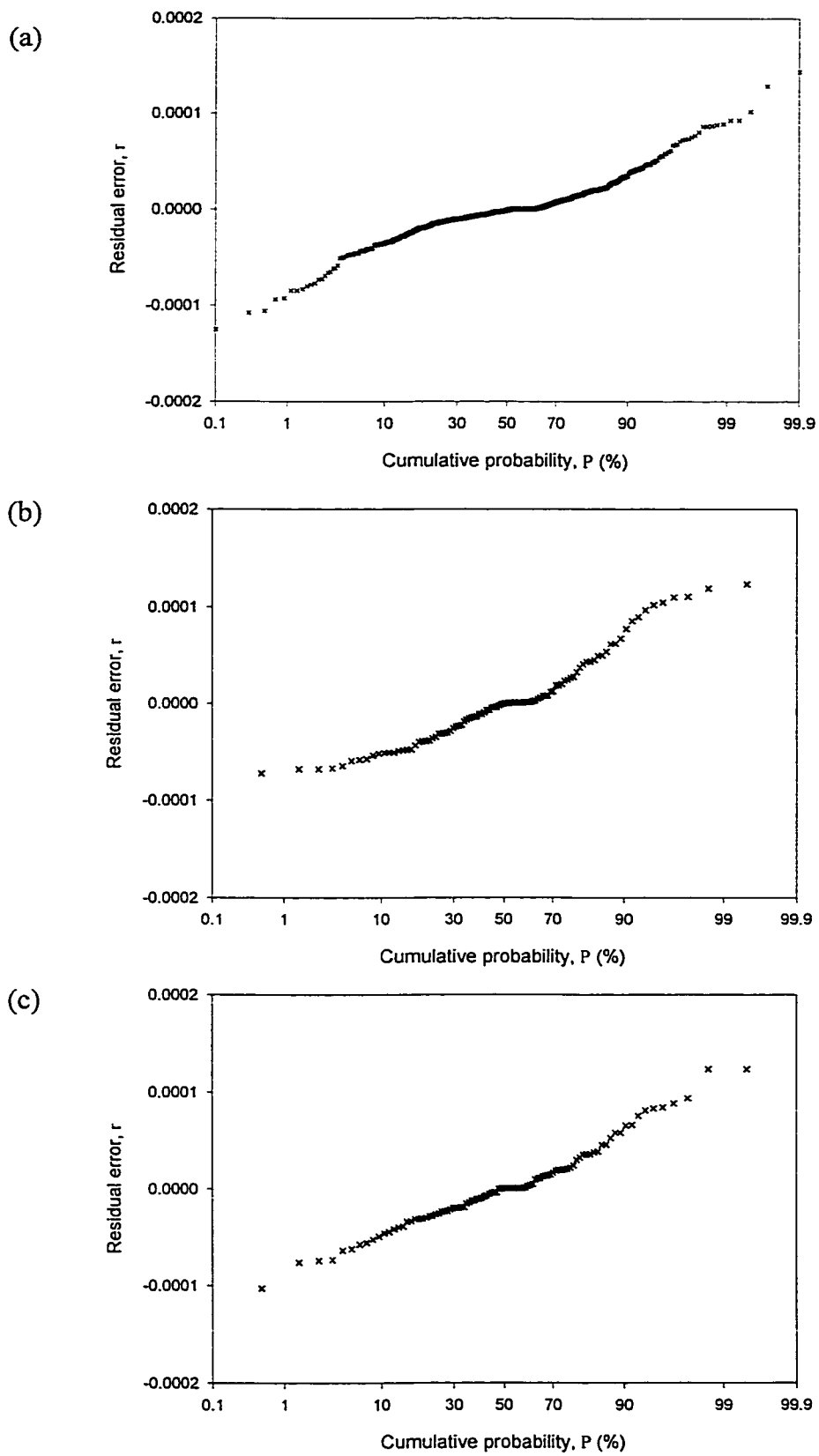


**Figure 6.30** Residual errors versus cumulative probability for  $p/p_y=0, 0.5,$  and  $0.8$

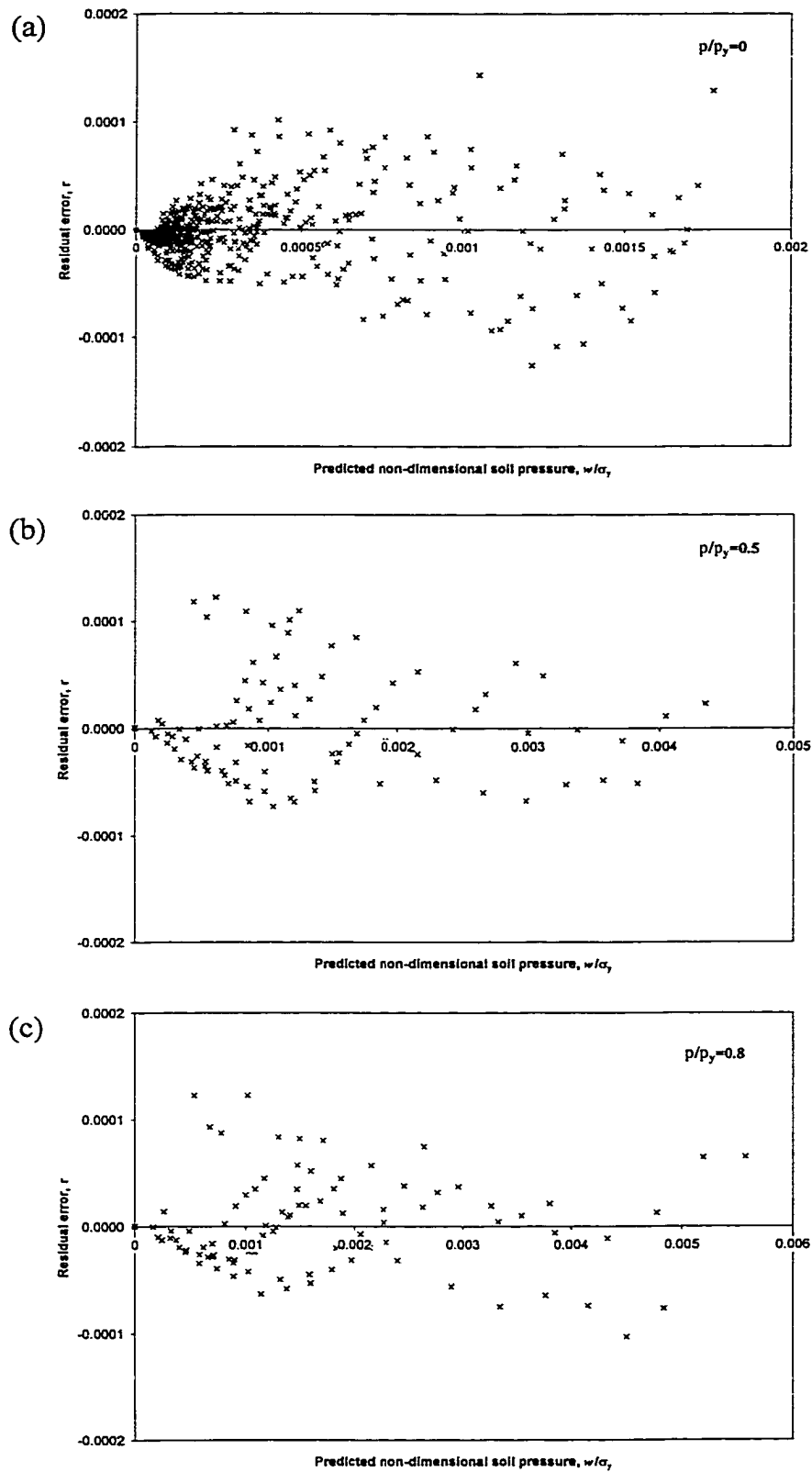


**Figure 6.31** Residual errors versus predicted response for  $p/p_y = 0, 0.5,$  and  $0.8$

## 7 ASSESSMENT OF PREDICTION EQUATIONS AND THEIR APPLICATION TO DESIGN

A finite element investigation of sleeper-supported piping systems that encompasses a wide range of dimensional, material, and operational parameters was presented in Chapter 6. From the finite element data, prediction equations [6-13], [6-14], and [6-16] were developed using non-linear regression analysis. These equations provide accurate predictions of the behaviour of idealized *in situ* sleeper-supported piping systems, and they will form the basis of a new design method.

Further verification of equations [6-13], [6-14], and [6-16] is desirable before they are implemented for use in design. This verification is necessary because the prediction equations are developed entirely from finite element data: the possibility that an error exists in the finite element model should be assessed. As an additional test of their validity, the prediction equations are compared with the behaviour that was observed in the laboratory tests of sleeper-supported pipes. A number of aspects are also examined in this chapter associated with practical on-site design issues and with the relationship that the new equations have with the limit states design philosophy. Finally, the new equations are compared with equation [1-3], which is the existing design formula proposed by Kormann and Zhou (1995).

### 7.1 PREDICTION OF BEHAVIOUR OBSERVED IN FULL-SCALE LABORATORY TESTS

It is clear that the new equations perform well when used to predict the response given by the finite element model of idealized *in situ* conditions. Unfortunately, there are no data available from real sleeper-supported piping systems with which to compare the predictive ability of the new equations. Although it is recognized that the loading and boundary conditions in the tests differ from the idealized *in situ* conditions, the laboratory results reported in Chapter 4 are the only source of experimental data available. If the new equations are able to make a reasonable prediction of the behaviour observed in the laboratory, a great deal of confidence can be gained in their veracity.

Several potential difficulties arise in the comparison of the prediction equations with the laboratory test data. The laboratory specimens had finite length and were loaded at discrete locations, as illustrated in Figure 2.3. In contrast, the idealized *in situ* finite

element model upon which the prediction equations are based considers an infinite length of pipe loaded by uniform soil pressure (see Figure 5.1). An additional difference between the cases is that steel plates stiffened the laboratory specimens to prevent excessive distortion at the supports; no such stiffeners are present in the finite element models used to derive the prediction equations. Consequently, it is not possible to implement the new equations directly to predict the behaviour of the laboratory specimens, and some simplifying assumptions are required.

To enable comparison of the two cases, it is useful to consider their free-body, shearing force, and bending moment diagrams (see Figure 7.1). It is reasonable to say that a laboratory specimen has shear force and bending moment diagrams with approximately the same shape as the middle half of those diagrams for the *in situ* finite element idealization. In other words, we compare only those regions that lie between the inflection points. Because the diagrams are similar between the inflection points, it is expected that the behaviour of an idealized *in situ* pipe having length  $L$  will be similar to a laboratory specimen having length  $\ell = L/2$ . Consequently, in order to calculate the predicted behaviour of the laboratory specimens, one should set  $L = 2\ell$  in the prediction equations. This calculation would give non-dimensional soil pressure,  $w/\sigma_y$ , at desired levels of out-of-roundness,  $o$ . However, the uniform soil pressure,  $w$ , is not directly applicable to the laboratory specimens because the loads in the tests were applied at discrete points. Consequently, the standard of comparison must be the total force,  $P$ , carried by a sleeper. This force can be calculated from the non-dimensional soil pressure as:

$$P = \frac{w}{\sigma_y} \times 2\ell \times D \times \sigma_y \quad [7-1]$$

Using this approach, the relationships between sleeper load and out-of-roundness for the laboratory specimens can be calculated using measured dimensions and material properties. Because the prediction equations were developed using an elastoplastic material model, it is necessary to choose a single representative value of the static yield stress,  $\sigma_y$ , for each laboratory specimen. This requires some judgement because, in the ancillary tests reported in Chapter 4, the stress-strain curves of the test specimens do not always have a well-defined static yield point. A standard practice in the pipeline industry

is to define yield stress as that stress in the material when the normal strain is 0.5%. Consequently, for each laboratory test specimen  $\sigma_y$  is assumed to correspond to the average static stress observed in the longitudinal tension coupon tests at a level of 0.5% strain. These static stress values and other measured dimensions of the laboratory specimens are reported in Appendix B.

The level of internal pressure must also be considered for specimens S3 and S9, which were pressurized to give a stress of 80% of the specified minimum yield strength (SMYS) in the hoop direction. Subsequent testing of tension coupons showed that the measured yield strength,  $\sigma_y$ , is greater than the SMYS. Consequently, the actual value of  $p/p_y$  is less than 0.8 for these specimens:  $p/p_y=0.68$  for specimen S3 and  $p/p_y=0.73$  for specimen S9. To obtain a prediction of the behaviour at these particular levels of internal pressure, linear interpolation is used between the prediction given by equation [6-13] for  $p/p_y=0.5$  and that given by equation [6-14] for  $p/p_y=0.8$ .

Using equations [6-13], [6-14], and [6-16], the predicted behaviour of each laboratory specimen is presented in Figures 7.2 through 7.12 in terms of sleeper load versus out-of-roundness. The values of parameters  $D/t$ ,  $p/p_y$ ,  $2b/D$ ,  $L/D$  and  $\epsilon_y$  upon which the predictions are based are also shown in each figure. As standards of comparison, the response observed in the laboratory tests and the response predicted by finite element analyses of the test specimens are also shown in the figures (these data were originally presented in Chapter 4). In general, all of the predictions correlate extremely well with the laboratory results, especially when one considers that the boundary and loading conditions of the laboratory tests are not identical to the conditions for which the prediction equations were derived. This similarity is extremely significant because it implies that the problem is not overly sensitive to the boundary and loading conditions, so the equations can be expected to give reasonable results even when actual conditions differ somewhat from the *in situ* idealization.

Although the new equations were developed based upon data having a maximum value of  $\sigma=25\%$ , the predictions given in Figures 7.2 through 7.12 for values of  $\sigma$  in excess of 25% are still quite good. Similarly, no adverse effects are evident even though values of  $L/D$  for the test specimens are greater than the maximum value of  $L/D$  that was investigated in the parametric study, at least for the unpressurized specimens. These facts

provide additional evidence that the new equations are not sensitive to deviations from those conditions considered in Chapter 6, and provide credibility to the argument that the new equations can be used for design.

Some differences between the predicted and actual behaviour of the specimens are apparent in Figures 7.2 through 7.12. Several of the unpressurized specimens exhibit a plateau on the load versus out-of-roundness curve that is not reflected in the predicted curve (see, for example, Figure 7.6). Such a plateau is attributed to a local loss of stiffness as the pipe in the area of contact with the sleeper undergoes a reversal of curvature, as described in Section 4.1.2.2. The predicted curves do not show this plateau: the form of the regression equation prevents points of inflection, so it is not expected that the plateau would be represented in the prediction. Despite the fact that the plateau is not represented, the predictions still give a reasonably good representation of the behaviour in this region.

The predictions for the pressurized specimens, S3 and S9, are quite good up a level of about  $\sigma=6\%$  (see Figures 7.4 and 7.10, respectively). However, the predicted sleeper load is too large beyond  $\sigma=6\%$ . The reason for the difference is likely attributable to the relatively small sleeper spacings examined in the parametric finite element study. The prediction equations were derived from data that have a maximum value of  $L/D=9$ , while the laboratory specimens have  $L/D$  values that are effectively in excess of 14. In the finite element analyses, the relatively short span lengths reduce the level of moment in the pipe and delay the onset of moment-induced yielding. With relatively greater span lengths, the laboratory specimens must carry greater bending moments and the maximum load that can be applied is correspondingly reduced. Another factor that may play a role in the difference between the laboratory specimens and the finite element model of *in situ* conditions relates to the level of axial stress. In the laboratory tests, end caps were welded to each pressurized pipe so as to form a pressure vessel, causing the internal pressure to give rise to a large tensile primary load in the axial direction. In contrast, the idealized *in situ* pipe is infinitely long, so internal pressure does not cause primary axial stresses. The presence of primary axial stress reduces the maximum amount of moment, and thus sleeper force, that can be carried by a laboratory specimen. Consequently, the prediction

equations tend to overestimate the maximum strength of the pressurized laboratory specimens. The predictions at lower levels of force are still valid, however.

To predict the behaviour of the pressurized specimens, it was stated that values were interpolated between those given by equation [6-13] for  $p/p_y=0.5$  and by equation [6-14] for  $p/p_y=0.8$ . Such interpolation is probably reasonable because all pressurized pipes examined in this study exhibited similar behaviour. However, it is known that the deformational characteristics of unpressurized systems differ significantly from those that are at high pressure. Consequently, as a note of caution, if a system under examination has a value  $0 < p/p_y < 0.5$  it is not necessarily reasonable to interpolate linearly between the results given by equation [6-16] for  $p/p_y=0$  and by equation [6-13] for  $p/p_y=0.5$ . In practice, few North American pipelines have such a low value of design pressure, so the usefulness of such interpolation is likely to be limited.

## **7.2 USE OF EQUATIONS AND APPLICATION OF LIMIT STATES DESIGN**

A number of on-site considerations should be examined to help determine how the new equations can be implemented in design. The most important aspect is whether sleepers should be used at all. It is known that some pipeline operators, such as Enbridge Inc., do not use sleepers to support buried piping in their compressor station yards. Instead, they use quality backfill having proper compaction to provide resistance to soil forces and surface loads—a valid alternative to sleeper supports. Consequently, the use of sleeper supports is not a necessity in the design process. In fact, it stands to reason that sleepers concentrate reaction forces at discrete locations, thereby increasing local distortion and stresses in the pipe. From this perspective, the use of sleepers may actually be detrimental.

There are, however, many practical reasons to use sleepers, and the work performed in this study shows that the adverse effects that their use has on cross-sectional distortion can be controlled satisfactorily. The most important benefit of sleeper supports is cost savings realized by reducing the need to ensure quality of backfill material and compaction. In addition, Kormann and Zhou (1995) point out that sleepers serve to aid in the accurate alignment of piping during installation and to reduce the influence that inclement weather might have on the construction process by elevating the pipe above the bottom of the trench. Concrete sleepers or horizontal steel beams supported by piles are

also used for buried mainline piping where heavy valves or tee connections must be supported. Consequently, it is expected that the use of sleeper-type supports will continue, and the new equations will provide a more rational approach to their design.

Taken alone, equations [6-13], [6-14], and [6-16] allow the behaviour of sleeper-supported piping systems to be predicted, but these equations can not necessarily be considered as design equations per se. First, it must be appreciated that the equations relate specifically to one limit state only—that of excessive distortion, a serviceability limit state. To use the equations properly in a limit states design context, the probability distributions associated with all loads and with the strength and stiffness of the system must be considered, along with the severity of the consequences of failure and the inherent conservatism of the design equation. Such an assessment will allow appropriate load and resistance factors to be developed that will provide an acceptable level of system performance.

Generally speaking, load factors and resistance factors are not used for limit states related to serviceability, but they can be used if a more conservative estimate of the behaviour is desired. As reported in Section 1.2.4.2.3, Price and Anderson (1991) recommend different out-of-roundness limits for various service conditions: 2.5% for installation acceptance, 15.0% at zero pressure, and 6.0% at full pressure. Different pipeline operators may have alternative requirements, however, based upon the specific specifications of their systems and of their pigging devices. Along with these rather subjective limits, Price and Anderson also give recommendations regarding appropriate resistance factors for out-of-roundness. Specifically, they recommend a resistance factor of 1.0 for installation acceptance, 0.75 for operations at zero pressure, and 1.0 at full pressure. It is noted that Price and Anderson appear to have established these values only on the basis of engineering judgement and experience, so these values should be used with caution.

Although there is no way to judge how they affect serviceability, the finite element studies show that the limits proposed by Price and Anderson (1991) are probably reasonable for sleeper-supported piping systems. Collapse or local wrinkling of a sleeper-supported pipe would occur at a level of out-of-roundness far beyond the limits proposed by Price and Anderson, at least within the range of parameters investigated in

the finite element study. This suggests that if the serviceability limit state is satisfied, ultimate limit states related to collapse will also be satisfied. It is important to note that a designer must also consider all other applicable limit states, such as limits on maximum tensile strains, the effect of accumulated plastic strain (ratchetting) from large pressure fluctuations, vibration-induced fatigue, and others.

Based on the available information, the author recommends that the new prediction equations be used in their current form without modification by load and resistance factors. In any event, the specific values chosen for the acceptable limits of distortion are subjective: the values chosen are, to some extent, at the discretion of the designer, which could negate the usefulness of load and resistance factors. The limit of 6% given by Price and Anderson (1991) for pressurized conditions is comparable to the recommendations of others that are reported in Chapter 1. Their suggested limit of 15% in conjunction with a resistance factor of 0.75 would effectively limit out-of-roundness to 11.25% for unpressurized conditions. These values are judged by the author to be appropriate first estimates of acceptable limits of distortion that can be used in conjunction with the new prediction equations.

One limitation of the finite element work reported herein is that the influence of cross-sectional distortion at installation is not considered. Consequently, the author judges that the criteria for acceptable distortion be reduced somewhat to reflect the influences of initial distortion, although there is no physical evidence available to estimate the magnitude of the correction. Price and Anderson (1991) recommend that out-of-roundness be limited to 2.5% at installation (presumably measured before backfilling). Assuming that this worst-case condition applies, it would be reasonable to reduce the limit on distortion at zero operating pressure from 11.25% to 8.75%, or, more conveniently, 8.5%. (It is recognized, however, that the effects of initial out-of-roundness are probably not additive arithmetically.) Similarly, the author recommends that the allowable out-of-roundness at full operating pressure should also be reduced somewhat, from 6% to a value of about 5%. Such a recommendation seems to be realistic considering that NOVA Gas Transmission Ltd. currently uses a distortion limit of 5% on out-of-roundness.

Additional perspective can be gained by examining those values of limiting distortion recommended by the Canadian standard, CSA Z662-96, that are discussed in Chapter 1. The Standard, however, defines distortion in terms of ovalization rather than the out-of-roundness definition that is used herein. Because the calculation made for ovalization in equation [1-10] is very similar to that calculation for out-of-roundness in equation [1-12], it is reasonable to neglect the fact that different definitions of distortion are used. As reported in Section 1.2.4.2.1, the Standard states that the critical ovalization,  $\Delta_{\theta}^{\text{crit}}$ , as a result of bending loads shall be determined by valid analysis methods or physical tests, or both, in order to control cross-sectional collapse. In the absence of such data, the limit on ovalization is to be taken as  $\Delta_{\theta}^{\text{crit}}=3\%$ . Because the experimental and finite element data gathered in this study show that cross-sectional collapse is not likely to be the failure mode for sleeper-supported pipes even at levels of ovalization far beyond 3%, a serviceability requirement in the Standard would apply instead. To allow unhindered passage of pigging devices,  $\Delta_{\theta}^{\text{crit}}$  must be limited to 6% "...in the absence of more detailed information..." This 6% limit is very similar to the 5% limit on out-of-roundness that is recommended by the author for operations at full pressure. Further assessment of appropriate distortion limits and of load and resistance factors is beyond the intended scope of this work, and more study of this issue should be undertaken to ensure that the equations give a satisfactory level of system performance.

### **7.3 COMPARISON OF PREDICTION EQUATIONS WITH EXISTING DESIGN EQUATION**

It is desirable to compare the new prediction equations with equation [1-3], which was proposed by Kormann and Zhou (1995), to assess their relative performance. In Chapter 1 it is identified that equation [1-3] is believed to give results that are much too conservative, that is, the sleepers are spaced too closely in the opinion of the designers that use the equation. Before a comparison can be made, it must be remembered that equation [1-3] is based upon working stress design methods that are an attempt to limit stresses in the pipe wall to a level below the yield stress. It considers only sleepers of length  $2b/D=1.5$ , only loads from soil having a density of  $15 \text{ kN/m}^3$ , and it applies only to systems that are pressurized so that the hoop stress equals 50% of the specified minimum

yield strength. Consequently, only equation [6-13] can be compared directly with equation [1-3], since both equations consider the same level of internal pressure.

A large number of possible design scenarios exist that could be analysed to make a comparison between the methods. Consequently, the methods will be compared only for one design scenario that is representative of a typical sleeper-supported piping application. In this hypothetical scenario, a pipe at a compressor station is to be supported by sleepers having length  $2b=1.5D$ , and the spacing of the sleepers,  $L/D$ , is to be determined. The pipe is to be embedded with a depth of cover of 3 m in soil having a density of  $15 \text{ kN/m}^3$ . Under normal conditions, the line will operate at a pressure of 8450 kPa, so this value is used as the design pressure. The pipe has a specified minimum yield strength of 483 MPa, an elastic modulus of 207 000 MPa, and is 762 mm in diameter. Given these facts and assuming that all installation conditions are typical, the minimum wall thickness,  $t$ , required by the Canadian pipeline standard, CSA Z662-96, is calculated to be 13.3 mm using equation [5-6].

For these design parameters,  $L/D$  is calculated by the Kormann and Zhou (1995) approach given in equation [1-3] as:

$$\begin{aligned} \frac{L}{D} &= 20000 \frac{S}{H} \left( \frac{D}{t} \right)^{-1.75} \\ &= 20000 \frac{483 \text{ MPa}}{3000 \text{ mm}} \left( \frac{762 \text{ mm}}{13.3 \text{ mm}} \right)^{-1.75} && [7-1] \\ &= 2.7 \end{aligned}$$

The result  $L/D=2.7$  means that the sleepers would be spaced very closely: the sleepers are 1.5D in length, so the clear span between sleepers is only 1.2D (smaller than the length of the sleepers themselves). On the basis of engineering judgement, such close spacing does not seem to be reasonable.

Using the prediction equation [6-13], and assuming that the maximum allowable out-of-roundness is 5% in accordance with the recommendations in Section 7.2, the required sleeper spacing is calculated as:

$$\begin{aligned}
\frac{L}{D} &= 3.3505 \left( \frac{D}{t} \right)^{-1.1443} \left( \frac{2b}{D} \right)^{0.3021} \left( 1 - 0.9689^{(100 \times o)} \right) \left( \frac{w}{\sigma_y} \right)^{-1} \\
&= 3.3505 \left( \frac{762 \text{ mm}}{13.3 \text{ mm}} \right)^{-1.1443} (1.5)^{0.3021} \\
&\quad \left( 1 - 0.9689^{(100 \times 0.05)} \right) \left( \frac{15 \times 10^{-6} \text{ N/mm}^3 \times 3000 \text{ mm}}{483 \text{ MPa}} \right)^{-1} \\
&= 58.0
\end{aligned} \tag{7-2}$$

This unrealistically large value of L/D is vastly greater than that given by equation [1-3], and, by itself, it can not be used for design purposes. However, equation [7-2], which is based upon finite element analyses and has been proven by test data, does support the argument that the approach of Kormann and Zhou (1995) is much too conservative.

A distinct advantage of the new equations is that they are not limited to the specific set of service conditions considered in equation [1-3]. For example, equation [1-3] applies only to pressurized pipes, but the new prediction equations allow the limit state at zero internal pressure to be checked. Using equation [6-16], a distortion limit of 8.5% on out-of-roundness, and considering the specified soil pressure as the only external load:

$$\begin{aligned}
\left( \frac{L}{D} \right)^{0.9144} &= 1.4017 \left( \frac{D}{t} \right)^{-2.2045} \left( \frac{2b}{D} \right)^{0.1468} (\epsilon_y)^{-0.4891} \left( 1 - 0.904^{(100 \times o)} \right) \left( \frac{w}{\sigma_y} \right)^{-1} \\
&= 1.4017 \left( \frac{762 \text{ mm}}{13.3 \text{ mm}} \right)^{-2.2045} (1.5)^{0.1468} \left( \frac{483 \text{ MPa}}{207\,000 \text{ MPa}} \right)^{-0.4891} \\
&\quad \left( 1 - 0.9040^{(100 \times 0.085)} \right) \left( \frac{15 \times 10^{-6} \text{ N/mm}^3 \times 3000 \text{ mm}}{483 \text{ MPa}} \right)^{-1} \tag{7-3} \\
&= 23.8 \\
\frac{L}{D} &= 32.0
\end{aligned}$$

This value of L/D, while more realistic than that given by [7-2], is still very large. However, it must be noted that the loads used in this equation, which have been chosen to be consistent with those used in Kormann and Zhou's approach, are not complete. All

other sources of surface live and dead load—structures, trucks, cranes, etc.—must also be taken into account in the design process. The principal advantage of the new prediction equations is that they are adaptable, allowing the inclusion of these additional loads. The vertical soil pressures that the additional loads impart on the pipe can be determined using the Boussinesq or similar approaches that were described in Chapter 5.

Because the surface loads depend largely on the nature of the equipment used by a particular pipeline operator, it is difficult to approximate their values in the design example. However, it can be shown that the resultant of [7-3] would be reduced to about  $L/D=25$  if it is assumed that a fully loaded standard tandem-axle dump truck were parked on the surface directly above the pipe. Although, the effect of surface live load is not great in this design example, its influence would be much more significant if the depth of cover were to be decreased. In fact, when the depth of cover is small, surface loads can give rise to live load soil pressures greater than those from soil self-weight. Although it is not conservative to neglect these loads, they are not considered in equation [1-3]. This fact further demonstrates the improvement offered by the new design equations.

Examining the values of  $L/D$  given by the new design equations, there is a clear indication that out-of-roundness is likely to be of minimal concern in this particular design example: the maximum allowable sleeper spacing would be about  $L/D=25$ . This result is desirable because it gives the designer the flexibility to place the sleepers at the most practical locations—away from girth welds, for example—rather than at extremely close intervals.

It is, however, necessary to recall that the new design equations were developed from data having a maximum value of  $L/D=9$ . Consequently, any value of  $L/D$  given by the equations that is in excess of nine should be used with some caution. However, the correlation of the equations with the experimental tests—for which  $L/D$  is always effectively in excess of 14—is shown to be good in Figures 7.2 through 7.12. Therefore, it is probably reasonable to extrapolate the equations up to about  $L/D=14$ . Accordingly, unless additional data become available that indicate otherwise, the maximum allowable sleeper spacing should not exceed about  $L/D=14$  under any circumstances. Using this ‘rule of thumb,’ the number of sleepers required in the design example would be reduced by a factor of five as compared to the design values given by equation [1-3]. Of course,

issues such as the bearing capacity of the soil beneath the sleepers should also be checked, which could place additional constraints on the sleeper size and spacing.

In conclusion, the equations developed in Chapter 6 support the argument that the approach recommended by Kormann and Zhou (1995) is usually much too conservative. The new design equations also offer an improvement over equation [1-3] in that they allow conditions to be checked at various levels of internal pressure, consider different sizes of sleepers, and account for soil pressures that arise from both live loads and dead loads. Furthermore, the solutions provided by the new design equations are compatible with the limits states design philosophy, which is generally considered to be preferable to allowable stress design. Consequently, the new equations are judged to form an appropriate method for the design of sleeper-supported piping systems that offers many improvements over the method that existed previously.

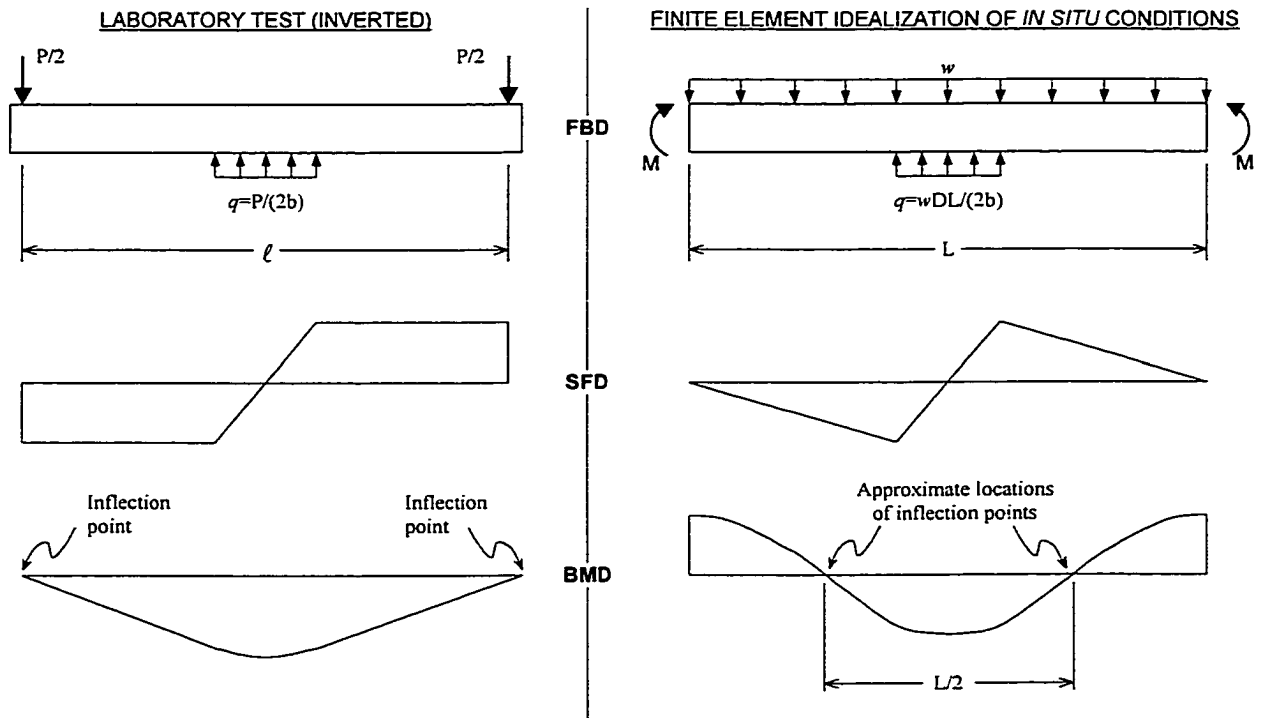


**Figure 7.1** Free-body, shear force, and bending moment diagrams of laboratory tests and the *in situ* idealization

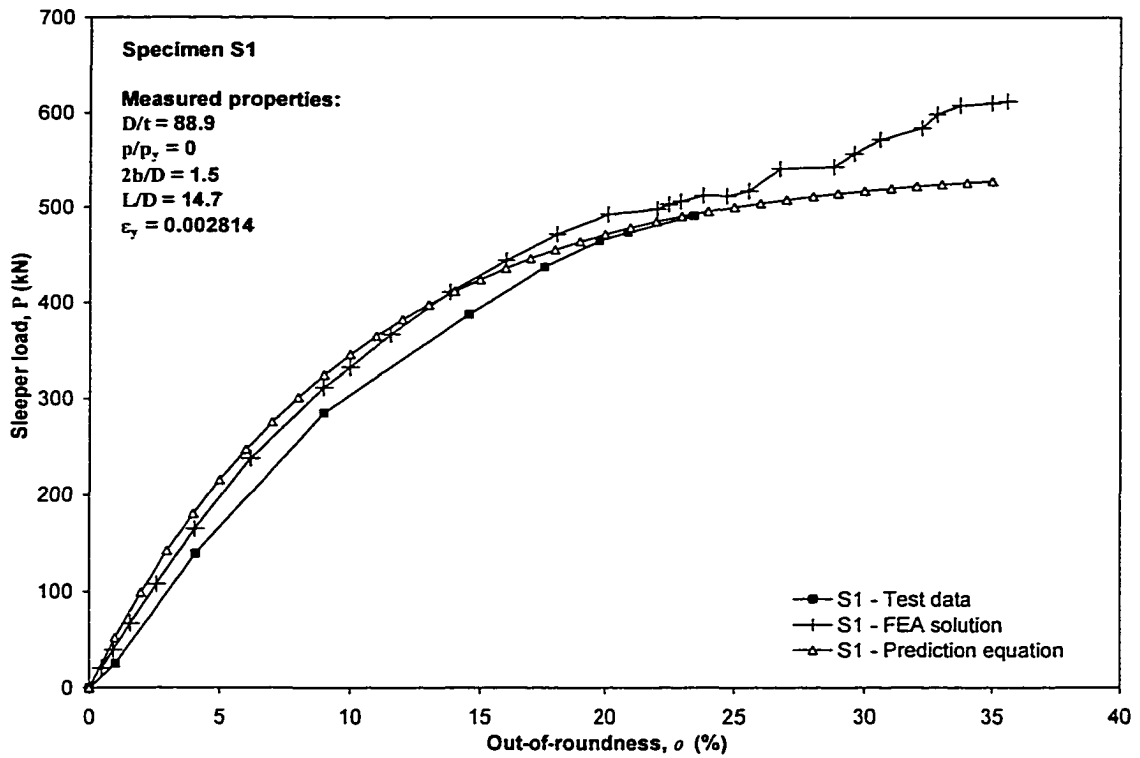


**Figure 7.2** Comparison of laboratory test, finite element solution, and regression prediction equation for Specimen S1

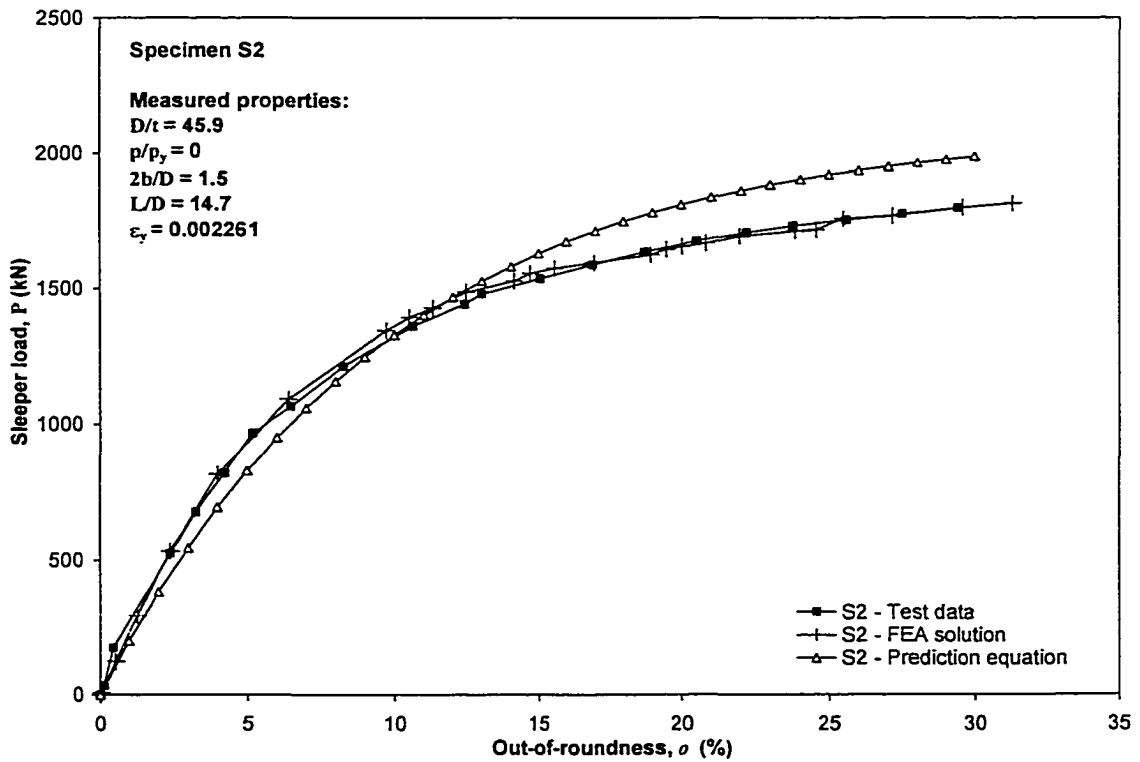


**Figure 7.3** Comparison of laboratory test, finite element solution, and regression prediction equation for Specimen S2

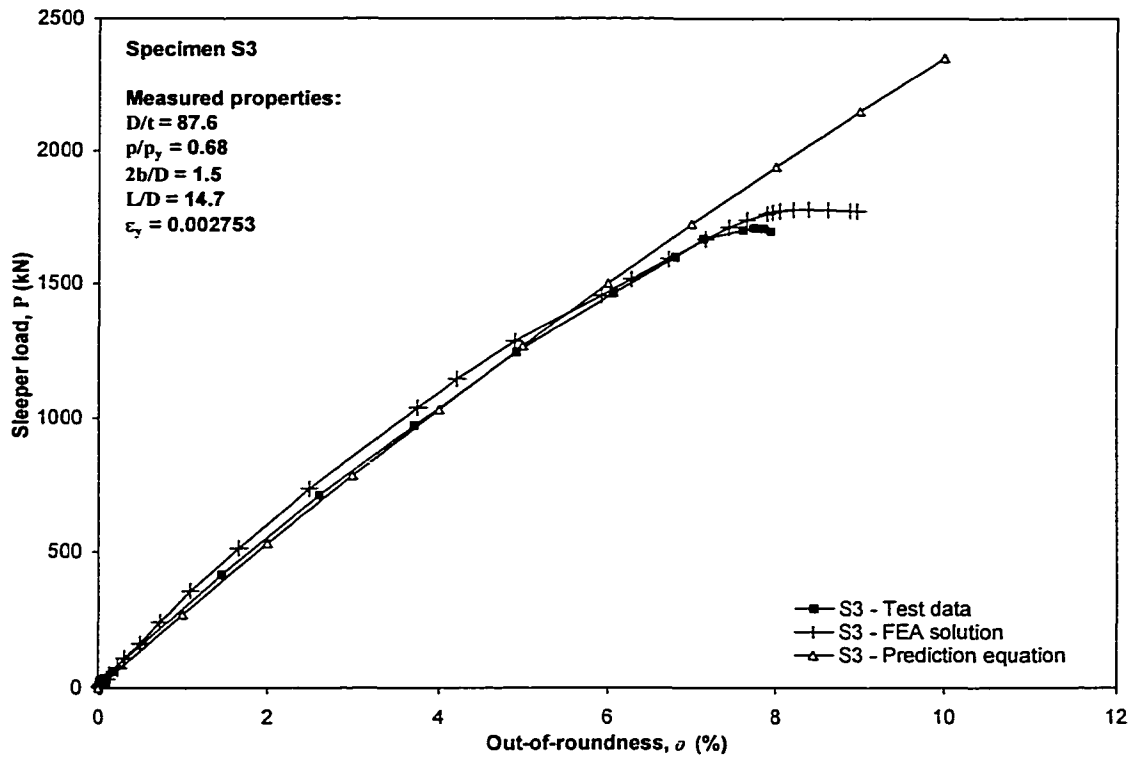


**Figure 7.4** Comparison of laboratory test, finite element solution, and regression prediction equation for Specimen S3

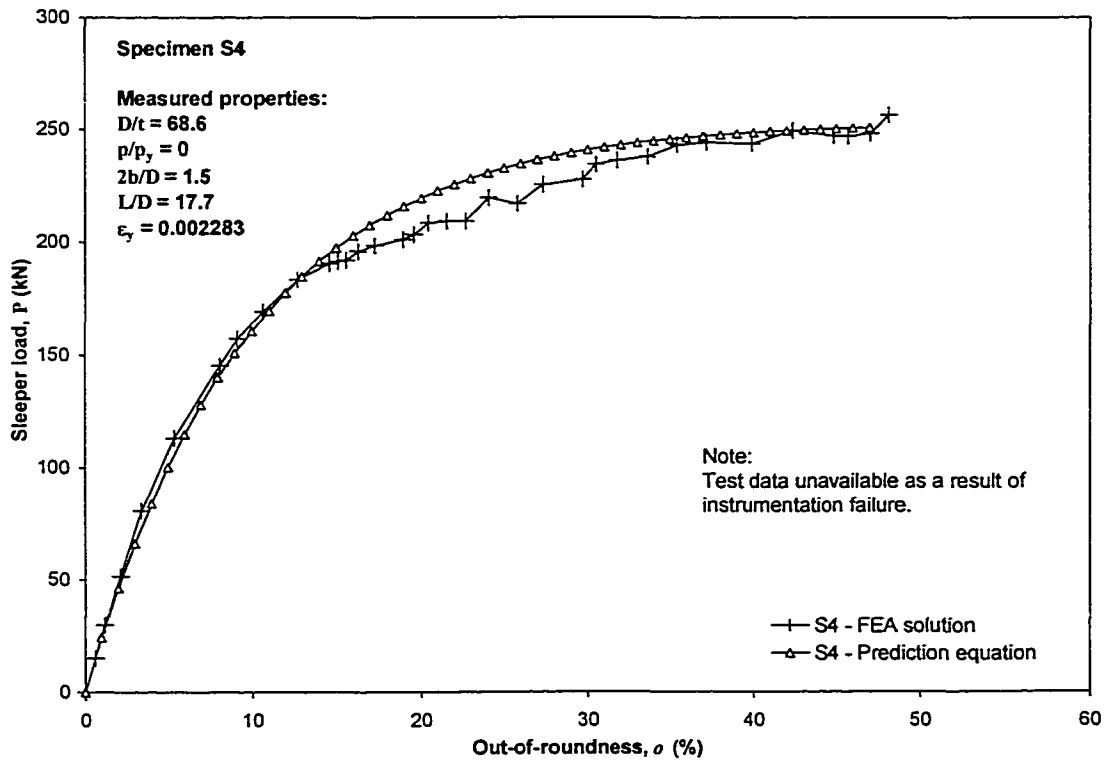


**Figure 7.5** Comparison of laboratory test, finite element solution, and regression prediction equation for Specimen S4

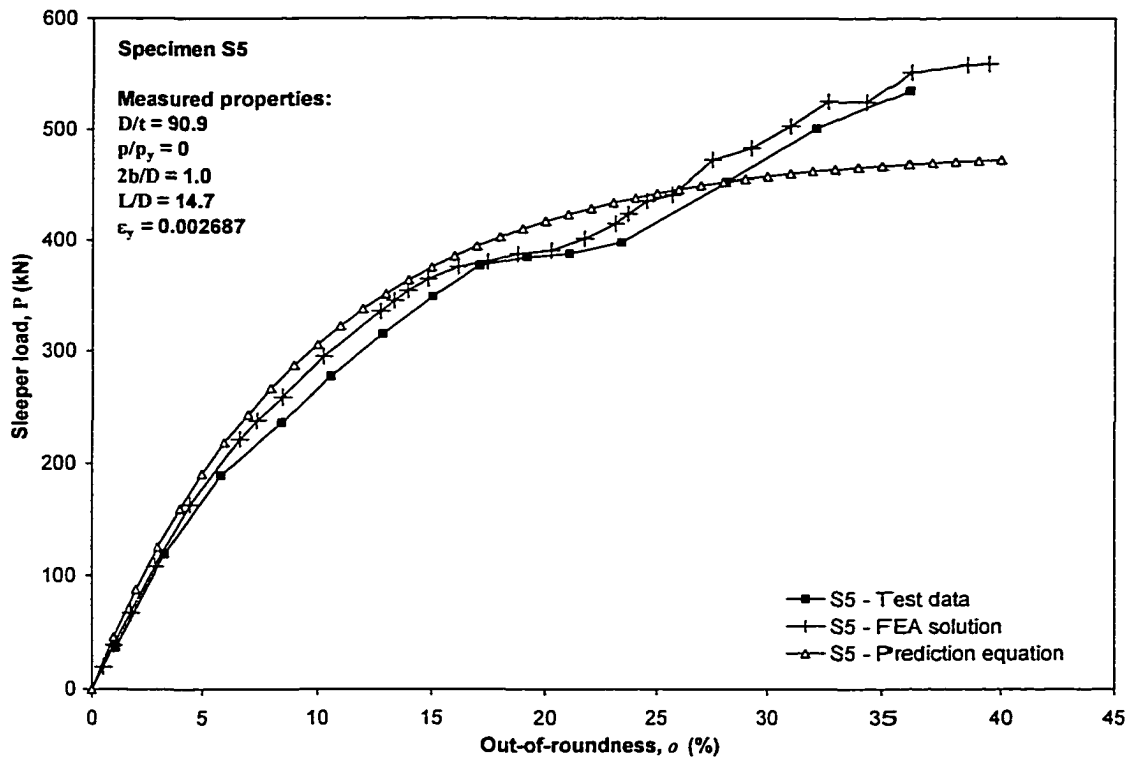


**Figure 7.6** Comparison of laboratory test, finite element solution, and regression prediction equation for Specimen S5

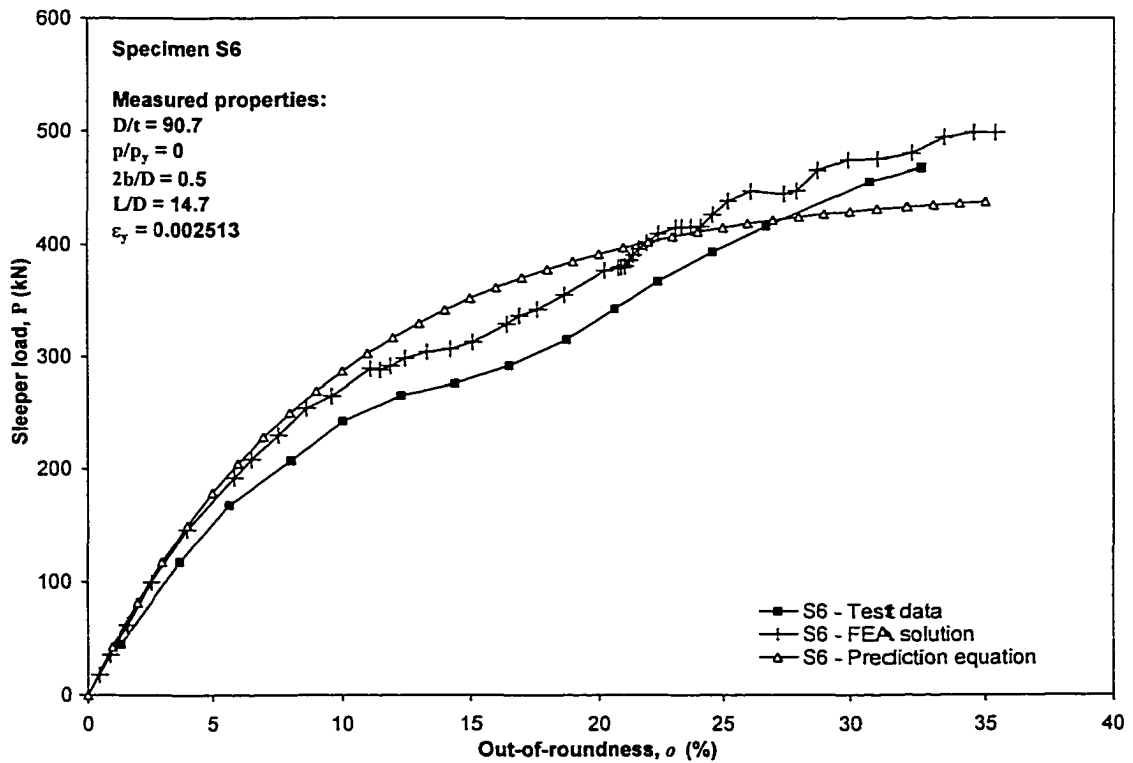


**Figure 7.7** Comparison of laboratory test, finite element solution, and regression prediction equation for Specimen S6

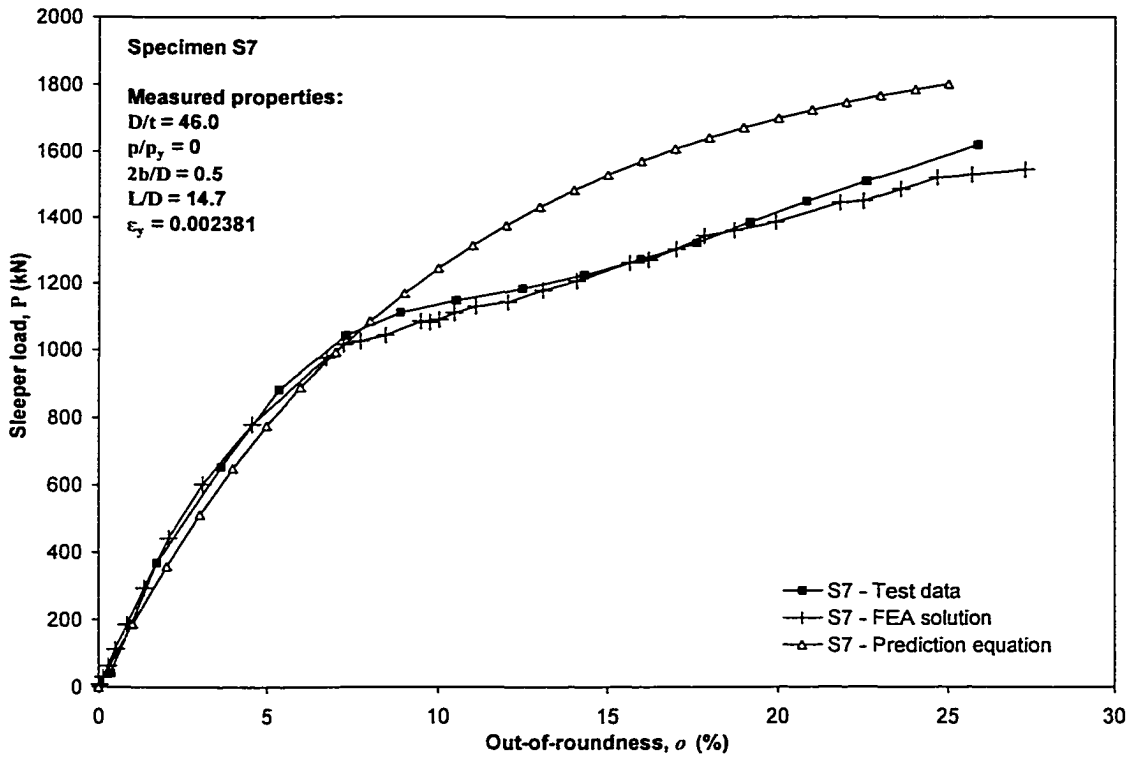


**Figure 7.8** Comparison of laboratory test, finite element solution, and regression prediction equation for Specimen S7

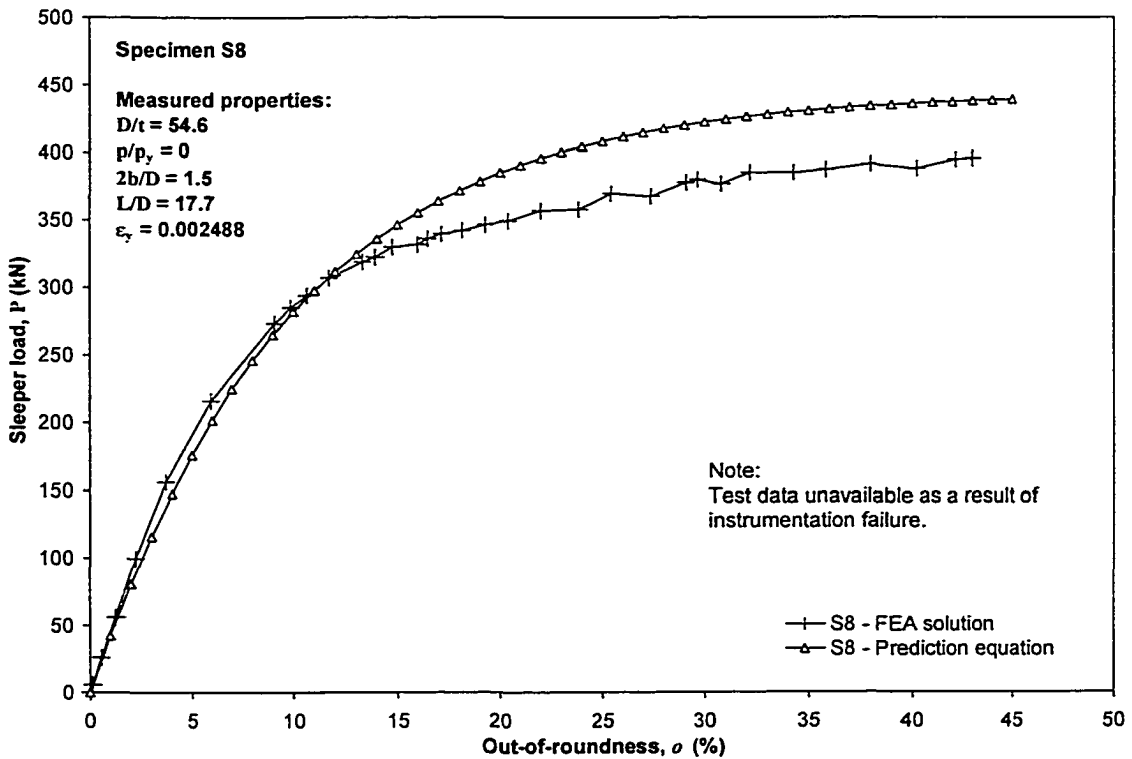


**Figure 7.9** Comparison of laboratory test, finite element solution, and regression prediction equation for Specimen S8

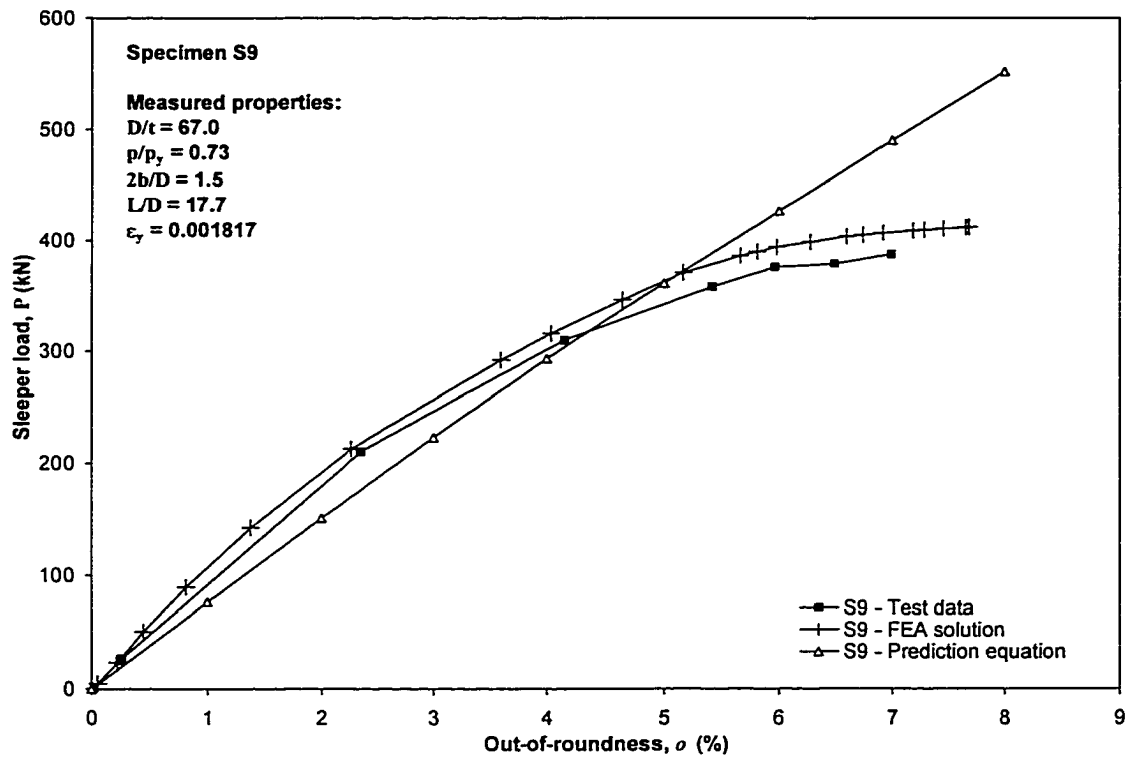


**Figure 7.10** Comparison of laboratory test, finite element solution, and regression prediction equation for Specimen S9

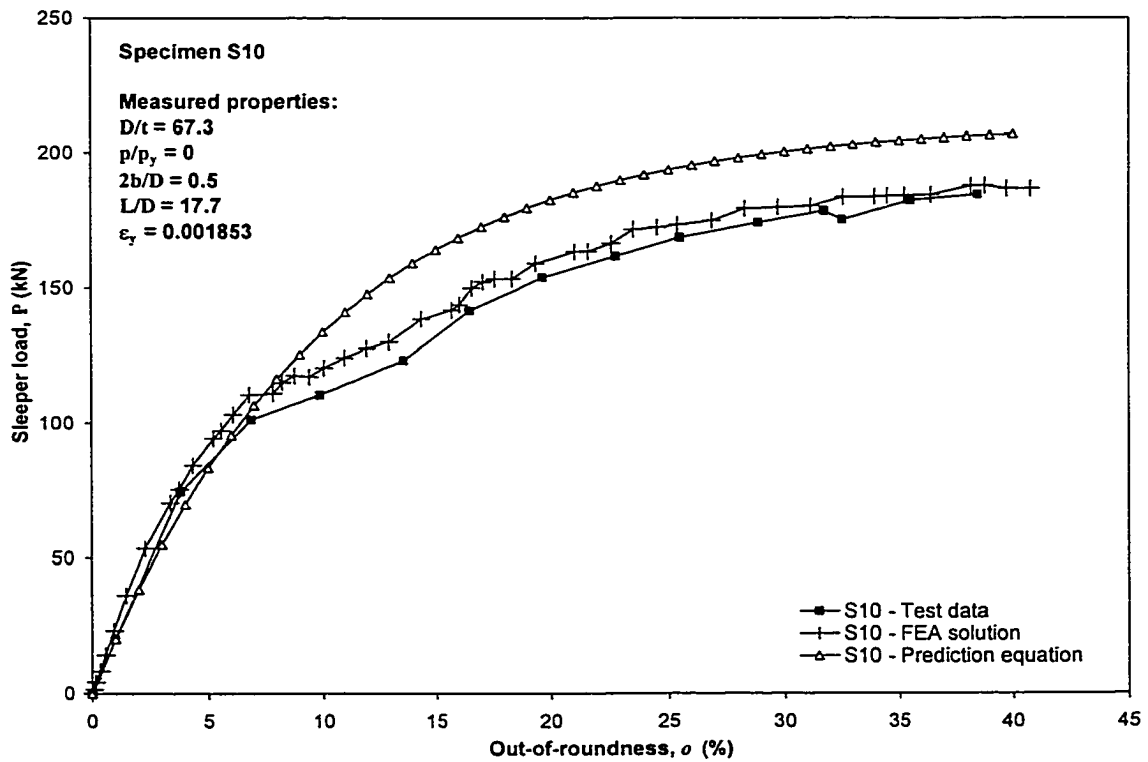


**Figure 7.11** Comparison of laboratory test, finite element solution, and regression prediction equation for Specimen S10

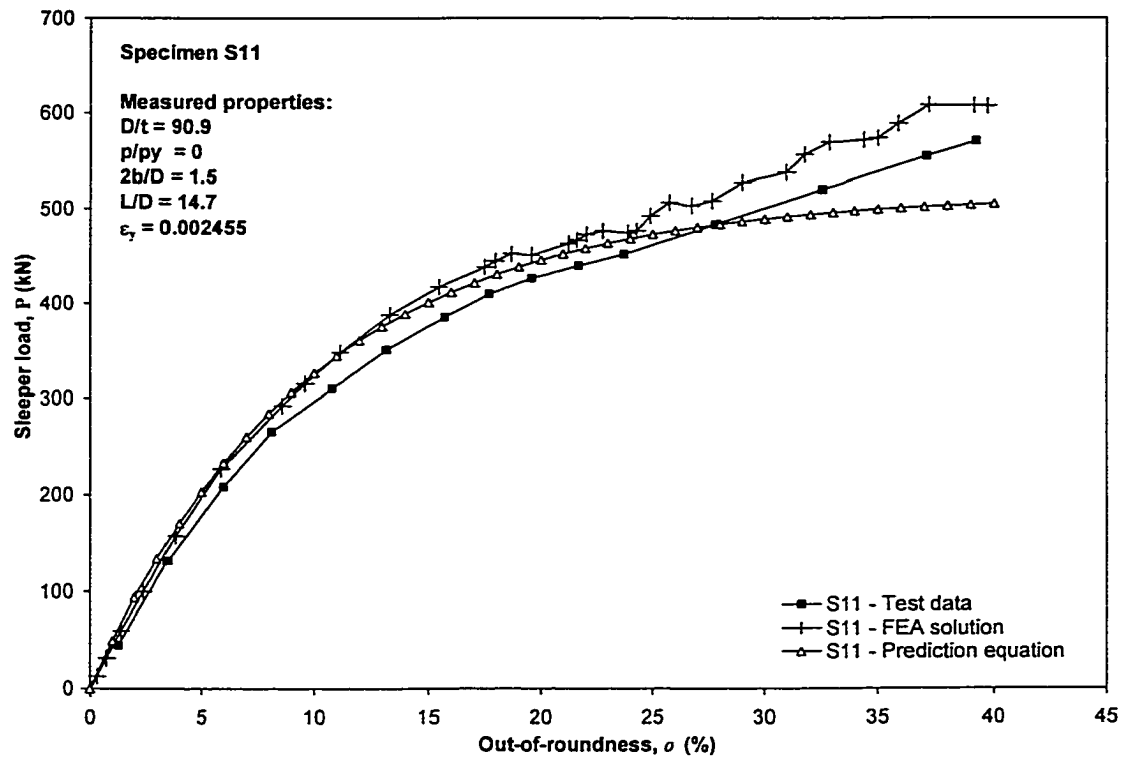


**Figure 7.12** Comparison of laboratory test, finite element solution, and regression prediction equation for Specimen S11

## 8 SUMMARY, CONCLUSIONS, AND RECOMMENDATIONS

### 8.1 SUMMARY

Flat reinforced concrete ‘sleepers’ are currently used by some pipeline operators to support buried pipes. The contact condition between the sleeper and the pipe can impose high levels of stress in the pipe wall and can potentially cause significant deformation of the cross-section. As described in the literature review, a design method for sleepers has been in use by the industry, but the solutions that it provides are believed to be much too conservative. No rational method by which to approach the design of sleeper supports was available, which led to the implementation of this study. The intent throughout the study has been to develop a new design approach that is consistent with the limit states design philosophy.

As a first step toward obtaining fundamental information on the behaviour of sleeper-supported pipes, a series of 11 full-size line pipe specimens were tested at the University of Alberta. The parameters considered were the pipe diameter and wall thickness, the internal pressure, and the size of the sleeper support. This experimental work provided data to enhance basic understanding of sleeper-to-pipe interaction in terms of both strength and local deformation criteria. In all cases the response of the specimens was stable and ductile, and cross-sectional distortion would be the governing limit state. A series of ancillary material tests were also conducted.

The desire to explore the behaviour of other sleeper-supported piping configurations required the construction of a numerical model. A finite element modelling technique was developed accounting for large deformations, non-linear material behaviour, and sleeper-to-pipe contact. The pipe itself was represented by shell elements, the sleeper by solid elements. Comparisons with the experimental data show that the modelling technique is reliable and that its use for the analysis of other sleeper-supported piping systems is likely appropriate.

It is recognized that the behaviour of those specimens tested in the laboratory differs from *in situ* sleeper-supported pipes—the loading and boundary conditions are not identical. Consequently, an idealized model of *in situ* conditions was developed by modifying the finite element models used for the laboratory specimens. The idealized

model became the means through which to study the parameters that influence sleeper-supporting piping behaviour.

Nine variables in the idealized model were deemed to have a significant influence on the behaviour. In order to limit the complexity of the study, the problem was cast in terms of non-dimensional parameters using the Buckingham Pi theorem, which reduced the number of variables to seven:  $D/t$ ,  $p/p_y$ ,  $2b/D$ ,  $L/D$ ,  $\varepsilon_y$ ,  $w/\sigma_y$ , and  $o$ . A series of experiments were then designed to examine how the out-of-roundness,  $o$ , was affected as the other parameters were varied through a range of realistic values. In this context, the finite element model played the role of the experiment, and it provided a database of information on the expected behaviour of *in situ* sleeper-supported pipes. By means of non-linear regression analysis of the data, simplified empirical equations were developed that predict the behaviour of idealized *in situ* sleeper-supported piping. An excellent degree of correlation was obtained between the regression equations and the finite element data. The equations also provide good predictions of the behaviour that was observed in the laboratory tests.

## 8.2 CONCLUSIONS

Considerable progress has been made toward the understanding of sleeper-supported line pipe behaviour. A number of significant conclusions have been drawn:

1. The design method currently used for sleeper-supported piping appears to be too conservative, is not rational, and is not based upon the well-established principles of limit states design. Improved design methods are required.
2. There is currently no consensus in industry regarding the definition of limiting states of acceptable behaviour for pipelines, particularly as related to the sleeper pipe-support problem. A variety of criteria are used as general limits on cross-sectional distortion, but most appear to be based solely on engineering judgement.
3. The laboratory tests of full-scale sleeper-supported line pipes reveal that the deformational mechanism that develops is stable and ductile. Distortion of the

cross-section is significant and is likely to be the governing limit state in the design process.

4. Both strength and cross-sectional distortion characteristics of sleeper-supported pipes can be modelled accurately by representing the pipe as a shell structure and incorporating finite membrane strains, large displacements, non-linear material properties, and contact into the formulation. The finite element models described in Chapter 3 are judged to form the basis of a general modelling technique for sleeper-supported pipes.
5. Hydraulic ring expansion testing is believed to give the best representation of the actual stress-strain characteristics for the hoop direction of pipeline steel. However, testing procedures must be controlled carefully to ensure that the results are not affected adversely by the many possible sources of error inherent in such tests. Flattened transverse tensile coupons do not give an acceptable representation of material properties for use in advanced numerical modelling. For the work performed in this study, the coupons taken from the longitudinal direction of the pipe wall are judged to provide the most useful data.
6. The forces that act on sleeper-supported piping in compressor station yards are expected to be load-controlled rather than displacement-controlled. The finite element model developed in Chapter 5 is believed to be a reasonably realistic, albeit simplified, representation of *in situ* conditions for sleeper-supported pipes. In this idealization, forces transmitted through the soil act on the pipe only in the vertical downward direction. This model should give a conservative estimate of the true behaviour because, among other assumptions, the potentially beneficial effects of lateral earth pressure on the pipe are neglected.
7. Data were generated by the finite element models of idealized *in situ* conditions for parametric values that typically pertain to pipelines. Based upon non-linear regression analysis of that data, the behaviour of *in situ* sleeper-supported pipes is described by the following empirical equations:

For zero internal pressure:

$$\frac{w}{\sigma_y} = 1.4017 \left( \frac{D}{t} \right)^{-2.2045} \left( \frac{2b}{D} \right)^{0.1468} \left( \frac{L}{D} \right)^{-0.9144} (\epsilon_y)^{0.4891} (1 - 0.9040^{(100 \times o)}) \quad [6-16]$$

For internal pressure that imparts a hoop stress of 50% of the tensile yield strength:

$$\frac{w}{\sigma_y} = 3.3505 \left( \frac{D}{t} \right)^{-1.1443} \left( \frac{2b}{D} \right)^{0.3021} \left( \frac{L}{D} \right)^{-1} (1 - 0.9689^{(100 \times o)}) \quad [6-13]$$

For internal pressure that imparts a hoop stress of 80% of the tensile yield strength:

$$\frac{w}{\sigma_y} = 3.2793 \left( \frac{D}{t} \right)^{-1.0759} \left( \frac{2b}{D} \right)^{0.3473} \left( \frac{L}{D} \right)^{-1} (1 - 0.9689^{(100 \times o)}) \quad [6-14]$$

For levels of hoop stress between 50% and 80% of the yield strength, it is probably reasonable to interpolate linearly between the values given by equation [6-13] and [6-14]. Additional study of the behaviour at levels of hoop stress between 0% and 50% of the yield strength is required to determine an appropriate means of interpolation between equations [6-16] and [6-13]. In practice, few North American pipelines have such a low value of design pressure, so the usefulness of such interpolation is likely to be limited.

8. Equations [6-13], [6-14], and [6-16], which are based upon data from the idealized *in situ* finite element model, each provide coefficients of multiple determination in excess of 0.99—a very good level of predictive ability. The equations also provide excellent predictions of the behaviour observed in the laboratory tests, even though the tests had loading and boundary conditions that differed from the *in situ* idealization. Because the equations give predictions that are insensitive to the loading and boundary conditions, they are expected to provide reasonable estimates of sleeper-supported piping behaviour even when design conditions are not identical to those assumed in the idealization. Comparisons with the laboratory tests also indicate that the equations are valid up to values of about  $L/D=14$ , even though the maximum value of  $L/D$  investigated in the parametric study was only nine.
9. By choosing appropriate limits on allowable distortion, equations [6-13], [6-14], and [6-16] form a new method for the design of sleeper-supported pipes. The equations should relieve the designer of the need to perform detailed finite element analyses for routine design scenarios and should provide solutions that are more rational than those that were available previously.

### 8.3 RECOMMENDATIONS

To refine design techniques further and to gain additional confidence in them, field monitoring of sleeper-supported piping would be helpful. Gathering of field data would allow a more detailed assessment to be made of the effectiveness of equations [6-13], [6-14], and [6-16]. In addition, the effect of a girth weld in close proximity to a sleeper support was not specifically studied in this work. Unless new data become available that indicate otherwise, girth welds should be located remotely from the sleeper supports whenever possible.

Much of the work reported in the literature related to material properties in the hoop direction of pipeline steels is based upon data that the author judges to be unreliable: among other limitations, the effect of residual stresses on the behaviour of flattened coupons is not recognized. Ring expansion testing offers a promising alternative, but improved test methods are required over those used in this study and those reported in the literature. In particular, a ring expansion study should be conducted using more advanced test control systems. With improvements in the control systems, static yield stress values, which are an essential descriptor of material behaviour, can be obtained.

Equations [6-13], [6-14], and [6-16] could be made somewhat more useful to the designer by consolidating them into a single equation. As stated previously, it is expected that additional study of the behaviour at levels of hoop stress between 0% and 50% of the yield strength is required before an appropriate means of interpolation between equations [6-16] and [6-13] can be determined. Consequently, the effect of internal pressure at about  $p/p_y=0.2$  should be investigated before attempting to develop a single, comprehensive, equation in any future work.

The new design equations that have been developed in this work are based upon conservative estimates of the soil loads. It is recognized that the soil model used is greatly simplified, and the beneficial effects of lateral soil pressure have been intentionally neglected. The potential exists to improve the *in situ* idealization to reflect the true interaction between the pipe structure and the soil more realistically. However, future work in this area is likely useful only if the new design equations are perceived to provide an inadequate level of economy.

There is a need for the pipeline industry to clarify the specific definitions of ovality, ovalization, and out-of-roundness, all of which are used for describing cross-sectional distortion. There also appears to be an absence of field data on what limits should be placed on distortion, and further study in this area is required so that rational, quantitative, limits can be defined. In the absence of more detailed information, the author recommends that equations [6-13], [6-14], and [6-16] be used without load or resistance factors. Based upon the available literature, reasonable maximum limits on distortion are 8.5% out-of-roundness at zero internal pressure and 5% out-of-roundness at operating pressure. If these values are used, the test data and finite element results from this study show that the serviceability limit state for distortion of the cross-section is likely to govern the design. All sources contributing to vertical downward soil pressure should be considered in the calculations, including soil self-weight and surface loads. Using this approach, equations [6-13], [6-14], and [6-16] constitute a new method for the design of sleeper-supported pipelines.

## REFERENCES

- American Petroleum Institute (1995). Specification for Line Pipe, API Specification 5L, 41st Edition, Washington, D.C.
- American Society for Testing and Materials (1994). "Standard Test Methods and Definitions for Mechanical Testing of Steel Products," ASTM Designation A370-94.
- American Society of Mechanical Engineers (1992). Boiler and Pressure Vessel Code, Section VIII, Division 2: Alternative Rules, ASME, New York, New York.
- Bathe, K.-J. (1996). Finite Element Procedures, Prentice Hall, Englewood Cliffs, New Jersey.
- Box, G.E.P., Hunter, W.G., and Hunter, J.S. (1978). Statistics for Experimenters, John Wiley and Sons, New York, New York.
- Brazier, L.G. (1927). "On the Flexure of Thin Cylindrical Shells and other 'Thin' Sections," Proceedings of the Royal Society of London, Series A, Vol. CXVI, pp. 104-114.
- Brooks, P., and Smith, M. (1995). "Pipeline Integrity Assessment and Rehabilitation," Advances in Underground Pipeline Engineering, Second International Conference, ASCE, Bellevue, Washington, pp. 845-854.
- Canadian Standards Association (1996). Z662-96 Oil and Gas Pipeline Systems, Canadian Standards Association, Etobicoke, Ontario.
- Canadian Standards Association (1994). CAN/CSA-S16.1-94—Limit States Design of Steel Structures, Canadian Standards Association, Toronto, Ontario.
- Canadian Standards Association (1974). S16.1-1974 Steel Structures for Buildings—Limit States Design, Canadian Standards Association, Etobicoke, Ontario.
- Collberg, L., and Mørk, K. (1999). "Update of DNV'96 into an Offshore Standard, An Introduction," Proceedings of the OMAE, 18th International Conference on Offshore Mechanics and Arctic Engineering, St. Johns, Newfoundland.
- Davis, H.E., Troxell, G.E. Troxell, and Hauck, G.F.W. (1982). The Testing of Engineering Materials, Fourth Edition, McGraw-Hill, New York, New York.
- Det Norske Veritas (1996). Rules for Submarine Pipeline Systems, Det Norske Veritas, Høvik, Norway.
- Devore, J.L. (1991). Probability and Statistics for Engineering and the Sciences, Third Edition, Brooks/Cole Publishing Company, Pacific Grove, California.
- Dinovitzer, A.S., and Smith, R.J. (1998). "Strain-Based Pipeline Design Criteria Review," International Pipeline Conference, ASME, Calgary, Alberta, pp. 763-770.

- Galambos, T.V. (Editor) (1998). Guide to Stability Design Criteria for Metal Structures, Fifth Edition, John Wiley & Sons, New York, New York.
- Glover, A.G., Horsley, D.J., and Dorling, D.V. (1999). "High-Strength Steel becomes Standard on Alberta Gas System," *Oil and Gas Journal*, Vol. 97, No. 1, pp. 44-50.
- Gunst, R.F., and Mason, R.L. (1980). Regression Analysis and Its Application: A Data-Oriented Approach, Marcel Dekker Inc., New York, New York.
- Hibbitt, Karlsson, & Sorenson, Inc. (HKS) (1997a). ABAQUS/Standard, Version 5.7-1 (computer software). Hibbitt, Karlsson, & Sorenson Inc., Pawtucket, Rhode Island.
- Hibbit, Karlsson, & Sorenson, Inc. (HKS) (1997b). ABAQUS/Standard Theory Manual, Version 5.7. Hibbitt, Karlsson, & Sorenson Inc., Pawtucket, Rhode Island.
- Hibbit, Karlsson, & Sorenson, Inc. (HKS) (1997c). ABAQUS/Standard User's Manual, Version 5.7. Hibbitt, Karlsson, & Sorenson Inc., Pawtucket, Rhode Island.
- Hibbit, Karlsson, & Sorenson, Inc. (HKS) (1997d). ABAQUS/Standard Example Problems Manual, Version 5.7. Hibbitt, Karlsson, & Sorenson Inc., Pawtucket, Rhode Island.
- Kennedy, D.J.L. (1974). "Limit States Design—An Innovation in Design Standards for Steel Structures," *Canadian Journal of Civil Engineering*, Vol. 1, No. 1, pp. 1-13.
- Khuri, A.I., and Cornell, J.A. (1996). Response Surfaces: Designs and Analyses, 2nd Edition, Marcel Dekker Inc., New York, New York.
- Kormann, P., and Zhou, Z. (1995). "Support Spacing of Buried and Above-ground Piping," Second International Conference on Advances in Underground Pipeline Engineering, ASCE, Seattle, Washington, pp. 54-64.
- Langhaar, H.L. (1951). Dimensional Analysis and Theory of Models, John Wiley and Sons, New York, New York.
- Lay, M.G. (1982). Structural Steel Fundamentals – An Engineering and Metallurgical Primer, Australian Road Research Board, Vermont South, Australia.
- Llewellyn, D.T. (1992). Steels: Metallurgy and Applications, Butterworth-Heinemann, Oxford, UK.
- Mak, D.K., and Tyson, W.R. (1998). "Material Assessment of Canadian SAW Line-pipes," International Pipeline Conference, ASME, Calgary, Alberta, pp. 711-721.
- McCarthy, D.F. (1988). Essentials of Soil Mechanics and Foundations, Prentice Hall, Englewood Cliffs, New Jersey.
- Montgomery, D.C. (1976). Design and Analysis of Experiments, John Wiley & Sons, New York, New York.
- NORSOK (1997). Subsea Pipelines, NORSOK Standard Y-001, Revision 1, Norsk sokkels konkuransesposisjon (competitive standing of the Norwegian offshore sector), Oslo, Norway.

- NOVA Gas Transmission Ltd. (1999). December 1999 Annual Plan, Report to Alberta Energy and Utilities Board, NOVA Gas Transmission Ltd. (a subsidiary of TransCanada PipeLines Limited), Calgary, Alberta.
- Petroleum Communication Foundation (1995). Pipelines—A Backgrounder, Petroleum Communication Foundation, Calgary, Alberta.
- Prevost, R.C., and Kienow, K.K. (1994). "Basics of Flexible Pipe Design," *Journal of Transportation Engineering*, ASCE, Vol. 120, No. 4, pp. 652-671.
- Price, P.St.J., and Anderson, H.A. (1991). "Integrity Monitoring and Maintenance Criteria for New and Existing On Land and Marine Pipelines," *Proceedings of the First International Offshore and Polar Engineering Conference*, Edinburgh, UK, pp. 386-393.
- Price, P.St.J., and Barnette, J.A. (1987). "Pipeline Codes and Structural Criteria for Pipelines in Arctic and Earthquake Regions," *Sixth International Symposium and Exhibit on Offshore Mechanics and Arctic Engineering*, Houston, Texas, pp. 89-97.
- Ramm, E. (1980). "Strategies for Tracing Nonlinear Responses Near Limit Points," *Nonlinear Finite Element Analysis in Structural Mechanics*, Europe-U.S. Workshop, Bochum, Germany.
- Riks, E. (1972). "The Application of Newton's Method to the Problem of Elastic Stability," *Journal of Applied Mechanics*, ASME, pp. 1060-1065.
- Riks, E. (1979). "An Incremental Approach to the Solution of Snapping and Buckling Problems," *International Journal of Solids and Structures*, Vol. 15, pp. 529-551.
- Roark, R.J., and Young, W.C. (1975). Formulas for Stress and Strain, Fifth Edition, McGraw-Hill, New York, New York.
- Row, D.G., Hollings, J.P., Sause, R., and Der Kiureghian, A. (1987). "Limit State Probabilistic Design of Offshore Arctic Pipelines," *Sixth International Symposium and Exhibit on Offshore Mechanics and Arctic Engineering*, Houston, Texas, pp. 115-123.
- Sabnis, G.M., Harris, H.G., White, R.N., and Mirza, M.S. (1983). Structural Modeling and Experimental Techniques, Prentice-Hall, Englewood Cliffs, New Jersey.
- Saikaly, W.E., Bailey, W.D., and Collins, L.E. (1996). "Comparison of Ring Expansion vs. Flat Tensile Testing for Determining Linepipe Yield Strength," *International Pipeline Conference*, ASME, Calgary, Alberta. pp. 209-213.
- Shoemaker, A.K. (1984). "The Effects of Plate Stress-Strain Behavior and Pipemaking Variables on the Yield Strength of Large-Diameter DSAW Line Pipe," *Journal of Engineering Materials and Technology*, ASME, Vol. 106, pp. 119-126.
- Souza, L.T., and Murray, D.W. (1999). "Analysis for Wrinkling Behavior of Girth-Welded Line Pipe," *Journal of Offshore Mechanics and Arctic Engineering*, *Transactions of the ASME*, Vol. 121, No. 1, pp. 53-61.

- Spangler, M.G., and Handy, R.L. (1973). Soil Engineering, Third Edition, Intext Educational Publishers, New York, New York.
- SPSS, Inc. (1997). SigmaPlot 4.0 (computer software), SPSS Inc., Chicago, Illinois.
- Standards Australia (1997). Pipelines—Gas and Liquid Petroleum, Part 1: Design and Construction, Australian Standard 2885.1—1997, Standards Australia, Homebush, New South Wales, Australia.
- Stelpipe (1993). Steel Pipe for Commercial, Industrial, and Process Use, Fifth Edition, Stelpipe (A Unit of Stelco, Inc.), Welland, Ontario.
- Sterling, R. (Facilitator) (1996). “Working Group Report, Pipeline Design,” Workshop of Pipeline Research Needs, Pipeline Division, Pipeline Research Committee, ASCE, Leesburg, Virginia.
- Streisselberger, A., Bauer, J., Bergman, B., and Schütz, W. (1992). “Correlation of Pipe to Plate Properties—Model Calculations and Application in the Design of X80 Line Pipe Steels,” Canadian International Conference on Pipeline Reliability, pp. III-3-1 through III-3-13.
- Tabachnick, B.G., and Fidell, L.S. (1996). Using Multivariate Statistics, Third Edition, HarperCollins College Publishers, New York, New York.
- Taylor, E.S. (1974). Dimensional Analysis for Engineers, Oxford University Press, London, UK.
- Tiratsoo, J.N.H. (editor) (1987). Pipeline Pigging Technology, Pipes & Pipelines International, Scientific Surveys Ltd., Beaconsfield, UK.
- Troitsky, M.S. (1982). Tubular Steel Structures: Theory and Design, James F. Lincoln Arc Welding Foundation, Cleveland, Ohio.
- Young, W.C. (1989). Roark’s Formulas for Stress and Strain, Sixth Edition, McGraw-Hill, New York, New York.
- Yoosef-Ghods, N., Kulak, G.L., and Murray, D.W. (1994). Behavior of Girth-Welded Line Pipe, Structural Engineering Report No. 203, Department of Civil Engineering, University of Alberta, Edmonton, Alberta.
- Zhou, Z., and Kormann, P. (1995). “Behavior of Sleeper-Supported High Pressure Piping,” Proceedings of the OMAE-95, Vol. V, Pipeline Technology, AMSE, Copenhagen, Denmark, pp. 403-408.
- Zimmerman, T.J.E., Price, P.St.J., Colquhoun, I.R., and Smith, R.J. (1992). “Development of a Limit States Guideline for the Pipeline Industry,” Proceedings of the 11th International Conference on Offshore Mechanics and Arctic Engineering, ASME, Vol. V, Part A, Calgary, Alberta, pp. 85-89.

**APPENDIX A—PROPAGATION OF RANDOM  
EXPERIMENTAL ERRORS**

## PROPAGATION OF RANDOM EXPERIMENTAL ERRORS

### *Estimates of error in measuring devices*

Manual measurements—ruler (MM)		±2 mm
Cable transducers (CT)	±0.15% of full scale for 20 in. transducers = ±0.762 mm	
Load cells (LC)	±0.15% of full scale for 300 kip load cells = ±2.0 kN	
	±0.4% of full scale, 500 kip range on MTS 6000 = ±8.9 kN	
Strain gauges (SG)		±10 µε

### *Sample calculations for the propagation of random errors*

#### Out-of-roundness

$$o = \text{out-of-roundness} = \frac{D_{\max} - D_{\min}}{D} \quad [1-12]$$

$$D_{\max} = \Delta MM_1 + \Delta MM_2 + D = (MM_{1f} - MM_{1i}) + (MM_{2f} - MM_{2i}) + D$$

$$D_{\min} = \Delta CT_I = CT_{1f} - CT_{1i}$$

where,

- ΔMM<sub>1</sub> = lateral deflection of pipe wall based on manual measurements (east side)
- ΔMM<sub>2</sub> = lateral deflection of pipe wall based on manual measurements (west side)
- MM<sub>1f</sub> = final lateral position of pipe wall (east side)
- MM<sub>1i</sub> = initial lateral position of pipe wall (east side)
- MM<sub>2f</sub> = final lateral position of pipe wall (west side)
- MM<sub>2i</sub> = initial lateral position of pipe wall (west side)
- ΔCT<sub>I</sub> = vertical diametrical deflection measured by internal cable transducer
- CT<sub>1f</sub> = final extension of internal cable transducer
- CT<sub>1i</sub> = initial extension of internal cable transducer

D is constant, and using equation [4-1]:

$$\begin{aligned}
 e_{\text{oor}} &= \sqrt{\left(\frac{\partial o}{\partial MM_{1f}} e_{MM_{1f}}\right)^2 + \left(\frac{\partial o}{\partial MM_{1i}} e_{MM_{1i}}\right)^2 + \left(\frac{\partial o}{\partial MM_{2f}} e_{MM_{2f}}\right)^2} \\
 &\quad + \sqrt{\left(\frac{\partial o}{\partial MM_{2i}} e_{MM_{2i}}\right)^2 + \left(\frac{\partial o}{\partial CT_{1f}} e_{CT_{1f}}\right)^2 + \left(\frac{\partial o}{\partial CT_{1i}} e_{CT_{1i}}\right)^2} \\
 &= \sqrt{\frac{4(2\text{mm})^2 + 2(0.762\text{mm})^2}{D^2}} \\
 &= \frac{\pm 4.14\text{mm}}{D} \\
 &= 0.54\% \text{ out-of-roundness for } 762 \text{ mm pipe} \\
 &= 1.0\% \text{ out-of-roundness for } 406 \text{ mm pipe}
 \end{aligned}$$

where,

- $e_{oor}$  = error associated with out-of-roundness
- $e_{MM_{1f}}$  = error associated with manual measurement  $MM_{1f}$
- $e_{MM_{1i}}$  = error associated with manual measurement  $MM_{1i}$
- $e_{MM_{2f}}$  = error associated with manual measurement  $MM_{2f}$
- $e_{MM_{2i}}$  = error associated with manual measurement  $MM_{2i}$
- $e_{CT_{1f}}$  = error associated with cable transducer measurement  $CT_{1f}$
- $e_{CT_{1i}}$  = error associated with cable transducer measurement  $CT_{1i}$

Gap between sleeper and pipe caused by local reversal of pipe wall curvature

$$\text{Gap} = \Delta CT_E - \Delta CT_I = (CT_{Ef} - CT_{Ei}) - (CT_{1f} - CT_{1i})$$

where,

- $\Delta CT_E$  = vertical deflection of bottom of pipe with respect to the sleeper, as measured by an external cable transducer
- $CT_{Ef}$  = final extension of external cable transducer
- $CT_{Ei}$  = initial extension of external cable transducer

$$\begin{aligned} e_{gap} &= \sqrt{\left(\frac{\partial \text{gap}}{\partial CT_{Ef}} e_{Ef}\right)^2 + \left(\frac{\partial \text{gap}}{\partial CT_{Ei}} e_{Ei}\right)^2 + \left(\frac{\partial \text{gap}}{\partial CT_{1f}} e_{1f}\right)^2 + \left(\frac{\partial \text{gap}}{\partial CT_{1i}} e_{1i}\right)^2} \\ &= \sqrt{4(0.762\text{mm})^2} \\ &= \pm 1.5 \text{ mm} \end{aligned}$$

where,

- $e_{gap}$  = error associated with size of gap
- $e_{CT_{Ef}}$  = error associated with cable transducer measurement  $CT_{Ef}$
- $e_{CT_{Ei}}$  = error associated with cable transducer measurement  $CT_{Ei}$

## **APPENDIX B—RESULTS OF ANCILLARY TESTS**

Notes: L indicates a longitudinal coupon  
T indicates a flattened transverse coupon  
R indicates a hydraulic ring expansion specimen

**Table B.1** Measured specimen parameters

Specimen	Measured Size $D \times t \times \ell$ (mm)	$\sigma_y^\dagger$ (MPa)	$E^\ddagger$ (MPa)
S1	762 × 8.57 × 5600	560	199 000
S2	762 × 16.60 × 5600	450	199 000
S3	762 × 8.70 × 5600	545	198 000
S4	406 × 5.92 × 3600	460	201 500
S5	762 × 8.38 × 5600	540	201 000
S6	762 × 8.40 × 5600	540	214 900
S7	762 × 16.58 × 5600	510	214 200
S8	406 × 7.43 × 3600	510	205 000
S9	406 × 6.06 × 3600	390	214 600
S10	406 × 6.03 × 3600	390	210 500
S11	762 × 8.38 × 5600	520	211 800

<sup>†</sup>Average static yield stress at 0.5% strain from longitudinal coupon tests.

<sup>‡</sup>Average elastic modulus from longitudinal coupon tests.

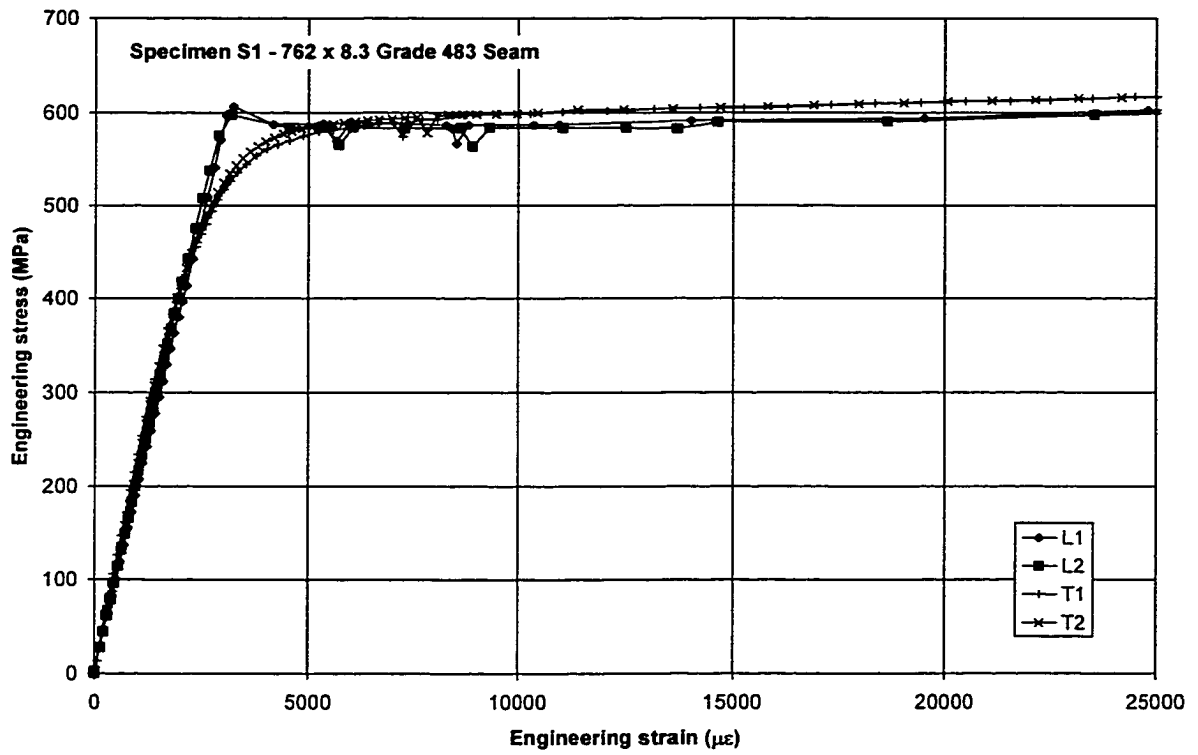


**Figure B.1** Ancillary test results, Specimen S1

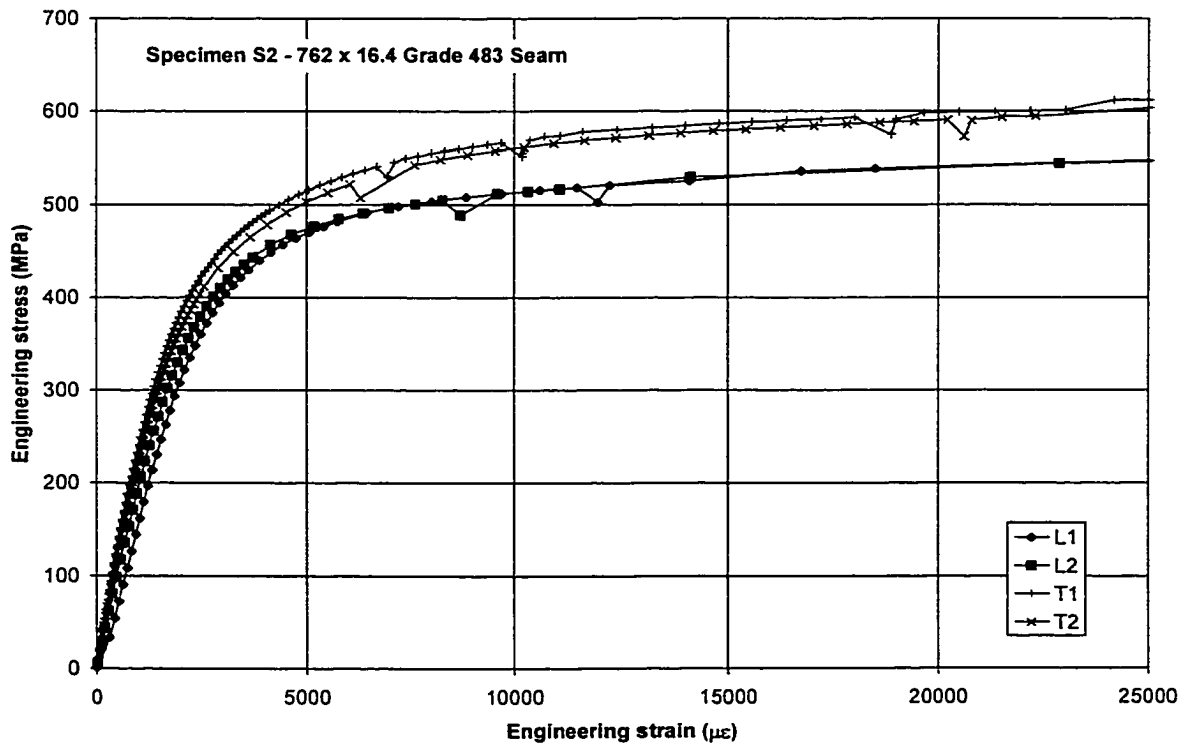


**Figure B.2** Ancillary test results, Specimen S2

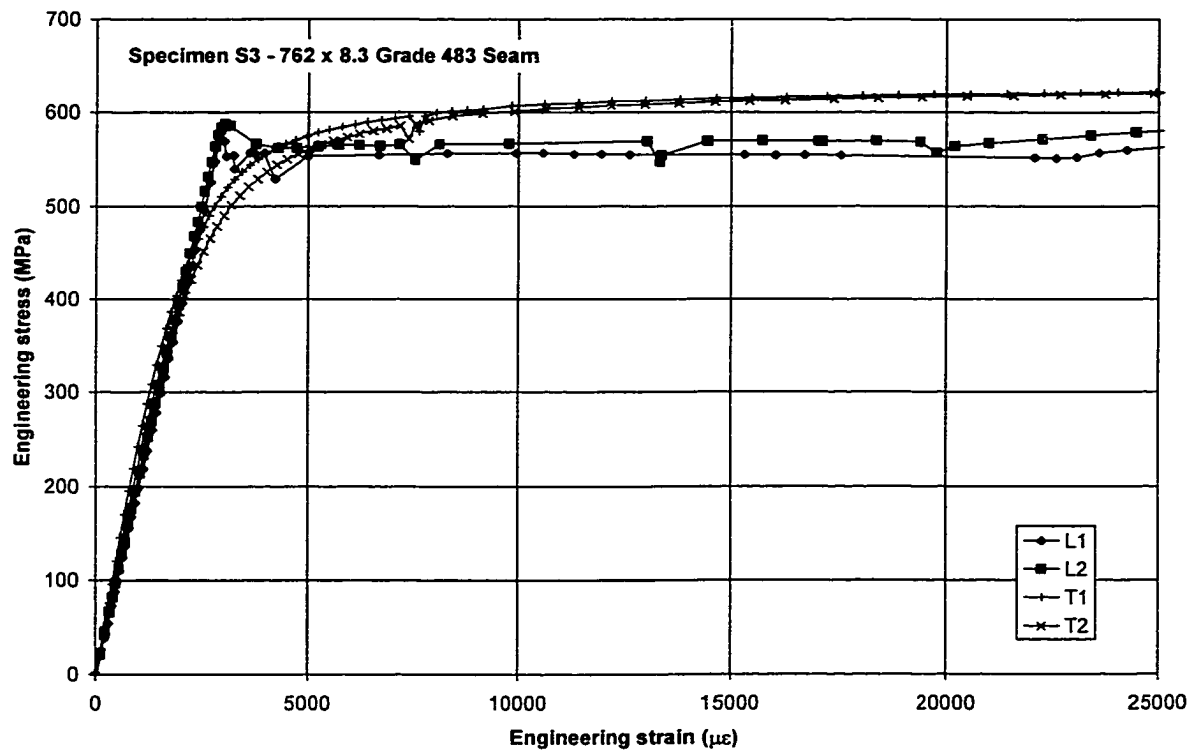


**Figure B.3** Ancillary test results, Specimen S3

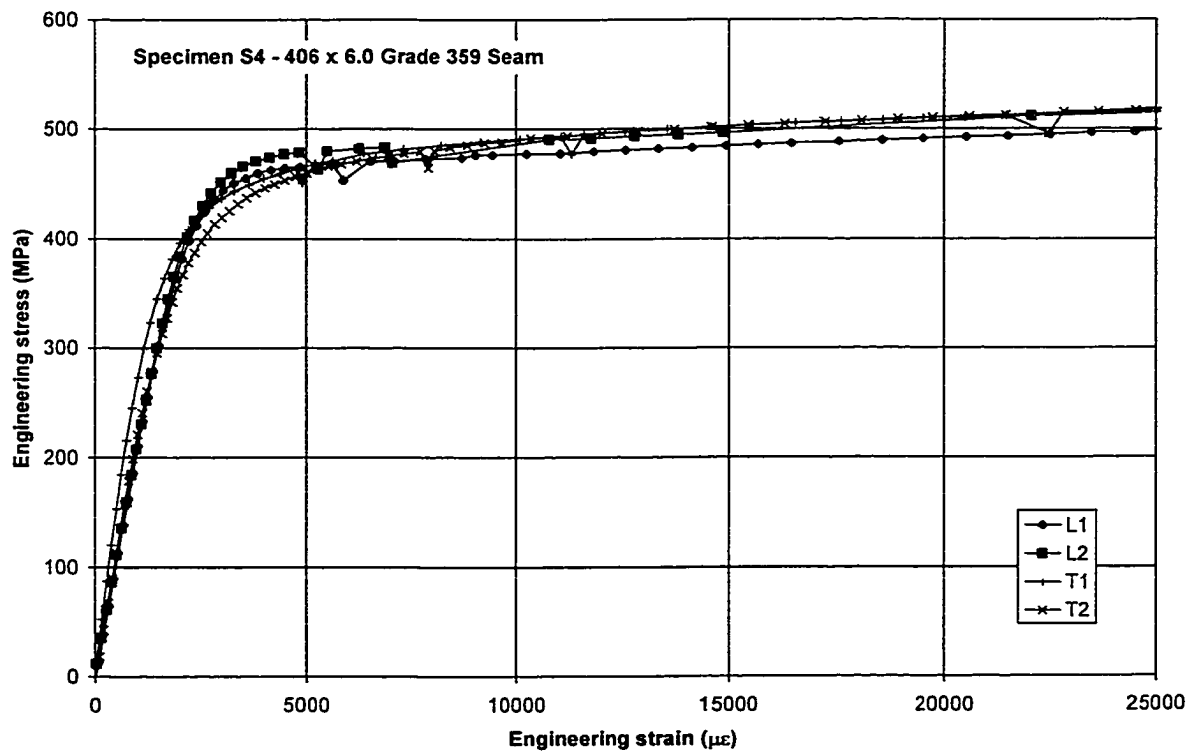


**Figure B.4** Ancillary test results, Specimen S4

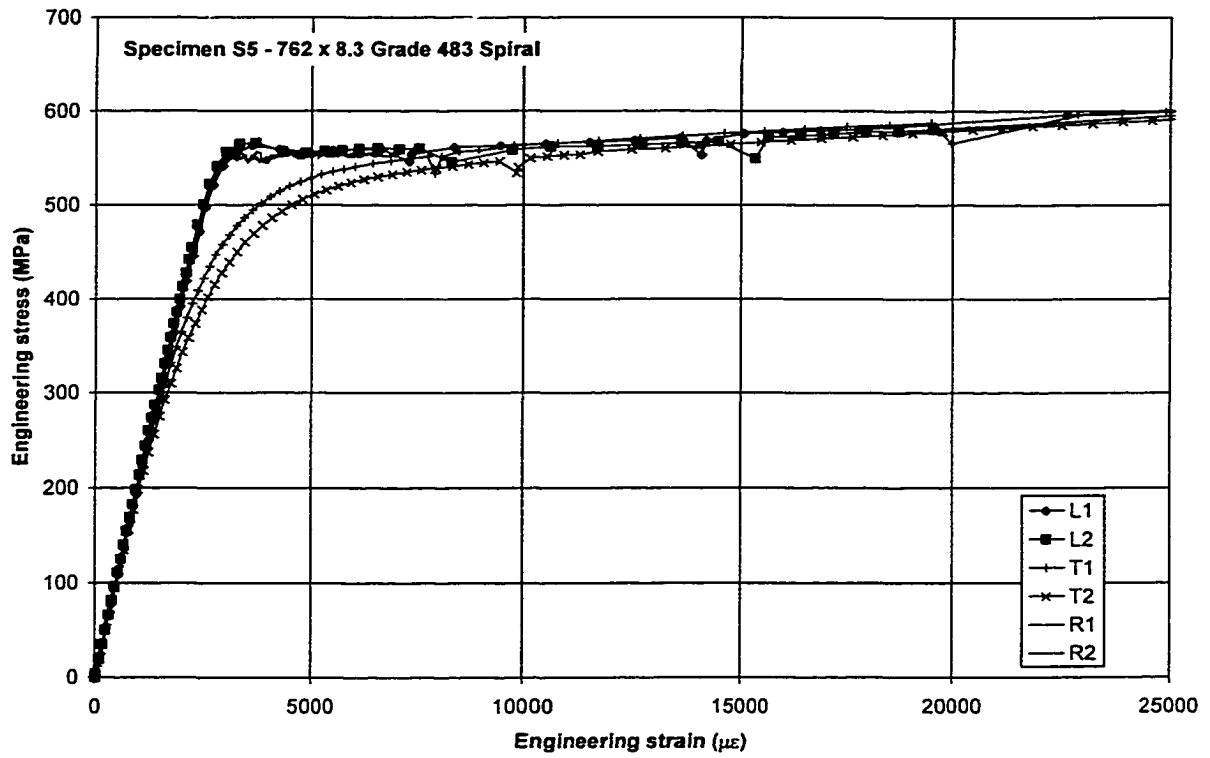


Figure B.5 Ancillary test results, Specimen S5

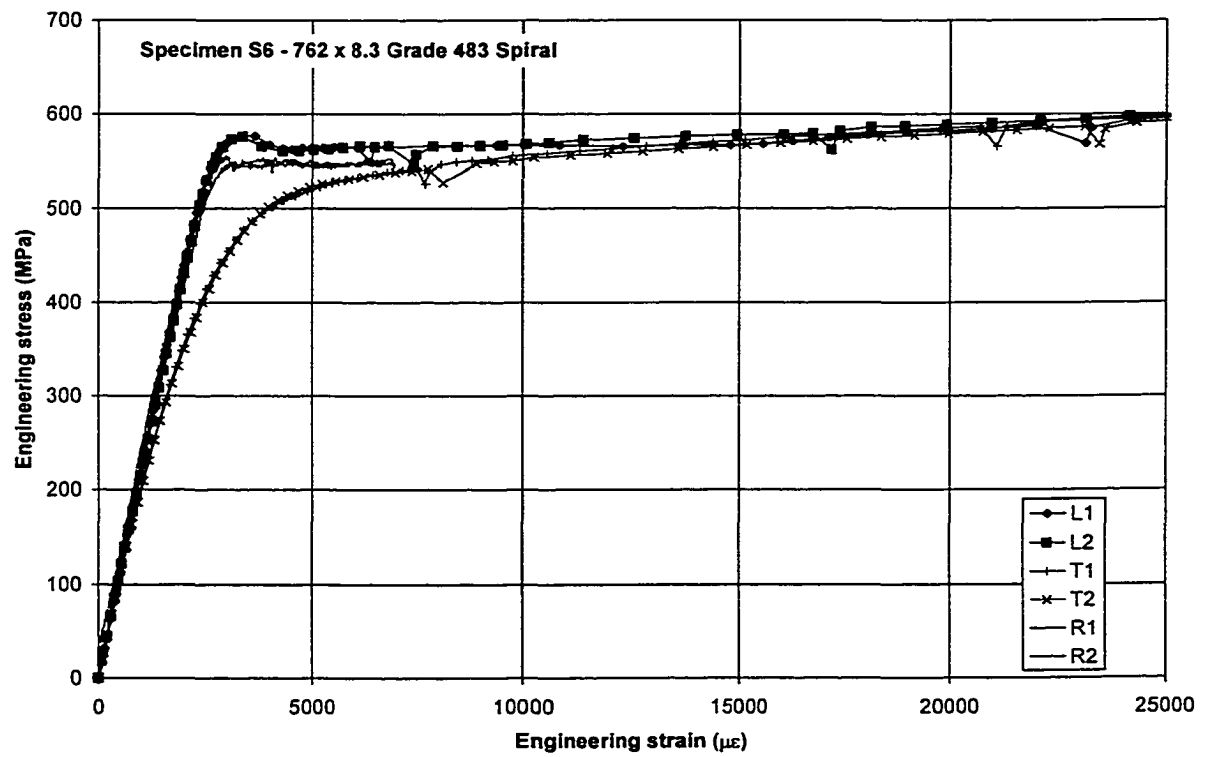
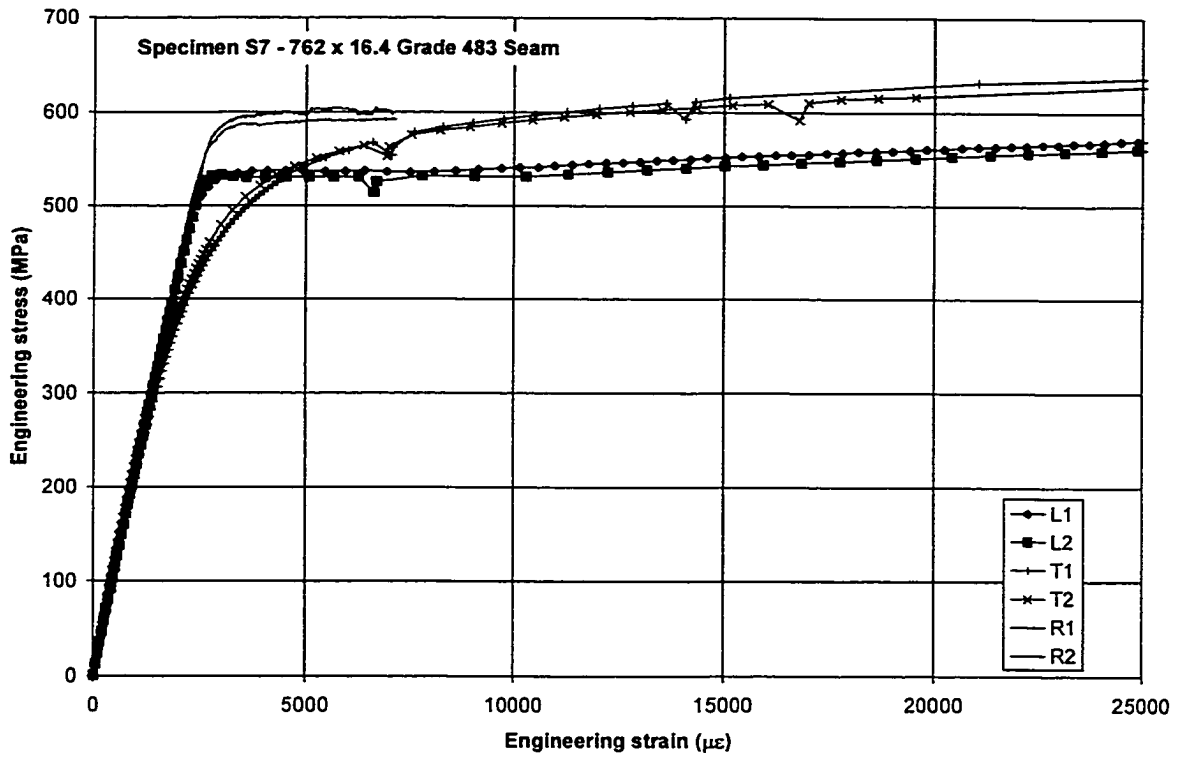
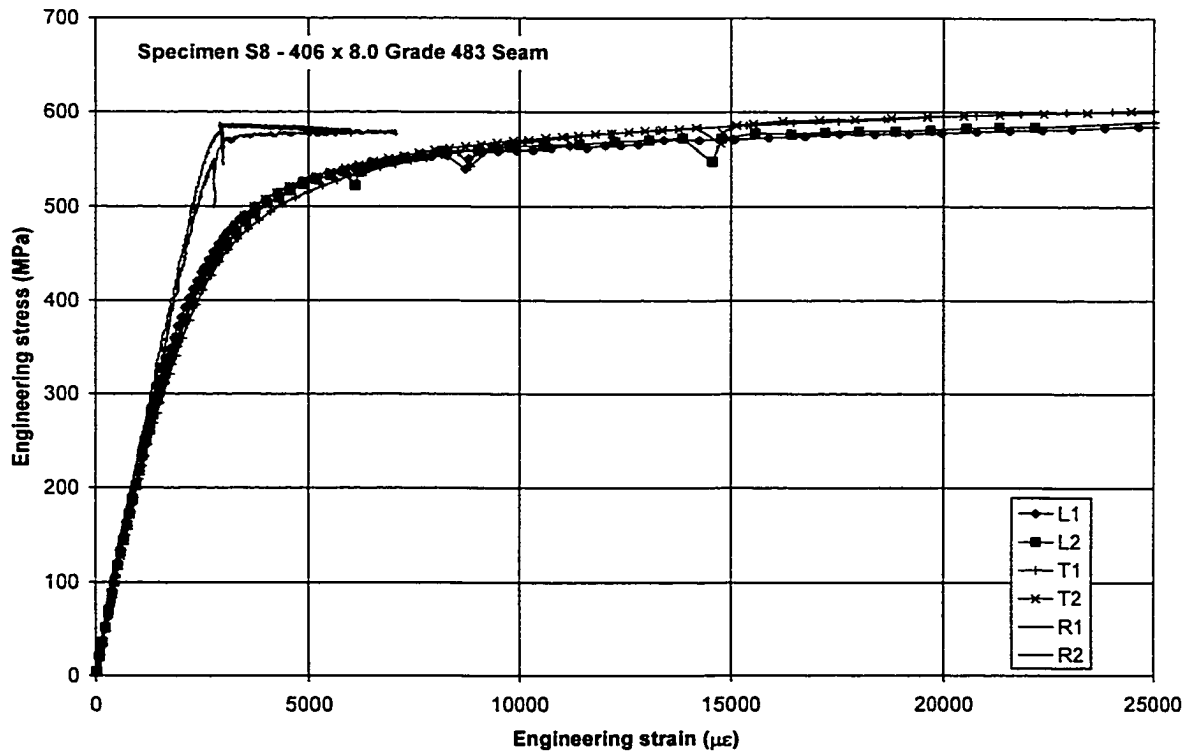


Figure B.6 Ancillary test results, Specimen S6



**Figure B.7** Ancillary test results, Specimen S7



**Figure B.8** Ancillary test results, Specimen S8

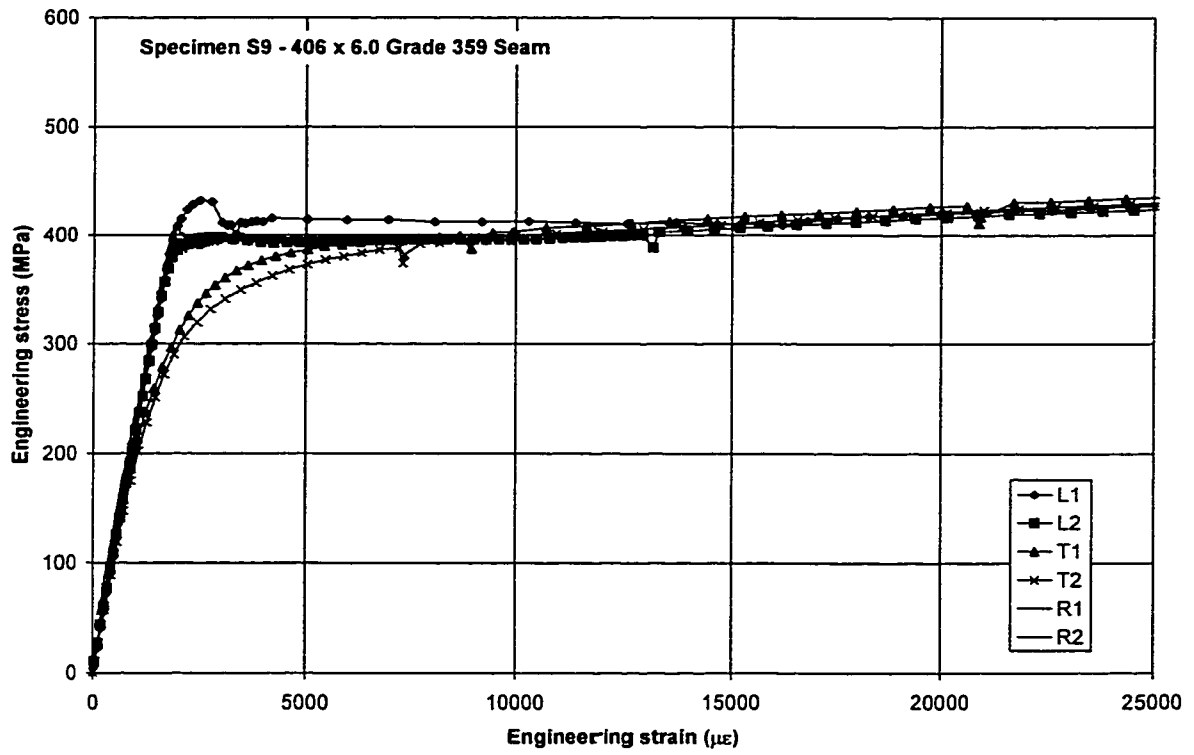


Figure B.9 Ancillary test results, Specimen S9

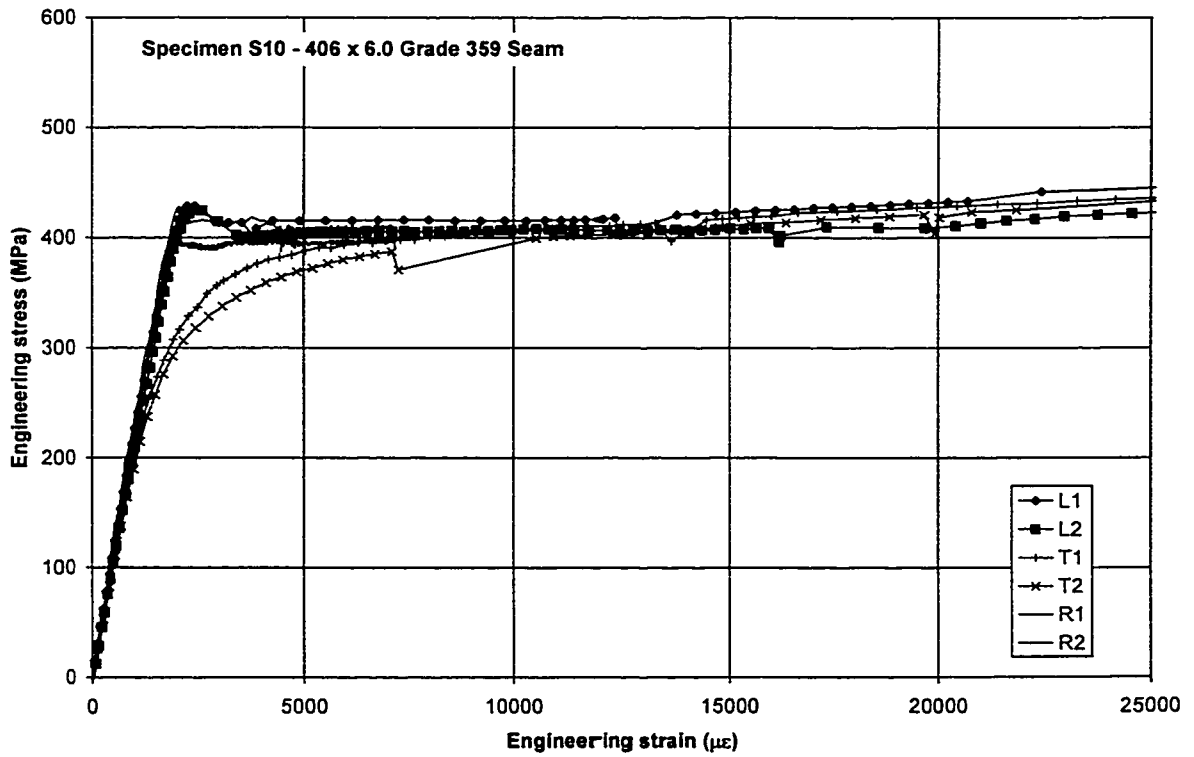
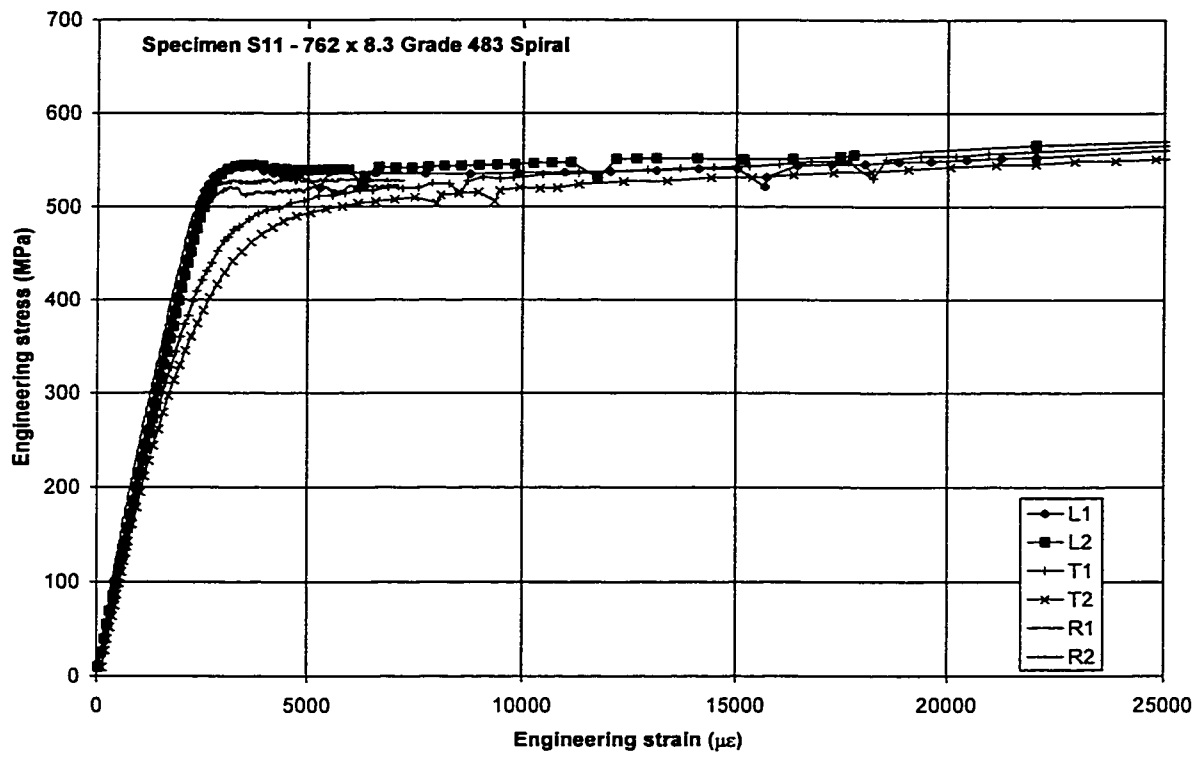
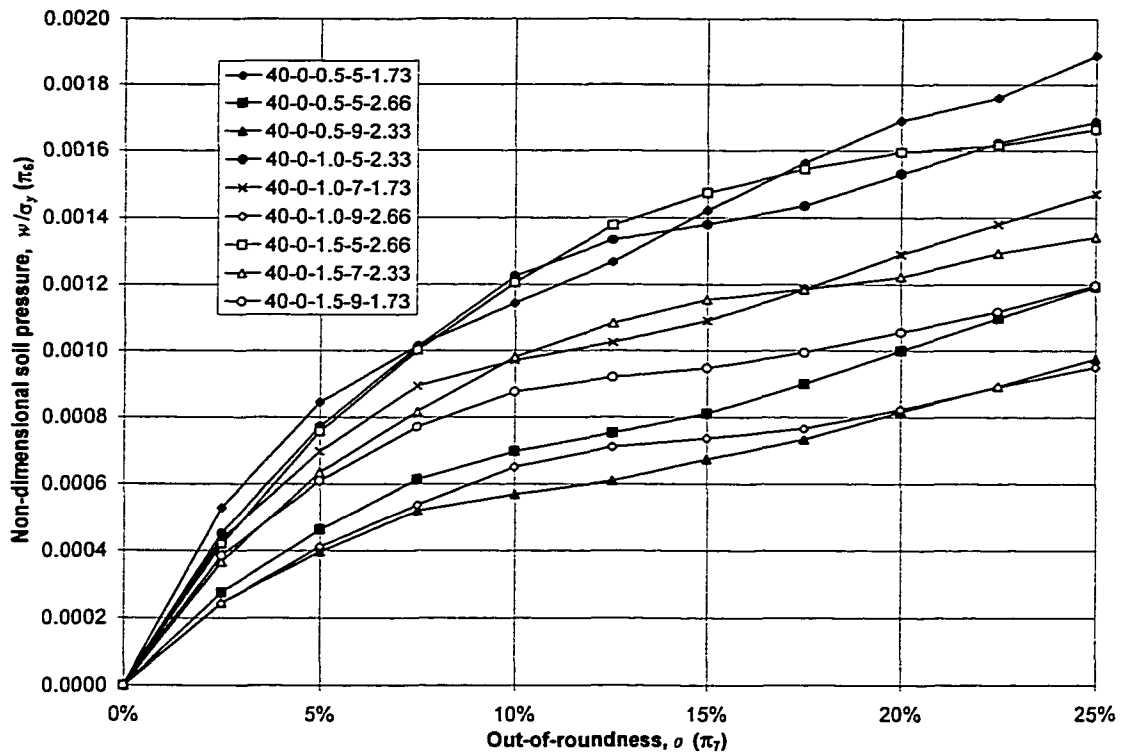


Figure B.10 Ancillary test results, Specimen S10



**Figure B.11** Ancillary test results, Specimen S11

**APPENDIX C—FINITE ELEMENT ANALYSIS  
RESULTS FOR PARAMETRIC STUDY OF  $p/p_y=0$**



**Figure C.1** Results from finite element analysis for parametric study of  $p/p_y=0$  when  $D/t=40$

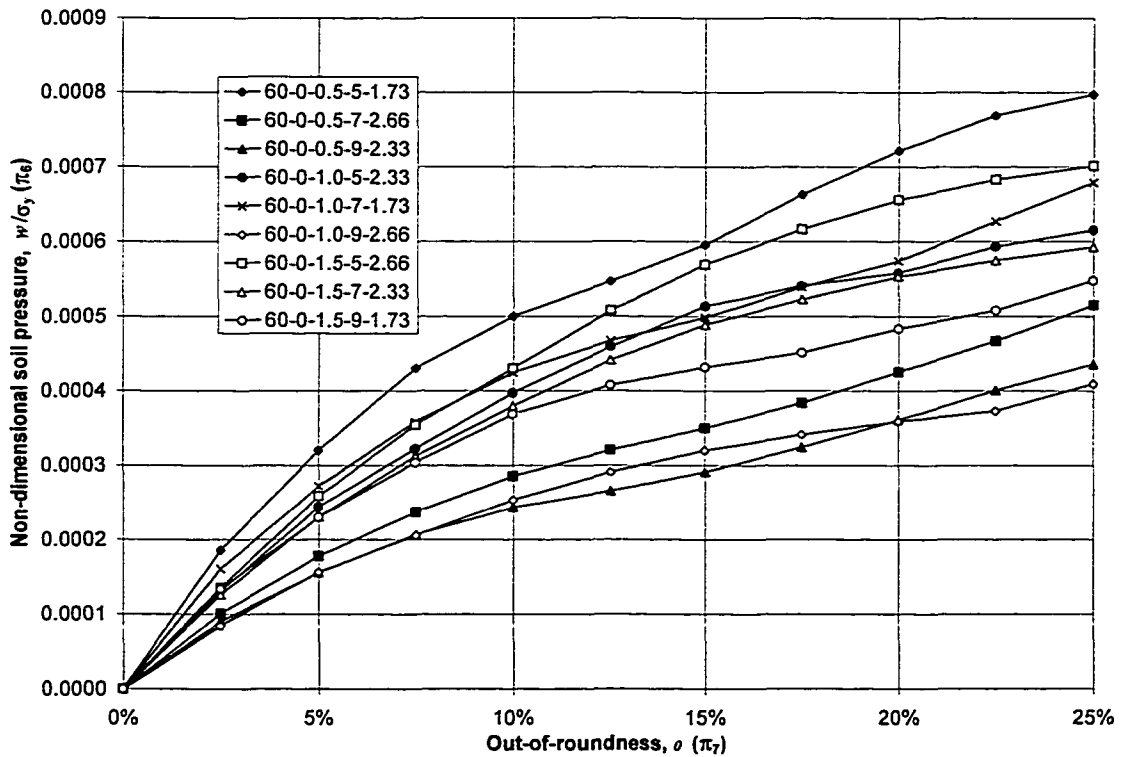


**Figure C.2** Results from finite element analysis for parametric study of  $p/p_y=0$  when  $D/t=60$

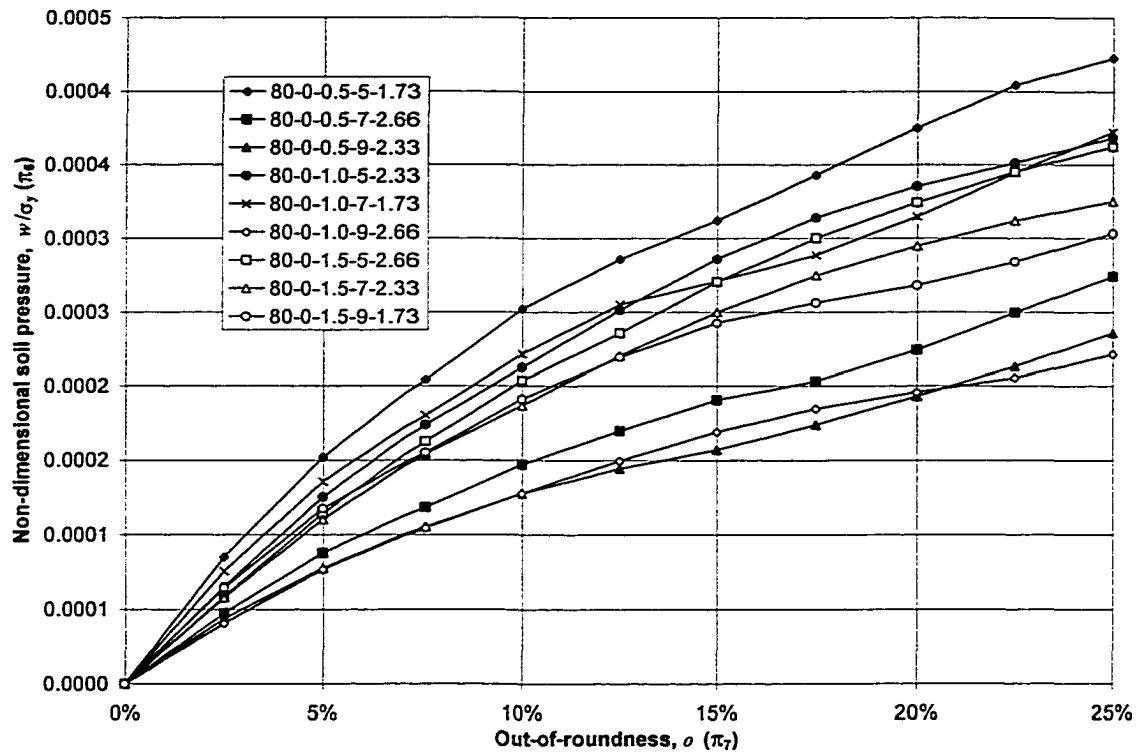


**Figure C.3** Results from finite element analysis for parametric study of  $p/p_y=0$  when  $D/t=80$

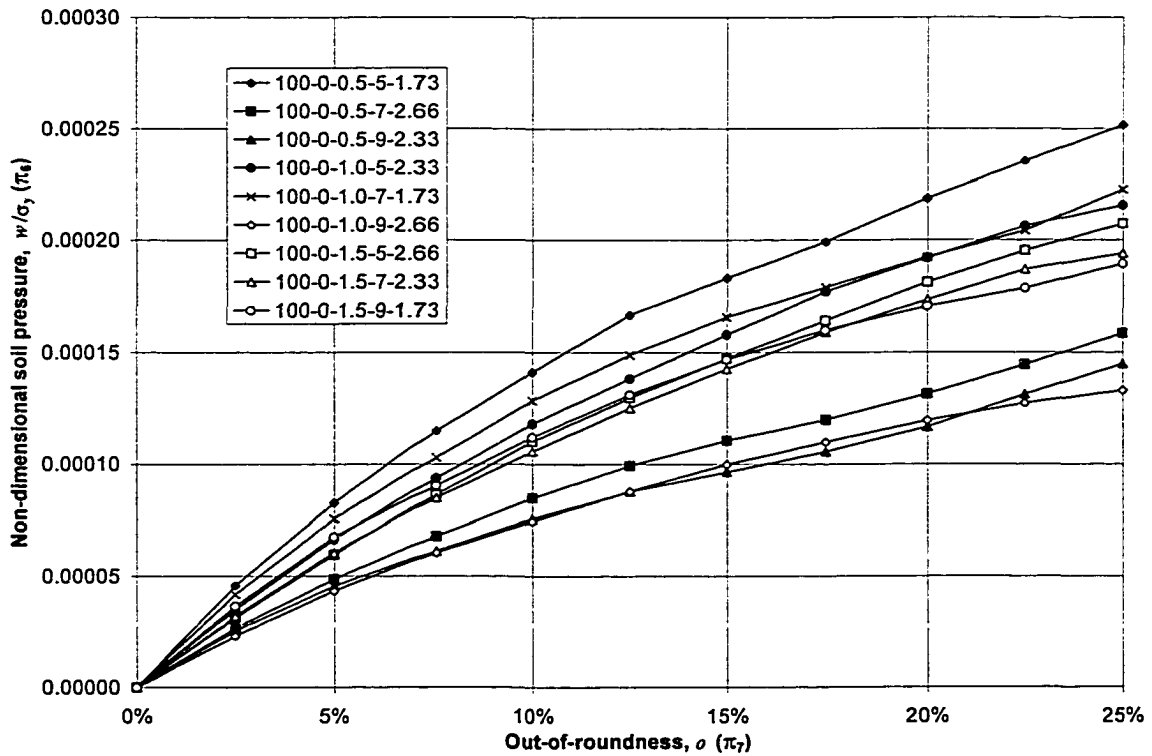


**Figure C.4** Results from finite element analysis for parametric study of  $p/p_y=0$  when  $D/t=100$

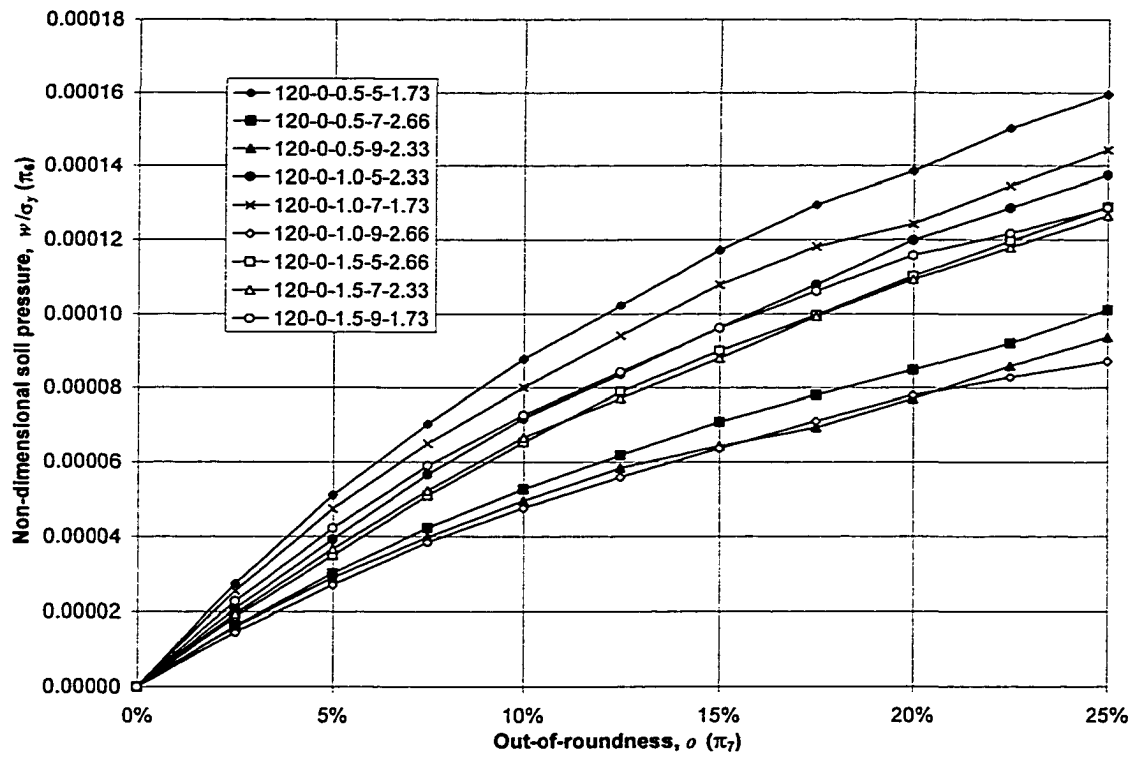


**Figure C.5** Results from finite element analysis for parametric study of  $p/p_y=0$  when  $D/t=120$